Safety Report

15-Foot Bubble Chamber

15-Foot Bubble Chamber

Safety Report

July 1972

Volume 2

National Accelerator Laboratory
Batavia, Illinois

safety report, 15-foot bubble chamber, July 1972

Operated by Universities Research Association Inc.
Under Contract of the United States Atomic Energy Commission

TABLE OF CONTENTS

VOL. I

TABLE OF CONTENTS

VOL. II

LIST OF DRAWINGS

VOL. II

2621.ME-26072	Expansion System Schematic
2621.ME-26071	Expansion System Schematic
2621.ME-33202	Oil & Air Compressor - Floor Plan Layout
2621.MR-33168	9" Valve Actuator System 9" Valve - Check Valve Layout
2621.MR-33280	Expansion System Elevation View
2621.MD-25378	Piston & Rod Guide Assembly
2621.ME-25534	Piston & Rod Seal - Assembly Lower
2621.ME-25129	Expansion Piston
2621.MC-25369	Piston Rod Fitting Assembly
2621.MD-25461	Wood Core
2629.ME-25308	General Assembly Illustration
2621.MC-25336	Lip Seal Section
2621.MB-25973	Piston Lip Seal
2621.MB-25974	Piston Lip Seal
2623.ME-25250	Optical Fisheye Assembly (Section)
2623.ME-25421	Optical Fisheye Port - Plug
2627.MD-25798	Optics Vacuum System Schematic
2623.ME-25432	Optics System - Optical Fisheye Port
2627.MC-25971	Main Vacuum System Schematic

TABLE OF CONTENTS

VOL. III

TABLE OF CONTENTS

VOL. III (Cont'd)

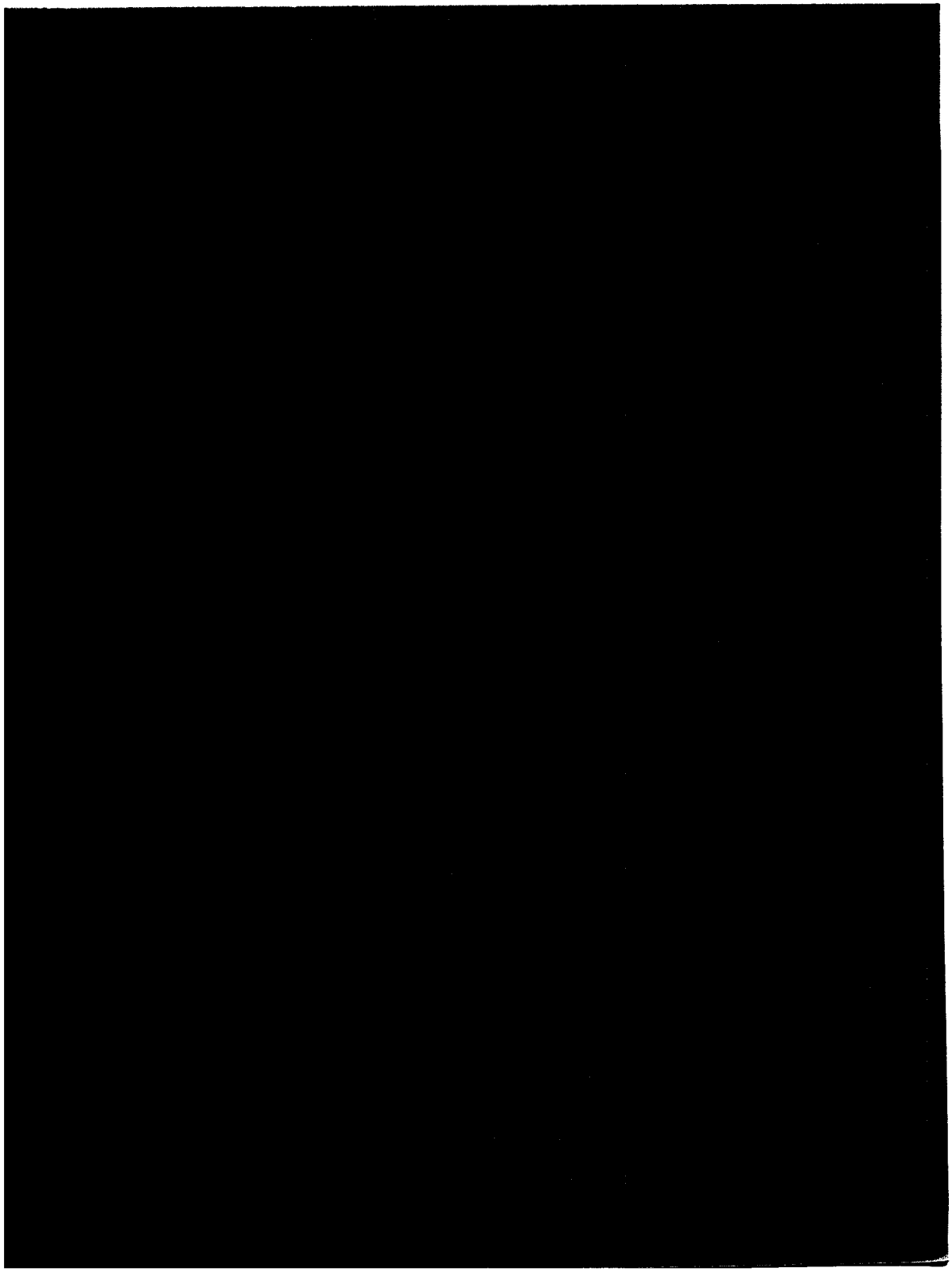

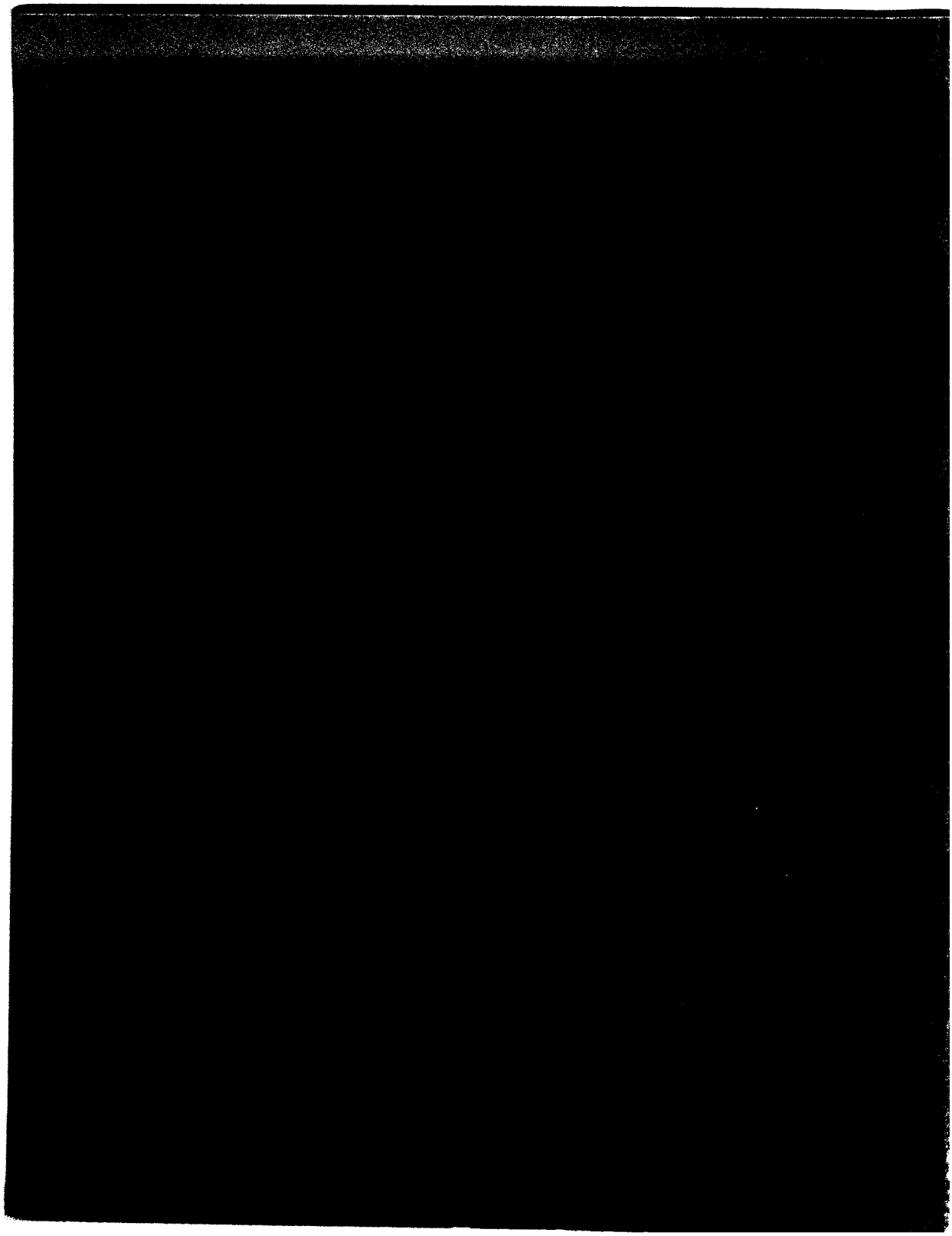

IV. *EQUIPMENT*

E. Expansion System Actuator

Prepared by

Stanford Linear Accelerator Center,
Bubble Chamber Group

TABLE OF CONTENTS

LIST OF FIGURES

LIST OF TABLES

IV. E. EXPANSION SYSTEM ACTUATOR

(1) INTRODUCTION

The National Accelerator Laboratory (NAL) asked the Stanford Linear Accelerator Center (SLAC) to design and implement the expansion system for the 15-foot bubble chamber. This report describes some of the basis for the design and details the equipment which has been constructed.

The SLAC Bubble Chamber Group has had experience at Lawrence Radiation Laboratory, Berkeley, and at SLAC with several chambers with a total of over 50 million expansions. The design for NAL is directly scaled from the SLAC 82" chamber (former Lawrence Radiation Laboratory 72" chamber) and the SLAC 40" hydrogen bubble chamber. These chambers use resonant hydraulic expansion systems with partial pneumatic control systems. "Tuning" the resonance for the different chamber operating liquids (hydrogen, deuterium, neon) is accomplished by changing the mass of the "bouncer" piston which serves as a mass multiplier in the resonant system.

At this point in time all the components have been designed, assembled, and checked out at SLAC. Previous experience with these systems indicates extensive tests and modifications are usually necessary for successful routine operation. These test are scheduled to begin in December 1971 at NAL with the expansion actuator and all support equipment installed in its final position.

(2) CRITERIA

1. The National Accelerator Laboratory will provide the chamber expansion piston. It is to weigh less than 2,000 pounds including the shaft and clamp.

2. NAL will provide the coupling between the piston and the expansion system 9-inch shaft.

3. NAL is to provide a 1,000-ton foundation block with 1,500,000 pound post-tensioned reinforcing rods on which the expansion system will

be bolted.

4. NAL will provide a 15-ton elevator for access to the expansion pit and will provide a cart on which the expansion assembly and the alignment and maintenance jigs and fixtures can be installed.

5. SLAC will specify the necessary pneumatic compressors and oil pumps. NAL will provide installation and piping to SLAC's schematic drawings.

6. When operated with hydrogen the actuator should be able to provide four expansion-recompression cycles per accelerator cycle and a one percent (approximately 5.7" stroke) expansion ratio. The period of the H_2 pulse will be about 50 milliseconds.

7. Time between each expansion-recompression cycle should be ~250 milliseconds. The average repetition rate is to be once per second.

8. For neon operation, the period of the pulse will probably be approximately 150-250 milliseconds, and the repetition rate will be correspondingly lower.

9. The design is to include failure-mode analysis; parts will be designed for the worst failure condition that can be visualized.

10. System reliability is to be accomplished by using proven components at conservative ratings. Maintenance will be facilitated by design that allows replacement of major subsystems.

11. Remote indication and control of critical parameters will be provided to the control room.

(3) SYSTEM DESCRIPTION AND OPERATION

The whole expansion system (see Figure 1) is extremely simple in both concept and content. It consists of a large gas-driven, oil-retarded actuator drive piston which is connected to the chamber piston rod. The piston is exposed to high pressure gas at its top and held in balance by oil at its bottom.

The expansion valve is an axial flow, air-driven device which has a large, high capacity radial/axial flow sleeve seal at one end and a smaller radial flow sleeve seal at the other. The function of the large

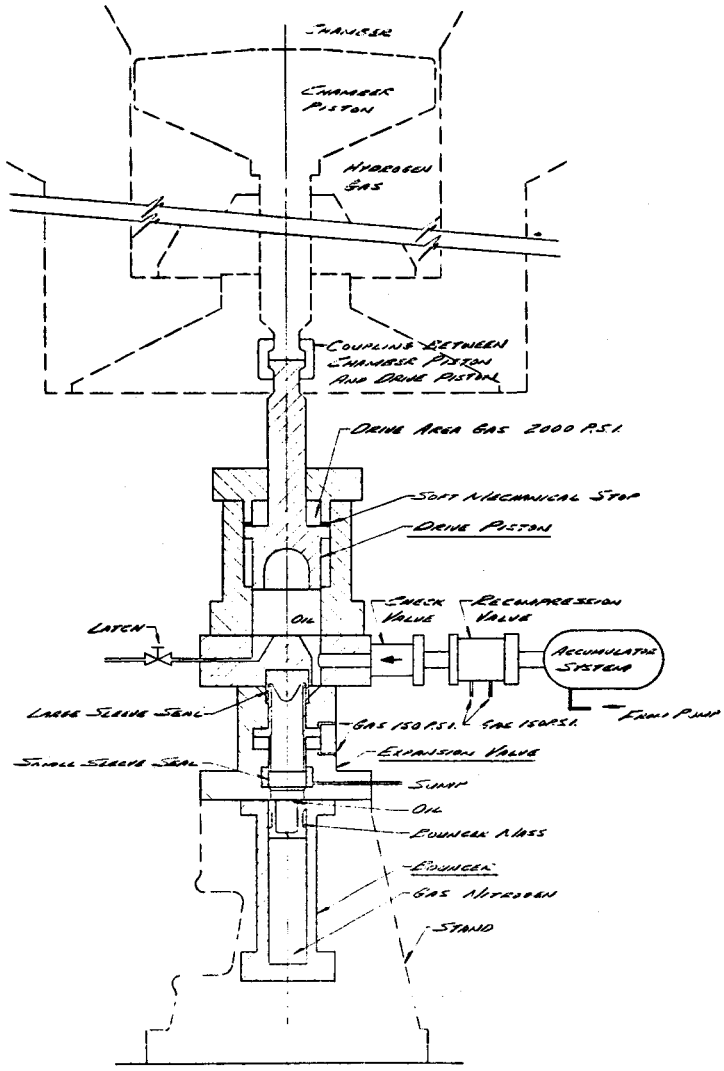
Chamber
Chamber Piston
Hydrogen Gas
Coupling Between Chamber Piston And Drive Piston
Drive Area Gas 2000 P.S.I.
Soft Mechanical Stop
Drive Piston
Check Valve
Recompression Valve
Oil
Latch
Accumulator System
Large Sleeve Seal
Gas 150 P.S.I.
Gas 150 P.S.I.
Expansion Valve
Small Sleeve Seal
Sump
Oil
Bouncer Mass
Bouncer
Gas Nitrogen
Stand

FIGURE 1

axial valve is to handle the main flow of oil during expansion and recompression, while the smaller radial seal portion exhausts the unreturned oil from the bouncer region to the sump.

The bouncer is one of the several energy storage regions used during the stroke, and its pressure and volume, at the beginning of the stroke, control to a large degree the length of the stroke.

The bouncer mass moves several times faster than the drive piston and transforms back into the chamber system as the ratio of the velocities squared. The duration, or period, of the pulse is controlled by both the mass and the velocity of the bouncer, and alternate bouncer assemblies will be used to time the pulse period when different operating fluids are put in the chamber.

Operation

The expansion system is a resonant one in which potential energy is stored in the gas in the drive area until the expansion valve is opened, at which time the chamber piston is pulled downward, gaining kinetic energy as it speeds up. As motion progresses downward, oil drives the bouncer down. Gas is compressed below the bouncer piston; this compression is essentially adiabatic. Simultaneously, the main chamber liquid piston moves to reduce the chamber pressure and raises the pressure by about 60-75 percent in the gas region which exists below it. At the bottom of the stroke the kinetic energy, which has been carried by the moving masses in the chamber piston, oil piston and in the bouncer and its oil, is stored as potential energy in the bouncer gas and in the pressure difference between the chamber liquid and the gas space below. The motion then reverses itself, and the piston returns nearly to its starting point, at which time the expansion valve is closed. Since the cycle is not completely reversible and losses occur, it is necessary to replace the lost energy by injecting a small amount in the form of high-pressure oil, and this is done through the recompression valve via a check valve and accumulator system which puts a predetermined volume of oil back into the system. The timing of the injection is not critical

and is done sometime during the return stroke of the expansion piston, while the expansion valve is still open.

The depth of the stroke is controlled by varying the starting pressure in the bouncer or the gas pressure above the drive piston. Curves are given to show the results of such variations in Appendix A.

The main chamber piston always returns to the same position after each pulse; this requires mechanical stops. These stops consist of elastomer pads which compress gas in circumferential convolutions as the piston reaches the rest position. Even though the stops are in the nature of snubbers or shock absorbers, it is undesirable to bump them with any real velocity. Therefore, the whole cycle is designed so that the recompression make-up is one percent to three percent less than the amount needed for complete reset; a small oil supply, called the "latch", bleeds a predetermined amount of oil into the region between the expansion valve and main oil piston to produce a ramp-like approach to the mechanical stops. The latch valve remains open at all times except during chamber pulses.

Theory

A simplified model of the expansion system will suffice as an introduction to the essential operating parts. The much more complete model, which was used in the final computer analysis, was described by K. Skarpaas (January 8, 1971, revised November 3, 1971) and is included here in somewhat abstracted form as Appendix A.

The piston body M_1 is acted upon by the forces (see Figure 2)

F_1 = (chamber pressure)x(chamber piston area;)

F_2 = (gas region pressure)x(chamber piston area minus shaft area;)

F_3 = (pusher pressure)x(drive piston pusher area;)

F_4 = (oil pressure)x(drive piston oil area.)

The bouncer body M_2 is acted on by the forces

F_5 = (oil pressure)x(bouncer area;)

F_6 = (bouncer gas pressure x bouncer area.)

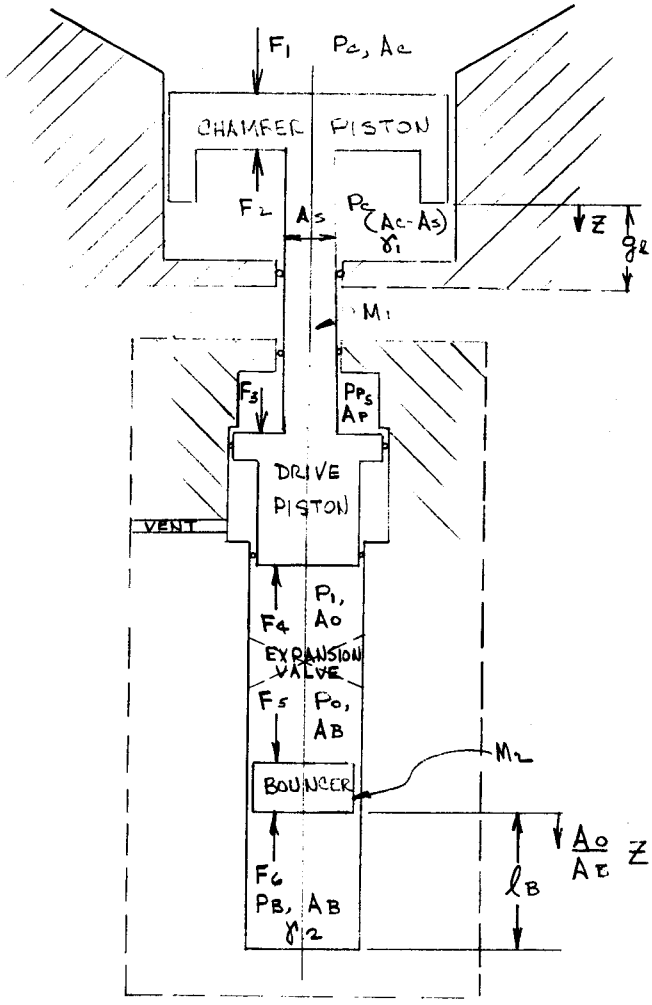
F1
Pc, Ac
CHAMFER
PISTON
F2
As
Pc (Ac-As)
γ1
Z
g2
M1
F3
Pps Ap
DRIVE PISTON
VENT
F4
P1, Ao
EXPANSION VALVE
F5
Po, AB
M2
BOUNCER
F6
PB, AB
γ2
lB
Ao/At Z

FIGURE 2

A closer look at the various forces shows that, to a first approximation,

F_1 = (P_o - KZ) x chamber piston area, where P_o is the initial chamber pressure and KZ is the term for the Δ P which results from the piston motion;

$F_2 = P_o \left(\frac{V_o}{V_f}\right)^{\gamma_1}$ x (piston area minus shaft area); V_o, V_f = initial, final volume beneath piston. The ratio of specific heats in the "below piston area" does not stay constant as the stroke progresses; the best guess at γ_1 is between 1.8 and 2.

F_3 will be nearly constant because it is a gas region with large accumulators connected to it.

F_4 is a term in which the oil pressure varies during the stroke. Just prior to the opening of the expansion valve, the oil pressure is high: the order of 2,000 - 2,500 psi. When the valve is opened, the pressure quickly drops to about one-half this value and remains there while the chamber piston starts to move. At the same time the bouncer starts to move down and compress the gas in its energy storage region. The oil pressure between the bouncer and piston slowly builds up until at the very bottom of the pulse, when deceleration is the greatest, the oil pressure may exceed the value it had prior to the start of expansion. As the piston starts its upward travel, the oil pressure in this region once again drops back down to reach a low at the time the upward piston velocity is the greatest. As the piston slows down on the final return stroke, the oil pressure in this region approaches the value it had previous to the start of expansion.

F_5, being a product of the oil pressure times the area, will follow nearly the same pattern as F_4. Both F_4 and F_5

must be slightly modified by a term which takes into account the fact that, as the bouncer moves down, the column of oil, which changes diameter, and therefore velocity, must be accelerated; and as this column height grows with the stroke, the amount of oil mass to be accelerated also grows. It is necessary to use $f = \frac{d\ (mv)}{dt}$ and not $m \frac{dv}{dt}$ so this changing oil mass won't be neglected. This was done in computer study but is not shown here.

F_6 is a term in which the gas pressure changes almost adiabatically with the stroke and follows the expression $F_6 = P_B\left(\frac{\ell_o}{\ell_o - S_B}\right)^{\gamma_2} A_B$, where ℓ_o is the original length of the gas-occupied region below the bouncer, and S_B is the bouncer stroke (γ_2 is 1.4 if N_2 gas is used in the bouncer). $S_B = \frac{A_O}{A_B} Z$.

These forces combine to give the two coupled equations:

$$A_c\ (P_0 - KZ) - P_0\left(\frac{g_L}{g_L - Z}\right)^{\gamma_1} (A_c - A_s) + P_P A_P - P_1 A_0 = M_1 \ddot{Z}$$

$$P_O A_B - A_B P_B\left(\frac{\ell_B}{\ell_B - \frac{A_O}{A_B} Z}\right)^{\gamma_2} = M_2 \frac{A_0}{A_B} \ddot{Z}$$

These are very enlightening and useful equations which give solutions that describe very well the overall picture of the piston motion, but they do not include the many losses which occur during the motion, such as friction through the valves, the impedance presented by a valve which does not open as a step function but which actually takes 15 to 20 milliseconds to open, the bulk modulus of the oil in the system and the oscillations this can cause. The dynamic picture of the whole system is extremely complicated, and a much more detailed and thorough study was made,

one which included the spring action of the supports, the motion of the liquid in the chamber, the elongation of the fiberglass drive rod during the pulse, and many other items of interest.

(4) COMPONENT SPECIFICATION

The major components are listed and briefly described in Table I. Five drawings[1] included here illustrate the major components, their mechanical assembly, and the schematic relationship. A complete list of detail drawings is appended (Appendix B), copies of which are available at SLAC and NAL.

A workbook was kept at SLAC with a copy at NAL of detailed calculations, purchase specifications, pertinent correspondence, etc., which further delineate the expansion system component design. An index of this workbook is attached as Appendix C.

---

1 NAL 2621.ME-26072, Pit Area Schematic.
NAL 2621.ME-26071, Compressor Oil and Air Schematic.
NAL 2621.ME-33202, Floor Plan Layout.
NAL 2621.MR-33168, 9-Inch Valve - Check Valve Layout.
NAL 2621.MR-33280, Expansion System Elevation View.

TABLE I

NAL EXPANSION ACTUATOR

Drive Piston	
Weight	1250 lbs.
Bore	20 in., gas side; 16 in., oil side
Maximum stroke	10 in.
Rod diameter	12 in. gas side
Piston area	200 sq. in.
Displacement	.88 gal.
Pressure	2,500 psi
Housing material	Steel
Liner material	Steel, hard chrome plated (two items)
Piston material	316 and A286 stainless steel
Seal bearing material	Aluminum bronze (three items)
Seals	Commercial "Polypack" (U-cups)
Expansion Valve	
Type	Axial flow, gas drive, three way
Diameter	7.5 in.
Material	Steel
Opening time	.017 sec.
Shuttle weight	172.5 lbs.
Shuttle material	A286 with aluminum bronze weld inserts
Cage and bearing material	Aluminum bronze Ampco 18
Seals, oil	"Polypack"
Seals, gas and static	Rubber compound
Recompression Valve, 2 each	
Type	Axial flow, air driven, three way
Diameter	3.0 in.
Opening time	.006 sec.
Material	Steel, aluminum bronze

TABLE I (continued)

Bouncer	
Size	9 in. dia.
Housing material	Steel
Variable length	20 in. to 28 in.
Weight	32 lbs.
Piston material	Aluminum
Accumulators, Bladder Type, 3,000 psi	
Storage	8-10 gal. std. Greer A106-200
Buffer	2-5 gal. std. Greer A105-200
Kick	4-10 gal. hi-flow Greer A3501-200
Latch	1-10 gal. std. Greer A106-200
Return	4-10 gal. std. Greer A106-200
Hydraulic System	
One booster pump	Warren Pump Inc., Type 400-TS-Screw
Two high pressure variable volume pumps	Dennison, Model PXX-1223-604 RIPX542
Fluid	Petroleum-base oil SAE 5
Maximum pressure	3,000 psi
Maximum delivery	2 x 72 = 144 gpm
Filtration	30 and 10 micron on supply line; 30 micron on return line
Reservoir capacity	560 gal.
Power requirement	1 x 30 = 30 hp 2 x 150 = 300 hp
N_2/He System	
One two-stage horizontal compressor	Ingersoll-Rand, 12 1/2 and 7 x 6 Type PHE-2
Fluid	Nitrogen or helium
Maximum pressure	150 psig
Maximum delivery	400 SCFM
150 psig storage tanks	70 cu. ft.
Regulated pressure	100 psig

TABLE I (continued)

Air/He System (continued)	
100 psig storage tanks	15 cu. ft.
Low pressure	Max. 17 psia
LP buffer volume tanks	190 cu. ft.
Power requirement	100 hp
Drive System	
One three-stage compressor	Ingersoll-Rand, Type 223
Fluid	Nitrogen
Maximum pressure	3,000 psi
Maximum delivery	4.4 SCFM
3,000 psi storage	9.6 cu. ft.
Power requirement	5 hp
Typical H_2 Expansion	
Piston stroke	3.743 in.
Maximum piston velocity	191.7 in./sec.
Maximum piston acceleration	52.8 to 64.6 g
Bounce stroke	11.805 in.
Maximum bounce velocity	618.6 in./sec.
Maximum bounce acceleration	Erratic (27.9 to 227 g)
Maximum oil pressure	2072 psi
Minimum oil pressure	672 psi
Maximum bouncer pressure	1722 psi
Start bouncer pressure	800 psi
Percent expansion	.73 percent

(5) THE CRITICAL COMPONENT ANALYSIS

The component design was accomplished with the requirements of failure-mode analysis very much in mind. Except where specified, pressure vessels and piping were designed in accordance with the ASME Code for Unfired Pressure Vessels, Section VII.

Drive Piston and Drive Piston Housing

The internal housing pressure is 3,000 psi. The stress on all parts is less than 10,000 psi.

Expansion Valve

Wall Thickness of Ring

The material is steel. At the minimum section, ID is 16 inches, the OD is 23 inches, and the oil pressure is 3,000 psi. Using the conservative Barlow's formula, the stress is 9,900 psi.

Shuttle

The material is A286. The yield is 100,000 psi. Hoop stress due to normal differential pressure is 10,000 psi, and hoop stress due to extreme differential pressure is short 16,000 psi. The shuttle reaches a velocity of approximately 200 inches/second and it stops in a distance of approximately .250 inches. This is equivalent to an acceleration of 320,000 inches/second^2. The force to stop the cylindrical part of the shuttle (98 lbs. of mass) is 143,000 lbs. The shear area is 56.5 in.^{2}. The shear stress is 14,300 psi.

The 3 inch bolts must absorb the kinetic energy of stopping the shuttle. The kinetic energy of a 170 lb. shuttle moving at 200 inches/second is 8,900 inch lb. The bolts have a total stressed volume of about 2,400 in.^{3} and Young's modulus of 30,000,000 psi. Since the bolts are initially stressed to 70,000 psi, the calculated strain is .052 mil/inch, or a stress of 1,500 psi. (This does not include the spring constant of the flanges which further reduces the stress.)

Bouncer

Piston Body

Normal acceleration load of 250 g is equivalent to 127 psi pressure differential load. If the piston gets stuck, the maximum stress is 21,400 psi.

Cylinder Wall

The cylinder is 9 inches ID x 12 3/4 OD. The maximum internal pressure is 3,000 psi. The hoop stress is 4,150 psi.

Bouncer Cap

The cap is 3.250 thick plate. There is a 10.5 inch diameter load circle at 3,000 psi. Maximum stress is 5,870 psi for a rigid plate.

Stand

The stand wall is 4 inches thick. The minimum cross-section area is greater than 250 square inches. Stress is 500,000 lbs./250 $in.^2$ = 2,000 psi.

Drive System

The nitrogen compressor is rated for a maximum of 3,000 psi; all components used in that system are items of commerce with a 3,000 psi working rating. The nitrogen compressor will have a relief valve set at 3,300 psig. The four 3,000 psig receivers should be ASME Code stamped and the piping will be tested at 4,500 psig.

Hydraulic System

The hydraulic system, which has a maximum pressure of 3,000 psi, is made from commercial components of this rating whenever possible. Manufactured items are designed for a stress of less than 10,000 psi and representative x-rays of welds are taken. Each pump has a relief valve adjustable from 200 to 3,100 psig. The main oil supply line has a 3,000 psig relief valve. Supply lines will be tested to 4,500 psig.

Accumulators

The oil accumulators are rated at 3,000 psig and carry the ASME "U" Code stamp.

Air/He System

All six helium tanks have a 150 psig rating and will be ASME Code stamped. All pipes are rated at 150 psig and will be tested to 225 psig.

Bolts

The main assembly bolts are listed in Table II, which lists recommended pre-load torques, stresses and female thread strength.

(6) TEST PROGRAM

Prototype expansion systems are working at SLAC, but prior experience indicates that the degree of scaling up required by the NAL design will require an extensive test program. Although individual components have been manufactured, assembled, tested, and have met the required design conditions, a full system test is visualized that will undoubtedly disclose problems requiring greater or less rework of the components described herein. In particular, problems associated with the vibration and noise will be of concern. Oil and gas system contamination may also be a problem.

Fortunately, it was discovered[2] that with relatively minor changes in the operating parameters a full scale operating test of the expansion system can be conducted without connection to the bubble chamber. A dummy chamber which has also been used for testing of other installations is also not required.

This freedom to test in situ without major interference with the other chamber systems should encourage an extensive program, on the order of a million cycles, so that the expansion system will be proven before it need be mated to the hydrogen chamber.

Experience on other chambers has shown that the relation of the expansion system actuator with the hydrogen chamber piston must be carefully aligned and monitored. The test program will give some indication of

---

2 Private communication: R. Watt and K. Skarpaas to W. Fowler, January 27, 1971.

TABLE II

BOLTS

Bolt Function	Number	Size and Length	Pre-Load Torque (Ft-Lb)	Pre-Load (Lb/Bolt) (1)	Pre-Load Stress (Psi) (1)	Cyclic Load (Lb/Bolt) (2)	Female Thread Engagement (Diam.)	Female Shear Stress (Psi) (3)	Female Shear Strength (Psi) (4)	Shear Stress/Shear Strength for Female Thread
Stand to Base	33	2 1/2x12NFx16	5,000	180,000	40,000	2,200	.9	18,500	60,000	.31
Valve to Stand	12	2-12NF2x16.5	4,500	200,000	70,000	6,000	1.75	16,700	60,000	.28
9" Valve Assembly	12	3-12NFx36	15,000	420,000	70,000	6,000	1.75	16,700	60,000	.28
9" Valve to Cage	1	3-12NFx7.5	15,000	420,000	70,000	-	1.0	29,000	67,000	.43
			10,000	300,000	45,000	-	1.0	18,800		.28
Piston to 9" Valve	24	1.75-5NCx11.75	3,000	150,000	80,000	3,000	1.75	19,200	60,000	.32
Piston Assembly	16	1.75-5NCx16.0	3,000	150,000	80,000	4,500	1.75	19,200	60,000	.32
Bouncer to 9" Valve	16	1.25x12NFx6.5	1,100	80,000	75,000	4,500	1.75	19,200	60,000	.32
Bouncer Cap	16	1.25x12NFx9	1,100	80,000	75,000	4,500	.9(5)	34,000	160,000	.21

(1) Calculated on a coefficient of friction of .135.

(2) Calculations made using flange stiffness four times that of bolt and cyclic load amplitude of 360,000 pounds.

(3) Calculated for 60 percent thread engagement for entire length of designated thread length.

(4) .75 x ultimate tensile strength.

(5) Nut used.

alignment variations with time.

A detailed operating procedure is under preparation to help familiarize NAL personnel with the start-up and operation of the actuator during the test program. NAL will conduct the test. SLAC will act as consultant.

APPENDIX A

COMPUTER PROGRAM SIMULATING THE DYNAMIC BEHAVIOR OF THE 15-FOOT NAL HYDROGEN BUBBLE CHAMBER

NOTE: Pages 7-39, which have been deleted for the NAL Design Report, contain evaluations of most of the constants listed on pages 3 and 4.

IV. E. APPENDIX A

COMPUTER PROGRAM SIMULATING THE DYNAMIC BEHAVIOR OF THE 15-FOOT NAL HYDROGEN BUBBLE CHAMBER

The computer program KXSREACM was written at Stanford Linear Accelerator Center for the National Accelerator Laboratory. This program was written to determine what forces, accelerations, velocities, and displacements one should expect during pulsing of the 15-foot bubble chamber. Some additional relative displacements were also calculated. The program treats the bubble chamber as a lumped mass system considering only vertical motions.

The optional data outputs from the computer are listed on pages 5 of 44 and 6 of 44 where positive values generally indicate a downward direction.

The program divides the chamber liquid mass into several horizontal liquid slabs with their proper stiffnesses, to approach a more correct response between the chamber liquid and the piston--expansion system. This part of the program was introduced because of the heavy H_2 - Neon mixtures. The program assumes as shown on Figure 1, page 2 of 44, that all these liquid masses are connected in series and, therefore, that only the uppermost liquid mass is connected to the chamber. In the actual chamber all these liquid masses do, of course, interact with the chamber walls as well as surrounding liquid masses. Therefore, although the program does produce a more correct response between the chamber liquid and the piston, the optional pressure distribution output should not be used to predict pressure uniformity throughout the chamber.

The program does not correct for repressurization of the liquid after the chamber has been expanded, nor does it include any damping except for the damping caused by the valves.

To use this program, approximately 80 variables must be given. Pages 3 of 44 and 4 of 44 show as an example which values we have been using to simulate a chamber running with liquid hydrogen. The values

of these variables and also those used for deuterium and hydrogen-neon mixtures runs are given on pages 5 of 44 through 39 of 44.

We have at SLAC used this program extensively during the design of the expansion system. The program was used to determine the main valve size, the bouncer volume and bouncer diameter, to be compatible with the required chamber period and stroke recoveries.

To demonstrate how we used this program we have chosen to show the effect on the stroke of the chamber piston of small variations of the bouncer pressure, page 40 of 44; the main valve opening time, page 41 of 44; bouncer volume length, page 42 of 44; and the driving pressure, page 43 of 44.

During the design one would, of course, also continuously check miscellaneous accelerations and displacements. Table I on page 44 of 44 shows the maximum differential displacement between the lens mount on the chamber and the vacuum tank, the maximum tension in the piston rod, and the maximum tension between the expansion system and the base for all the conditions considered for the previous four graphs.

Since the time the above-mentioned tables and graphs were prepared, the program has been modified slightly to include the effect of varying the size of the driving accumulators, and the size of the piping for the recompression valves. The results of varying the driving accumulator size from infinite to 5,000 cubic inches are seen on page 45.

Finally, page 46 contains two curves, one showing the expansion stroke for "normal" hydrogen operating conditions, and the other showing an acceptable test condition of the bare expansion system produced by using a somewhat lower driving pressure and a higher bouncer pressure.

Stanford Linear Accelerator Center — Stanford University

ENGINEERING NOTE

STATUS	SUBJECT CODE	FILE NO.

AUTHOR: K. SKARPAAS

DATE: NOV 25-70 PAGE: 2 OF 44

PROJECT—JOB:

TITLE: DIAGRAM FOR COMPUTER-PROGRAM KKSREACM

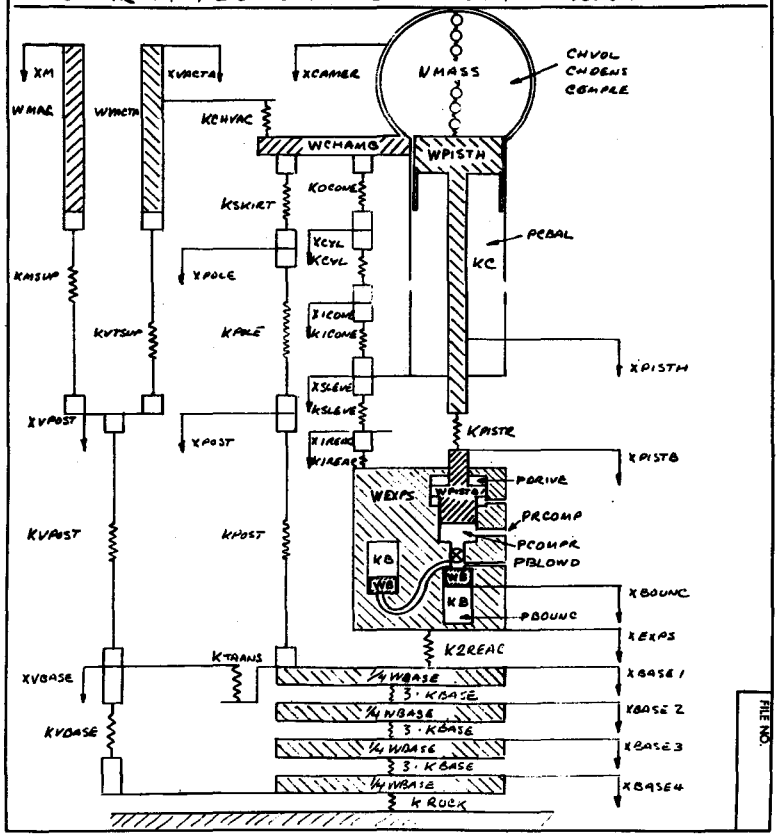

PARAMETERS FOR COMPUTER PROGRAM KXSREACM

WEIGHT OF THE MAIN BASE CASON	=	1956000.
WEIGHT OF THE POLES WHICH SUPPORT THE CHAMBER	=	12245.
WEIGHT OF THE SKIRT WHICH SUPPORTS THE CHAMBER	=	4380.
WEIGHT OF THE CHAMBER	=	21296.
WEIGHT OF THE OUTSIDE CONICAL PART OF CHAMBER	=	8440.
WEIGHT OF THE CYLINDER WHICH CONTAINS THE PISTON	=	5610.
WEIGHT OF THE CONE UNDERNEATH THE PISTON	=	3260.
WEIGHT OF THE SLEEVE CONTAINING THE PISTON ROD	=	936.
WEIGHT OF THE PISTON ROD	=	770.
WEIGHT OF THE UPPER VACUUM TANK SUPPORT CYLINDERS	=	1025.
WEIGHT OF THE VACUUM TANK	=	40000.
WEIGHT OF THE VACUUM TANK BASE CASONS	=	1.
WEIGHT OF THE POSTS WHICH SUPPORT THE CHAMBER	=	82650.
WEIGHT OF THE POSTS WHICH SUPPORT THE VACUUM TANK	=	81000.
WEIGHT OF THE PISTON HEAD	=	1400.
WEIGHT OF THE PISTON BASE	=	1580.
WEIGHT OF THE BOUNCER	=	32.
WEIGHT OF THE EXPANSION SYSTEM	=	23692.
WEIGHT OF THE MAGNET SUPPORT CYLINDERS	=	3075.
WEIGHT OF THE MAGNET ASSEMBLY	=	200000.

STIFFNESS OF THE MAIN BASE CASON	=	362999808.
STIFFNESS OF UPPER POLES THAT SUPPORT THE CHAMBER	=	404000000.
STIFFNESS OF THE SKIRT THAT SUPPORTS THE CHAMBER	=	130000000.
STIFFNESS OF THE CHAMBER LIQUID (AS CALCULATED)	=	62155.
STIFFNESS OF THE BOTTOM CONE OF THE CHAMBER	=	55500000.
STIFFNESS OF THE CYLINDER CONTAINING THE PISTON	=	96200000.
STIFFNESS OF THE CONE UNDERNEATH THE PISTON	=	13300000.
STIFFNESS OF THE SLEEVE CONTAINING THE PISTON ROD	=	38000000.
STIFFNESS OF THE PISTON ROD	=	6000000.
STIFFNESS OF THE UPPER VAC. TANK SUPPORT CYLINDERS	=	26000000.
STIFFNESS OF THE MAIN BASE TO VACUUM TANK BASE	=	1000000.
STIFFNESS OF THE VACUUM TANK BASE	=	1.
STIFFNESS OF THE POSTS WHICH SUPPORT THE CHAMBER	=	170000000.
STIFFNESS OF THE POSTS WHICH SUPPORT THE VAC. TANK	=	115000000.
STIFFNESS OF THE LIME ROCK FOUNDATION	=	2000000000.
STIFFNESS OF THE EXPANSION SYSTEM TO CHAMBER	=	1.
STIFFNESS OF THE EXPANSION SYSTEM TO MAIN BASE	=	75000000.
STIFFNESS OF THE CHAMBER TO VACUUM TANK CONNECTION	=	10000.
STIFFNESS OF THE MAGNET SUPPORT CYLINDERS	=	49700000.

CHAMBER PRESSURE BEFORE EXPANSION	=	80.000
STARTING OIL PRESSURE UNDER THE PISTON	=	2100.000
STARTING BLOWDOWN PRESSURE	=	20.000
STARTING BOUNCER PRESSURE	=	800.000
RECOMPRESSION PRESSURE	=	2200.000
DRIVING PRESSURE	=	1750.000

PARAMETERS FOR COMPUTER PROGRAM KXSREACM (continued)

CHAMBER RADILS	=	75.500
CHAMBER THICKNESS	=	1.000
RATIO OF SPEC. HEATS FOR THE BOUNCER GAS	=	1.400
RATIO OF SPEC. HEATS FOR GAS UNDER CHAMBER PISTON	=	2.000
RADIUS OF BOUNCER VOLUME	=	4.500
LENGTH OF BOUNCER VOLUME	=	28.000
RADIUS OF DRIVING VOLUME	=	10.000
ROD RADIUS IN DRIVING VOLUME	=	5.000
ROD RADIUS UNDER PISTON HEAD	=	6.000
RADIUS OF CHAMBER PISTON	=	35.433
RADIUS OF COMPRESSION CHAMBER	=	8.000
EFFECTIVE RADIUS OF EXPANSION VALVE IN INCHES	=	4.500
OBSTRUCTION LOSS IN EQUIVALENT FEET	=	106.000
EFFECTIVE RADIUS OF RECOMPRESSION VALVE	=	1.500
OBSTRUCTION LOSS IN EQUIVALENT FEET	=	51.000
EFFECTIVE DIAMETER OF BLOWDOWN PIPE	=	0.750
OBSTRUCTION LOSS IN EQUIVALENT FEET	=	5.000
DENSITY OF OIL IN LBS/CUBIC FOOT	=	50.000
VISCOSITY OF OIL IN LBS/(SEC*FOOT)	=	0.023
BULK MODULUS OF OIL IN PSI	=	180000.000
STARTING OIL VOLUME IN COMPRESSION CHAMBER	=	3730.000
STARTING OIL VOLUME IN BOUNCER CHAMBER	=	1900.000
STARTING GAS VOLUME UNDER CHAMBER PISTON	=	130000.000

COMPUTER TIME INCREMENT	=	0.000002
TIME INTERVAL BETWEEN WRITTEN OR PLOTTED DATA	=	0.002000
TIME AT WHICH RECOMPRESSION IS APPLIED	=	0.200000
TOTAL TIME OF WRITTEN DATA	=	0.100000
TOTAL TIME OF PLOTTED DATA	=	0.100000
TIME REQUIRED FOR EXPANSION VALVE TO OPEN / CLOSE	=	0.017000
TIME REQUIRED FOR RECOMPRESSION VALVE TO OPEN/CLOSE	=	0.004000
TIME AT WHICH EXPANSION VALVE IS COMPLETELY CLOSED	=	0.068000
TIME AT WHICH RECOMPR. VALVE IS COMPLETELY CLOSED	=	0.200000

CHAMBER VOLUME IN CUBIC INCHES	=	2010000.
DENSITY OF CHAMBER LIQUID IN GR/CUBIC CM	=	0.062500
COMPRESSIBILITY OF CHAMBER LIQUID IN SQ CM/KG	=	0.001830

The first four data cards are used as described below.

Notes on the data cards.

First three data cards are title cards, and usually contain title, date, etc.

Fourth data card specifies:

NMASS NMASS must be a multiple of 20, and not greater than 200

MODE MODE = 1, is used if one wants to force the displacement of the chamber piston to follow a (1-COS(0*time)) type displacement.

CASE CASE = 1, is used if bouncer mass moves in the same direction as the piston.

CASE CASE = 2, is used if bouncer mass moves in the opposite direction as the piston.

TABLE (1) = 1, is used to tabulate acceleration, velocity, and displacement of the expansion piston and the bouncer piston.

TABLE (2) = 1, is used to tabulate acceleration, velocity, and displacement of the chamber piston and the chamber.

TABLE (3) = 1, is used to tabulate acceleration, velocity, and displacement of the expansion system and the base.

TABLE (4) = 1, is used to tabulate acceleration, velocity, and displacement of the vacuum tank and the relative displacement between the camera mount in the chamber and the ground, and the relative displacement between the camera mount in the chamber and the vacuum tank.

TABLE (5) = 1, is used to tabulate acceleration, velocity, and displacement of the expansion system and the vacuum tank base.

TABLE (6) = 1, is used to tabulate displacement-distribution from bottom to top of chamber.

GRAPH (1) = 1, is used to plot the displacement of the expansion piston.

GRAPH (2) = 1, is used to plot the displacement of the bouncer piston.

GRAPH (3) = 1, is used to plot the displacement of the chamber piston.

GRAPH (4) = 1, is used to plot the displacement of the chamber.

GRAPH (5) = 1, is used to plot the displacement of the expansion system housing.

GRAPH (6) = 1, is used to plot the displacement of the base.

GRAPH (7) = 1, is used to plot the displacement of the vacuum tank.

GRAPH (8) = 1, is used to plot the displacement of the camera mount in the chamber with respect to the ground.

GRAPH (9) = 1, is used to plot the displacement of the camera mount in the chamber with respect to the vacuum tank.

GRAPH (10) = 1, is used to plot the displacement of the vacuum tank base.
GRAPH (11) = 1, is used to plot the acceleration in G's of expansion piston.
GRAPH (12) = 1, is used to plot acceleration in G's of bouncer piston.
GRAPH (13) = 1, is used to plot acceleration in G's of chamber piston.
GRAPH (14) = 1, is used to plot acceleration in G's of chamber.
GRAPH (15) = 1, is used to plot acceleration in G's of expansion system housing.
GRAPH (16) = 1, is used to plot acceleration in G's of base.
GRAPH (17) = 1, is used to plot acceleration in G's of vacuum tank.
GRAPH (18) = 1, is used to plot acceleration in G's of vacuum tank base.
GRAPH (19) = 1, is used to plot displacement of the vacuum tank base.
GRAPH (20) = 1, is used to plot displacement of chamber and base.
GRAPH (21) = 1, is used to plot force between expansion system and base.
GRAPH (22) = 1, is used to plot force in the piston rod.
GRAPH (23) = 1, is used to plot chamber pressure distribution.

DEBUG (1) through DEBUG (10) are used for debugging.
(in space No. 71)

Stanford Linear Accelerator Center — Stanford University

ENGINEERING NOTE

STATUS	SUBJECT CODE	FILE NO.

AUTHOR: K. Skarpaas

DATE: [illegible]

PAGE: 40 OF 45

PROJECT—JOB:

TITLE:

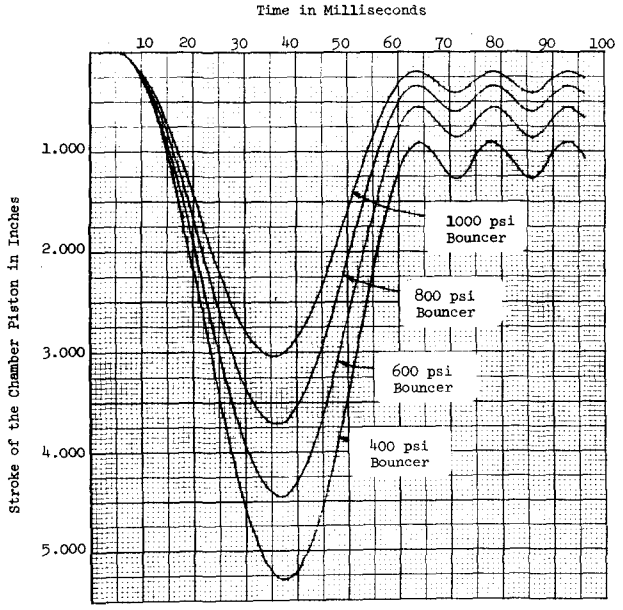

This graph shows how the stroke of the chamber piston is varied by varying the starting pressure in the bouncer. All other variables are as shown on pages 3 and 4.

FILE NO.

Stanford Linear Accelerator Center — Stanford University

ENGINEERING NOTE

STATUS	SUBJECT CODE	FILE NO.

AUTHOR: K. Skarpaas

DATE: [illegible] -71

PAGE: 41 OF 44

PROJECT--JOB

TITLE

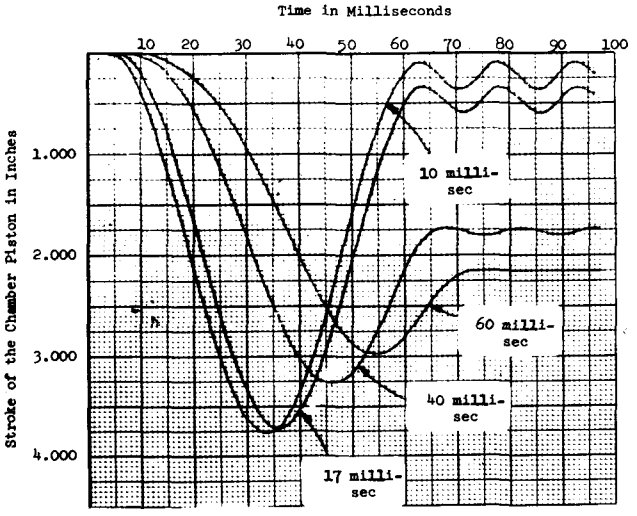

This graph shows how the recovery of the chamber piston stroke varies with the time it takes to open the main valve. There is little change in the chamber recovery if the main valve slows down from 10 to 17 milliseconds, but if it slows down much more than that, the recovery suffers drastically. The total times the valves were kept open were also changed for these curves, and were 63, 68, 78, and 88 milliseconds respectively for the 10, 17, 40, and 60 millisecond valve opening times.

All other variables are as shown on pages 3 and 4.

FILE NO

Stanford Linear Accelerator Center — Stanford University

ENGINEERING NOTE

STATUS	SUBJECT CODE	FILE NO.

AUTHOR: K. Skarpaas

DATE: Jan 7 - 71

PAGE: 42 OF 44

PROJECT—JOB:

TITLE:

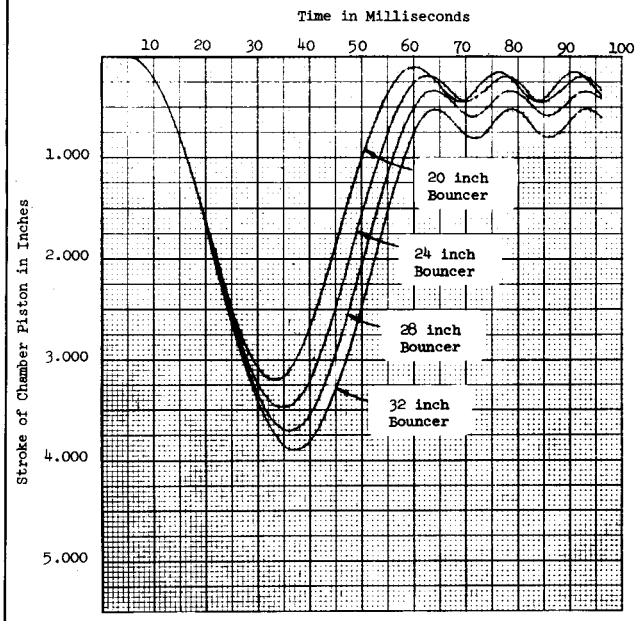

This graph shows how the stroke of the chamber piston is varied by different choices of bouncer volume lengths. All other variables are as shown on pages 3 and 4.

FILE NO.

Stanford Linear Accelerator Center — Stanford University

ENGINEERING NOTE

STATUS	SUBJECT CODE	FILE NO.

AUTHOR: K. Skarpaas

DATE: JAN 7-71

PAGE: 43 OF 44

PROJECT—JOB

TITLE

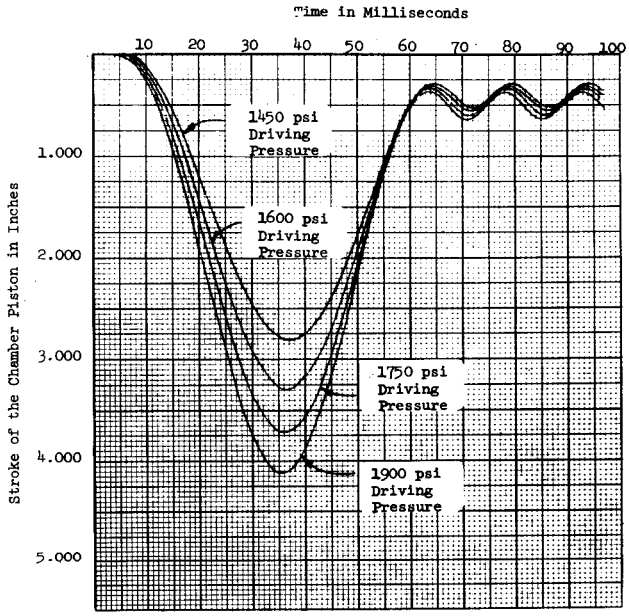

This graph shows how the stroke of the chamber piston is varied by varying the driving pressure.

FILE NO.

TABLE I

BOUNCER PRESSURE IN PSI	VALVE OPENING TIME IN SECONDS	BOUNCER VOLUME LENGTH IN INCHES	DRIVING PRESSURE IN PSI	MAXIMUM MOTION BETWEEN LENS MOUNT & VAC-TANK	MAXIMUM TENSION IN PISTON ROD	MAXIMUM TENSION BETWEEN EXPANSION SYSTEM & BASE
1000	.017	28	1750	.0114	215200	257400
800	.017	28	1750	.0141	261000	326500
600	.017	28	1750	.0170	308500	403000
400	.017	28	1750	.0204	364200	514100
800	.010	28	1750	.0141	285100	337300
800	.040	28	1750	.0126	243300	333200
800	.060	28	1750	.0110	250900	328800
800	.017	32	1750	.0150	281000	375200
800	.017	24	1750	.0127	235000	280000
800	.017	20	1750	.0120	201800	197500
800	.017	28	1900	.0153	295000	326900
800	.017	28	1600	.0125	240900	287800
800	.017	28	1450	.0107	198700	251800

This table shows the maximum values of three variables for all the conditions considered for the previous four graphs. The first variable is the maximum vertical motion between the lens mount on the chamber and the vacuum tank. No attempt has been made to account for the motion caused by the natural axial frequency which the filled chamber has of its own. The second variable is the maximum tension in the piston rod, and is intended to give a clue to what maximum dynamic forces the clamp should be designed to sustain. The last variable is the maximum value of the tension in the support between the expansion system and the base.

Stanford Linear Accelerator Center — Stanford University

ENGINEERING NOTE

STATUS	SUBJECT CODE	FILE NO.

AUTHOR: K. Skarpaas

DATE: March 15,1971 PAGE 45 OF

PROJECT—JOB: NAL Expansion System

TITLE: Chamber Piston Stroke Versus Driving Accumulator Size

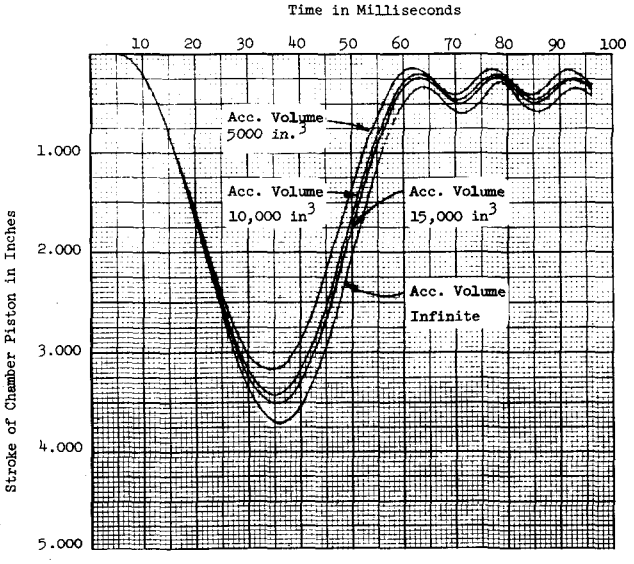

This graph was produced to help determine the sizes of the driving accumulators; it shows the decrease in chamber piston stroke by decreasing accumulator sizes. All other variables are as shown on pages 3 and 4 of the KXSREACM computer program write-up.

By comparing with p. 43 of that write-up, one will conclude that to drive the expansion system with accumulators having a total volume of 10,000 in^3, rather than an infinite volume, the driving pressure would have to be raised approximately 90 psi.

FILE NO.

Stanford Linear Accelerator Center — Stanford University

ENGINEERING NOTE

STATUS	SUBJECT CODE	FILE NO.

AUTHOR: R. Watt and K. Skarpaas

DATE: March 10, 1971

PAGE: 46 OF

PROJECT–JOB: NAL Expansion System

TITLE: Mechanical Test of the NAL Pulser System

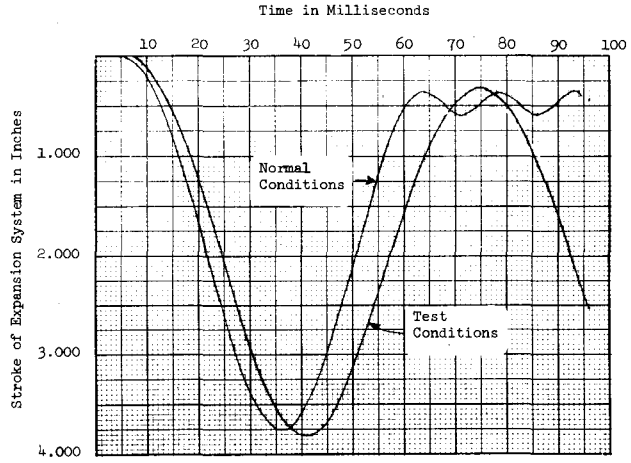

Normal Hydrogen Operating Conditions:

Driving pressure is 1750 psi.
Bouncer pressure is 800 psi.
Expansion valve is closed at .068 sec.
Estimated chamber period is 60 msec.

Test Operating Conditions:

Driving pressure is 1300 psi.
Bouncer pressure is 1000 psi.
Chamber piston is not mounted, only weight mounted is weight of clamp, estimated 200 lbs.
Expansion valve was left open to ease estimation of test period; we estimate it to be 70 msec.

FILE NO.

APPENDIX B

NAL EXPANSION SYSTEM

DRAWINGS ORIGINATING AT SLAC

IV. E. APPENDIX B

NAL EXPANSION SYSTEM
DRAWINGS ORIGINATING AT SLAC

SLAC DRAWING NUMBER AND SUB-SYSTEM		NAL DRAWING NUMBER
915-701	Drive Piston	2621.MC-33000-33059
915-702	9-Inch Valve	33060-33099
915-703	Bouncer	33100-33139
915-704	Stand	33140-33149
915-705	9-Inch Valve Actuator System	33150-33199
915-706	Compressor	33200-33239
915-707	Oil System	33240-33279
915-708	Assembly	33280-33309
915-709	Electronics	33310-33339
915-710	Recompression	33340-33400

GROUP LOG SHEET
DRIVE PISTON

PRE-FIX	BASE	SUF-FIX	REV	DRWG SIZE	NAL NO.	TITLE OR DESCRIPTION	ASSIGNED TO	DATE
SA	915-701	01	1	E	2621.ME-33000	Assembly	Maruyama	3-25-71
SA	915-701	02	1	R	2621.MR-33001	Cover Plate	Barden	3-25-71
PF	915-701	03	1	E	2621.ME-33002	Piston Housing	Maruyama	3-25-71
PF	915-701	04	1	E	2621.ME-33003	Piston	Maruyama	3-25-71
PF	915-701	05		D	2621.MD-33004	Piston Sleeve	Maruyama	3-25-71
PF	915-701	06	1	D	2621.MD-33005	Upper Liner	Barden	3-25-71
PF	915-701	07	1	D	2621.MD-33006	Lower Liner	Barden	3-25-71
SA	915-701	08		D	2621.MD-33007	Upper Seal Flange	Maruyama	3-25-71
PF	915-701	09	1	D	2621.MD-33008	Upper Seal Ring	Maruyama	3-25-71
SA	915-701	10	1	D	2621.MD-33009	Lower Seal Fangle	Maruyama	3-25-71
PF	915-701	11	1	D	2621.MD-33010	Lower Seal Ring	Maruyama	3-25-71
PF	915-701	12	1	D	2621.MD-33011	Top Seal Ring	Barden	3-25-71
PF	915-701	13	1	D	2621.MD-33012	Top Seal Flange	Barden	3-25-71
PF	915-701	14	1	C	2621.MC-33013	Bearing Ring	Maruyama	3-25-71
PF	915-701	15	1	C	2621.MC-33014	Upper Bumper	Maruyama	3-25-71
PF	915-701	16	1	C	2621.MC-33015	Lower Bumper	Maruyama	3-25-71
PF	915-701	17	1	B	2621.MB-33016	Thick Spacer	Maruyama	3-25-71

DRIVE PISTON (continued)

PRE-FIX	BASE	SUF-FIX	REV	DRWG SIZE	NAL NO.	TITLE OR DESCRIPTION	ASSIGNED TO	DATE
PF	915-701	18	1	B	2621.MB-33017	Thick Spacer - Slotted	Maruyama	3-25-71
PF	915-701	19	1	B	2621.MB-33018	Thin Spacer	Maruyama	3-25-71
PF	915-701	20	1	B	2621.MB-33019	Thin Spacer - Slotted	Maruyama	3-25-71
PF	915-701	21		A	2621.MA-33020	Upper Liner Bolt Modification	Barden	3-25-71
PF	915-701	22		A	2621.MA-33021	Lower Liner Bolt Modification	Barden	3-25-71
PF	915-701	23	1	B	2621.MB-33022	Bleed Down Valve	Maruyama	3-25-71
PF	915-701	24	1	A	2621.MA-33023	Bleed Down Valve Locking Screw	Maruyama	3-25-71
SA	915-701	25	1	E	2621.ME-33024	Piston and Sleeve Machining	Maruyama	3-25-71
SA	915-701	26		E	2621.ME-33025	Piston Sleeve	Maruyama	4-27-71
PF	915-701	27		C	2621.MC-33026	Bumper Retaining Ring	Maruyama	7-27-71
PF	915-701	28		A	2621.MA-33027	Bumper Retaining Ring Screen	Maruyama	7-27-71
					33028			
					33029			
					33030			
					33031			
					33032			
					33033			

GROUP LOG SHEET
9-INCH VALVE

PRE-FIX	BASE	SUF-FIX	REV	DRWG SIZE	NAL NO.	TITLE OR DESCRIPTION	ASSIGNED TO	DATE
SA	915-702	01	1	E	2621.ME-33060	Ring #1	Maruyama	3-3-71
SA	915-702	02	1	D	2621.MD-33061	Ring #2	Maruyama	3-3-71
SA	915-702	03	1	E	2621.ME-33062	Ring #3	Maruyama	3-3-71
SA	915-702	04	1	D	2621.MD-33063	Ring #4	Maruyama	3-3-71
SA	915-702	05	1	E	2621.ME-33064	Base Plate	Maruyama	3-3-71
PF	915-702	06	1	E	2621.ME-33065	Top Plate	Maruyama	3-3-71
SA	915-702	07	1	D	2621.MD-33066	Spool	Maruyama	3-3-71
SA	915-702	08	3	D	2621.MD-33067	Cage	Maruyama	3-3-71
PF	915-702	09		C	2621.MC-33068	Bumper	Maruyama	3-3-71
SA	915-702	10	1	E	2621.ME-33069	Assembly	Maruyama	3-3-71
PF	915-702	11		C	2621.MC-33070	Bearing Ring	Maruyama	3-3-71
PF	915-702	12		A	2621.MA-33071	Washer	Maruyama	7-30-71
PF	915-702	13		C	2621.MC-33072	Spool Blank	Barden	8-3-71
					33073			
					33074			
					33075			
					33076			

GROUP LOG SHEET
BOUNCER

PRE-FIX	BASE	SUF-FIX	REV	DRWG SIZE	NAL NO.	TITLE OR DESCRIPTION	ASSIGNED TO	DATE
SA	915-703	01	1	D	2621.MD-33100	Piston	Barden	1-28-71
PF	915-703	02		C	2621.MC-33101	Upper Piston Bearing	Barden	1-28-71
PF	915-703	03		C	2621.MC-33102	Lower Piston Bearing	Barden	1-28-71
PF	915-703	04		D	2621.MD-33103	Piston Body	Barden	1-28-71
PF	915-703	05		D	2621.MD-33104	Filler Block	Barden	1-28-71
PF	915-703	06	2	D	2621.MD-33105	Bottom Plate	Barden	1-28-71
SA	915-703	07	1	D	2621.MD-33106	Water Jacket	Barden	1-28-71
PF	915-703	08	1	D	2621.MD-33107	Cap Off Plate	Barden	1-28-71
PF	915-703	09		D	2621.MD-33108	Flange	Barden	1-28-71
PF	915-703	10		D	2621.MD-33109	Cylinder	Barden	1-28-71
SA	915-703	11	1	D	2621.MD-33110	Bouncer Weldment	Barden	1-28-71
SA	915-703	12	2	D	2621.MD-33111	Bouncer Finish Machine	Barden	1-28-71
SA	915-703	13	1	D	2621.MD-33112	Assembly for Test	Barden	1-28-71
SA	915-703	14		E	2621.ME-33113	Assembly	Barden	1-28-71
PF	915-703	15		B	2621.MB-33114	Washer	Barden	1-28-71
					33115			
					33116			

GROUP LOG SHEET
STAND

PRE-FIX	BASE	SUF-FIX	REV	DRWG SIZE	NAL NO.	TITLE OR DESCRIPTION	ASSIGNED TO	DATE
PF	915-704	01	5	D	2621.MD-33140	Casting	Middleton	3-4-71
PF	915-704	02		D	2621.MD-33141	Spacer Plate	Maruyama	7-30-71
PF	915-704	03		A	2621.MA-33142	Washer	Maruyama	7-30-71
					33143			
					33144			
					33145			
					33146			
					33147			
					33148			
					33149			

GROUP LOG SHEET
9-INCH ACTUATOR SYSTEM

PRE-FIX	BASE	SUF-FIX	REV	DRWG SIZE	NAL NO.	TITLE OR DESCRIPTION	ASSIGNED TO	DATE
						Ross Valve Modification		
PF	915-705	01	1	D	2621.MD-33150	Valve Cylinder, Lower	Adamson	4-26-71
PF	915-705	02	1	D	2621.MD-33151	Valve Piston, Lower	Adamson	4-26-71
PF	915-705	03	1	D	2621.MD-33152	Valve Cylinder, Upper	Barden	4-26-71
PF	915-705	04		D	2621.MD-33153	Valve Piston, Upper	Barden	4-26-71
PF	915-705	05		B	2621.MB-33154	Shaft Piston Connection	Barden	4-26-71
PF	915-705	06		B	2621.MB-33155	Shaft Bumper	Barden	4-26-71
PF	915-705	07		B	2621.MB-33156	Upper Piston Bumper	Barden	4-26-71
PF	915-705	08		B	2621.MB-33157	Lower Piston Bumper	Barden	4-26-71
PF	915-705	09		B	2621.MB-33158	Shaft Bushing	Barden	4-26-71
SA	915-705	10		B	2621.MB-33159	Ross Valve Modification Assembly	Barden	6-9-71
SA	915-705	11		D	2621.MD-33160	2-Inch Ross Valve Can	Barden	
PF	915-705	12		C	2621.MC-33161	Hose Clamp Flange #1	Maruyama	7-20-71
PF	915-705	13		C	2621.MC-33162	Hose Clamp Flange #2	Maruyama	7-20-71
SA	915-705	14		E	2621.ME-33163	Helium Supply Manifold - R.F.	Maruyama	8-13-71
SA	915-705	15		E	2621.ME-33164	Helium Supply Manifold - L.H.	Maruyama	8-13-71
SA	915-705	16		D	2621.MD-33165	Ross Valve Exhaust Tank - R.H.	Maruyama	8-17-71
SA	915-705	17		D	2621.MD-33166	Ross Valve Exhaust Tank - L.H.	Maruyama	8-17-71

9-INCH VALVE ACTUATOR SYSTEM (continued)

PRE-FIX	BASE	SUF-FIX	REV	DRWG SIZE	NAL NO.	TITLE OR DESCRIPTION	ASSIGNED TO	DATE
GP	915-705	18		R	2621.MR-33167	Piston Drive - High Pressure N_2	Maruyama	11-2-71
GP	915-705	19		R	2621.MR-33168	9-Inch Valve - Check Valve Layout	Maruyama	11-2-71
GP	915-705	20		R	2621.MR-33169	9-Inch Valve - Ross Valve Layout	Maruyama	11-2-71
GP	915-705	21		R	2621.MR-33170	9-Inch Valve - Oil Return Layout	Maruyama	11-2-71
					33171			
					33172			
					33173			
					33174			
					33175			
					33176			
					33177			
					33178			
					33179			
					33180			
					33181			
					33182			
					33183			

GROUP LOG SHEET
COMPRESSOR

PRE-FIX	BASE	SUF-FIX	REV	DRWG SIZE	NAL NO.	TITLE OR DESCRIPTION	ASSIGNED TO	DATE
GP	915-706	01		D	2621.MD-33200	Oil and Air Compressor Floor Plan Layout	E.K.Wong	2-11-71
PS	915-706	02	1	A	2621.MA-33201	Technical Specifications	Petersen	2-17-71
GP	915-706	03		E	2621.ME-33202	Oil and Air Compressor Floor Plan Layout	E.K.Wong	5-12-71
GP	915-706	04		E	2621.ME-33203	Oil and Air Compressor South and East Elevation	E.K.Wong	5-12-71
GP	915-706	05		E	2621.ME-33204	Oil and Air Compressor North Elevation	E.K.Wong	5-12-71
GP	915-706	06		A	2621.MA-33205	Technical Specifications for N_2 Compressor	Petersen	6-12-71
PF	915-706	07		D	2621.MD-33206	Helium Reservoir Tank - 42 diameter (South Wall)	E.K.Wong	7-14-71
PF	915-706	08		D	2621.MD-33207	Helium Reservoir Tank - 42 diameter (North Wall)	E.K.Wong	7-20-71
PF	915-706	09		D	2621.MD-33208	Helium Reservoir Tank - 18 diameter (South Wall)	E.K.Wong	7-21-71
PF	915-706	10		D	2621.MD-33209	Helium Reservoir Tank - 18 diameter (North Wall	E.K.Wong	7-21-71
PF	915-706	11		D	2621.MD-33210	Helium Reservoir Tank - 24 diameter (South Wall)	E.K.Wong	7-23-71
PF	915-706	12		D	2621.MD-33211	Helium Reservoir Tank - 24 diameter (North Wall)	E.K.Wong	7-23-71

COMPRESSOR (continued)

PRE-FIX	BASE	SUF-FIX	REV	DRWG SIZE	NAL NO.	TITLE OR DESCRIPTION	ASSIGNED TO	DATE
PF	915-706	13		D	2621.MD-33212	Pipe Support Bracket	E.K.Wong	7-29-71
PS	915-706	14		A	2621.MA-33213	Technical Specifications Six Helium Tanks	Petersen	8-11-71
PS	915-706	15		A	2621.MA-33214	Technical Specifications Gas Piping	Petersen	8-13-71
ML	915-706	16		A	2621.MA-33215	Material List Gas Piping System	E.K.Wong	8-16-71
ML	915-706	17		A	2621.MA-33216	Material List Oil Piping System	E.K.Wong	8-16-71
SD	915-706	18		E	2621.ME-33217	Oil and Air Compressor Schematic Diagram	E.K.Wong	10-26-71
SD	915-706	19		F	2621.MF-33218	Pit Area Schematic	F.Barrera	11-1-71

GROUP LOG SHEET
OIL SYSTEM

PRE-FIX	BASE	SUF-FIX	REV	DRWG SIZE	NAL NO.	TITLE OR DESCRIPTION	ASSIGNED TO	DATE
PS	915-707	01		A	2621.MA-33240	Technical Specifications	Petersen	3-11-71
SD	915-707	02		A	2621.MA-33241	Diagram	Petersen	3-11-71
PS	915-707	03		A	2621.MA-33242	Oil Supply System	Petersen	7-7-71
SA	915-707	04		D	2621.MD-33243	Oil Tank	Petersen	7-8-71
SD	915-707	05		C	2621.MD-33244	Oil Supply Diagram	Petersen	7-9-71
PS	915-707	06		A	2621.MA-33245	Oil Piping	Petersen	7-12-71
					33246			
					33247			
					33248			
					33249			
					33250			
					33251			
					33252			
					33253			
					33254			
					33255			
					33256			

GROUP LOG SHEET
ASSEMBLY

PRE-FIX	BASE	SUF-FIX	REV	DRWG SIZE	NAL NO.	TITLE OR DESCRIPTION	ASSIGNED TO	DATE
SA	915-708	01		R	2621.MR-33280	Expansion System Elevation View	Barden	5-4-71
					33281			
					33282			
					33283			
					33284			
					33285			
					33286			
					33287			
					33288			
					33289			
					33290			
					33291			
					33292			
					33293			
					33294			
					33295			
					33296			

GROUP LOG SHEET
ELECTRONICS

PRE-FIX	BASE	SUF-FIX	REV	DRWG SIZE	NAL NO.	TITLE OR DESCRIPTION	ASSIGNED TO	DATE
	915-709				2621.M -33310			
					33311			
					33312			
					33313			
					33314			
					33315			
					33316			
					33317			
					33318			
					33319			
					33320			
					33321			
					33322			
					33323			
					33324			
					33325			
					33326			

GROUP LOG SHEET
RECOMPRESSION

PRE-FIX	BASE	SUF FIX	REV	DRWG SIZE	NAL NO.	TITLE OR DESCRIPTION	ASSIGNED TO	DATE
SA	915-710	01		D	2621.MD-33340	Piston and Cage Details and Sub-assembly	Barden	2-10-71
SA	915-710	02		D	2621.MD-33341	Check Valve - Housing	Maruyama	5-27-71
PF	915-710	03		C	2621.MC-33342	Check Valve - Cover Plate	Maruyama	5-28-71
PF	915-710	04		C	2621.MC-33343	Check Valve - Poppet	Maruyama	5-28-71
SA	915-710	05		D	2621.MD-33344	Check Valve - Manifold - Left Hand	E.K.Wong	6-7-71
SA	915-710	06		D	2621.MD-33345	Check Valve - Manifold - Right Hand	E.K.Wong	6-7-71
PF	915-710	07		C	2621.MC-33346	Flange - Modified	E.K.Wong	6-7-71
PF	915-710	08		C	2621.MC-33347	Manifold Block	E.K.Wong	6-7-71
PF	915-710	09		B	2621.MB-33348	90° Elbow - Modified	E.K.Wong	6-7-71
SA	915-710	10		D	2621.MD-33349	Hose Coupling Manifold - R.H	E.K.Wong	6-7-71
SA	915-710	11		D	2621.MD-33350	Hose Coupling Manifold - L.H.	E.K.Wong	6-7-71
PF	915-710	12		C	2621.MC-33351	Manifold Block	E.K.Wong	6-7-71
PF	915-710	13		B	2621.MB-33352	90° Male Elbow - Modification	E.K.Wong	6-7-71
SA	915-710	14		C	2621.MC-33353	Hose and Coupling Assembly	E.K.Wong	6-8-71
SA	915-710	15		D	2621.MD-33354	Valve Coupling - 3"	E.K.Wong	6-9-71
SA	915-710	16		D	2621.MD-33355	B.W. Valve Coupling	E.K.Wong	6-9-71

RECOMPRESSION (continued)

PRE-FIX	BASE	SUF-FIX	REV	DRWG SIZE	NAL NO.	TITLE OR DESCRIPTION	ASSIGNED TO	DATE
SA	915-710	17		E	2621.ME-33356	Test Set-Up	Maruyama	6-10-71
SA	915-710	18		D	2621.MD-33357	High-Flow Accumulator Manifold	Maruyama	5-20-71
PF	915-710	19		C	2621.MC-33358	Recompression Valve Mounting Plate	Maruyama	6-10-71
PF	915-710	20		C	2621.MC-33359	Recompression Valve Manifold	Maruyama	6-10-71
PF	915-710	21		B	2621.MB-33360	Recompression Valve - Stud	Maruyama	6-10-71
PF	915-710	22		D	2621.MD-33361	Ball Valve Mounting Plate	Maruyama	6-10-71
PF	915-710	23		D	2621.MD-33362	Regulator Mounting Plate	Maruyama	6-10-71
SA	915-710	24		E	2621.ME-33363	Regulator Assembly	Barden	6-17-71
PF	915-710	25		B	2621.MB-33364	Regulator - Stud	Barden	6-17-71
SA	915-710	26		B	2621.MB-33365	Regulator - Seal	Barden	6-17-71
PF	915-710	27		C	2621.MC-33366	Regulator - End Cap	Maruyama	6-17-71
PF	915-710	28		D	2621.MD-33367	Regulator - Ring #1	Barden	6-17-71
PF	915-710	29		D	2621.MD-33368	Regulator - Ring #2	Barden	6-17-71
PF	915-710	30		D	2621.MD-33369	Regulator - Ring #3	Barden	6-17-71
SA	915-710	31		D	2621.MD-33370	Regulator Spool and Cage	Barden	6-17-71
PF	915-710	32			2621.M -33371	Regulator Disogrin Pad	Barden	6-17-71
PF	915-710	33		D	2621.MD-33372	Regulator - Ring #4	Barden	6-17-71
PF	915-710	34		D	2621.MD-33373	Regulator - End Plate W/O Sleeve	Barden	6-17-71

RECOMPRESSION (Continued)

PRE-FIX	BASE	SUF-FIX	REV	DRWG SIZE	NAL NO.	TITLE OR DESCRIPTION	ASSIGNED TO	DATE
SA	915-710	35		D	2621.MD-33374	Regulator - End Plate With Sleeve	Barden	
SA	915-710	36		D	2621.MD-33375	Check Valve Assembly	Maruyama	7-20-71
PF	915-710	37		B	2621.MB-33376	Check Valve Stud	Maruyama	7-20-71
SA	915-710	38		D	2621.MD-33377	Accumulator High Flow Piping	Maruyama	8-2-71
SA	915-710	39		D	2621.MD-33378	Recompression Valve Piping	Maruyama	8-2-71
SA	915-710	40		D	2621.MD-33379	Regulator Valve Piping	Maruyama	8-3-71
PF	915-710	41		D	2621.MD-33380	Regulator - Insert #1	Barden	8-6-71
PF	915-710	42		B	2621.MB-33381	Regulator - Insert #2	Barden	8-9-71
SA	915-710	43		D	2621.MD-33382	Recompression to Regulator Piping	Maruyama	8-12-71

APPENDIX C

CONTENTS OF NAL BOOK

(as of November 2, 1971)

IV. E. APPENDIX C

CONTENTS OF NAL BOOK
(as of November 2, 1971)

Meeting Notes, November 24, 1970 to date.

Purchase Requisitions, August 26, 1970 to date.

Work Orders, February 24, 1971 to date.

Memo, F. Barrera to K. Skarpaas, some major decisions on NAL handling, support and alignment of Actuating System, January, 1971.

Memo, R. Blumbert to G. Mulholland, SLAC bubble chamber crew shift operations, June 11, 1971.

Engineering Note, R. Byrns, Arguments for drive rod extension, February 11, 1971.

Memo, R. Byrns to F. Barrera, NAL 15-Foot HBC handling, January 19, 1971.

Letter, H. Petersen to G. Mulholland, Information on pipe and fittings, September 20, 1971.

Specification, H. Petersen, Gas Piping System, PS-915-706-15, August 13, 1971.

Specification, H. Petersen, Oil Piping System, PS-915-707-06, August 12, 1971.

Specification, H. Petersen, Six Helium Tanks, PS-915-706-14-RO, August 11, 1971.

Specification, H. Petersen, Oil Supply System, PS-915-707-03-RO, July 7, 1971.

Specification, H. Petersen, One Nitrogen Compressor Unit, PS-915-706-060RO, June 11, 1971.

Specification, H. Petersen, Two Hydraulic Oil Power Units, Tank and Accumulators, Complete, PS-915-707-01-RO, March 17, 1971.

Memo, H. Petersen to M. LaBrie, Request for Proposal for Air and Helium Compressor Unit(s) Complete; Technical Specification PS-915-706-02-R1, March 15, 1971.

Letter, H. Petersen to G. Mulholland, Specifications for the Air or Helium Compressor, March 5, 1971

Specification, H. Petersen, One Air and Helium Compressor Unit, Complete, PS-915-706-02-R1, February 18, 1971.

Engineering Note, K. Skarpaas, Chamber Piston Stroke Versus Driving Accumulator Size, March 15, 1971.

Engineering Note, K. Skarpaas and D. Talaska, Test of Markite Model #9303 Rectilinear Potentiometer, March 10, 1971.

Engineering Note, R. Watt and K. Skarpaas, Mechanical Test of the NAL Pulser System, March 10, 1971.

Memo, K. Skarpaas to R. Huson, Piston to Expansion System Clamp, December 18, 1970.

Engineering Note, K. Skarpaas, Seals in Top Plate, February 19, 1971.

Memo, K. Skarpaas, List of Materials to be Ordered for the Bouncer Assemblies, February 12, 1971.

Memo, K. Skarpaas to F. Barrera, Nonmagnetic Versus Magnetic Steels for the NAL Expansion System, February 18, 1971.

Quotation, Ryerson Steel to K. Skarpaas, Rings and Plate, February 18, 1971.

Engineering Note, K. Skarpaas, Bouncer Assembly, February 10, 1971.

Mwmo, K. Skarpaas to F. Barrera and R. Byrns, Telephone Call with G. Mulholland about 9-Inch Sleeve Valve, February 10, 1071.

Engineering Note, K. Skarpaas, Computer Program Simulating the Dynamic Behavior of the 15-Foot NAL HBC, January 8, 1971.

Memo, A. Fluter to R. Huson, Suggested NAL Stores Item, July 16, 1971.

Memo, D. Nauenberg to F. Barrera, High Pressure Test on 2-Inch Hose, Undated.

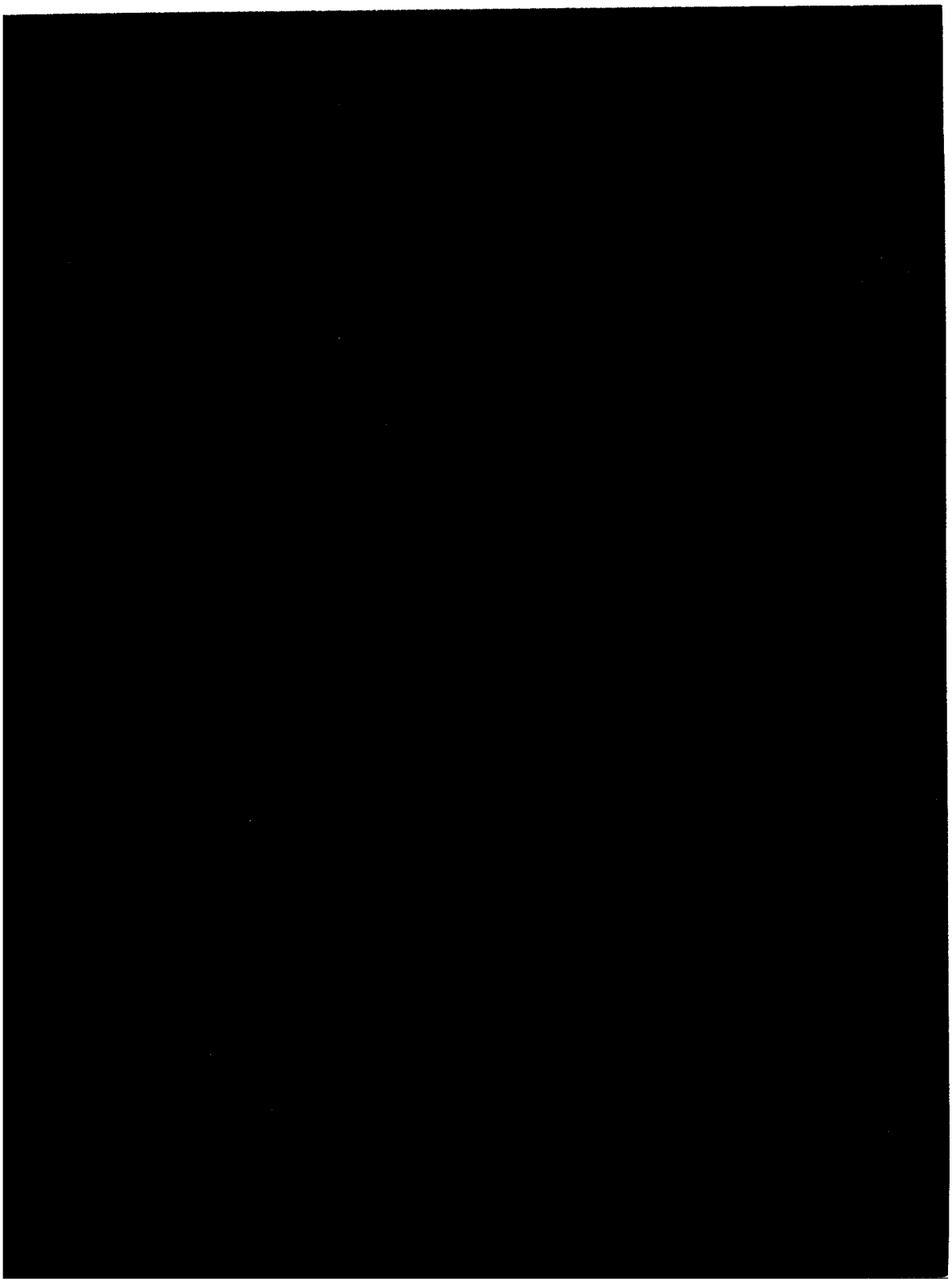

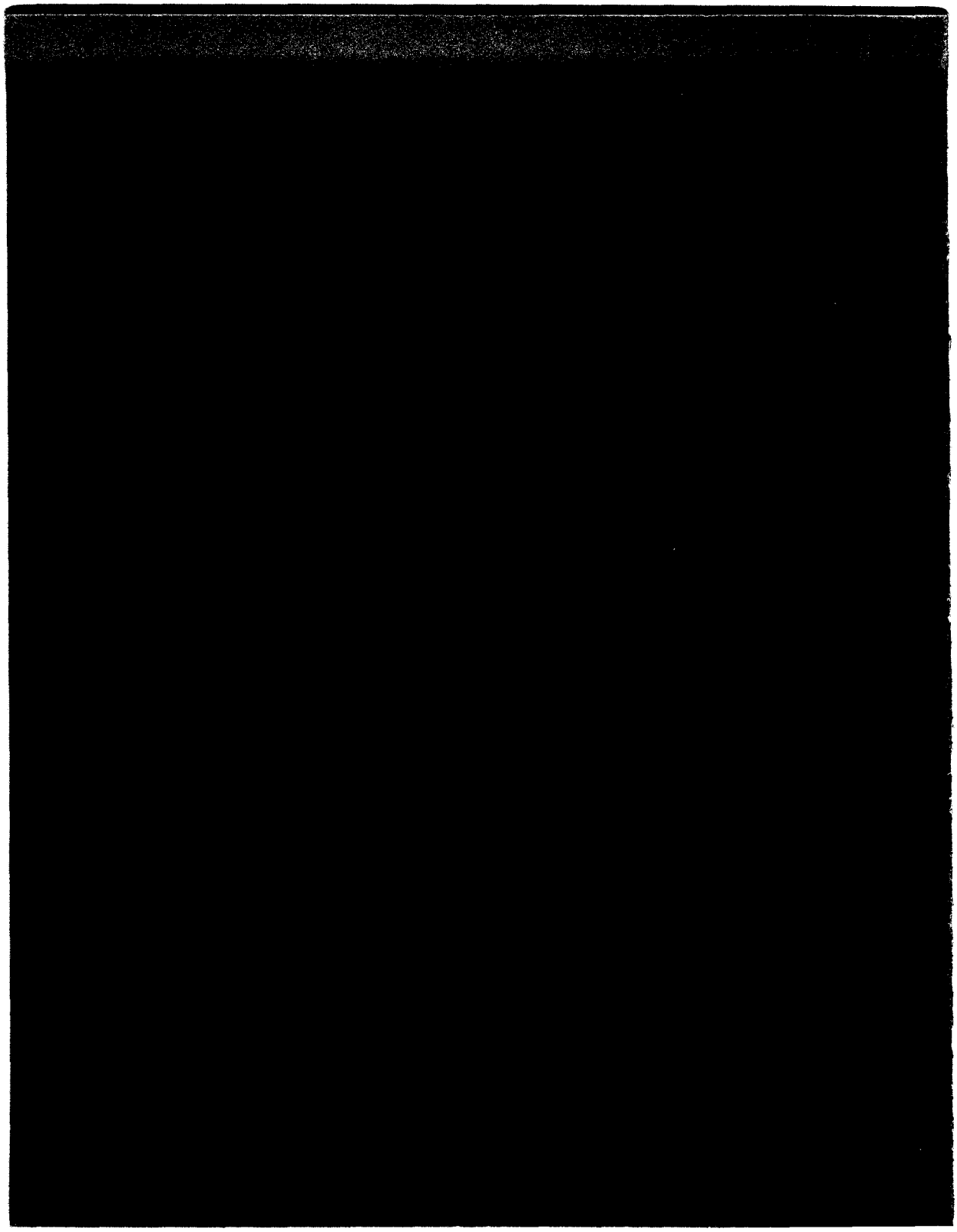

IV. EQUIPMENT

F. Failure Mode Analysis: EXPANSION SYSTEM ACTUATOR

Prepared by

Stanford Linear Accelerator Center,
Bubble Chamber Group
and National Accelerator Laboratory

IV. F. FAILURE MODE ANALYSIS: EXPANSION SYSTEM ACTUATOR

The components of the expansion system actuator for the National Accelerator Laboratory (NAL) 30,000 Liter Bubble Chamber (30 KLBC) were designed and built at the Stanford Linear Accelerator Center.

This portion of the failure mode analysis pertains only to the expansion system actuator. A failure mode analysis of interactions with the other systems is found elsewhere in this report.

General design of the NAL chamber system with respect to the actuator is somewhat different from previous experience and provides generally more favorable conditions in the event of actuator failures. The chamber liquid pressure is designed to be in balance with the liquid-gas volume beneath the chamber piston so that a failure in the expansion system actuator would find a restoring force from the chamber, tending to hold the system in a neutral position. Also, the reaction forces for the actuator are not carried directly to the chamber vacuum tank system. The actuator is fastened to ground, and the restoring forces to the actuator are carried to the foundation. Failures in the actuator system tend to be self-isolating and self-limiting.

The following possible failure cases are considered:

1. Loss of Actuator Restoring Pressure

This could occur to greater or lesser extent if (a) gas pressure was lost below the bouncer, (b) oil pressure was lost, (c) electrical power supply shut down.

This condition was analyzed by the computer program KXSREACM. The assumptions were that there was no bouncer in the system and that all the oil was lost and there was no recompression. The assumption was made that the chamber piston did have the liquid-gas volume on the lower side, which provided the restoring force. This program showed that the restoring force proved to be high enough to prevent over-travel of the

chamber piston. The chamber piston was found to go 8 inches, and the permissible travel of the piston assembly is 10 inches. The chamber piston, actuator coupling, and actuator piston were accelerated to 80 G's. The drive piston is designed to handle this acceleration.

An electrical power supply shutdown could also cause this case of failure since the valve timing would be affected; however, oil is stored in the system accumulators, and there would be no noticeable initial effect. In the worst case it would be a normal expansion with no recompression force and some degree of bouncer restoring force.

2. Loss of the Restoring Force Below the Chamber Piston

If this restoring force loss is not detected, the system could pulse. Prior to the pulse, the drive piston will drop approximately 1/4 inch increasing the oil pressure below it and above the closed expansion valve to approximately 5,000 psi from 2,000 psi. If this condition is undetected, there will be a violent pulse. In addition to monitoring the restoring force; i.e., pressure in the volume below the chamber piston, the maximum oil pressure; i.e., via latch piping, will be monitored during pulsing and is to be interlocked to prevent pulsing when the pressure exceeds design values. In addition, the stroke will be monitored with interlocks for full reset and excessive stroke. These interlocks will stop pulsing of the system. If such a pulse occurs, the nine inch shaft would see a million pounds force; i.e., 16,000 psi.

The loss of restoring force by this means is very improbable since the seals between the chamber liquid and the liquid-gas volume below the chamber piston will begin to leak when the pressure above the piston slightly exceeds the pressure below the piston. Thus, chamber liquid will enter the lower volume and maintain pressure there. In addition, this case implies 200 liters of liquid-gas mixture beneath the piston have gone somewhere, which in itself is a failure condition.

3. Hydraulic Line Failure

In case of a high pressure oil leak, personnel could be injured if

the high velocity oil stream impinged upon them. Personnel in the hydraulic system areas are required to wear safety glasses or other eye protection. The hydraulic controls are arranged so that the operator is generally protected from oil streams. Occupancy in the hydraulic pit area during operation is minimized. The oil temperature is expected to be less than 100°F. Both small and large hydraulic leaks will be monitored by observing the rate of oil level change in the sump and an oil mist detector in the pit area. Small leaks will cause an alarm to be sounded, while large leaks will stop pulsing and the pumps.

The flexible hydraulic lines are installed high enough above normal head height so that a whipping hydraulic line would be unlikely to strike any personnel in the immediate vicinity. Additionally, the ends of the lines are to be secured with mechanical restraints.

4. Failure of Bolt or Post-Tensioning Rod

The design provides the bolts with a high pre-load in order to decrease the effect of cyclic loads. In general, the loss of an individual bolt or two would cause oil or gas leakage and ultimately shut down the system on a low pressure interlock. In the unlikely event that all the bolts in one bolt circle fail simultaneously, there are three possibilities. The first, in general, is the same as the first case considered above--the actuator restoring is lost. This is a case where the bouncer separates from the valve or the expansion valve separates from the piston. The second case is where there is a bolt circle failure in the support system and the bolts or post-tensioning rods separate and the actuator becomes disconnected from the ground. Here again there is no actuator restoring force and this becomes essentially the same as the first case above, except for secondary piping failures. A remote possibility would be failure of the complete bolt circle of the drive piston assembly cover plate. This would allow the drive piston cover plate to be accelerated up to the coupler and would bang against the coupler. This would accelerate the expansion piston-rod-drive-piston

assembly upward until decelerated by the Z section of the vacuum tank. The probability of this occurring is very low due to the stringent design, assembly, and inspection procedures.

Another dangerous case would be failure of a portion of a bolt circle resulting in a rocking-tipping action of the actuator. Such motion will be monitored by a vibration indicator which will stop pulsing. This is similar to the actuator-expansion piston misalignment in problems that have occurred on other big chambers. In addition to very careful alignment procedures, horizontal and vertical position interlocks located at the top plate of the drive piston will be provided.

5. Earthquake

The loads imposed by an earthquake of .2 or .3 G or superimposed by an earthquake while pulsing are trivial compared to the forces handled during normal pulsing.

6. Tornado

As standard procedure, all chamber systems will be shut down to a safe condition at the sounding of a tornado warning.

7. Fatigue

Fatigue has always been a problem with high forces and accelerations. Previous experience indicates that there will be, at least until experience is gained, fatigue failure of piping fittings and supports, although all parts have been designed to operate at stress below the fatigue limit for the selected material in the most heavily loaded operating mode, and extremely heavy supports are used. Constant inspection is necessary until confidence is insured.

8. Fire Caused by Ignition of Hydraulic System Oil

Petroleum base hydraulic fluid was chosen for the working fluid in this system. The petroleum base fluid was chosen because the possible fire hazard is considered a lesser risk than the toxic effects of the phosphate-ester fluids available and its detrimental effects on seals which could cause leaks and other failures in the system. (A detailed

argument for the use of the petroleum base hydraulic fluid is given by Appendix I.)

A fire in the expansion pit will initiate two automatic responses. One being the activation of the sprinkler heads by virtue of melting of the control elements, and the other being the issuance of an alarm from sensors which monitor both the absolute temperature and the rate of temperature rise in the area. In parallel, the elevator area pit is protected by a foam-type system. (Foam is employed in this area since any oil spills in the expansion pit drain to the elevator pit.) The alarm will be transmitted to both the bubble chamber control room and to the NAL Fire Department. Reaction in the control room will be to stop pulsing the system and to dispatch an individual to assess the situation. Further response will follow the report of the investigating person.

The oil and gas circuits can be remotely unloaded. This will remove the stored energy. It should be noted that at no place in the system is there a possibility of a mixture of high pressure oil and air since the drive gas is helium and both the Ross and bouncer gas is nitrogen.

If a fire occurs in the area while personnel are present, there are both adequate portable extinguishers to fight the fire and, if required, three exits out of the area. One exit leads directly out of the building proper and is isolated by a fire door.

9. Hazards from "Missiles" Caused by Failure of Mechanical Components

The system is thoroughly pre-tested at operating pressure and protected from over-pressure by relief valves on the discharge of the pumps and elsewhere. High pressure piping is securely anchored and shielded. High pressure accumulators are supported and braced to prevent motion during pulsing of the chamber. If a component were to fail at high pressure despite these precautions, a person struck by such a "missile" could be seriously injured.

The number of people near this equipment during operation will be kept to a minimum. Routine control is done remotely from the control

room and no major adjustments made while the expansion system is actuating to reduce the likelihood of malfunction causing injury to personnel. Periodically, inspection of the system is required by operating personnel.

10. Operator Error

A single pulse without restoring force is not catastrophic, as demonstrated particularly in Case 1 above. However, multiple pulses without restoring forces should be avoided. Therefore the following interlocks are to be provided: Chamber pressure high and low, space pressure below the chamber piston high and low, oil pressure at the drive piston high and low, gas drive pressure high and low, return line pressure high and low, gas and oil supply pressures high and low, piston reset and length of stroke.

Appendix I

November 18, 1971

To: Dr. W. Fowler, NAL

From: R. Watt, SLAC

Subject: Justification for the Use of Petroleum Oil as a Driving Media in the Expansion System

The expansion system as designed is simply an extrapolation of that in use on the two SLAC chambers and a tremendous amount of experience with these has shown that, if one wishes a reasonable seal lifetime, it is necessary to use polyurethane compounds in the sliding seals. A conservative estimate of our experience indicates a pulse-lifetime ratio of 10 to 1 in favor of the polyurethane over the various rubbers.

In the early stages of the chamber operation we attempted to use phosphate-ester hydraulic fluids and found that our seals were destroyed very quickly. Replacing the Skydrol fluids with petroleum enabled us to attain a seal lifetime of the order of millions of pulses with no deterioration in seal performance.

The expansion system has many moving parts, each of which has to move freely with very small friction forces involved. In order to do this the drive media must have a very low coefficient of friction (high lubricity). Petroleum oil fills this requirement admirably.

We include the manufacturer's recommendations showing the effects of various fluids on the Molythane seals in use.

It is quite clear from our previous experience and the enclosed information that the operation of the system will be severely affected by the use of a fluid other than that recommended. We suggest that you take a very firm stand against any change in the system as now proposed.

A further consideration of extreme importance to the people involved with the maintenance and repair is the effect of exposure of the eyes, skin, lungs and other sensitive body parts to the fluid in use. Experience both at SLAC and Argonne has shown that some very painful skin problems can be caused by working with phosphate-ester fluids, and on several occasions eye exposure caused lost time for people involved in operations. Exposure to fluids may not be an important thing in most hydraulic systems, such as airplanes, etc. For bubble chamber systems it is not uncommon to make repairs and do maintenance several times a day.

IV. EQUIPMENT

G. Piston and Seals

1. DESIGN

Prepared by

F. R. Huson

IV. G. 1. DESIGN

The criteria used to design the piston were as follows:

(a) It must follow roughly the contour of the chamber.

(b) It must be "easy" to photograph.

(c) It must not produce heat in the chamber due to eddy currents caused by movement in the magnetic field.

(d) It must cause a minimum of liquid currents in the chamber.

(e) The "rings" must not produce boiling in the chamber.

(f) It must be compatible with the overall design of the chamber.

(g) The size of the chamber requires that it be expanded by up to 23,000 in^3.

These led to a fiberglass piston of approximately 6 feet diameter using lip seals for rings. The success of the CERN 1-meter model chamber obviously effected our design. In fact, since the diameter of our piston should be about 6 feet, we have picked 70.866 inches to match the diameter of the CERN BEBC Chamber, although our piston is much shorter.

The intrinsic design of a piston chamber with sliding seals requires a gas volume behind the piston, thus as the piston moves to lower the pressure in the chamber the gas pressure behind the piston increases adiabatically (PV^2 = constant). To have a gas volume under the piston requires the temperature under the piston to be at least 2°K warmer than the chamber liquid to maintain gas and thus there must be a temperature gradient near the liquid-gas interface. To maintain this temperature gradient there is a honeycone structure under the piston (see drawing 2621.MD-25378) to avoid convection currents in the liquid and a cooling loop on the cone to maintain temperature. The piston skirt has a wall thickness of 1/8 inch where it is in the liquid to minimize the rise (1 mm) of the liquid-gas interface during a pulse. The epoxy fiberglass has a balsa wood sandwich structure in this region to decrease the heat

leak through the skirt. There are 100 watts heat leak up the rod guide and rod, and 15 watts heat produced in the rod guide because of the steel sleeve on the piston rod moving in the magnetic field. Approximately 50 watts will be removed from the gas through the piston skirt and the rest will be removed by the cooling loop on the cone. This system will set up convection currents in the gas so that the gas does not develop a large temperature gradient. The heat leak to the chamber through the piston head is less than 50 watts.

The head of the piston is made of wood for structural reasons (see stress analysis). It is difficult to keep gas out of the head since gas penetrates fiberglass. In fact, it is advantageous to have pressure in the wood head to balance the pressure on the outside of the head. This keeps deflections near the lip seals to a minimum during the piston motion. To have a controlled pressure in the wood head requires communication with the gas volume. From tests it was found that approximately 200 - 1/8 inch holes (one to each block of wood in the head, since the epoxy between blocks decreases the flow of gas) in the fiberglass between the gas volume and the wood permits the pressure in the head to follow the gas pressure under the piston with a time constant of 3 minutes (time for Δp to decrease by 1/2).

The design of the lip seal region has evolved from the CERN design for the 1-meter model. There were pictures taken in the 1-meter model which had good tracks in the chamber and no visible boiling at the lip seal region when the liquid around the lip seal region was approximately 0.5°K colder than the chamber liquid. Leakage by the lip seal was small (200 cm^3/sec at 1Kg Km^2 or 10cm^3/ normal pulse of 3 Kg/cm^3). The 15-foot design (see drawing 2621.MD-25378) has two lip seals with an intermediate volume. The diameters of the two lip seals differ (.016 inch) such that the intermediate volume expands the same as the chamber when there is no leakage past the seals. In this case the upper seal acts only as a bubble catcher and wall between chamber and intermediate volume.

The lower seal takes the full pressure drop(80 psi for hydrogen). The intermediate volume is held a few degrees colder than the chamber liquid to absorb the heat produced at the seal. If the lower seal leaks then the pressure will build up in the intermediate volume and the upper seal will develop a pressure difference making it seal. There is a small cooling loop above the upper seal to absorb heat produced there.

The materials chosen for the lip seals and bearing on the head of the piston are beryllium-copper and Rulon A (produced by the Dixon Corp., Bristol, Rhode Island) respectively. Tests were made in liquid N_2 for glass filled Teflon, Rulon A, fiberglass, high density polyethylene, 316 stainless steel, and beryllium-copper to check wear and static coefficient of friction. When the same material was used for seal and bearing or anything on 316 stainless steel some binding and/or galling were observed. The measurements for beryllium-copper on Rulon A gave a wear rate of 0.3 (Rulon A) mils per million pulses. The coefficient of friction is assumed to be $\eta = 0.1 + 0.3|\sin 2\pi t/\tau|$. Note the dynamic coefficient of friction for Teflon is larger than the static and proportional to velocity and inversely proportional to load. For this coefficient of friction and the expected pressure difference (80 psi max.) across the lip seal there will be ~1300 joules of heat produced by the lower seal per pulse. The heat produced by the upper seal will be small since the pressure across the lip seal is small.

The chamber piston is coupled to the actuator piston making a rigid system (3500 lb). To not be redundant this system is guided in only 2 places, at the lip seals of the chamber piston and at the large diameter seal of the actuator piston. The seals on the piston rod are floating seals and can operate continuously with a horizontal displacement of .020 inches and take a displacement of .100 inches for a few hundred pulses. This displacement will be continuously monitored during operation (see instrumentation section). The allowed horizontal displacement on the actuator is 0.028 inches and will also be continuously

monitored.

The seal on the rod (see drawing 2621.ME-25534) has 2 emergency seals which are actuated by pressure and 3 dynamic seals. There are pump outs between all the seals. There is also an emergency seal at the top of the rod guide which is closed by lowering the piston (see drawing 2621.MD-25378).

IV. EQUIPMENT

G. Piston

2. A DETAILED STRESS ANALYSIS OF NATIONAL ACCELERATOR LABORATORY'S CHAMBER EXPANSION PISTON ASSEMBLY

Prepared by

F. A. Simonen and M. Vagins

IV. EQUIPMENT

G. Piston

2. A DETAILED STRESS ANALYSIS OF NATIONAL ACCELERATOR LABORATORY'S CHAMBER EXPANSION PISTON ASSEMBLY

TABLE OF CONTENTS

TABLE OF CONTENTS (Cont'd)

LIST OF TABLES

LIST OF FIGURES

LIST OF FIGURES (Cont'd)

LIST OF FIGURES (Cont'd)

IV. G. 2. A DETAILED STRESS ANALYSIS OF NATIONAL ACCELERATOR LABORATORY'S CHAMBER EXPANSION PISTON ASSEMBLY

INTRODUCTION

Since August of 1970 Battelle's Columbus Laboratories have been involved in a program of assistance in design and analysis for the construction of National Accelerator Laboratory's 30,000 Liter Capacity Bubble Chamber Facility. During this period almost every component of the bubble chamber structure, including the bubble chamber proper, the vacuum tank, the super-conducting magnet and cryostat, the chamber support system and the piping system, has either been completely analyzed by Battelle, or, if components have been analyzed by others such analyses have been critically reviewed by Battelle. The detailed stress analysis of the chamber expansion piston assembly described in this report is a part of this overall program of assistance in design.

The chamber expansion piston assembly forms an extremely important part of the operational system of the chamber. It is the means by which the pressure in the fluid medium contained in the main portion of the chamber is rapidly lowered to bring that medium to the state of a superheated fluid. The piston assembly, which is a composite structure fabricated from a combination of fiberglass-epoxy laminate, wood of various types and grades, and stainless steel, operates in a cryogenic temperature environment with temperatures as low as -423°F. By its nature of operation the piston will be subjected to significant pressure differentials across the piston head and to large tensile forces in the piston stem. These loads are cyclic, being induced by the rapid vertical motion of the piston itself. The design requirement for the piston assembly is that it must successfully perform its mission for at least 10^7 pressure pulsations.

The main responsibility for the design and fabrication of the piston assembly lies with the Brunswick Corporation of Marion, Virginia.

However, because of the very complex nature of its construction, the large cyclic loads to be imposed on it for a long period of time, and the need to assure a high level of confidence in its operational abilities NAL requested Battelle to carry out an independent analysis of the main components of the assembly. Included in this work is a description of the effort to develop an effective lip seal configuration to operate in conjunction with the piston assembly.

DESCRIPTION OF CHAMBER EXPANSION PISTON ASSEMBLY

The chamber expansion piston assembly is fully defined by the following NAL drawings:

Drawing Number	Title	Revision
2621.ME-25129	30K Liter Hydrogen BC Expansion Piston	F
2621.MC-25369	Piston Rod Fitting Assembly	A
2621.MD-25461	30K Liter Hydrogen BC Wood Core	-

The positioning of the piston assembly in the chamber and the positioning of the lip seal arrangement when the piston assembly is at the bottom of its stroke are shown in the following NAL drawings:

Drawing Number	Title	Revision
2629.ME-25308	30K Liter Hydrogen Bubble Chamber General Assembly Illustration	-
2621.MC-25336	30K Liter Hydrogen BC Lip Seal Section	-

The piston assembly is a composite structure fabricated from fiberglass-epoxy laminate, wood of various types and grades, and stainless steel. The assembly consists of a piston head, a piston skirt, a piston stem, upper and lower bearing sleeves, and a coupling. The assembly is shown schematically in Figure 1.

The piston head is a composite structure. It has an outer shell of fiberglass-epoxy laminate surrounding and bonded to an inner core of balsa wood and douglas fir. The grain of the wood core is aligned vertically; i.e., parallel to the center axis of the assembly. The dia-

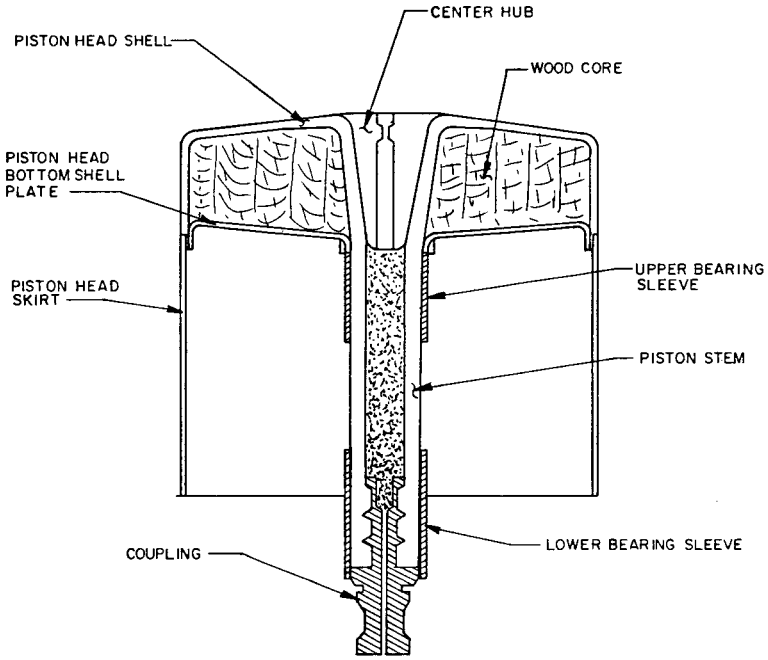

FIGURE 1. SCHEMATIC OF PISTON ASSEMBLY

meter of the piston head is 70.865 inches. The depth of the piston head varies from 22 inches at its center to approximately 17 inches at its outer diameter. A fiberglass-epoxy cylindrical skirt attaches to the bottom of the outer periphery of the piston head and hangs vertically downward for approximately 48 inches.

The outer surface, top, and inner surface of the piston head are formed integrally with the piston stem. The bottom surface of the piston head, also formed of fiberglass-epoxy laminate is a separate piece which is attached to the upper shell by glue and pin joints. It is also bonded to the wood core upon assembly. The piston stem has an outer diameter of 11 inches and an inner diameter of 7 inches. At the bottom of the piston stem is embedded the stainless steel coupling which in operation is attached to the stem of the hydraulic actuator. At both the bottom (near the coupling) and at the top (at the base of the piston head) of the stem there are stainless steel bearing sleeves.

The laminate material is composed of Epon 828 epoxy resin reinforced with fiberglass cloth. The piston head and the skirt are laminated using a bi-directional glass fabric. The piston stem is fabricated using a highly directional glass fiber oriented vertically so as to maximize its extensional stiffness in the axial direction. The piston core is a laminated wood assembly made up of several densities of end grain balsa and douglas fir bonded with resorcinol adhesive. At the center of the core (adjacent to the stem) there is a 34 pcf density douglas fir. Succeeding adjacent sections of the core, moving outward radially, are composed of 15.5, 11.0, and 6.0 pcf densities of end grain balsa, respectively.

The piston assembly is basically a body of revolution. It deviates from this form at several points. First there are pin reinforcements of joints in the head to skirt and head bottom plate to piston stem locations. Second, there are a number of holes cut into the bottom plate of the piston head to allow the buffer zone gas to soak into the piston

head and thus allow the core of the piston head to reach the equilibrium pressure.

As the development of the piston progressed the method of supporting and guiding the piston went through several changes. Originally it was intended to guide and align the piston assembly-actuator stem system by means of two strategically placed bearings; one in the actuator and the other in the spool piece of the "Z" section, or lower chamber. The bearing in the spool piece was to act against the upper bearing sleeve described above. It was intended that the lip seals themselves would see no bearing loads. As work progressed it was shown that alignment difficulties could make the lip seals inoperative. It was thus decided to remove the upper guidance bearings and employ the lip seals not only in a sealing mode but also for lateral guidance purposes.

CONCLUSIONS AND RECOMMENDATIONS

The work carried out as detailed in this report showed that some modifications of the original design of the piston assembly were required to allow that structure to be both structurally and operationally adequate. These modifications are a thickening of the outer radial wall of the piston head assembly and a substantial change in the geometry of the stainless steel coupling. With the inclusion of these design changes the piston assembly has been shown to be a structurally acceptable component which has a very high probability of successfully completing its design operational life of in excess of 10^7 pressure pulses.

The lip seal study resulted in the development of a lip seal configuration that can successfully perform the two missions required of it: the maintenance of the pressure boundary and at the same time acting as the upper lateral guide for the piston. Because of the relative rigidity of the proposed new lip seals tolerance requirements on both the lip seal geometry and the plastic coating become problem areas. These problems can be overcome by sizing these two components to have an

interference fit when initially assembled and cold. The assurance of a good fit is then developed by preliminary cycling of the piston so as to "wear in" the plastic surface and the achievement of a lap fit on the mating sliding surfaces.

GENERAL CONSIDERATIONS

Loading Conditions

The anticipated loading conditions for the piston assembly are as follows:

(1) The piston assembly, coupled to an being driven by the hydraulic actuator, moves vertically with a versine pulse form of motion.

(2) The displacement of the piston and the time period of each pulse is dependent upon the type of fluid in the main chamber.

The displacement can vary from approximately 4.0 to 6.0 inches. The time period of each pulse can vary from about 0.05 second for the hydrogen operation to about 0.130 second for the neon operation.

(3) For all types of operation the piston starts in a pressure equilibrium position with pressurized fluid above the piston and cold gas at a pressure equal to that of the fluid below the piston head in the "Z" section or lower chamber. The equilibrium pressures for the hydrogen, deuterium, and neon operations are approximately 80.0, 90.0, and 140.0 psia, respectively.

(4) In each type of operation the versine motion of the piston causes the pressure in the fluid in the main chamber to drop until the piston reaches the bottom of its stroke. At the same time the pressure in the gas in the lower chamber is raised by the compressive action of the volume reduction. At the bottom of the piston stroke a significant pressure differential

exists across the head of the piston. For the hydrogen and deuterium operations this differential is approximately 100.0 psi while for the neon operation the pressure differential equals approximately 130.0 psi.

(5) The maximum inertial loading of the piston occurs during the hydrogen operation when the piston will experience a peak loading of about 165 "g"s. This loading is seen at the start and stop of each stroke (at the equilibrium position) as well as at the bottom of each stroke. At the beginning and at the end of each stroke there is no pressure differential across the piston head. At the bottom of the stroke the pressure differential across the head is at its maximum. However, at this position the effect of the inertial load is in direct opposition to the effect of the pressure differential.

(6) Because of the very light weight construction of the piston head the effect of the inertial loading, taken by itself, will, for the types of operation considered, always be less severe than the maximum pressure differential across the head, again taken by itself. The effects of the maximum pressure differential across the head are mitigated by the effect of the inertial loads. Thus for a conservative model analysis, at least for the piston head, the omission of the inertial loads from the stress calculations is called for.

Based upon the data presented above it was decided that the only loading condition to be used in this analysis would be a maximum pressure differential across the head. This pressure differential would consist of a pressure of 70.0 psia above the piston and a pressure of 200.0 psia acting along its outer radial surface and underneath the piston head. This loading pattern was based on the erroneous belief that at the bottom of the stroke the main piston seal would be accomplished at the top of the piston. This was later found not to be the case. The main seal

is to be achieved at a position approximately halfway down the outer radial surface of the piston head. The original analyses were carried out with the erroneous pressure boundary conditions. Examination of the results indicated that a new analysis with the correct pressure boundary conditions was not called for since such conditions would in all cases induce less severe stresses and deformations in the piston head assembly than those induced by the original set of conditions. However, a single check run on the final piston configuration was carried out using the correct pressure distribution.

Limits of Analysis

The analysis is limited to the study of the piston assembly and coupling configuration acted upon by the pressure differential described above. The effects of the inertial loadings are not considered. Such loadings have been considered by Brunswick. A report[1]* submitted to NAL by Brunswick, dealing with their stress analysis of the piston assembly and which has been reviewed by Battelle dealt quite adequately with the effects of the inertial loads.

The piston assembly is subject to considerable thermal stress due to the slight differences in the coefficients of linear thermal contraction among its constituent materials. During cool-down these materials attempt to contract differentially and the restraints between them induce the indicated thermal stresses. The Brunswick report, cited above, gave full consideration to these stresses and showed that they were sufficiently small as to present no structural adequacy problem.

FINITE ELEMENT STRESS ANALYSIS OF THE PISTON HEAD AND COUPLING

The stress analysis of the bubble chamber piston assembly was carried out in two parts. The first part concerned the stresses where the

* Numbers in superscripted parentheses refer to references found at the end of this report.

stainless steel coupling joined the fiberglass-epoxy stem. The second part concerned stresses and deflections in the piston head. The same approach was used for both analyses, namely the application of Battelle's finite element computer stress analysis program AXISOL. A detailed description of this program and the manipulation of the element's stress-strain relations necessary to carry out this work are given in the Appendix.

The steps taken in this investigation are characteristic of any finite element stress analysis. Initially the structures were sub-devided into continuous grids of finite elements to give an accurate and efficient idealization of the structure. All the elements and nodal points in this idealization were then numbered. This numbering scheme together with coordinates giving the locations of all nodal points were then coded as input for the computer program. A checkout procedure, which included plotting of the specified gridwork, verified that the input data was correct in every detail. Following specification of the assumed pressure and displacement loadings, the program was run to give a complete output of the stresses and deformations induced throughout the structure. A critical examination of the predicted stresses was then made to determine if the stress patterns were reasonable and consistent with the applied loadings. This was followed by plotting certain pertinent stresses to give a clear picture of the stress distribution within the structure. The final step involves comparison of the predicted stresses with the strength values for the materials to allow conclusions concerning the structural adequacy of the structure.

Analysis of Coupling

Modeling Considerations

Mathematical models of the piston coupling are shown in Figure 2. Each of the models has a total of 800 nodal points and 729 elements. For the initial model (Figure 2a) a perfect bond was assumed between the metal and the epoxy-fiber composite. When the stress calculations indi-

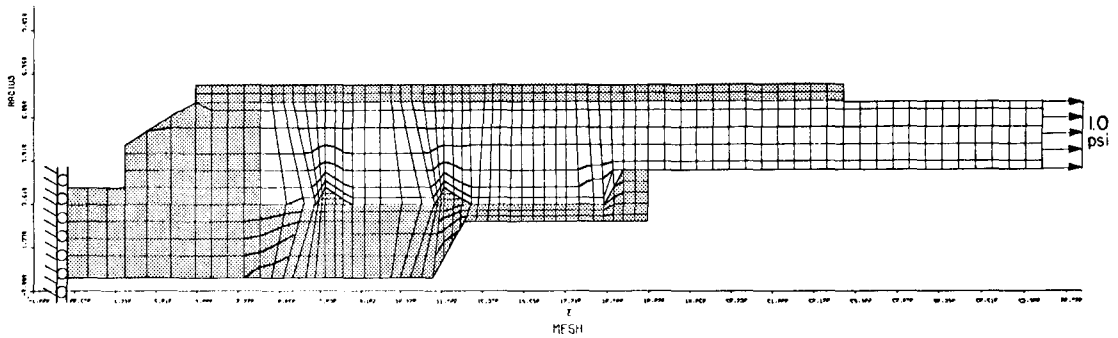

a) Fully Bonded

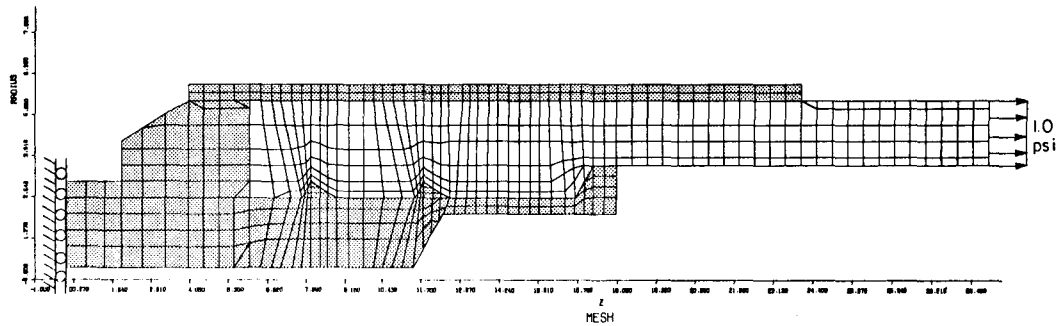

b) Broken Bond

FIGURE 2. FINITE ELEMENT MODELS OF PISTON COUPLING

cated that the integrity of the bond could not be guaranteed, the mathematical model was revised as shown in Figure 2b to allow separation of the bond under load. The finite element grid included pairs of superimposed (but distinct)nodal points along the interfaces between the materials. Input data to the computer program allowed the bond to be restored at specified points by forcing the displacements of paired points to be mathematically equal.

The stress analyses were performed for a unit axial loading in the fiber shaft of 1.0 psi. The shaft stress in operation was estimated as 8,800 psi, and the stress results may be scaled by this factor.

For convenience both the shaft and the end of the spool were truncated away from the joint. A displacement boundary condition was imposed at the end of the spool as indicated in Figure 2.

In order to calculate bending stresses, at least two elements were used through the thickness of each material (e.g., the outer metal sleeve). The grid was designed to be sufficiently detailed to show load paths through the coupling and also general variations and levels of stress. No attempt was made to determine precise stress concentrations at the various discontinuities in the coupling assembly.

Stresses With Full Bonding

In the initial stress calculations it was assumed that the entire bond between the epoxy composite and the metal remained intact. Figure 3 shows the radial distribution of axial stress over different cross sections down the length of the coupling. The results show the transfer of the axial stress from the epoxy into the stiffer metal components. Calculations were performed first for stainless steel and then for titanium. Changing to the lower modulus titanium slightly increased the stress in the epoxy while decreasing the stress in the metal. For both cases, Figure 3 shows the decrease in the axial load carried by the epoxy at locations successively further removed from the point of insertion into the coupling. However it should be cautioned that the

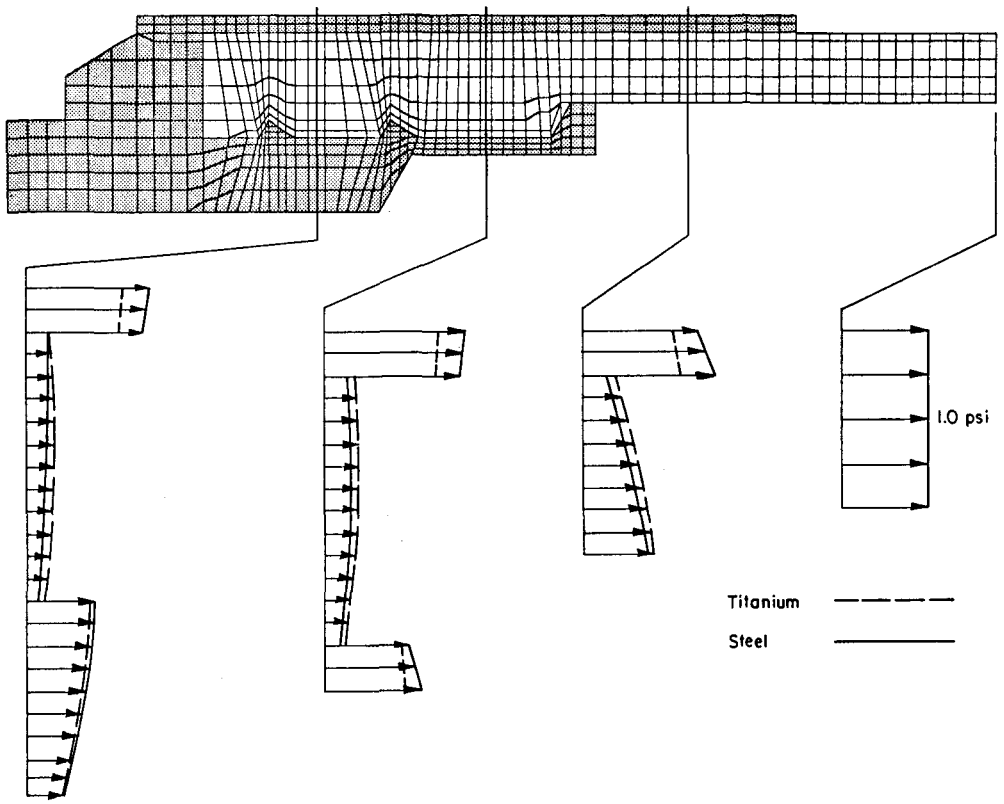

FIGURE 3. REDISTRIBUTION OF AXIAL STRESS DOWN LENGTH OF COUPLING, FULL BONDING ASSUMED

stresses shown in Figure 3 are at cross sections at locations remote from points of stress concentrations, and do not indicate the peak stresses in the epoxy.

Figure 4 shows the stress carried in shear by the bond along the epoxy-metal interface. These stresses have their maximum value at the end of the outer metal sleeve, and are greater than 0.4 times the applied axial loading of 1.0 psi. On the basis of the expected strength of these bonds, it was concluded that the bonding with the outer metal sleeve could not be maintained for stress levels of the calculated magnitude. The shear stresses shown in Figure 4 for the titanium construction were found to be somewhat lower than the stainless steel, but were not sufficiently reduced to suggest a change in material.

Although there were no specific data on the expected strength of the epoxy-metal bond in shear, the indications were that the bond could not be considered reliable under the predicted stress levels. Therefore, it was decided to evaluate the design on the basis of a strictly mechanical interlock between the metal and epoxy fiber materials.

Stresses With Broken Bond

It was assumed for the purposes of the stress calculations that the bond could support no tensile or shear stresses, but could transmit compressive contact stresses. A trial and error procedure was used to determine the contact (or separation) conditions along the various interfaces.

Table 1 lists all the cases analyzed, including those described previously for the fully bonded assumption. For case 3 a condition of zero shear was imposed along the bond interfaces, but with no separation of the adjoining materials. When tensile stresses were calculated across the bonds, the conditions of case 4 were imposed with contact only on the lugs. These results however indicated contact between the epoxy and outer metal sleeve. Consistent results were finally obtained for the conditions of case 5, with contact at the lugs and also along the outer

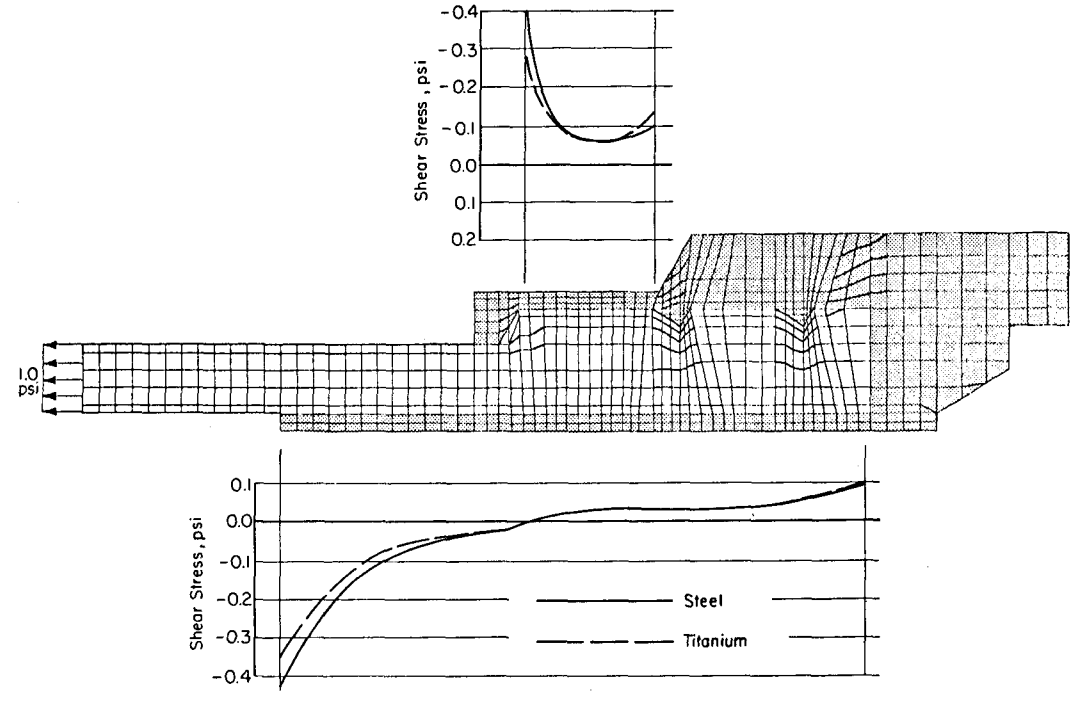

FIGURE 4. BOND SHEAR STRESS, τ_{rz}, IN PISTON COUPLING

TABLE 1. CASES ANALYZED IN STUDY OF COUPLING STRESSES, LISTED IN ORDER OF CONSIDERATION

Case	Type of Bonding	Spool Material	Center Plug	Comments
1	Fully bonded	Steel	No	
2	Fully bonded	Titanium	No	
3	Bonded - with bond assumed to transmit normal stress but no shear stress	Steel	No	Tensile bond stress calculated
4	Contact only at lugs - frictionless contact condition assumed	Steel	No	Results indicated that outer surface of epoxy will contact steel - incorrect contact assumption
5	Contact at lugs and outer surface of epoxy - frictionless contact condition assumed	Steel	No	Correct contact assumption
6	Contact at lugs and outer surface of epoxy - frictionless contact condition assumed	Steel	Yes	Correct contact assumption

sleeve.

The contact conditions of Case 6 were the same as for Case 5 with the difference being that the end of the spool was restrained against rotation. This restraint was obtained mathematically by imposing a condition of zero radial displacement for three nodal points at the end of the spool. This was to simulate the addition of a metal plug-plate, which was suggested as a design change to reduce the bending stresses at the end of the spool.

Figure 5 shows the calculated axial stresses in both the metal and epoxy for comparison with those of Figure 3 for the fully bonded assumption. It is seen that the outer sleeve carries no axial stress, which results in an increase in stress in both the epoxy and the inner spool.

A more complete picture of the stress in the end of the spool is shown in Figure 6. Fixing the end of the spool does result in some decrease in stress, but the bending stress is still about 7.5 times the applied axial stress of 1.0 psi.

Figure 7 is a computer plot of the deformed finite element grid, with the deflections exaggerated by a factor of 250,000. This Figure shows how the epoxy rides up on the lugs in a ramp type of motion, and how this in turn causes the epoxy to bear against the outer sleeve.

Figures 8-11 give calculated stresses for that portion of the epoxy material which is imbedded into the coupling. The results are given for Case 6 of Table 1. Numbers marked within each element which give the value of stress calculated for that element. For example, Figure 8 shows the variation in axial stress σ_z. The other figures successively show the shear, radial and hoop components of stress. The critical locations are seen to be where the lugs are imbedded into the epoxy material. These give rise to geometric discontinuities as shown by the intense stress peaks. The particular stress values given at these locations however, should not be interpreted as actual maximum stresses, since a much more refined finite element grid would be required for this purpose.

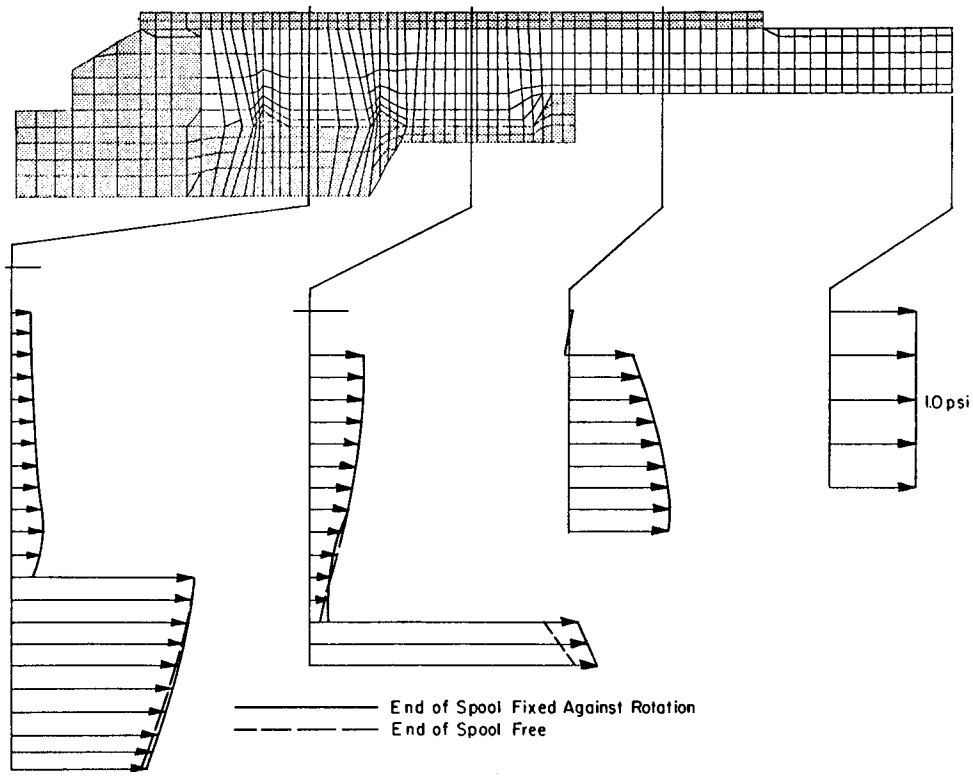

FIGURE 5. REDISTRIBUTION OF AXIAL STRESS DOWN LENGTH OF COUPLING, BROKEN BOND ASSUMED

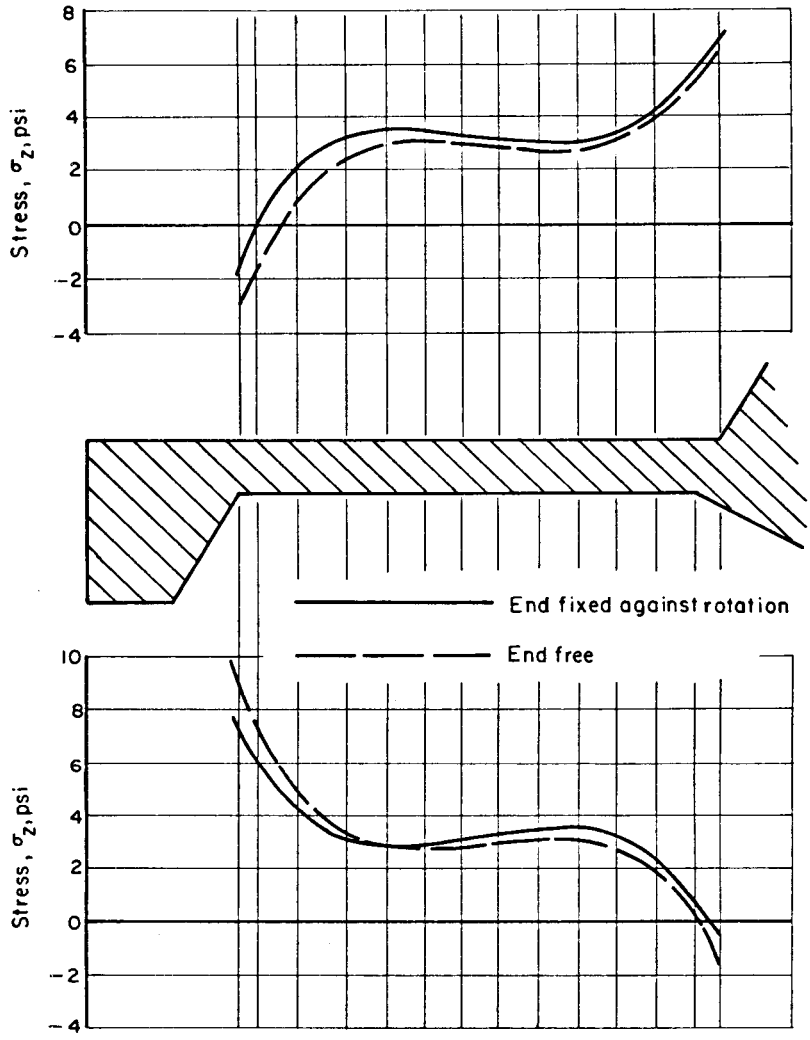

FIGURE 6. AXIAL STRESS, σ_Z, ALONG END OF SPOOL

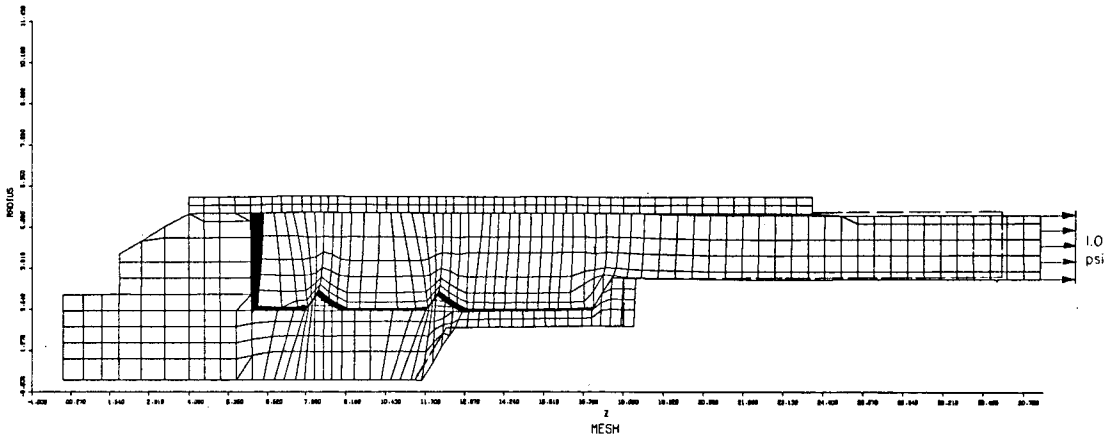

FIGURE 7. DEFORMED SHAPE OF PISTON COUPLING, END FIXED AGAINST ROTATION

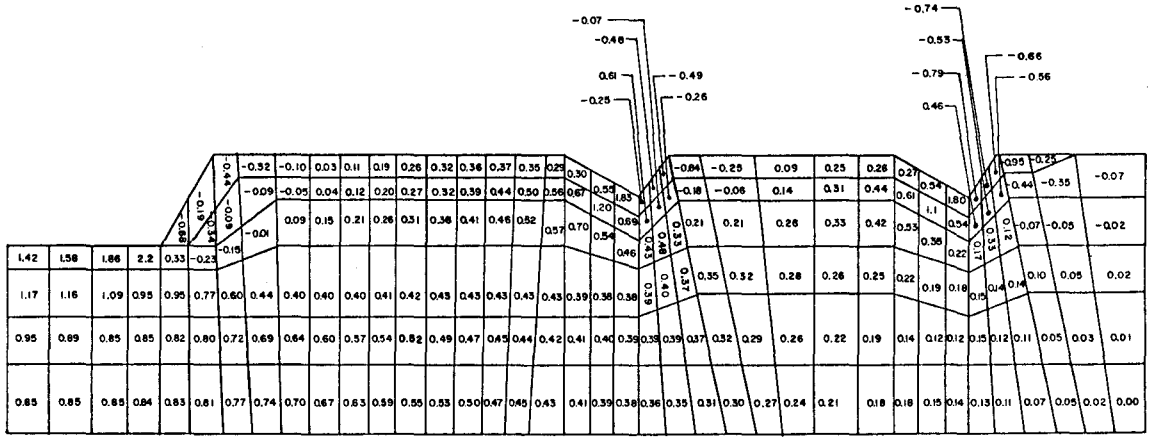

FIGURE 8. AXIAL STRESS, σ_z, IN FIBERGLASS-EPOXY, END OF SPOOL FIXED AGAINST ROTATION

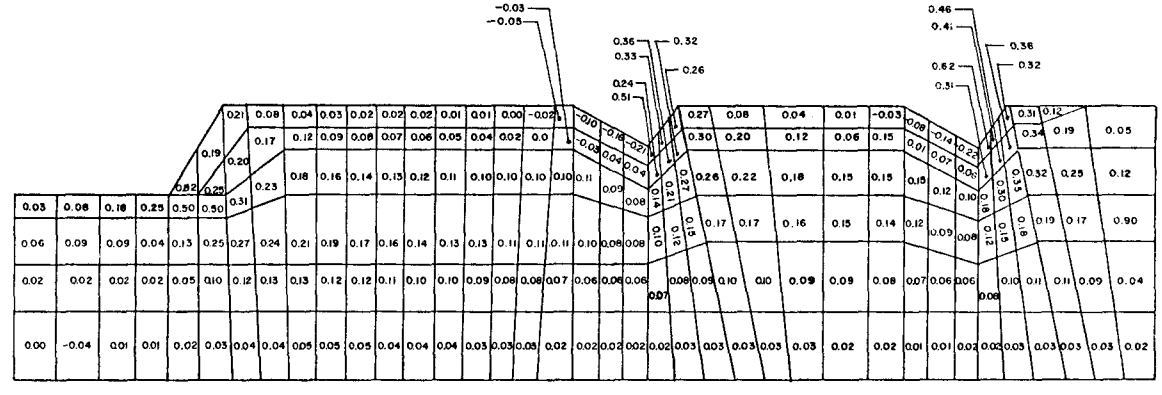

FIGURE 9. SHEAR STRESS, τ_{rz}, IN FIBERGLASS-EPOXY, END OF SPOOL FIXED AGAINST ROTATION

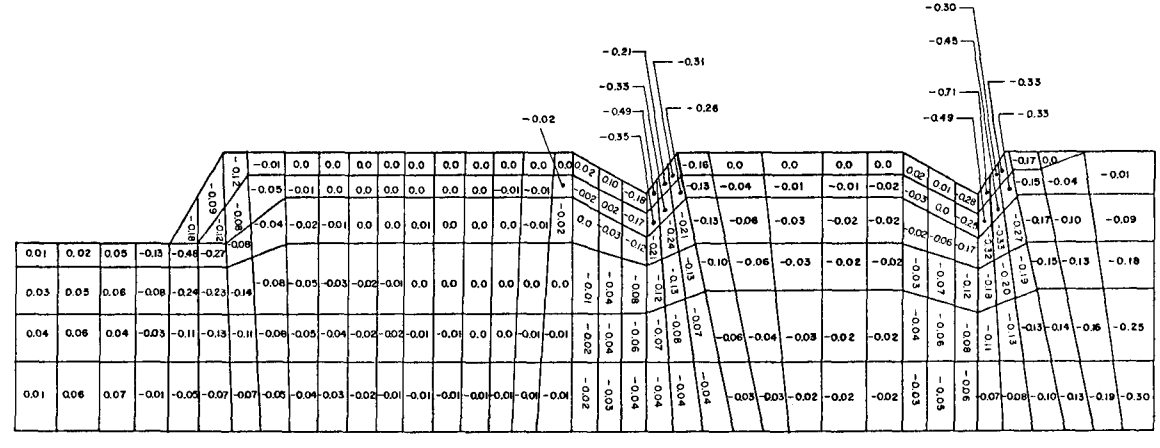

FIGURE 10. RADIAL STRESS, σ_r, IN FIBERGLASS-EPOXY, END OF SPOOL FIXED AGAINST ROTATION

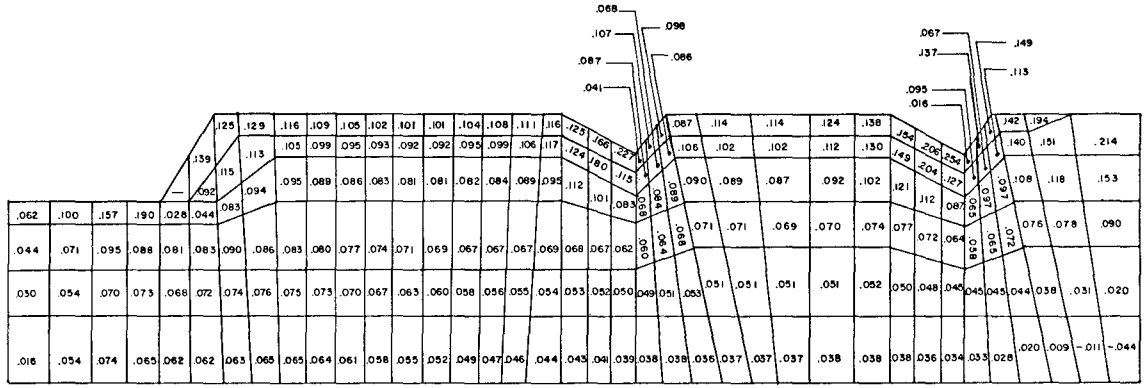

FIGURE 11. HOOP STRESS, σ_θ, IN FIBERGLASS-EPOXY, END OF SPOOL FIXED AGAINST ROTATION

Even if calculated, such peak stresses would be of limited value in evaluating the strength of the structure in the presence of sharp notches of the type involved here. Such an evaluation requires specific test data showing the sensitivity of material to notches.

In summary, the stress analysis of the coupling area of the piston revealed locations of high stress. The first location was at the end of the spool, where high bending stresses were calculated. A design modification consisting of a plug-plate to give structural support should reduce these stresses somewhat. However, the end of the spool still remains as a potential fatigue problem. The remaining locations of high stress are where the lugs are imbedded into the epoxy material. Some design changes have been developed to help relieve these geometric discontinuities. These changes are described below.

Modified Coupling

Based on the data generated by the AXISOL analyses of the proposed coupling as described above a modified coupling geometry was developed. As was shown, particularly by the broken bond model, high localized stresses in both the fiberglass-epoxy material and the stainless steel occurred at each of the lugs. The stresses in the steel at these locations had large bending stress components. The tensile and shear stresses induced in the fiber at these locations were caused by the abrupt changes in geometry of the lug configurations. The bending stresses in the steel occurred at the root of each lug with the greatest stress being found at the root of the last lug. The large stresses in the fiber stem occurred at the top of each lug with the maximum stress being developed at the end of the last lug.

To ameliorate these localized stress conditions a modified coupling geometry was developed which incorporated the following:

(1) All reentrant corners on the lugs were generously filleted. The addition of these fillets substantially reduced the local

stress concentrations at the root of the lugs and in all cases increased the wall thickness of the coupling at these locations by a minimum of 30 percent. Assuming that the local moment distribution is not significantly affected by the addition of this material the bending stresses at these locations will be greatly reduced. The bending stresses will be reduced by a factor equal to the square of the ratio of the old wall thickness, in this case by at least 70 percent. The addition of these fillets also presents a much smoother flow path for the bearing of the fiber material against the lugs while still maintaining the physical interlock feature.

(2) All external corners on the lugs were generously radiused. These rounded corners should prevent the development of highly localized stresses in the fiber material during operation.

(3) A tapered sleeve was added to the last lug extending to the end of the outer sleeve. In addition, one-half inch thick plug-plates were emplaced propping both the last lug and the end of the added tapered sleeve. These plug-plates considerably siffen the end of the coupling in a uniform bending mode while not at all affecting the axial stiffness of the coupling. This radial stiffening reduces the moment induced at the root of the last lug thereby reducing the bending stresses generated at that location. The tapered sleeve also prevents the fiber material from deforming around the end of the last lug. This action reduces the bearing stress in the fiber material and in general this new shape presents a much more satisfactory bearing surface.

(4) The flat cylindrical section of the coupling between the first and second lugs was changed to a one and one-half inch radius groove which blends smoothly into each lug face. This new geometry reduces the wall thickness of the coupling at this

location thereby allowing it to be more flexible in the axial direction. This change permits the first lug to carry slightly more load than was possible in the original configuration and so improves the load sharing amongst the three lugs. This new configuration also increases the contact area in the axial direction thus enlarging the amount of fiber and steel mating surfaces to be employed in the physical interlock mechanism.

The modified coupling is shown in Figure 12. No detailed stress analysis was carried out for this geometry. The anlysis of the original design showed that except in the localized areas discussed the coupling was completely adequate to sustain the anticipated loadings. The changes described above should correct these localized conditions. The adequacy of the modified coupling from the viewpoint of fatigue can be shown by the following.

From Figure 6, for the restrained condition in the original coupling, the maximum stress in the steel is shown to be 66,000 psi (i.e., 7.5 x 8,800 psi). This is a total stress which is composed of a membrane stress component of 30,800 psi and a bending stress component of 35,200 psi. For the modified coupling the membrane stress in this vicinity is reduced by the ratio of the old to new thicknesses while the bending stress is reduced by the square of this ratio. This results in a new membrane stress of approximately 23,600 psi and a new bending stress of approximately 20,700 psi. This gives a new combined total stress of 44,300 psi. The steel of the coupling is A-286 type stainless steel which has a tensile strength in excess of 110,000 psi, a yield strength of approximately 65,000 psi, and a fully reversed bending endurance limit in fatigue of greater than 35,000 psi amplitude. All these values taken at room temperature. The stresses induced in the coupling are cyclic in nature going from zero to maximum to zero for each pulse of the piston. The maximum stress in the steel calculated above can be converted to an equivalent fatigue stress from the following relation.

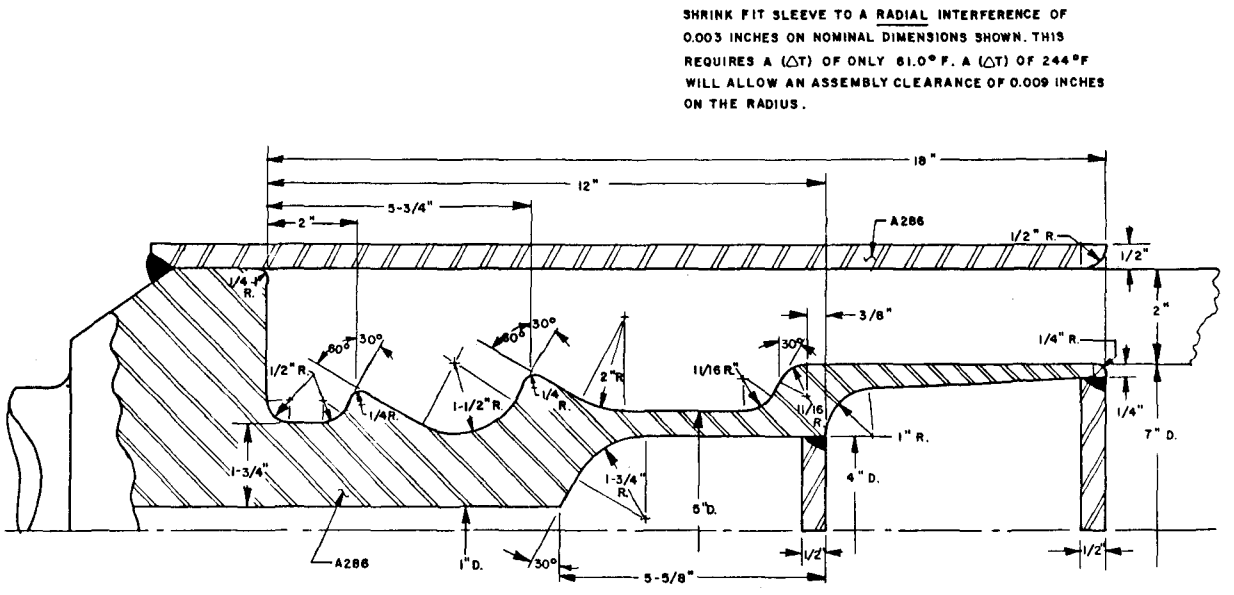

FIGURE 12. MODIFIED COUPLING DESIGN

$$\sigma_{eq} = \frac{\sigma_{r/2}}{1 - \sigma_m/\sigma_{ul}}$$

where σ_{eq} = the equivalent fully reversed bending fatigue stress

$\sigma_{r/2}$ = the stress range divided by 2

σ_m = the mean stress

σ_{ul} = the tensile strength

For this case

$\sigma_{r/2}$ = 22,150 psi

σ_m = 22,150 psi

σ_{ul} = 110,000 psi

Thus

$$\sigma_{eq} = \frac{22,150}{1 - \frac{22,150}{110,000}} = 27,735 \text{ psi.}$$

This figure compares very favorably with the fatigue limit of 35,000 psi.

From Figure 8, the maximum tensile stress occurring in the fiberglass-epoxy stem is shown to be 19,360 psi. Reference 1 gives the fatigue limit of this material in this direction as 21,000 psi. Thus, the stresses in the fiberglass-epoxy stem should cause no fatigue problem as long as no significant local fretting of the material occurs here. The new, smooth geometry should ensure the prevention of localized fretting.

Analysis of the Piston Head

The piston head together with the lip seal system forms the moving pressure boundary which ensures the rapid pressure drop in the fluid in the main chamber. This structure must not only be capable of sustaining many millions of cycles of pressure loading but must as well maintain the pressure seal. The purpose of this work is to show that the piston will maintain its structural integrity during its operational life. Further, the deformation of the outer radial surface of the piston head must be kept to an absolute minimum to ensure that the lip seals will be

capable of maintaining contact with this surface during each stroke.

To prevent excessive loading of the wood core of the piston head assembly the bottom fiberglass-epoxy laminate shell component is perforated by numerous circular holes. The concept behind this structural feature is that the presence of the holes would not significantly weaken the assembly but would allow the gas from the "Z" section or lower chamber to permeate the very porous core material. This gas would be at the equilibrium pressure and would be established by a soaking action taking place while the piston is dwelling at the equilibrium position. It is believed that the diffusion rate of the gas through the wood would be fairly rapid but not rapid enough to take place during the pulse period itself. This action should ensure that the core would always be subjected to the equilibrium pressure (except of course at start-up and shut-down) and that such pressure would tend to mitigate the effects of the large pressure differential which acts across the head of the piston during each stroke.

However, the wood core material and the bonding agents used for the core assembly cause the structure to be so non-homogeneous that the exact diffusion rates cannot be established to any great degree of accuracy. It was thus decided to analyze this structure as if this diffusion did not occur and to ensure its structural adequacy and deformation limitations under such a condition. Once an adequate structure has been developed the effects of the diffusion phenomenon on this assembly will be determined.

Modeling Considerations

The mathematical model of the piston head and assumed loading are shown in Figure 13. A total of 713 elements and 881 nodal points were used. The upward thrust resulting from the difference between the 200 psi and 70 psi pressures was reacted by tension in the piston shaft. As indicated in this figure a displacement boundary condition was imposed at the end of the shaft. Neither the full length of the shaft nor outer

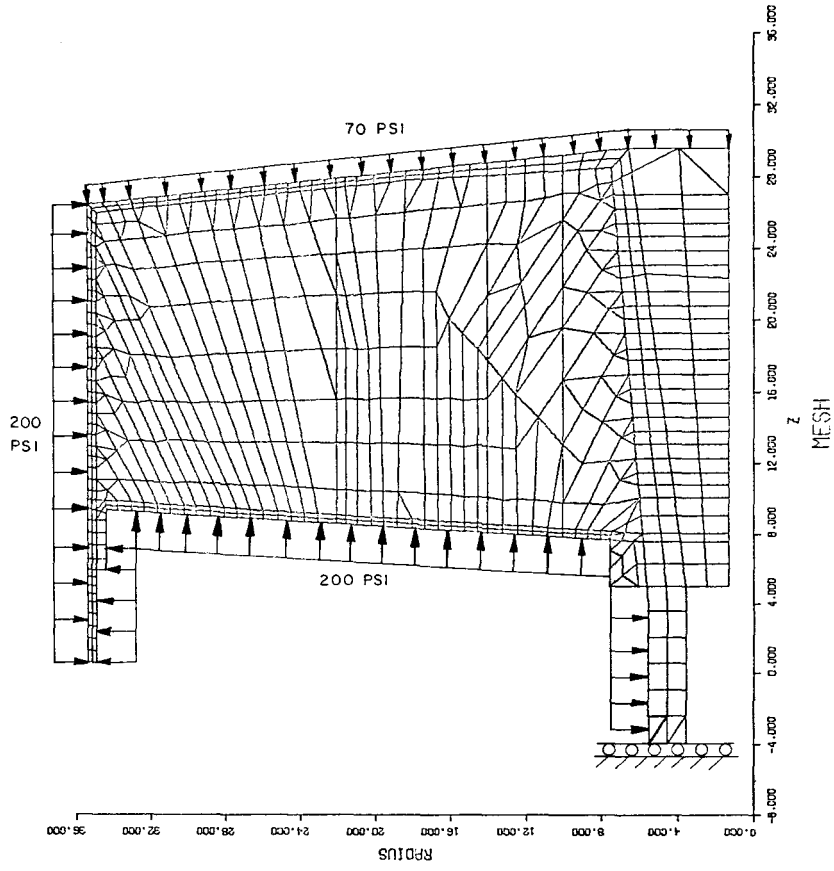

FIGURE 13. FINITE ELEMENT MODEL OF PISTON HEAD WITH PRESSURE LOADING

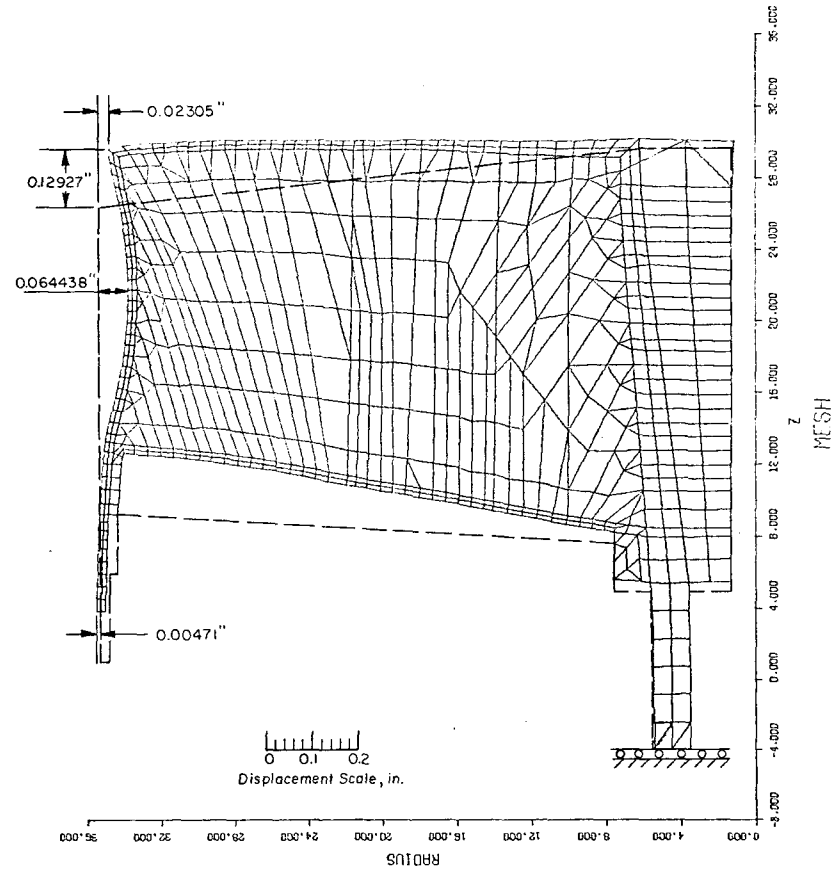

FIGURE 14. DEFORMED SHAPE OF PISTON HEAD (DISPLACEMENTS EXAGGERATED BY A FACTOR OF 25)

cylinder were analyzed, both being truncated as shown.

The 713 element model represented a relatively complex problem for the program AXISOL and the solution required over 6 minutes of central processor time on Battelle's CDC 6400 computer. Nevertheless, only two elements were used across the thickness of the fiberglass-epoxy outer shell. This represented the minimum number of elements that would allow an accurate calculation of the bending stress through the thickness of the shell. Within the wood core the element gridwork was constructed in a manner to connect at all points with the surrounding outer shell and also to align with the interfaces between the core materials. These two criteria were often in conflict, so that the resulting grid became quite irregular in certain regions. The grid was, however, quite adequate to calculate stresses to within the required degree of accuracy, approximately ± 5 percent.

In constructing the mathematical model provision was made to allow separation of the bond between the laminate shell and the wood core. However, the results of the ensuing stress calculations indicated that at no location would the bond break. Thus this additional degree of generality in the analysis did not prove necessary.

Each of the four types of wood within the core was designated as a separate material by input data to the program. Table 2 gives the elastic properties assigned to the different materials. Those for the balsa wood were obtained from data sheets issued by a vendor[2], and those for the douglas fir were from the Wood Handbook[3]. The stress strain equations corresponding to these elastic constants are described in a separate section in the Appendix. Properties for the epoxy-fiber glass material are given in Table 2 for the principal fiber orientation aligned with the axis (or center line of the piston). Within the upper and lower faces of the piston, the properties were taken as aligned with the faces. The mathematical transformations used to rotate the material properties to the desired oblique directions are also given in the Appendix to this

TABLE 2. ELASTIC PROPERTIES USED IN CALCULATION OF STRESSES IN PISTON

Material	E_r psi	E_z psi	E_θ psi	G_{rz} psi	ν_{rz}	$\nu_{r\theta}$	$\nu_{z\theta}$
Epoxy* - Fiber Glass	1,500,000	5,000,000	1,500,000	500,000	0.25	0.25	0.009
Douglas Fir 34 lb/ft^3	180,000	2,000,000	122,000	150,000	0.295	0.368	0.023
Balsa 15.5 lb/ft^3	55,000 55,000	1,164,000 1,164,000	19,900 19,900	63,500 63,500	0.23 0.23	0.23 0.23	0.01 0.01
Balsa 11 lb/ft^3	37,000	768,000	13,000	41,800	0.228	0.250	0.01
Balsa 6 lb/ft^3	16,000	330,000	5,100	18,000	0.237	0.20	0.009

*For the epoxy E_z is the modulus in the meridional direction, and E_r is the modulus in the corresponding normal direction.

report.

Computed Stresses

A computer plot of the deformed shape of the piston head is shown in Figure 14. The displacements have been exaggerated by a factor of 25. Three principal modes of deformation can be seen. First of all there is a general upward deflection of the entire piston head due to stretching of the inner shaft with respect to its restrained lower end. There is also an upward beam type, or more correctly, a shearing deflection of the outer diameter of the piston with respect to its inner diameter. Finally, there is a radial inward deflection at the outer diameter as the 200 psi external pressure produces radial compression of the low modules balsa wood core. Magnitudes of the deflections can be measured from the drawing and read from the deflection scale shown. The exact deflection values as given by the computer printout for certain locations are also indicated on Figure 14. These include a maximum radial deflection of 0.064438 inch and a maximum axial deflection of 0.12927 inch.

Stresses in Core. The distribution and levels of stress in the wood core will be discussed first before considering the stresses in the epoxy. Figure 15 shows the arrangement of the different grades of balsa and douglas fir within the core, and indicates the numbering scheme used to designate the radial interfaces between the materials (i.e., interfaces 1, 2, 3, 4, and 5). Figures 16 and 17 then show stress distributions along these interfaces. No plots are given of stresses within the layers since the maximum stresses were found to exist in all cases at the interfaces. Also the axial stress, σ_z, are not shown. These were compressive and quite small in magnitude in comparison with the relatively higher strengths in this direction (along the direction of the grain of the wood).

The curves of Figures 16 and 17 have the axial coordinate z as the vertical scale, with the bottom of the graph corresponding to the bottom

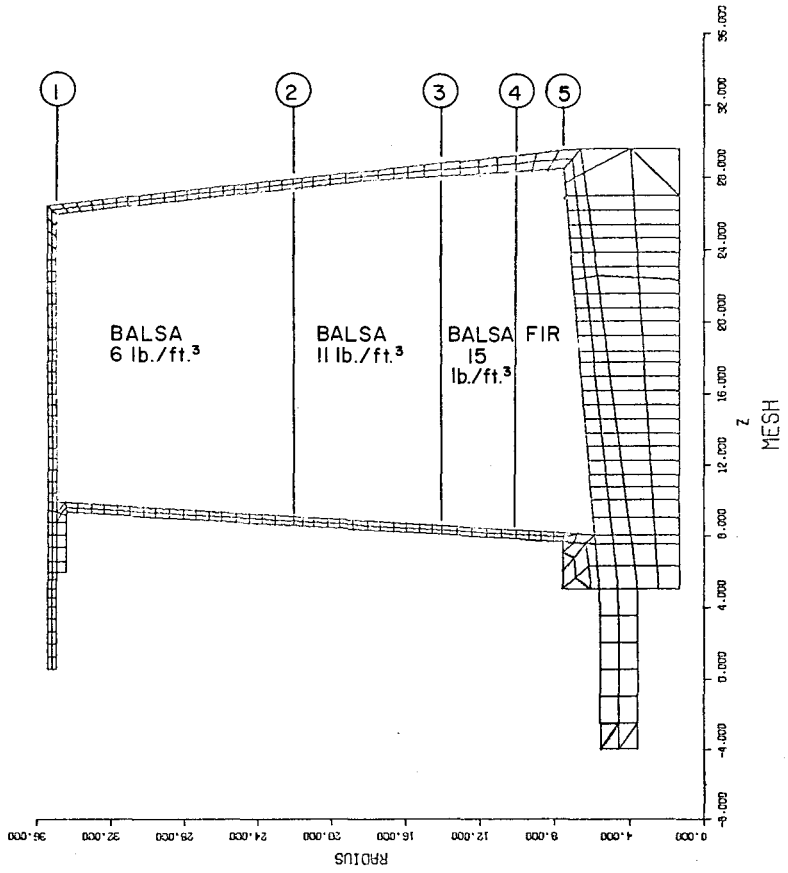

FIGURE 15. LOCATION OF MATERIAL INTERFACES WITHIN CORE

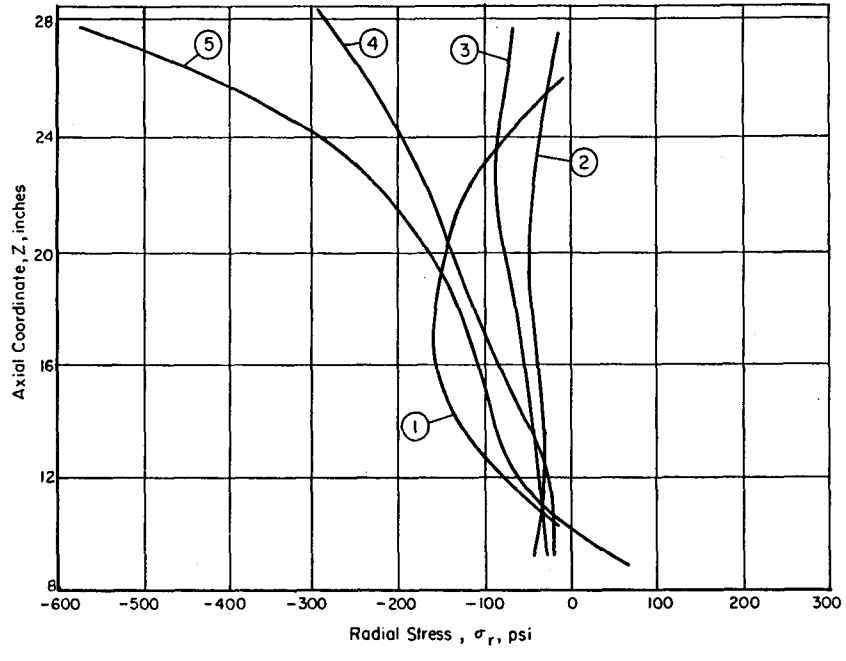

FIGURE 16. NORMAL STRESS DISTRIBUTION ALONG BONDS BETWEEN MATERIALS

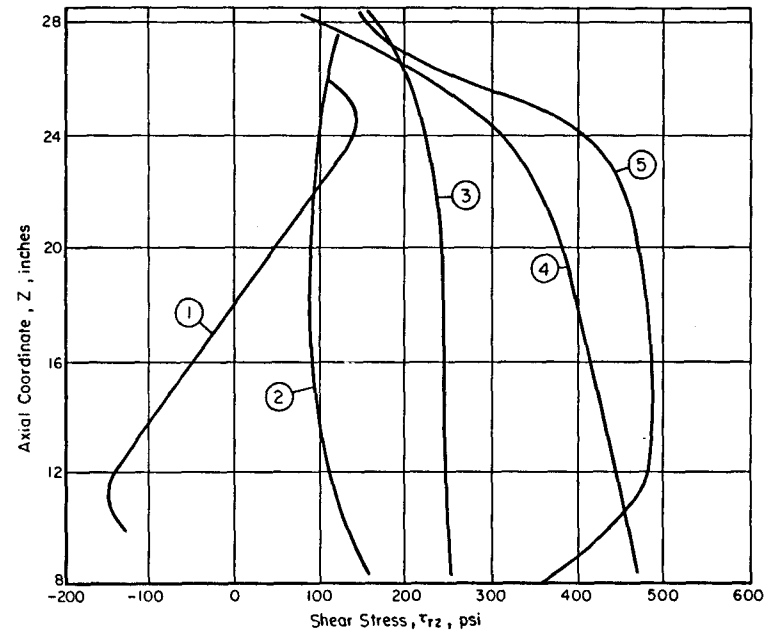

FIGURE 17. SHEAR STRESS DISTRIBUTION ALONG BONDS BETWEEN MATERIALS

face of the piston and the top of the graph corresponding to the top face of the piston. Certain trends can be seen from this collection of curves. For example, there is a relatively high compressive radial stress in the 6 lb/ft^3 balsa (curve 1 of Figure 16) which reflects the 200 psi radial pressure at the outside diameter. The radial stress distribution correlates with the deflections pattern (Figure 14) along the outer surface. Proceeding towards the center of the piston, the radial load is transferred to the stiffer epoxy upper and lower surfaces (curves 2 and 3 of Figure 16). There is, however, some increase in radial stress in the two innermost materials (balsa 15 lb/ft^3 and douglas fir), which reflects the higher elastic moduli of these materials.

The interpretation of the shear stress curves of Figure 16 is quite straightforward. There is a monotonic increase in this stress in the radial direction towards the center of the piston. The radial variation in this case is quite independent of the elastic properties of the core materials, but is governed by the pressure differential across the top and bottom of the piston. The resulting net axial load must be balanced by the shear stresses, τ_{rz}, which exists primarily in the core rather than the epoxy upper and lower faces.

Stresses in Epoxy. Stresses in the epoxy layers are shown in Figures 18 and 19. Here the stresses of interest are the meridional and hoop stresses, with the transverse normal and shear stresses being essentially negligible. The stresses are shown for both the inner and outer surfaces of the layers. Since the finite element computer program calculates stresses only at the centers of the elements, it was necessary to extrapolate to obtain stresses for points on the very surface of the epoxy layers. The meridional stresses are in general higher than the hoop stresses which follows from the higher modulus in the meridional direction. The maximum stresses occur in the shaft which reacts the net upward pressure loading. Here tensile stresses on the order of 8,800 psi occur, which are well below the material tensile strength of 40,000

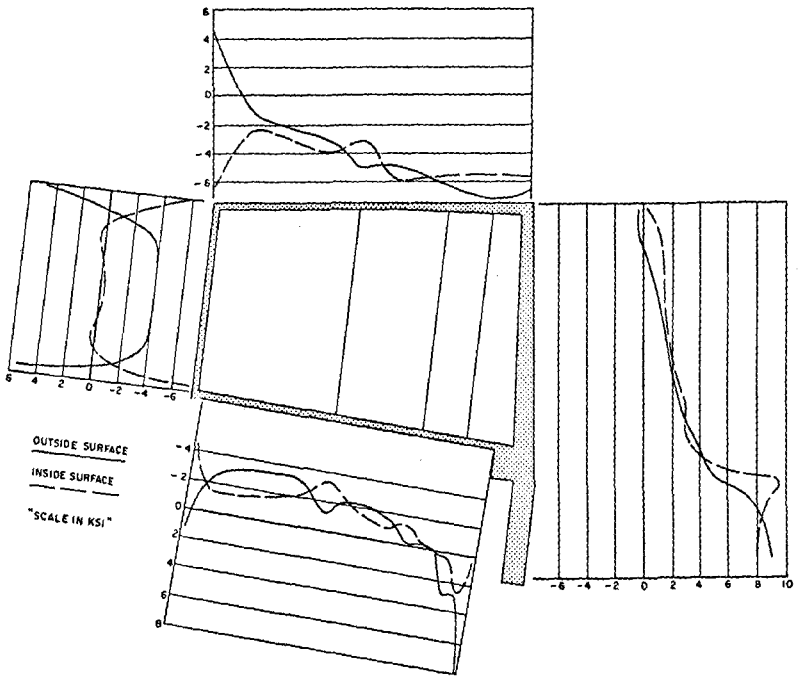

FIGURE 18. MERIDIONAL STRESSES IN FIBERGLASS-EPOXY SHELL

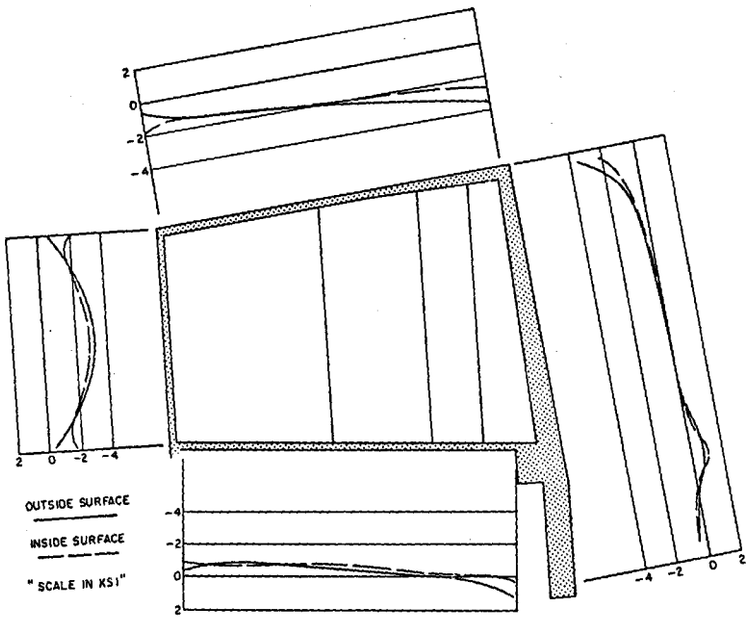

FIGURE 19. HOOP STRESS IN FIBERGLASS-EPOXY SHELL

psi. Other high stress locations occur at the corners, where bending gives rise to stresses in the 6,000 to 8,000 psi range. At no location were the calculated stresses at a level that approached the material strength, and it was concluded that the possibility of failure of the epoxy material is remote. However, the stress levels in the core indicated that at certain locations the balsa wood construction was marginal. The evaluation of these materials will be discussed below.

Comparison with Strength Data

The strengths of the three grades of balsa wood (Reference 2) and douglas fir (Reference 3) are given in Table 3. The z direction is the with-grain direction, r and θ, the two cross-grain directions, and the shear strength can be identified with the τ_{rz} stress of the finite element calculations. All strengths are for room temperature.

Since the core materials are exposed to multi-axial stresses a meaningful failure criterion is needed. Because no generally accepted criteria are available for anisotropic materials, two methods were used to compare the calculated stress levels with strength values. The first method involved the comparison of each component of stress with the corresponding material strength in that particular direction, while in the second method an effective stress was calculated.

Table 4 gives the maximum radial and shear stresses that were calculated in each material. In parentheses are the corresponding strength values from Table 3. On this basis it is seen that the shear stresses are less than the strength values for all materials. However the radial stress in the balsa 15.5 lb/ft^3 and the balsa 6 lb/ft^3 are significantly greater than the radial compressive strength of the wood.

An equation that has been used as a failure criterion for anisotropic materials under conditions of multi-axial stress is as follows:

$$\bar{\sigma} = (1/\sqrt{2}) \left[(\sigma_r/R - \sigma_\theta/\theta)^2+(\sigma_\theta/\theta-\sigma_z/Z)^2+(\sigma_z/Z-\sigma_r/R)^2+1.5(\tau_{rz}/RZ^2\right]^{1/2},$$

where R, Z, θ, and RZ are the material strengths in the respective di-

TABLE 3. STRENGTH PARAMETERS FOR WOOD CORE

Material	Proportional Limit in Compression			Shear Strength
	z-direction	r-direction	θ-direction	
Douglas Fir 34 lb/ft^3	5,850 psi	870 psi	870 psi	1,160 psi
Balsa 15.5 lb/ft^3	2,310 psi	198 psi	145 psi	522 psi
Balsa 11 lb/ft^3	1,450 psi	144 psi	100 psi	360 psi
Balsa 6 lb/ft^3	500 psi	84 psi	50 psi	180 psi

TABLE 4. MAXIMUM CALCULATED STRESSES IN WOOD CORE WITH COMPARISON WITH CORRESPONDING STRENGTHS

Material	Stress, psi	
	σ_r	τ_{rz}
Douglas Fir 34 lb/ft^3	-600 (-870)	490 (1160)
Balsa 15.5 lb/ft^3	-300 (-198)	475 (522)
Balsa 11 lb/ft^3	- 85 (-144)	250 (360)
Balsa 6 lb/ft^3	-160 (- 84)	150 (180)

rections. The quantity $\bar{\sigma}$ is an effective stress, or more precisely, the ratio of effective stress to the stress to produce material failure for the particular ratio of stress components being considered. In the current analysis of the piston head, if $\bar{\sigma}$ is less than 1.0 then the materials are stressed below their proportional limit. For $\bar{\sigma}$ greater than 1.0, the stress levels will produce permanent deformation. Table 5 gives the effective stress values for the four core materials. It is seen that both the douglas fir and balsa 11.0 lb/ft^3 are stressed below their proportional limits, while the balsa 15 lb/ft^3 and balsa 6 lb/ft^3 are stressed about 40 percent over their proportional limits. These conclusions are, of course, based on the failure criteria assumed above. The implication is that localized crushing of the balsa will occur due to biaxial compression in the radial and hoop directions. This, however, would by no means imply ultimate structural failure of the piston head. Rather a distribution of stress will occur, with the relatively low stressed epoxy laminate then carrying a greater proportion of the radial loading. Upon release of the applied pressure, some permanent deformation of the piston could be expected due to the remaining inelastic strains in the balsa (e.g., permanent curvature along the outer diameter of the piston into the form shown in Figure 14). Under the compressive biaxial stress field the inelestic strains in the balsa should, however, be relatively small and of an essentially contained nature.

It must be remembered that for the above analysis no credit was taken for two important conditions. First, the analysis was conducted with no gas pressure in the core. Second, no credit was taken for the increase in strength of the wood components of the core when subjected to a cryogenic environment. As discussed previously,it was decided that the adequacy of the piston head assembly was to be made in the absence of these factors. This being the case the original piston head configuration was judged to be structurally marginal and operationally unacceptable. This latter judgment is made on the basis of the large de-

TABLE 5. EFFECTIVE STRESSES IN CORE MATERIALS

Material	Location of Maximum Stress	Stress, psi				Effective Stress
		σ_r	σ_z	σ_θ	τ_{rz}	
Douglas Fir 34 lb/ft^3	Interface 5 @ Top	-507	299	-337	-180	0.577
Balsa 15.0 lb/ft^3	Interface 4 @ Top	-300	100	-49	75	1.410
Balsa 11.0 lb/ft^3	Interface 3 @ z = 22.5"	-90	-75	-23	245	0.780
Balsa 6.0 lb/ft^3	Interface 1 @ z = 13.5"	-120	5	-37	-120	1.375

flections of the outer radial surface of the piston head. As can be seen from Figure 14, radial displacements of the order of 23 mils and 65 mils occur at the top and the mid-line of the outer radial surface of the piston head, respectively, under the assumed loading condition. Such displacements are too great to be compensated for by the limited radial travel ability of the lip seals and consequently leakage will occur and the desired pressure drop in the chamber would never be achieved.

Modified Piston Head Analysis

The information developed during the analysis of the original piston head design gave ample direction for a design change that had a high probability of correcting the structural weaknesses of the head. From that work it was clear that the primary weakness of the head assembly lay in its inability to sustain the radial compressive loads induced by the 200 psi pressure acting on the outer radial surface of the structure. This surface is a cylinder supported at its ends by the upper and lower shells of the assembly and in between in an elastic manner by the wood core. Its deformation pattern can be broken into two parts; it deforms uniformly inward radially as a long cylinder under external pressure and, due to its end constraints, it deforms along its meridional generator in a bending mode. This radial deformation pattern can be significantly reduced by increasing the wall thickness of this surface or cylinder. The original cylinder had a wall thickness of one-half inch. It was decided to double the wall thickness of this section, thus making it one inch thick. This was the only change made to the original configuration and the modified piston head design is shown in Figure 20.

The number of nodal points, number of elements and the pressure and boundary conditions governing the analysis of this new mathematical model were the same as the original model. The difference between this model and the original model was simply that the two elements comprising the wall of the cylinder were each double in thickness.

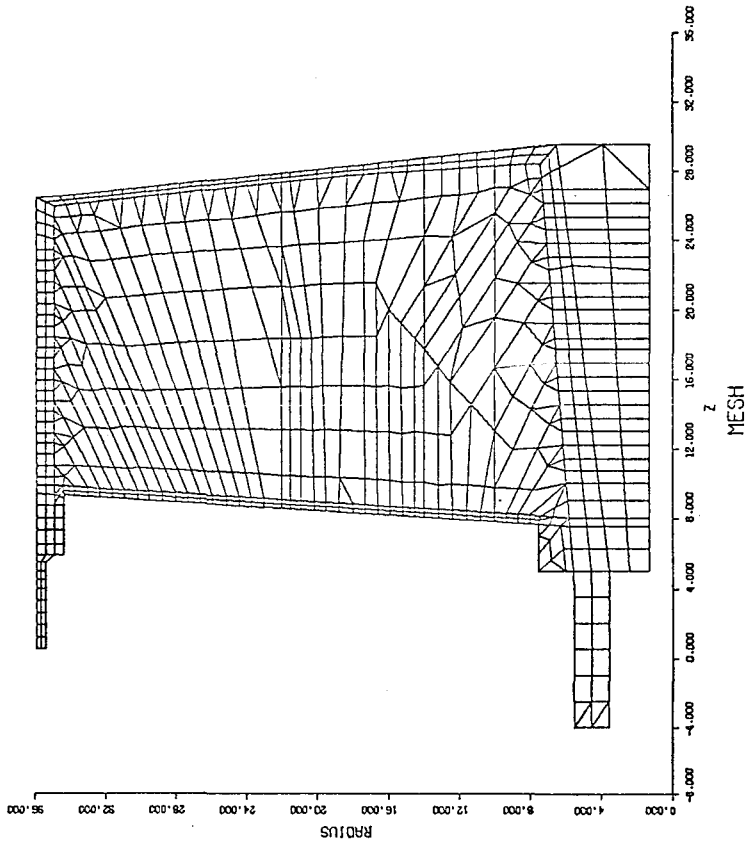

FIGURE 20. FINITE ELEMENT MODEL OF MODIFIED PISTON HEAD ASSEMBLY

A computer plot of the deformed shape of the piston head is shown in Figure 21. Here again the displacements were magnified by a factor of 25. As can be seen by comparing this figure to Figure 14 the radial displacements of the outer surface were drastically reduced.

The stresses developed in the core are shown in Figures 22 and 23 and the maximum stress of each type and in each of the wood components is presented in Table 6. In this table, as before, the proporational limit strength at room temperature is shown in each box in parentheses. It is noted that for the modified design the maximum stresses are, in all cases, less than the proportional limit strengths for the materials. Following the same procedure as for the core stresses in the original model these stress components were converted to effective stresses. These effective stresses are shown in Table 7. The greatest effective stress factor occurs in the balsa 6.0 lb/ft^3 and equals 0.914. Thus, since all the effective stress factors are less than 1.0 all the core deformations will remain elastic and no crushing of the core material is anticipated. The stresses in the fiberglass-epoxy laminate shell are shown plotted in Figures 24 and 25. Some redistribution of stress in the shell has been induced by the thickening of the outer cylinder wall. These stresses are again quite low when compared to the strength of the material and are acceptable.

Based on all the above and particularly in view of the rather stringent pressure conditions that were applied to the structure it is concluded that the piston head assembly as modified presents a structurally adequate and operationally effective configuration.

Saturated Core Model

At this point in the analysis-design procedure a completely satisfactory piston head configuration has been developed. It has been developed, however, to react to a pressure loading condition which is more severe than that which is anticipated during actual operation. It was anticipated that such a procedure would lead to a conservative design.

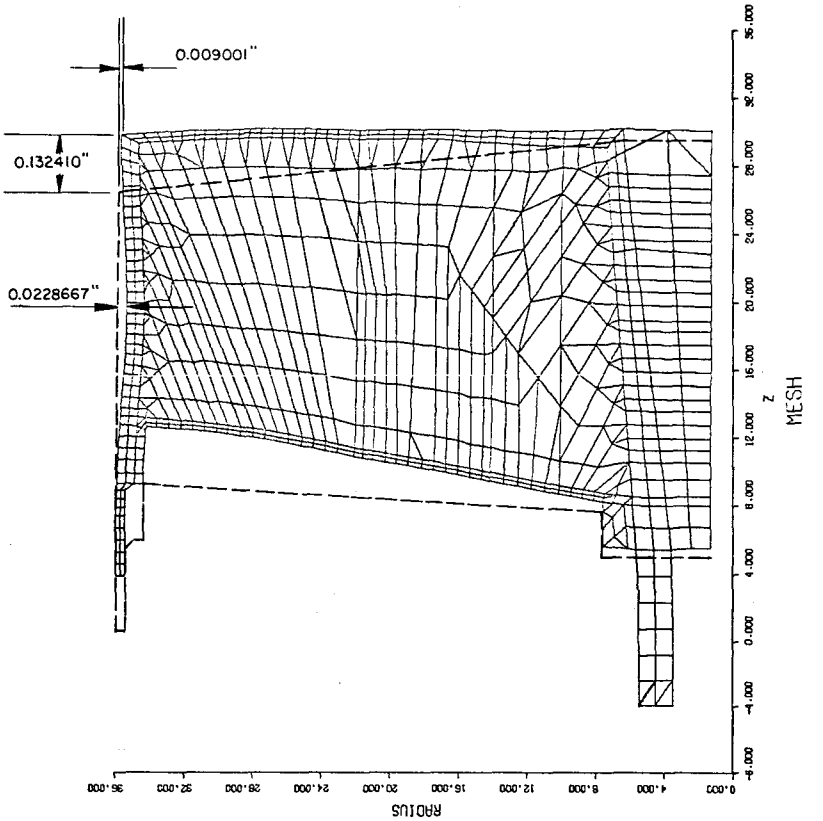

FIGURE 21. DEFORMED SHAPE OF MODIFIED PISTON HEAD ASSEMBLY UNDER ASSUMED LOADING

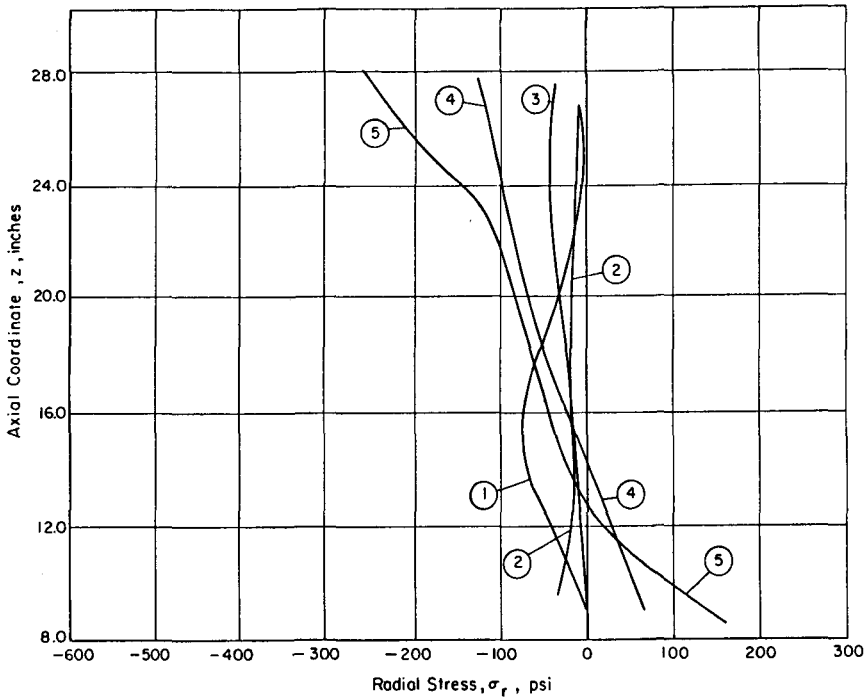

Figure 22. NORMAL STRESS DISTRIBUTION ALONG BONDS BETWEEN MATERIALS IN CORE OF MODIFIED PISTON HEAD

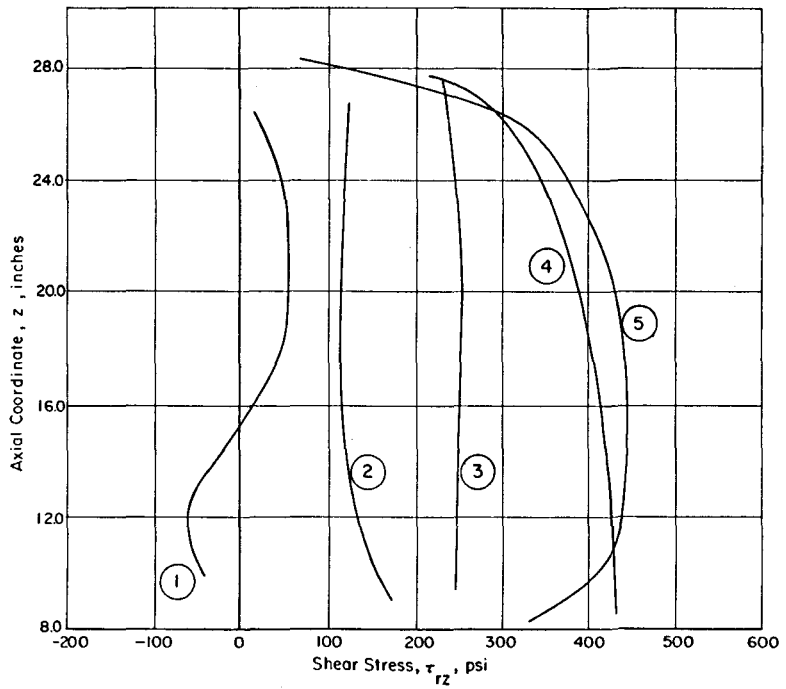

Figure 23. SHEAR STRESS DISTRIBUTION ALONG BONDS BETWEEN MATERIALS IN CORE OF MODIFIED PISTON HEAD

TABLE 6. MAXIMUM CALCULATED STRESSES IN WOOD CORE WITH COMPARISON WITH CORRESPONDING STRENGTHS FOR MODIFIED PISTON

Material	Stress, psi	
	σ_r	τ_{rz}
Douglas Fir 34 lb/ft^3	-260 (-870)	445 (1160)
Balsa 15.5 lb/ft^3	-125 (-198)	430 (522)
Balsa 11 lb/ft^3	- 40 (-144)	250 (360)
Balsa 6 lb/ft^3	- 75 (- 84)	175 (180)

TABLE 7. EFFECTIVE STRESS IN CORE MATERIALS FOR MODIFIED PISTON

Material	Location of Maximum Stress	Stress, psi				Effective Stress
		σ_r	σ_z	σ_θ	τ_{rz}	
Douglas Fir 34 lb/ft^3	Interface 5 @ z = 22.0"	-45	316	-20	445	0.413
Balsa 15.5 lb/ft^3	Interface 4 @ Bottom	70	-216	7	430	0.798
Balsa 11.0 lb/ft^3	Interface 3 @ z = 22.5"	-40	-94	-11	250	0.631
Balsa 6.0 lb/ft^3	Interface 2 @ Bottom	-45	-185	-6	175	0.914

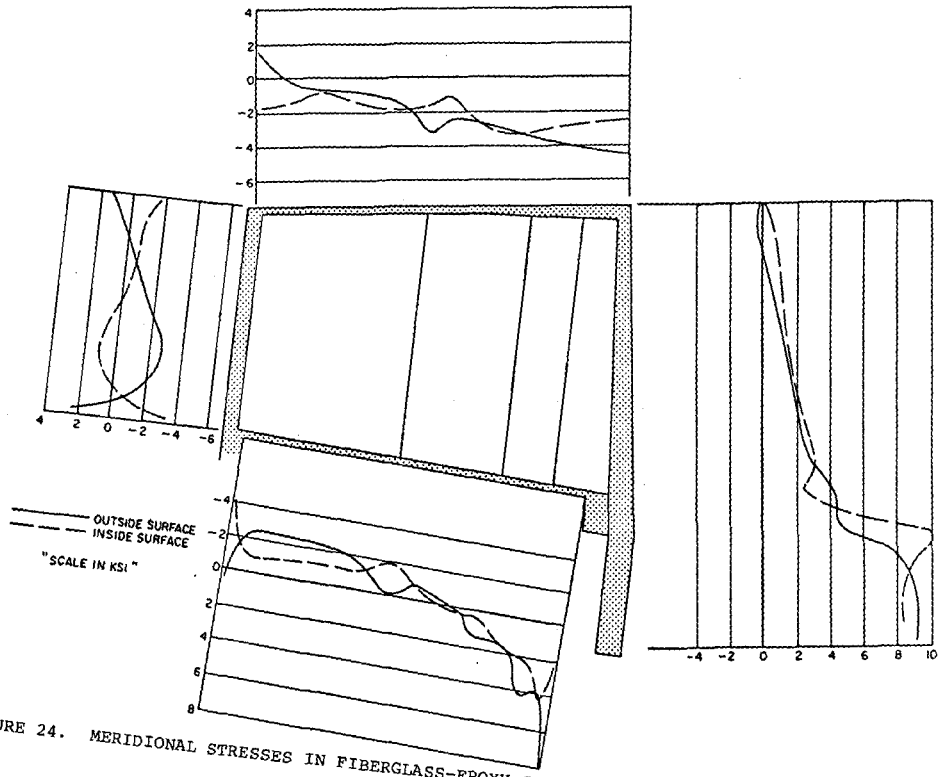

FIGURE 24. MERIDIONAL STRESSES IN FIBERGLASS-EPOXY SHELL OF MODIFIED PISTON HEAD

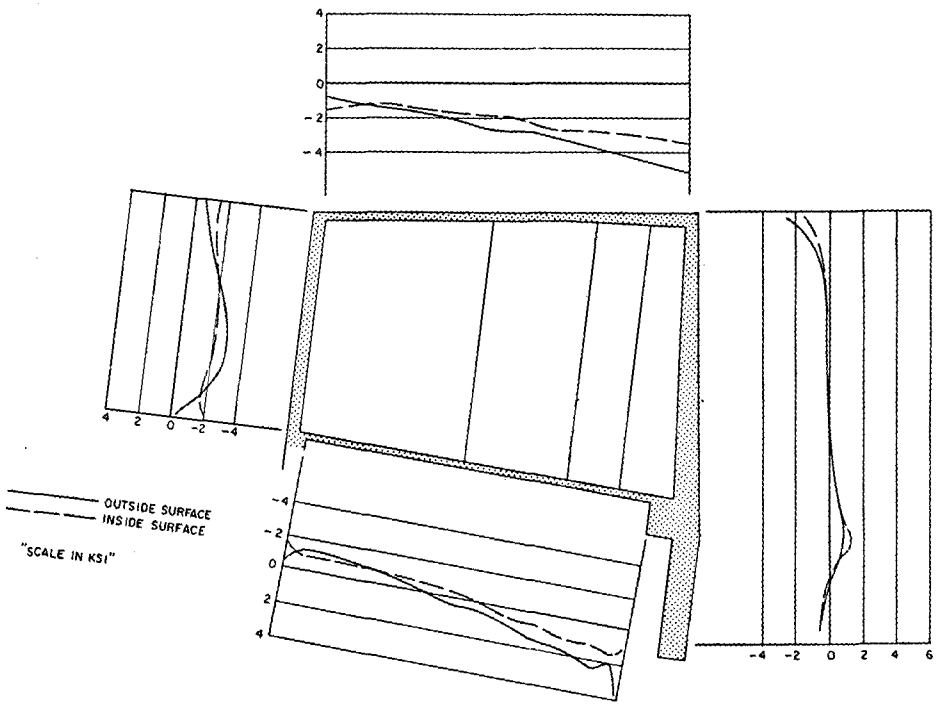

FIGURE 25. HOOP STRESSES IN FIBERGLASS-EPOXY SHELL OF MODIFIED PISTON HEAD

To determine the response of the modified piston head design to the actual predicted loading another AXISOL run was made. In this new run the only change made was in the pressure loading. Figure 26 shows the modified piston head assembly and the set of pressure loadings assumed. The pressures shown represent the condition of the piston at the bottom of the stroke in the neon operation. The 70.0 psi represents the pressure in the main chamber. The 200.0 psi represents the pressure in the lower chamber. The 140.0 psi represents the gas pressure in the core which has attained saturation level during the dwell time at the equilibrium position. It has been assumed that the pulse period is short enough to prevent any significant change in this saturation pressure. The intersection of the 70.0 and 200.0 psi pressure zones represents the actual position of the lower lip seal when the piston is at the bottom of its stroke. It is anticipated that this seal will form part of the main pressure boundary at the bottom of the stroke.

Figure 27 show the deformed shape of the modified piston head under the new assumed loadings. As shown the radial deformations of the outer cylinder are practically negligible. Figures 28 and 29 gives the stresses in the core material and Table 8 lists the maximum stress in each material along with the room temperature proportional limit strengths of those materials. Table 9 gives the effective stresses following the same procedure as previously employed. The largest effective stress factor developed is 0.830 which is again less than 1.0 and less than the previously determined values. Figures 30 and 31 show the stresses in the laminate shell. The stresses plotted in these last two figures do not reflect the presence of the circular holes cut into the bottom shell to allow the core to be saturated by the equilibrium pressure. However,if the number of these holes are limited and they are spaced such that there is at least a minimum ligament thickness between any two adjacent holes which equals twice the hole diameter then the maximum stress in this bottom shell should not be greater than twice those shown in these figures. Such stresses are still quite low when compared to the strength

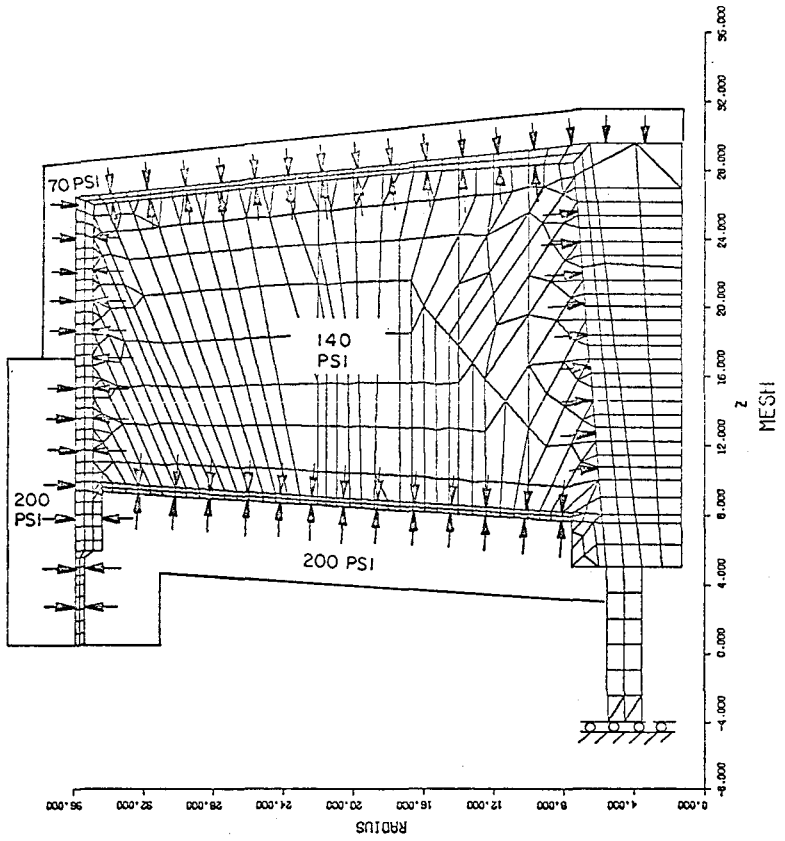

FIGURE 26. SATURATED, MODIFIED MODEL OF PISTON HEAD ASSEMBLY AND NEW ASSUMED LOADING

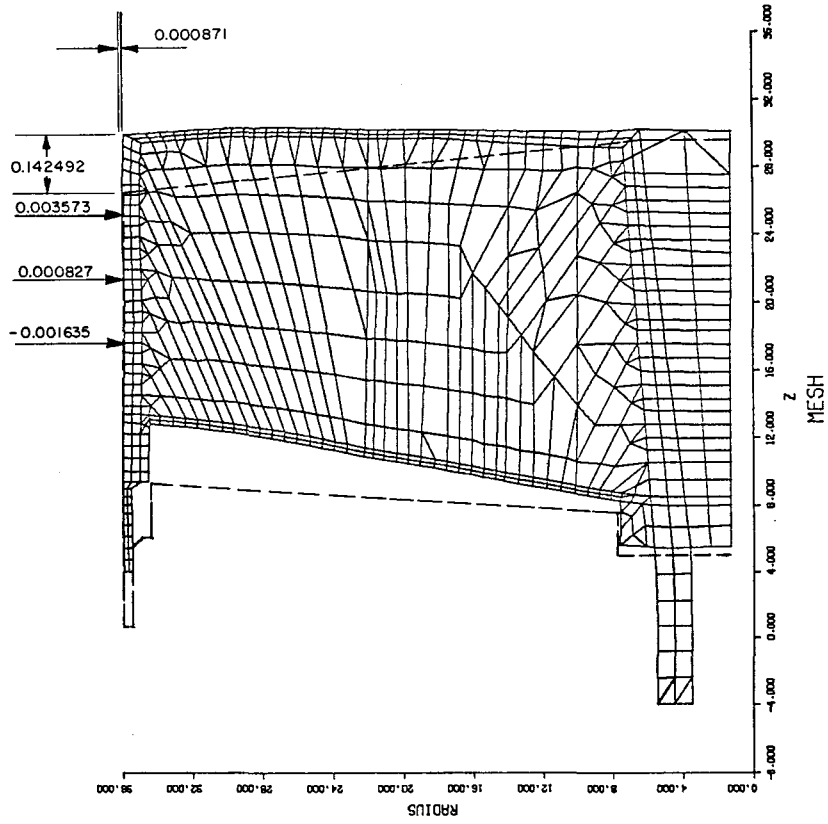

FIGURE 27. DISPLACEMENT PATTERN IN MODIFIED AND SATURATED PISTON HEAD UNDER THE ASSUMED LOADING

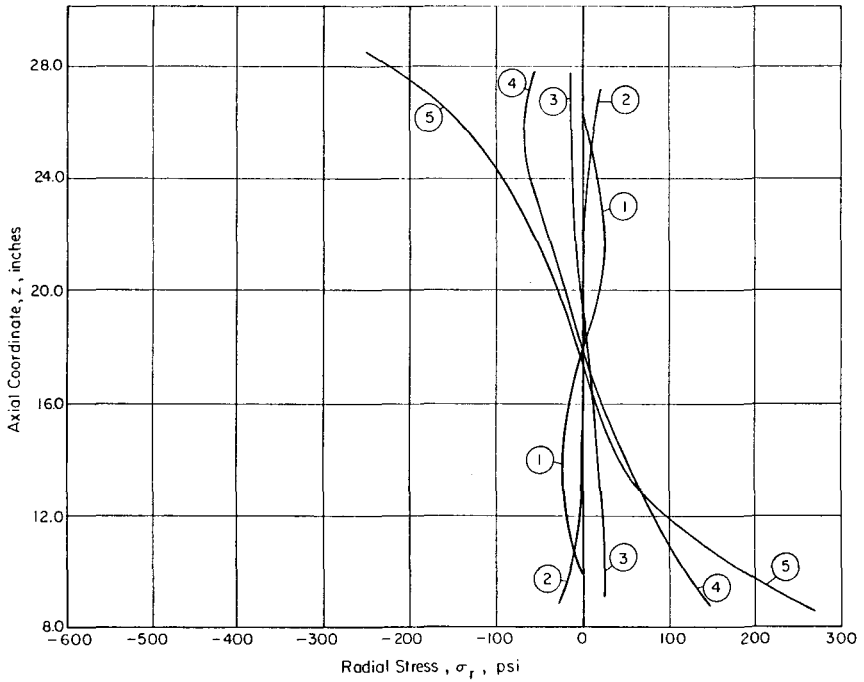

FIGURE 28. NORMAL STRESS DISTRIBUTION ALONG BONDS BETWEEN MATERIALS FOR MODIFIED AND SATURATED PISTON HEAD

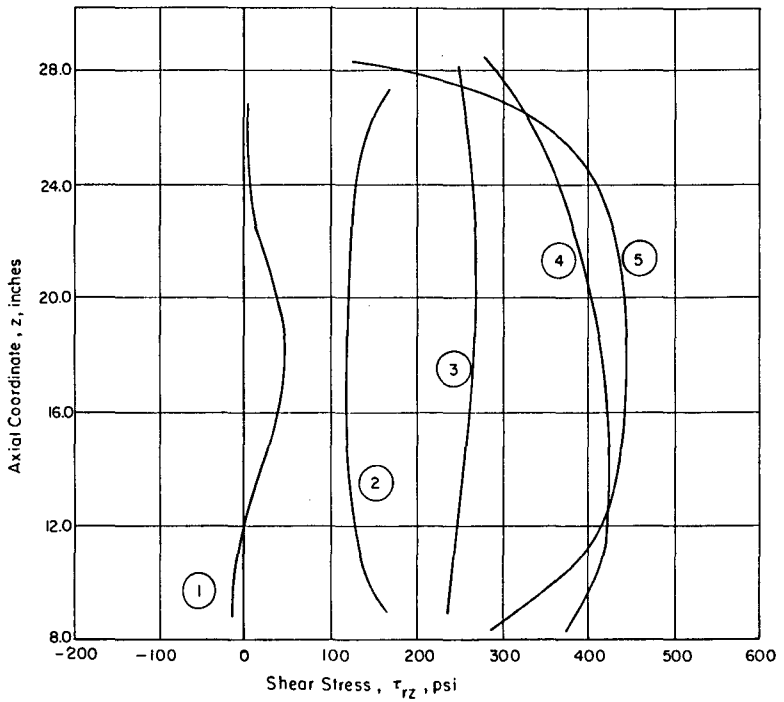

FIGURE 29. SHEAR STRESS DISTRIBUTION ALONG BONDS BETWEEN MATERIALS FOR MODIFIED AND SATURATED PISTON HEAD

TABLE 8. MAXIMUM CALCULATED STRESSES IN WOOD CORE WITH COMPARISON WITH CORRESPONDING STRENGTHS FOR THE MODIFIED-SATURATED PISTON HEAD

Material	Stress, psi	
	σ_r	τ_{rz}
Douglas Fir 34 lb/ft^3	+300 (870)	445 (1160)
Balsa 15.5 lb/ft^3	- 70 (-198)	420 (522)
Balsa 11 lb/ft^3	- 25 (-144)	270 (360)
Balsa 6 lb/ft^3	- 25 (- 84)	165 (180)

TABLE 9. EFFECTIVE STRESS IN CORE MATERIALS FOR THE MODIFIED AND SATURATED PISTON HEAD

Material	Location of Maximum Stress	Stress, psi				Effective Stress
		σ_r	σ_z	σ_θ	τ_{rz}	
Douglas Fir 34 lb/ft^3	Interface 5 @ z = 22.0"	-60	193	-26	425	0.329
Balsa 15.5 lb/ft^3	Interface 4 @ Bottom	90	-120	21	420	0.826
Balsa 11.0 lb/ft^3	Interface 3 @ z = 22.5"	5	8	-2	270	0.650
Balsa 6.0 lb/ft^3	Interface 2 @ Bottom	-25	-84	-1	165	0.830

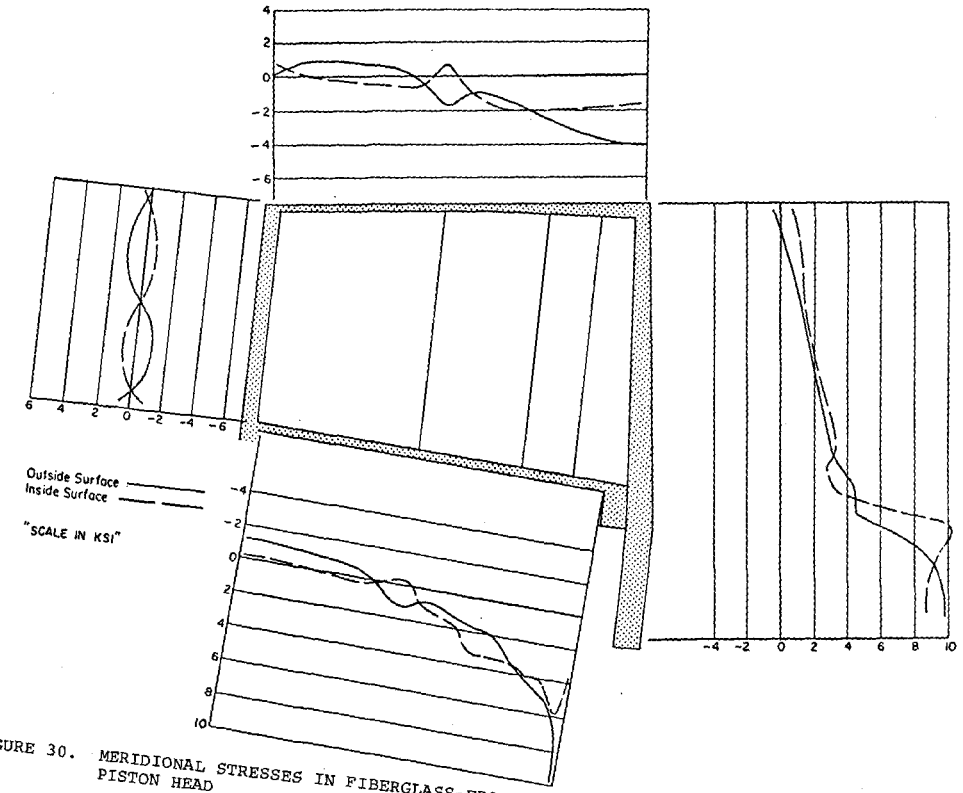

FIGURE 30. MERIDIONAL STRESSES IN FIBERGLASS-EPOXY SHELL FOR MODIFIED AND SATURATED PISTON HEAD

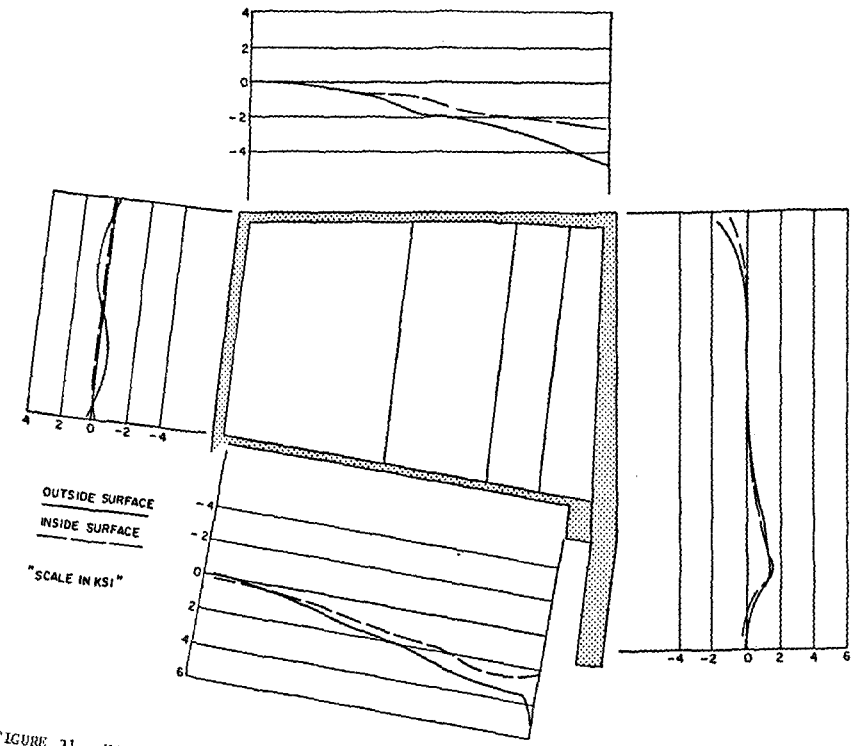

FIGURE 31. HOOP STRESSES IN FIBERGLASS-EPOXY SHELL OF MODIFIED AND SATURATED PISTON HEAD

of the material and are acceptable.

Thus the modified piston head design has been shown to be conservatively, structurally adequate.

LIP SEAL ANALYSIS

Early in 1971 NAL personnel designed a lip seal system to be employed with the piston head assembly. There were to be two lip seals; one mounted at the top and the other mounted at the bottom of the spacer ring installed between the bottom of the main chamber and the top of the "Z" section of lower chamber. Each seal consisted of a fiberglass-epoxy laminate back-up ring to which a grooved, teflon rub ring was to be bonded. These teflon surfaces were to slide on a teflon coating on the piston when the piston is in motion. The thickness of the teflon coating on the outer radial surface of the piston head is so arranged that when the chamber is cold and at the equilibrium pressure the bottom seal would just touch the piston while at the same time a slight gap would exist between the piston and the upper seal. As the piston starts its downward travel and pressure starts to build up in the lower chamber the lower lip seal would be pressure-activated to bear against the piston. This action is intended to maintain the pressure differential across this seal allowing the pressure to drop in the upper chamber and build up in the lower chamber. The upper seal is intended to act as a bubble trap and an emergency back-up for the lower seal.

The lip seals and their position in the bubble chamber are defined and shown in the following NAL drawings.

Drawing Number	Title	Revision
2621.MB-25973	30K Liter Hydrogen B. C. Piston Lip Seal	-
2621.MB-25974	30K Liter Hydrogen B. C. Upper Piston Lip Seal	-
2621.MC-25336	30K Liter Hydrogen B. C. Lip Seal Section	-

An evaluation of this seal system was carried out by Battelle. The results of this evaluation[4] predicted that the teflon on teflon sliding seal configuration would have an unacceptable wear rate and the seal system as originally defined would be inadequate from an operation life viewpoint. A basic point made in this study was that if sliding seals are to be employed, and this is a requisite design feature of this bubble chamber, then it would be advisable from the viewpoint of both heat generation and wear rate that a metallic-plastic sliding interface be achieved. Based on this finding NAL and Battelle personnel commenced an intensive effort to develop a lip seal that would incorporate a metallic rubbing surface and yet maintain the radial flexibility that is an inherent requirement for a successful lip seal configuration.

The original design specifications for the piston required that lateral guidance of the piston be accomplished by two bearings. One bearing would be in the actuator stem. The other would be in the spool piece of the lower chamber and would bear against the upper bearing sleeve of the piston stem. It was believed that such an arrangement would hold the vertical alignment of the piston and prevent any significant lateral loads from acting directly on the lip seals. However, it was found that the tolerance on the vertical misalignment of the piston center with the center-line of the lip seal rings could not be held to a difference less than 0.02 inch. Considerable effort was expended to develop a lip seal configuration that would be capable of accepting this misalignment and yet maintain the pressure differential and at the same time keep the interface pressure between the rubbing surface of the seal and the plastic coating on the piston low enough to prevent an excessive wear rate. It was determined that these requirements are mutually exclusive and can not be achieved.

This finding lead to reconsideration of the method of laterally guiding the piston. It was decided that the upper bearing, the one in the spool piece, would be removed and the lip seals themselves would act

as the upper bearings. For this system to be successful it must be shown that in order to achieve a small lateral displacement of the piston lateral forces greater than could be induced during operation must act on piston. In other words the lip seal ring must be quite stiff in this mode of displacement.

Based on the required wear characteristics as defined in Reference 4 and the decision to employ the lip seal as the upper lateral guide for the piston a new lip seal geometry was developed. This lip seal configuration is shown in Figure 32. It consists of the original fiberglass-epoxy laminate backing ring to which is inserted and bonded a berylium-copper rub ring. The piston is now coated with a layer of Rulon A instead of the teflon previously specified. Experiments conducted by NAL showed that the combination of Be-Cu sliding on Rulon A gave substantially better wear than did teflon on teflon or stainless steel on teflon or Rulon A.

Method of Analysis

The main analytic tool used to evaluate the new lip seal was Battelle's shell of revolution program MONSA-S. This program has been thoroughly described in previous reports to NAL[5] [6] and will not be further discussed here. This program is particularly applicable to the analysis of the lip seal because the lip seal is a body of revolution which can be considered a thin shell. (Because of the relatively simple input format and the short running time for this program compared,for instance, with finite element programs such as AXISOL, MONSA-S was extremely useful in the evaluation screening carried out on several other proposed lip seal configurations prior to this one.)

Three specific analyses were carried out using MONSA-S. These analyses were as follows.

Piston Following Ability

The Rulon A coating on the piston will be made as cylindrical as possible. However, there is a possibility that the coating will have ripples in its surface induced either during the manufacturing stage or

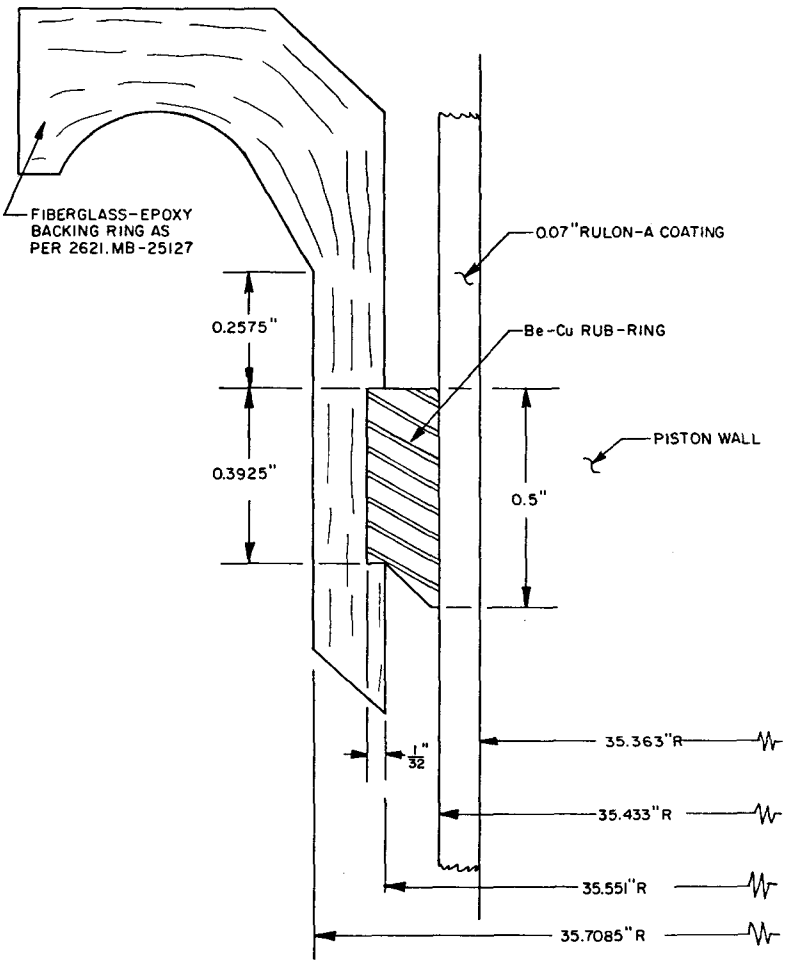

FIGURE 32. PROPOSED LOWER LIP SEAL CONFIGURATION

by non-uniform shrinkage when the piston is cooled down. This non-uniform shrinkage is sometimes a factor in composite structures with plastic constituents.

During operation, at the equilibrium pressure just before the beginning of the pulse it is intended that the lip seal rubbing surface will just be touching the Rulon A surface of the piston head. As the piston begins its downward motion and pressure starts to build up in the lower chamber the rub ring is to be forced against the plastic surface thus maintaining the pressure differential across the seal. The lip seal must have sufficient flexibility to follow the contour of the piston surface if there are ripples in it.

A model of the lip seal was generated for input to MONSA-S. This model is shown in Figure 33. The fiberglass-epoxy laminate backing ring was treated as an isotropic medium with a Youngs Modulus of 3.5×10^6 psi and a Poisson's ratio of 0.25. The rub ring, which is berylium copper, has a Youngs Modulus of 17×10^6 psi and a Poisson's ratio of 0.214. The seal is completely restrained at the top representing the clamp position in the wall of the spacer ring. The seal was loaded by the 100.0 psi pressure as shown. There is no restraint on the inward radial motion of the end of the seal. This artificial mathematical model represents the lip seal with the anticipated pressure differential acting across it but with the piston removed.

As is shown in Figure 33 the proposed lip seal configuration is quite stiff in the radial bending mode. This is due, essentially, to the presence of the 5/32 inch thick Be-Cu rub ring. Thus, theoretically, if there are depressions in the surface of the Rulon A greater than 0.005 inch from the equilibrium position of the seal then the lip seal will be incapable of following the surface at these locations and some high pressure fluid will blow by the seal.

Interface Pressure Study

The wear rate as well as the ability of the lip seal to maintain the

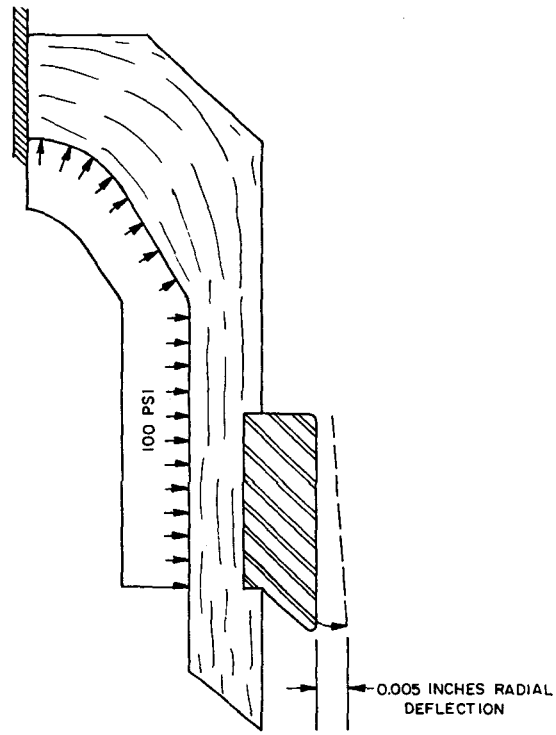

FIGURE 33. PISTON FOLLOWING MODEL OF LIP SEAL

required pressure boundary depends upon the magnitude of the interface pressure that occurs between the rub ring and the Rulon A surface. Figure 34 shows the mathematical model of the lip seal-piston surface interface when the piston is at the bottom of its stroke and with zero velocity. Because of the limitations of program MONSA-S it was necessary to model the Rulon A surface in contact with the rub ring as three separate rings. The Rulon A material was assumed to be an isotropic material with a Youngs Modulus of 1.0×10^6 psi and a Poisson's ratio of 0.5. The lip seal was restrained at the top as in the previous model. The Rulon A rings were fully restrained on their inner diameter surfaces. This location marks the interface between the 1.0 inch thick wall of the outer radial cylinder of the piston head assembly and the Rulon A coating.

The arrows shown represent the reactive forces between the Rulon A rings and the rub ring, acting on the rub ring. There is, of course, an equal and opposite set of forces acting on the Rulon A. N_θ represents a uniform circumferential line force and not a pressure and is denoted as pounds per inch of piston circumference (lb/in). Again, because of the limitations of the program these forces are not an exact representation of the pressure distribution existing at the interface. However, the following is true. Equilibrium of forces require that the sum of the forces N_θ shown equals the integration of the interface pressure over the contact surface divided by the contact length. The sum of the N_θ's equals 74.7 lb/in. The contact surface equals 0.5 inch. Thus, the average interface pressure between the rub ring and the Rulon A surface at the bottom of the stroke equals 149.4 psi. This is, of course, only the average and the actual pressure distribution would not be uniform along this length.

Additional computer runs were made to determine the effect that the friction between the two sliding surfaces would have on this interface pressure. Just before the piston reaches the bottom of its stroke

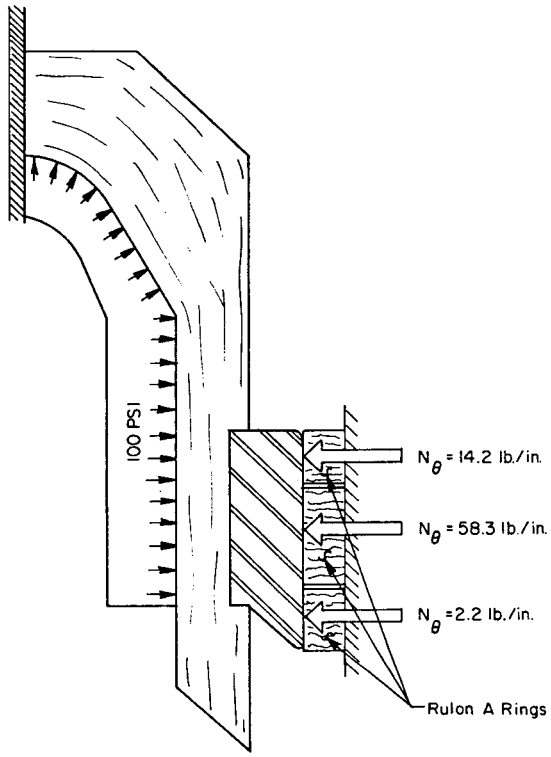

FIGURE 34. INTERFACE PRESSURE MODEL OF LIP SEAL

the pressure differential is almost completely achieved and there are friction forces acting downward on the rub ring and upward on the Rulon A surface. As the piston starts up from the bottom of its stroke the pressure differential still exists but now the relative direction of the friction forces are reversed. To carry out this study the Rulon A rings were removed from the mathematical model. They were replaced by boundary conditions which represented (1) the deflections of the Rulon A rings in the radial direction at each N_θ location, and (2) a friction force equal to 0.3 X N_θ location acting either vertically upwards or down depending upon which direction the piston was assumed to be moving. The output of each run gave a new N_θ acting at each location. These N_θ's were different from the original set. The next run consisted of changing the vertical forces to equal 0.3 times the new N_θ's. This procedure was continued until the output showed that the vertical forces assumed did approximately equal the friction coefficient times the N_θ's developed. The results of this work showed the interface pressure between the Be-Cu rub ring and the Rulon A surface was approximately 10 percent lower than that shown in Figure 34 when the piston was still moving downward at the bottom of the stroke and 10 percent higher when the piston started its upwards stroke.

Lip Seal Lateral Guide Stiffness

As discussed above the lip seal is now to be employed in a secondary role as the piston upper lateral guide. In order to determine the lip seal's lateral stiffness the nonsymmetric loading capability of program MONSA-S was used.

It was assumed that if the piston were to move over laterally it would cause the lip seal to deflect in a beam bending mode and contact it only along a line at the top of the Be-Cu rub ring and only along a 180 degree arc. The mathematical model for this study for input to MONSA-S is shown in Figure 35.

The manner in which MONSA-S analyses a nonsymmetric load problem is

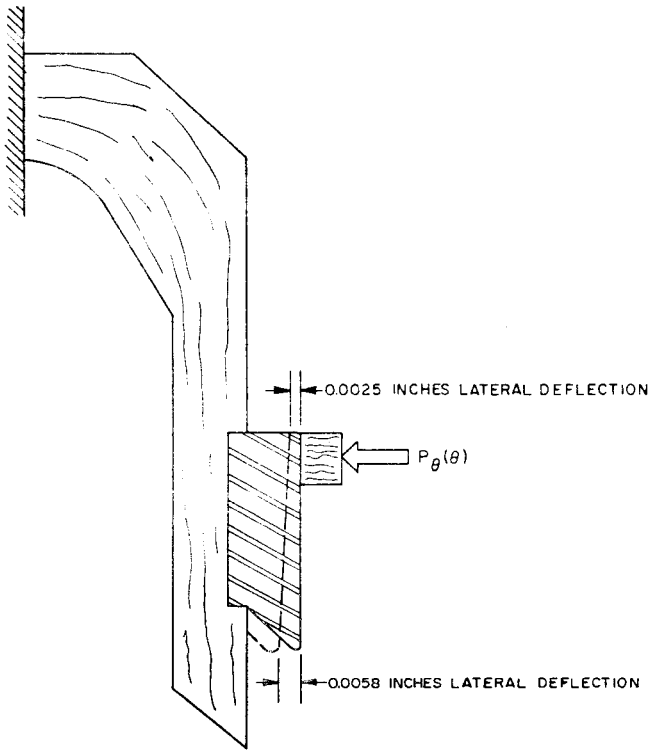

FIGURE 35. LATERAL DISPLACEMENT MODEL OF LIP SEAL

as follows. The load is broken into its cosine Fourier harmonic terms. That is, the load is considered as an infinite summation of cosine terms around the periphery of the shell. At any position θ, measured in radians from the theta equals zero position the load can be represented as:

$$P_\theta = P_O + P_1\cos(\theta) + P_2\cos(2\theta) + P_3\cos(3\theta) + \ldots\ldots$$

or

$$P_\theta = P_O + \sum_{n=1}^{N} P_n\cos(n\theta)$$

where,

$$P_O = \frac{1}{\pi}\int_o^\pi f(\theta)d\theta, \quad P_n = \frac{2}{\pi}\int_o^\pi f(\theta)\cos(n\theta)d\theta, \quad (n = 1,2,3,4,\ldots\ldots)$$

For the problem being analyzed

$f(\theta) = 100.0 \cos\theta$, lb/in $\qquad 0 \leq \theta \leq \frac{\pi}{2}$

$f(\theta) = 0.0 \qquad \frac{\pi}{2} \leq \theta \leq \pi$

where θ given in radians.

Battelle's computer program EXPAND was used to generate the harmonic terms for the cosine series representation of the load function, and the load function was plotted as a function of the number of terms of the cosine series used in the load approximation. Figure 36 shows the load function approximation using only five terms, P_O, P_1, P_2, P_4, and P_6. As can be seen from this figure these terms were sufficient to achieve a very good approximation of the complete function. For each of these P's MONSA-S calculates the shell response. A separate computer run must be made in each case. The program prints out the fundamental variables and stresses for each harmonic number as a function of the meridional generators. These quantities must be multiplied by either $\cos(n\theta)$ or $\sin(n\theta)$ to determine their values at positions other than θ = 0.0 or θ 90.0 degrees. The total shell response at any point of interest is then determined by superposition. This procedure was carried out for the model shown in Figure 35. The maximum deflection of the lip seal is shown and

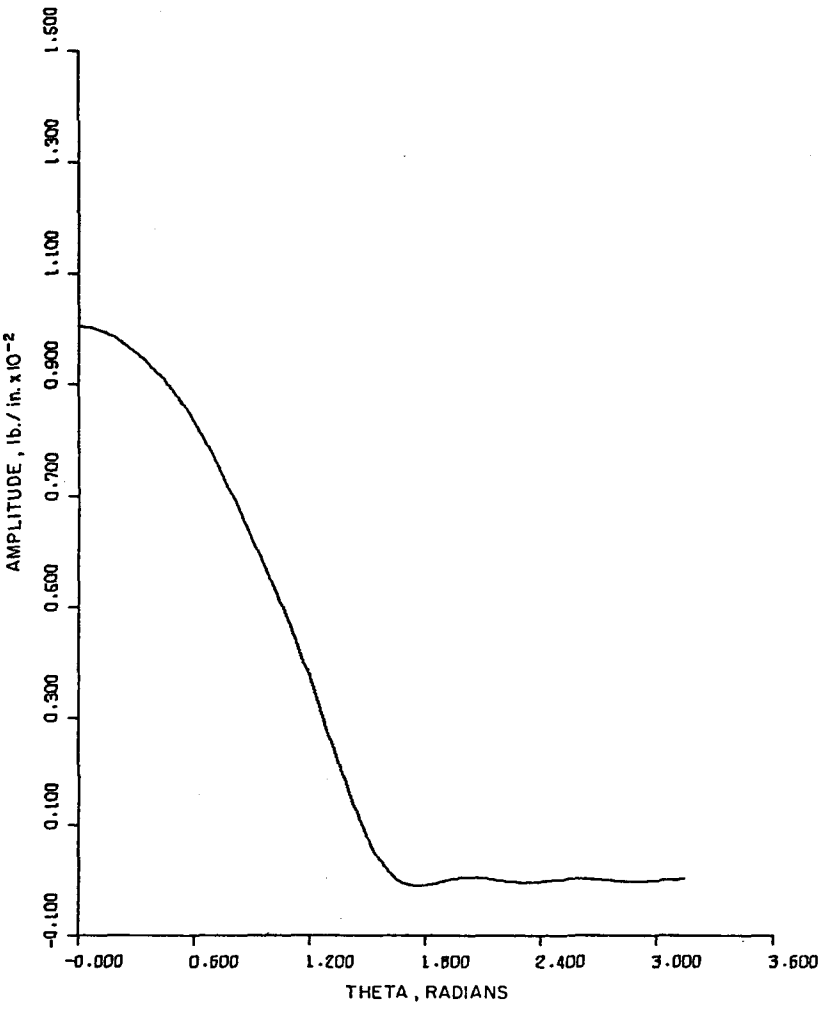

FIGURE 36. LOAD APPROXIMATION, 5 TERMS, n = 0, 1, 2, 4, AND 6

the assumption of single line contact is verified.

The total lateral load acting on the piston to achieve this deflection can be determined by taking only the force components in one direction and integrating as follows:

$$F_{lateral} = \int_0^{\pi} P(\theta) R \sin^2\theta \, d\theta$$

$$F_{lateral} = \int_0^{\pi} (100.0)(35.433)\sin^2\theta \, d\theta = 5{,}565 \text{ lb.}$$

Thus it can be seen that the lip seal does indeed form a stiff upper lateral guide having a spring stiffness equal to 2,226 lb/mil of lateral deflection.

Summary of Results

In all the studies described above the stresses induced in the fiberglass-epoxy laminate backing ring were quite small when compared to the strength of the material. Thus, from a structural viewpoint, the backing ring is quite adequate to perform its mission for an indefinitely long period. Care must be taken to insure a good bond between the Be-Cu rub ring and the backing ring. The 1/32 undercut in the backing ring does form a degree of mechanical interlock between the two components. However, the bonding agent acting between these two components should be capable of producing a bond strength in shear of at least 400 psi. This is a greater strength than will probably be required but the attainment of such a strength level increases the operational level of safety for this component.

As was shown in the first study, the piston following model, the proposed lip seal configuration has a fairly limited radial following ability. In order to ensure that no ripples in the Rulon A remain in the surface during operation it is recommended that upon initial assembly of the seal and piston the lip seal be fitted to the piston with an interference fit of approximately 5 mils on the diameter of the piston. The piston should then be cycled several times so as to wear in the Rulon

A surface and in effect achieve lap-fit mating surfaces.

The reason for the limited following ability is the stiffness of the 5/32 inch thick Be-Cu rub ring. This same stiffness however, is the primary reason why the interface pressures during operation are kept to reasonable bounds. A reduction in the thickness of this ring would increase its flexibility but would also allow an increase in the interface pressures. In addition, a reduction in the thickness of this ring would reduce the lateral spring stiffness of the lip seal. For these reasons it is not recommended that the Be-Cu ring thickness be reduced. It is recommended that the lapping procedure prescribed above be carried out. It is believed that if this is done then a good seal will be achieved.

REFERENCES

(1) "Stress Analysis Report on Chamber Expansion System for NAL 30,000 Liter Hydrogen Bubble Chamber", Report No. BR 311-23-001, submitted by the Brunswick Corporation to NAL under cover letter dated December 20, 1971.

(2) Data sheets supplied by the Balsa Ecuador Lumber Company.

(3) Wood Handbook, Agricultural Handbook No. 72, prepared by the Forest Products Laboratory, Forest Service, U. S. Department of Agriculture, (1955).

(4) Battelle Letter Report to Dr. William Fowler of NAL from W. A. Glaeser and S. S. Bupara of Battelle, dated January 27, 1972.

(5) Battelle Special Report to NAL, "A Stress Analysis of National Accelerator Laboratory's Proposed 30,000 Liter Bubble Chamber Vacuum Tank", by M. Vagins, dated October 19, 1970.

(6) Battelle Special Report to NAL, "A Stress Analysis of National Accelerator Laboratory's 30,000 Liter Capacity Bubble Chamber", by M. Vagins, R. H. Prause, and G. H. Workman.

APPENDIX A

Description of the Computer Program AXISOL

and

Stress-Strain Equations

APPENDIX A

DESCRIPTION OF THE COMPUTER PROGRAM AXISOL

The computer program AXISOL was used for the stress analysis of both the piston head and coupling. AXISOL is Battelle's version of the widely used "Wilson" program for the finite element stress analysis of axisymmetric and planar solids*. The discussion here will be limited to the basics of the finite element method. Some more specialized aspects of the computer program are described as they specifically relate to the analysis of the piston.

In applying the program AXISOL, an axisymmetric solid is modeled as an assembly of ring elements which can either be quadrilateral or triangular in cross section. It is assumed that the stress is uniform through the volume of each element, but that such stress is allowed to change from one element to the next. The elements are connected at their mutual corners, which are referred to as nodal points. Equilibrium equations in terms of the unknown displacements of these nodal points and the known element stiffnesses are formulated. In generating the equations, the element stiffnesses are calculated on the basis of the geometry of the elements and specified elastic properties. The solution of the resulting large system of linear algebraic equations describes the deformation of the finite element approximation of the continuous elastic solid.

The program AXISOL has no restriction on the geometrical shape of the solid to be analyzed. Stresses may be calculated for arbitrarily prescribed boundary deformations or boundary stresses, as well as for thermal loadings. The accuracy of the calculated stresses depends, of course, upon a suitably refined subdivision of the structure into the finite element gridwork. This subdivision is at the control of the

*Wilson, E. L.,and Jones, R. M., "Finite Element Stress Analysis of Axisymmetric Solids with Orthotropic, Temperature Dependent Material Properties", Air Force Report No. BSD-TR-67-222 (September, 1967).

analyst and is a critical step in the analysis procedure. For a complex structure, as represented in the current study of the piston configuration, a compromise is always required to obtain reasonable engineering accuracy within cost limitations. The costs involve both the effort in manpower to develop the mathematical model, and the subsequent computer running times.

AXISOL provides extensive output on calculated displacements and stresses, which represent an approximation to the theory of elasticity solution to the problem. Stresses include the components with respect to the coordinate axes, the components as resolved along the sides of the elements, principal stresses, and maximum shear stresses. Graphical output is provided as computer plots of the finite element gridwork, both as prescribed and as deformed by the acting loads.

STRESS-STRAIN EQUATIONS

Some changes in the program AXISOL were required to analyze the anisotropic epoxy-fiber material, and the various grades of balsa and douglas fir. The existing version of the program could treat only isotropic materials and a very specialized form of anisotropic material.

The required elastic stress strain relationship was of the matrix form

$$\{\varepsilon\} = [C]\{\sigma\} ,$$

where

$$\{\varepsilon\} = \begin{Bmatrix} \varepsilon_r \\ \varepsilon_z \\ \varepsilon_\theta \\ \gamma_{rz} \end{Bmatrix} ,$$

$$\{\sigma\} = \begin{Bmatrix} \sigma_r \\ \sigma_z \\ \sigma_\theta \\ \tau_{rz} \end{Bmatrix} ,$$

and [C] is a 4x4 material compliance matrix. The column matrixes give the stresses and strains in the cylindrical r, z, θ coordinate system. For axisymmetric deformations the shear stress components $\tau_{r\theta}$ and $\tau_{z\theta}$ are zero, and are omitted from the formulation. In the specialized case where the principal material directions align with the coordinate axes, the matrix [C] is given by

$$[C]= \begin{bmatrix} \frac{1}{E_r} & -\frac{\nu_{rz}}{E_z} & -\frac{\nu_{r\theta}}{E_\theta} & 0 \\ & \frac{1}{E_z} & -\frac{\nu_{z\theta}}{E_\theta} & 0 \\ \text{SYM.} & & \frac{1}{E_\theta} & 0 \\ & & & G_{rz} \end{bmatrix}$$

where SYM. indicates that the matrix is symmetric. The E's and ν's in the above expression can be recognized as the various Young's moduli and Poisson's ratios that describe the anisotropic material.

The relationship for the stresses in terms of the strains is simply

$$\{\sigma\} = [C]^{-1}\{\varepsilon\}$$

where $[C]^{-1}$ is the matrix inverse of [C]. AXISOL performs the inverse numerically, so there was no need to have an explicit expression for $[C]^{-1}$ in terms of the E's and ν's.

In the piston head, the epoxy material has fiber orientations which do not align with the coordinate axes. To allow for this, the program AXISOL was modified. The matrix $[C]^{-1}$ was first generated for the material directions, and then transformed to rotate the properties to the directions of the coordinate axes. The required transformation is given by Wilson* in the following matrix form

*Ibid

$$[C]^{-1} = [a]^T [C']^{-1}[a],$$

where

$$[a] = \begin{bmatrix} \cos^2\beta & \sin^2\beta & 0 & \sin\beta\cos\beta \\ \sin^2\beta & \cos^2\beta & 0 & -\sin\beta\cos\beta \\ 0 & 0 & 1 & 0 \\ -2\sin\beta\cos\beta & 2\sin\beta\cos\beta & 0 & \cos^2\beta-\sin^2\beta \end{bmatrix}$$

Here the matrix $[C']^{-1}$ represents the material stiffness matrix with respect to a coordinate system orientated at an angle β with respect to the (r,z) axes. The matrix $[C]^{-1}$ is the desired material stiffness matrix for the (r,z,θ) coordinate system, and $[a]^T$ is the transpose of the matrix [a]. Prior to analysis of the piston head, the above transformation equations were coded into the computer program AXISOL.

IV. EQUIPMENT

G. Piston

3. STRESS ANALYSIS REPORT ON CHAMBER EXPANSION PISTON

Prepared by

G. Vames
Brunswick Corp.

TABLE OF CONTENTS

IV. EQUIPMENT

G. Piston

3. STRESS ANALYSIS REPORT ON CHAMBER EXPANSION PISTON

IV. G. 3. STRESS ANALYSIS REPORT ON CHAMBER EXPANSION PISTON

(1) INTRODUCTION

This report is intended to verify the structural adequacy of the CHAMBER EXPANSION PISTON ASSEMBLY for the NAL 30,000 liter hydrogen bubble chamber, as defined by Brunswick Drawing BD0311001, for the structural loading specified by National Accelerator Laboratory Specification No. 2621-ES-7012.

(2) SUMMARY OF MINIMUM MARGINS OF SAFETY

Piston Head:		
	Laminate Facings	+2.38
	Wood Core	+0.18
Upper Bearing		+1.66
Piston Rod		high
Attach Fitting		+0.55
Attach Ftg/Piston Rod Interface		+0.67
Piston Skirt		high

(3) DESCRIPTION OF STRUCTURE

The structure analyzed herein is a cryogenic Piston Assembly as defined by Brunswick Drawing BD0311001. The assembly consists of a piston head and skirt, piston rod, upper and lower bearings, and attach fitting. The materials used in the assembly are epoxy laminate, steel and wood.

The piston head is a composite sandwich construction consisting of an outer shell of glass fabric reinforced epoxy laminate integrally bonded to a laminated wood core of end-grain balsa and fir. The diameter of the piston head is 70.865 inches, while its depth varies from approximately 22 inches at the center to approximately 17 inches at its outer periphery. A cylindrical skirt (also glass fabric laminate)

attaches to the outer periphery of the piston head, resulting in a total length of 65 inches from the upper face of the piston to the bottom of the skirt.

The upper face of the piston outer shell is a continuous extension of the piston rod and varies in thickness from 1.0 inch at the rod to 0.50 inch constant outside a 36.0 inch diameter center area. The lower face of the piston shell is a constant thickness of 0.50 inches, and the outer cylindrical surface of the piston head shell is a constant thickness of 1.0 inches. The cylindrical skirt tapers in thickness from 0.50 inch at its upper end to 0.375 inch at its bottom edge. An inner liner of balsa wood (0.50 inch thick) is bonded to the inner surface of the cylinder for thermal insulation.

The piston rod is also glass fabric reinforced epoxy laminate and has an outside diameter of 11 inches and an inside diameter of 7 inches. The rod extends through the piston head where its core is filled by a tapered solid laminate plug. The steel attach fitting is inbedded in the lower portion of the piston rod and protrudes 15.5 inches below the rod giving an overall assembly length of 96 inches. The upper and lower bearings are steel cylinders which encase the piston rod and are 16.5 and 21.0 inches in length respectively. The basic components of the assembly are illustrated in Figure 1.

The epoxy laminate materials employed consist of Epon 828 epoxy resin reinforced with fiberglass cloth. The piston head and skirt are laminatedusing a bi-directional (style 181 or equivalent) glass fabric whereas the piston rod employs a highly directional (style 143 or equivalent) glass fabric to maximize its extensional stiffness.

The piston core is a laminated wood assembly comprised of several densities of end grain balsa and douglas fir bonded with resorcinol adhesive. The centermost portion of the core, adjacent to the piston stem, is laminated using a 34 pcf density fir. Succeeding adjacent sections of the core, moving outward radially, employ 15.5, 11.0, and 6.0 pcf densities of end grain balsa.

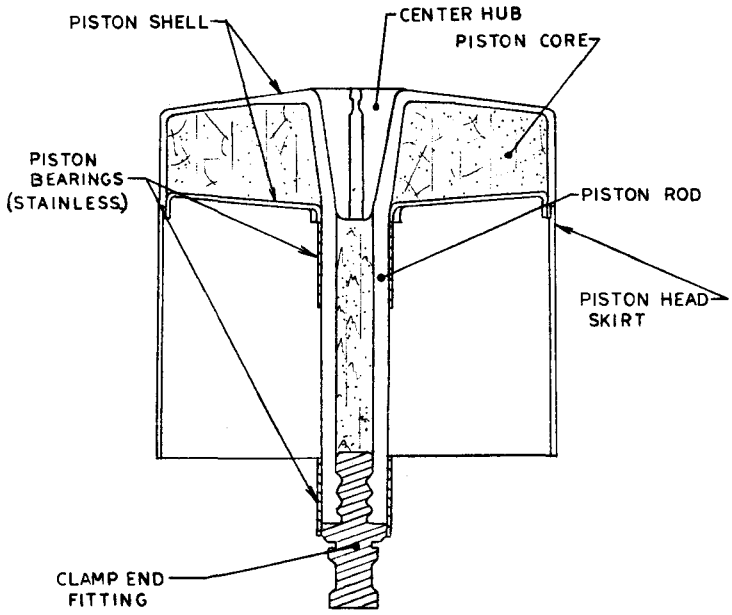

FIGURE 1. BASIC STRUCTURAL COMPONENTS

(4) LOADING CONDITIONS

4.1 Thermal

The chamber piston operates in a liquid hydrogen or liquid neon environment and thus operates at a constant temperature of 21°K or 35°K depending on which chamber filling liquid is employed. However, the lower end of the piston rod, the lower sleeve bearing, and the clamp-end and fitting are maintained at 70°F. A maximum temperature differential of approximately -495°F (room temperature to liquid hydrogen temperature) is employed herein for analysis purposes.

4.2 Cyclic Loads

The piston must withstand 10,000,000 cycles of expansion and recompression of the chamber filling liquid. During displacement the chamber piston lowers the pressure of the chamber filling liquid, while slightly increasing the pressure of the gas buffer. The maximum created pressure difference is 120 psi.

Typical displacement vs time diagrams for the piston for both liquid hydrogen and liquid neon are depicted in the following sketch:

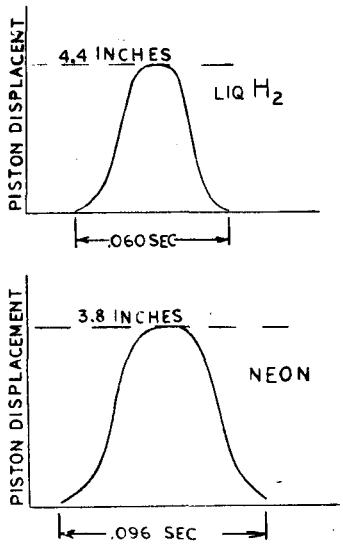

The piston displacement creates similar shaped pressure pulses acting across the piston head which interact with sizable inertia forces produced in the piston assembly. The tension in the piston rod resulting from the interaction of the pressure and inertia loading was determined by NAL computer analysis and is presented in the following diagrams for both liquid H_2 and liquid neon environments:

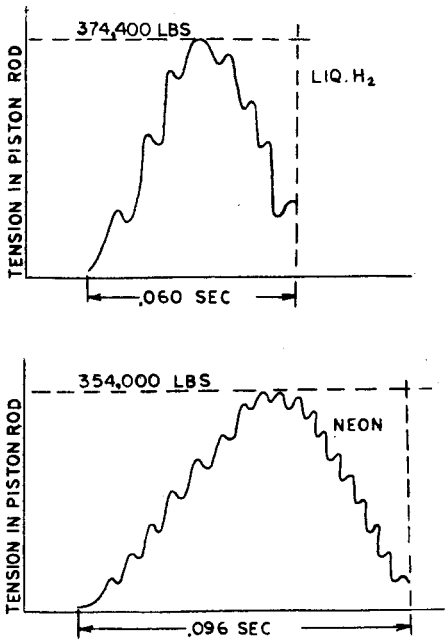

The maximum values of 374,400 lbs for liquid H_2 and 354,000 lbs for liquid neon are employed herein to compute peak stress values.

4.3 Static Loads

Due to proof test requirements, the piston assembly must be capable of withstanding (1) a static pressure of 300 psi from all sides and (2) a static pressure of 150 psi applied only underneath the piston head (i.e., piston rod side). This pressure results in a stem tensile load of approximately 574,000 pounds.

(5) GENERAL ANALYSIS APPROACH

Stress calculations and margins of safety are presented herein for the specified cyclic and thermal loads. Calculations for the specified static test loads are omitted since the stresses and margins of safety for the cyclic loads are in all instances more severe (i.e., the ratio of static to peak cyclic load is approximately 1.53, while the corresponding ratio of static to cyclic strength is approximately 1.80).

Margins of safety for the cyclic loads are calculated by comparing the peak load stresses to the material fatigue allowables for 10,000,000 cycles shown in Section 9.1. The thermal stresses are compared to static material strengths since the number of cool-down/warm-up cycles is small.

(6) STRESS AND MARGINS OF SAFETY

6.1 Piston Head

The maximum stresses in the piston head occur at the head/hub interface. The mechanical stresses at this point are calculated by treating the head as an annular plate fixed at the hub. The thermal stresses are calculated by treating the piston rod hub as a solid grp cylinder with an outer cylindrical shell of the wood core material.

Mechanical Stresses

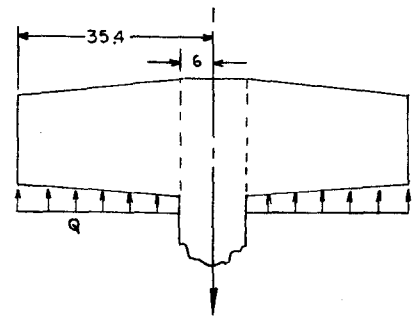

P = 374,400 lbs

$$Q = \frac{P}{A} = \frac{374,400}{\pi[(35.4)^2-(6)^2]} = 97.9 \text{ psi}$$

The maximum internal loads for a plate fixed at R=6 are given by:

$$M_{max} = \frac{\beta Q R^2}{6} = \frac{4.2(97.9)(35.4)^2}{6} = 85{,}900 \text{ in-lbs}$$

$$V_{max} = \frac{P}{2\pi R} = \frac{374{,}400}{2\pi(6)} = 9{,}930 \text{ lbs/in}$$

The section properties at R = 6 are shown below:

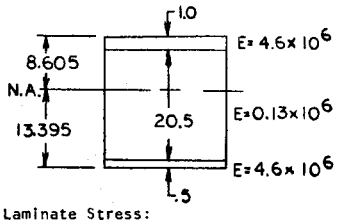

$EI = 814 \times 10^6$ lb-in^2/in

$EQ_{NA} = 41.0 \times 10^6$ lb-in/in

$EQ = 30.2 \times 10^6$ lb-in/in (lower interface)

Laminate Stress:

$$f_{b_{max}} = \frac{E\,Mc}{EI} = \frac{4.6 \times 10^6 (85{,}900)(13.395)}{814 \times 10^6} = 6{,}500 \text{ psi (tension)}$$

Core Stresses (34 pcf wood):

$$f_{b_{max}} = \frac{E\,Mc}{EI} = \frac{0.13 \times 10^6 (85{,}900)(12.895)}{814 \times 10^6} = 177 \text{ psi (tension)}$$

$$f_{b_{max}} = \frac{E\,Mc}{EI} = \frac{0.13 \times 10^6 (85{,}900)(7.605)}{814 \times 10^6} = 104 \text{ psi (compression)}$$

$$f_s = \frac{VEQ}{EI} = \frac{9930(41.0 \times 10^6)}{814 \times 10^6} = 500 \text{ psi (at neutral axis)}$$

$$f_s = \frac{VEQ}{EI} = \frac{9930(30.2 \times 10^6)}{814 \times 10^6} = 368 \text{ psi (at lower interface)}$$

Thermal Stresses

The thermal stress model is shown below:

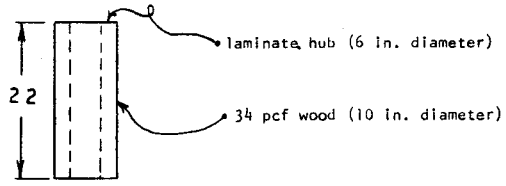

1. Laminate: $E = 4.6 \times 10^6$ psi ; $A = 113$ in^2; $\varepsilon = -.00200$ in/in (R.T. to -420°F)

2. 34 pcf Wood: $E = 2.6 \times 10^6$ psi; $A = 201$ in^2; $\varepsilon = -.00075$ in/in (R.T. to -423°F)

The differential strain of .00125 in/in produces a tensile load in the laminate and an equal and opposite compressive load in the wood.

$$\Delta\varepsilon = \frac{P}{EA_1} + \frac{P}{EA_2} \quad \text{or} \quad P = 325{,}000 \text{ lbs}$$

$$f_1 = \frac{P}{A_1} = \frac{326{,}000}{113} = 2{,}880 \text{ psi (tension in laminate)}$$

$$f_2 = \frac{P}{A_2} = \frac{326{,}000}{201} = 1{,}620 \text{ psi (compression in wood)}$$

The margins of safety are calculated below for the combined thermal and mechanical stresses.

34 psf wood core

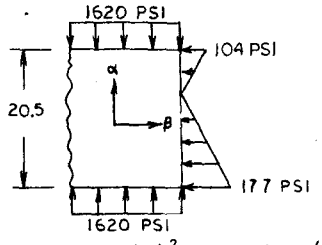

$F_\alpha = 8690$ psi (cycle compression)

$F_\beta = 478$ psi (cycle tension)

$F_{\alpha\beta} = 721$ psi (cycle shear)

$$R = \left(\frac{f_\alpha}{F_\alpha}\right)^2 - \left(\frac{f_\alpha f_\beta}{F_\alpha F_\beta}\right) + \left(\frac{f_\beta}{F_\beta}\right)^2 + \left(\frac{f_{\alpha\beta}}{F_{\alpha\beta}}\right)^2$$

At N.A. $f_\alpha = -1620$ psi; $f_\beta = 0$; $f_{\alpha\beta} = 500$ psi

$$R = \left(\frac{1620}{8690}\right)^2 + \left(\frac{500}{721}\right)^2 = .516$$

At Lower Interface $f_\alpha = -1620$ psi; $f_\beta = 177$ psi; $f_{\alpha\beta} = 368$ psi

$$R = \left(\frac{1620}{8690}\right)^2 - \frac{-1620(177)}{8690(478)} + \left(\frac{177}{478}\right)^2 + \left(\frac{368}{721}\right)^2 = .501$$

The minimum margin of safety for the 34 pcf wood core is:

$$M.S. = \frac{1}{\sqrt{.516}} - 1 = \underline{+ 0.39}$$

The cyclic tensile strength of the piston head and plug laminate (181) at -423°F is 22,000 psi. The margins of safety are shown below:

$$\text{Piston Head Laminate} \quad M.S. = \frac{22,000}{6,500} - 1 = \underline{+ 2.38}$$

$$\text{Plug Laminate} \quad M.S. = \frac{22,000}{2,880} - 1 = \underline{\text{High}}$$

The shear stresses in the lower density wooden core are shown below. The axial stresses are negligible since the internal bending load drops radically with increasing radius and decreasing core modulus.

$$V = \frac{QA}{C} = \frac{97.9[(35.4)^2 - R^2]}{2R}$$

$f_s = \frac{V}{d}$ where d = distance from centroid of top skin to centroid of bottom skin.

Density	R_{min}	V	d	f_s	F_s^*	M.S.
15.5	10	5644	20.5	275	324	+0.18
11.0	14	3696	20.0	185	224	+0.21
6.0	22	1711	18.8	91	112	+0.23

* Cyclic -423°F strengths

A Teflon seal is bonded to the outer periphery of the piston head. The thermal stresses and margin of safety for this interface are shown below.

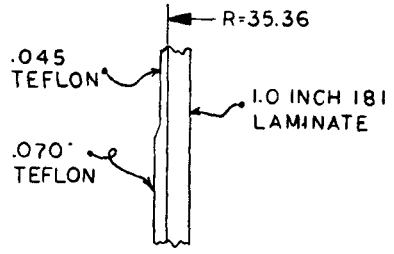

Teflon $E = 1.2 \times 10^6$

$\varepsilon = -.0090$

Laminate $E = 4.6 \times 10^6$

$\varepsilon = -.0020$

$\Delta\varepsilon = 7000 \times 10^{-6}$

0.045 Teflon $\quad Et = 1.2 \times 10^6 (.045) = .054 \times 10^6$ lbs/in

0.070 Teflon $\quad Et = 1.2 \times 10^6 (.070) = .084 \times 10^6$ lbs/in

1.00 Laminate $\quad Et = 4.6 \times 10^6 (1) = 4.6 \times 10^6$ lbs/in

$$P_i = \Delta\varepsilon \frac{(Et_1)(Et_2)}{Et_1 + Et_2}$$

$$P_{.045} = 7000 \frac{.054(4.6)}{.054+4.6} = 374 \text{ lbs/in}; \quad f_{.045} = \frac{374}{.045} = 8310 \text{ psi (tension)}$$

$$P_{.070} = 7000 \frac{.084(4.6)}{.084+4.6} = 577 \text{ lbs/in}; \quad f_{.070} = \frac{577}{.070} = 8240 \text{ psi (tension)}$$

$$\text{Teflon M.S.} = \frac{85,000}{8,310} - 1 = \underline{\text{High}}$$

6.2 Piston Rod and Upper Bearing

The piston rod transmits the cyclic load of 374,000 pounds between the piston head and the lower attach fitting. A steel bearing (sleeve) fits over the piston rod just below the piston head and is attached by six, 3/8 inch steel bolts. These parts operate at cryogenic temperatures. The bolt and rod margins of safety are calculated below.

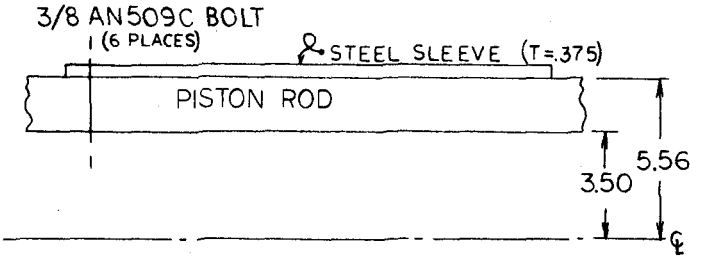

The thermal contraction of the piston rod is slightly greater than that of the steel sleeve; therefore no thermal stresses result. The maximum inertia load experienced by the assembly is approximately 100 g's. For the sleeve weight of 63 pounds the bolt shear load is:

$$P = \frac{Wg}{N} = \frac{63(100)}{6} = 1050 \quad \text{lbs per bolt}$$

The minimum single shear strength of each bolt is 5010 pounds at room temperature and 6810 pounds at -423°F. Using the unnotched fatigue strength factor for 10^7 cycles at -423°F of 41 percent results in the following bolt margin of safety.

$$M.S. = \frac{6810(.41)}{1050} - 1 = \underline{\underline{+ 1.66}}$$

The basic piston rod outside diameter is 11 inches and inside diameter is 7 inches. The resulting cyclic stress and margin of safety are calculated below for the 143 laminate construction.

$$f_t = \frac{P}{A} = \frac{374,400}{\pi/4[(11)^2-(7)^2]} = 6,620 \text{ psi}$$

$$M.S. = \frac{41,600}{6,620} - 1 = \underline{\underline{High}}$$

6.3 Lower Bearing and Attach Fitting

The attach fitting is fabricated into the lower end of the piston road and becomes an integral part of the rod. The lower bearing (sleeve) fits over the piston at this point and is bonded to the rod over 12 inches of its length. This end of the assembly operates at room temperature.

The maximum stress in the attach fitting below the piston rod occurs at the minimum cross-section where the outer diameter is 6 inches and the inner diameter is 0.75 inches.

$$f_t = \frac{P}{A} = \frac{374,400}{\pi/4[(6)^2-(.75)^2]} = 13,500 \text{ psi}$$

$$\text{R.T. Cyclic } M.S. = \frac{21,000}{13,500} - 1 = \underline{\underline{+ 0.55}}$$

The lower piston rod/attach fitting geometry is shown below.

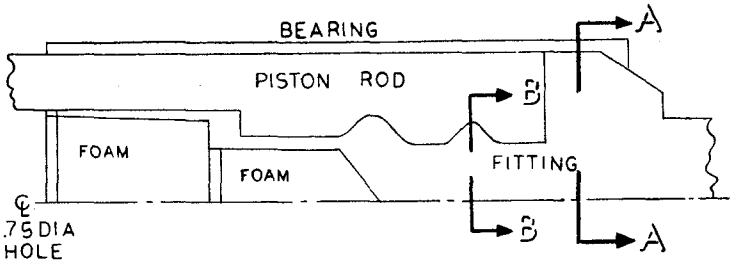

The joint will be conservatively analysed by assuming that the load in the bearing shears into the laminate and that the load in the fitting is transferred by compression at the nodes.

At A-A

$$A_{brg} = \pi/4\ [(11.81)^2-(11)^2] = 14.5\ in^2$$

$$A_{ftg} = \pi/4\ [(11)^2 - (.75)^2] = 94.6\ in^2$$

$$P_{brg} = \frac{374,400(14.5)}{14.5 + 94.6} = 49,800\ lbs$$

$$P_{ftg} = \frac{374,400(94.6)}{14.5 + 94.6} = 324,600\ lbs$$

The bearing bonded length is 12 inches resulting in an average shear stress between the bearing and piston rod of:

$$f_s = \frac{P}{A} = \frac{49,800}{\pi(11)(12)} = 120\ psi$$

$$M.S. = \frac{2680}{120} - 1 = \underline{High}$$

At B-B

Conservatively assume that 2/3 of the fitting load is reacted at the smallest node.

$$f_c = \frac{P}{A} = \frac{216,400}{\pi/4[(6.15)^2-(4.35)^2]} = 14,600\ psi$$

$$M.S. = \frac{24,400}{14,600} - 1 = \underline{+ 0.67}$$

The lower fitting operates at room temperature therefore no thermally induced stresses are present.

6.4 Piston Skirt

The piston skirt is bonded and bolted to the piston head by 55, 5/16 inch bolts. Assuming bond failure, the load per bolt is calculated below for 100 G's, 299 pounds.

$$P = \frac{100(299)}{55} = 544\ pounds$$

For the room temperature strength of 3910 pounds, a high margin of safety exists.

The piston assembly is subjected to a cyclic longitudinal load input of approximately 100 G's with a frequency of 160 cps. The natural frequency of the skirt is difficult to predict due to its tapering thickness. Therefore, to be conservative it is shown that the stress produced by resonance will be rapidly damped out before reaching a magnitude that approaches the endurance limit stress of the material.

Applied stress: $f = \frac{WG}{A} = \frac{299(100}{\pi(70.7)(.5)} = 269$ psi

Strain energy input: $SE = \frac{f^2}{2E} = \frac{(269)^2}{2(4.6 \times 10^6)} = .00787$ in-lbs/in^3

The damped energy per cycle for epoxy laminates is approximately 2.0 in-lbs/in^3 at the endurance limit of the material. Therefore, it is obvious that equilibrium between the input and the damped strain energy will occur at a small percentage of the endurance limit stress of the material.

(7) STIFFNESS CALCULATIONS

The overall spring constant of the piston assembly is calculated below. The contribution of the outer shell and wood core of the piston head is neglected in this calculation. The rod is divided into 19 elements starting at the bottom and the average diameter of each element is used.

	E-psi x 10^{-6}	
Material	RT	-423°F
143	5.1	6.7
181	3.5	4.6
Steel	27	29

Elem. No.	Temp. °F	Length Inches	143 OD	143 ID	181 OD	181 ID	Steel OD	Steel ID	EA lbsx10^{-6}	L/EA in/lbsx10^{-6}
1	R.T	2.2					9.0	.75	1706	
2	R.T	5.0					6.0	.75	751	
3	R.T	2.1					8.0	.75	1345	
4	R.T	2.0					6.0	.75	751	
5	R.T	1.2					9.0	.75	1706	
6	R.T	3.0					11.8	.75	2941	
7	R.T	7.0	11.0	5.0			11.8	11.0		
7	R.T						5.0	.75	1290	
8	R.T	5.0	11.0	5.0			11.8	11.0		
8	R.T						5.0	4.0	962	
9	-423	6.0	11.0	7.0			7.0	6.0	685	
10	-423	2.5	11.0	7.0					379	
11	-423	16.5	11.12	7.0			11.87	11.12	799	
12	-423	3.0			15.0	2.5			790	
13	-423	3.0			11.7	2.5			472	
14	-423	3.0			12.2	2.5			515	
15	-423	3.0			12.7	2.5			560	
16	-423	3.0			13.2	2.5			607	
17	-423	3.0			13.7	2.5			656	
18	-423	3.0			14.2	2.5			706	
19	-423	3.5			14.7	2.5			758	
Σ		96.0								.1504

$$\text{Spring Constant} = \frac{1}{.1504 \times 10^{-6}} = 6.65 \times 10^{6} \text{ lbs/in}$$

(8) CONCLUSIONS

The analyses of loads, stresses, deflections, and material strengths presented herein have demonstrated the structural adequacy of the chamber expansion piston assembly, as defined by Brunswick Drawing BD0311001, for the critical loading conditions defined by NAL Specification No. 2621-ES-7012. A summary of minimum margins of safety is presented in Section 2.

(9) APPENDICES

9.1 Material Properties

The following strength properties were taken from ML-TDR 64-280, Cryogenic Materials Data Handbook, AFSC, Wright-Patterson Air Force Base, dated August 1964 and from Forest Products Laboratory technical article entitled Wood at Low Temperatures, reprinted from the September 1954 issue of "Modern Packaging", Modern Packaging Corp., 575 Madison

Ave., New York 22, N.Y.

The cyclic strength data are based on notched fatique tests for 10^7 cycles.

Material	ROOM TEMPERATURE STRENGTH - psi									
	Static					Cyclic				
	Parallel		Perpendicular			Parallel		Perpendicular		
	Ten.	Comp.	Ten.	Comp.	Shear	Ten.	Comp.	Ten.	Comp.	Shear
181	40,000	43,000	37,700	36,500	5010	17,000	18,300	16,000	15,500	2130
143	75,600	57,300	9,070	25,100	6310	32,100	24,400	3850	10,700	2680
Steel	110,000	--	--	--	--	21,000	--	--	--	--
6# balsa	1375	500	112	80	180	756	275	62	44	99
11# balsa	3050	1450	170	144	360	1680	798	94	79	198
15.5# balsa	4525	2310	230	198	522	2490	1270	126	109	287
34# fir	7800	7430	340	870	1160	4290	4090	187	478	638
	-423°F STRENGTH - psi									
181	97,000	109,000	91,400	92,500	12,100	22,000	24,700	20,700	21,000	2740
143	183,300	145,200	22,000	63,600	15,300	41,600	32,900	4,990	14,400	3470
Steel	150,000	--	--	--	--	16,000	--	--	--	--
6# balsa	2300	1000	187	240	203	1260	550	103	132	112
11# balsa	5090	2900	284	432	407	2800	1600	156	238	224
15.5# balsa	7560	4610	384	594	590	4160	2540	211	327	324
34# fir	20,000	15,800	870	3710	1310	11,000	8690	478	2040	721

Material	E - psi x 10^{-6}				ϵ - in/in	
	R.T.		-423F		RT to -423F	
	∥	⊥	∥	⊥	∥	⊥
18l	3.5	3.5	4.6	4.6	-.0020	-.0020
1#3	5.1	2.2	6.7	2.9	-.0020	-.0030
Steel	27.0	27.0	30.0	30.0	-.0029	-.0029
6# balsa	.33	.016	.50	.023	-.0010	-.0040
11# balsa	.77	.037	1.13	.054	-.00090	-.0046
15.5# balsa	1.16	.056	1.70	.082	-.00091	-.0052
34# fir	1.75	.085	2.6	.13	-.00075	-.0075

9.2 Symbols

A - area
C - circumference
c - distance from neutral axis
d - depth
E - modulus of elasticity
F - material strength
f - applied stress
I - area moment of inertia
L - length
M - moment
M.S.- margin of safety
N.A.- neutral axis
P - load
Q - pressure, or first moment of area
R - radius, or interaction factor
RT - room temperature
SE - strain energy
V - shear
ϵ - strain

Subscripts:

eq - equivalent
b - bending
s - shear

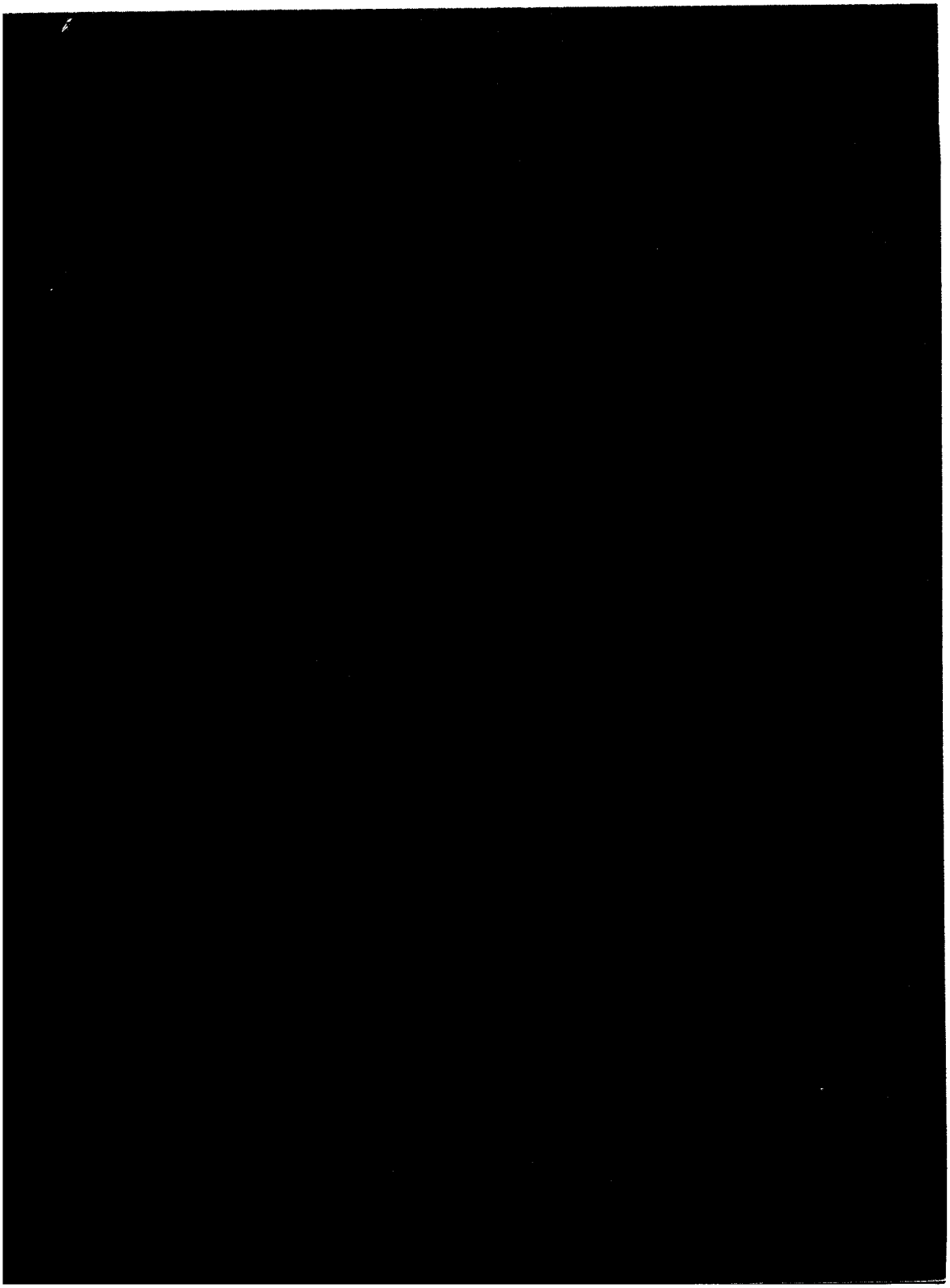

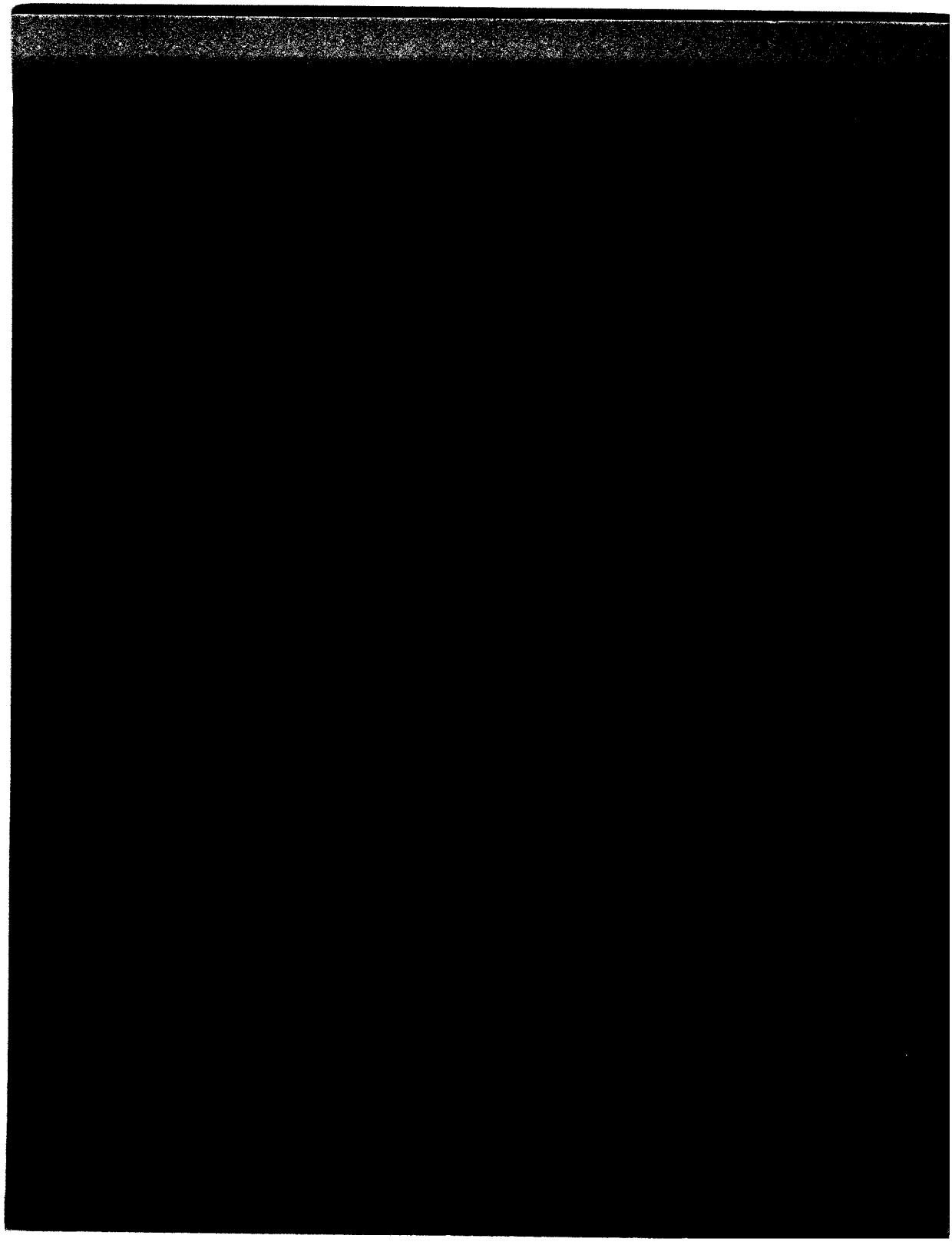

IV. EQUIPMENT

H. Failure Mode Analysis: PISTON AND SEALS

Prepared by

F.R.Huson

IV. H. Failure Mode Analysis: PISTON AND SEALS

The piston region has 3 dynamic seals and 3 emergency seals between the chamber field and atmosphere (see drawing No. 2621.MD-25378 and No. 2621.ME-25534) and a hydrogen detector near the seals at the end of the rod. The 2 pressure actuated emergency seals will have local controls at the chamber and remote controls.

Piston Out of Alignment

Should the piston pulse while it is misaligned horizontally more than .100 inches the A286 sleeve will ride on the aluminum-bronze seal mounts and the rod guide. This could result in either galling and/or aluminum-bronze particles attached to the sleeve and thus damaging the 3 dynamic seals. Chamber gas could leak past the damaged seals and, if so, would be detected by the hydrogen detector under the chamber. To stop this leak we have the 3 emergency seals.

Sleeve Becomes Free from Rod

Should the sleeve become detached from the rod, chamber gas will leak by the interior of the sleeve and be detected by the hydrogen detector under the chamber. To stop the leak the piston will be lowered, closing the emergency seal at the top of the rod guide.

Rod or Piston Head Breaks

If the fiberglass rod or piston head breaks, the expansion system will overexpand (larger stroke); however, the seals remain engaged on the sleeve and there is no leak to atmosphere.

Piston Not Attached to Actuator or Chamber

The lower limit for the piston is for it to rest on the seal at the top of the rod guide (see drawing No. 2621.MD-25378). There is not an upper limit for the piston; however, at 5 1/2 inches above the expanded position (normal stroke is approximately 4 inches) the piston bearing on

the head of the piston interferes with the upper lip seal by .008 inches. The piston can continue further up, resulting in a stress of 8000 psi in the Be-Cu lip seal. Above this point the piston is free.

If there is a static fluid in the chamber (liquid or gas) there is a balancing force, that is, if the piston rises, the pressure above the piston increases and below it decreases, tending to hold it at a given position.

Piston Unattached and a Pressure Difference Across It

It was found that for the CERN 1-meter model pressure differences could be held across the lip seal for only seconds. Thus an unbalance of pressure across the piston will only endure for seconds. However, should this occur such that the piston goes up (nothing happens downward) 18 inches above the down position, the lip seals will not be on their bearing and a pressure difference cannot be maintained. At this point the rod sleeve will be above the seals and the gas from under the piston will escape via the rod guide (assuming chamber pressure greater than 1 atmosphere) reducing the pressure under the piston. The piston will come back down, not damaging the seals, and reseal.

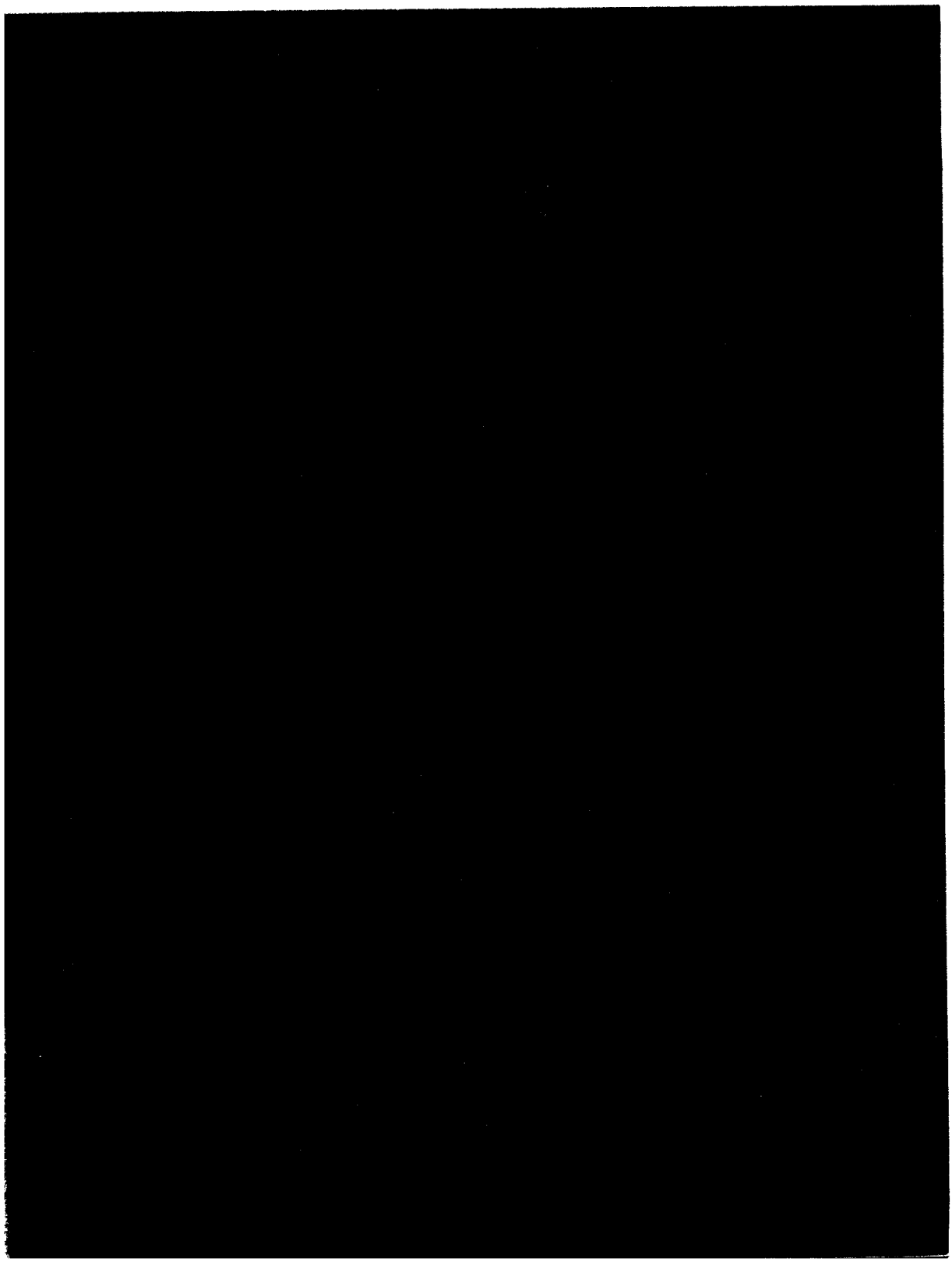

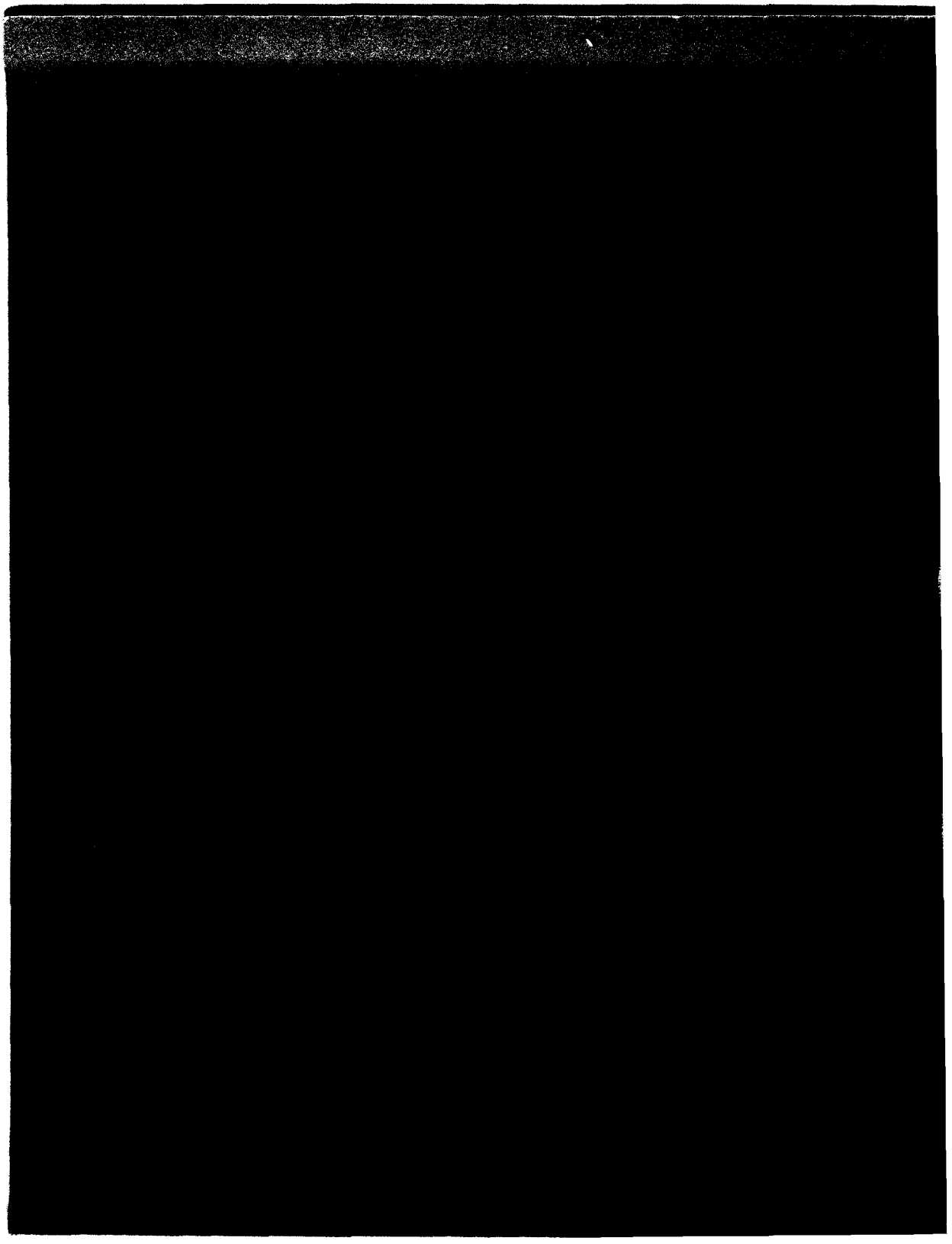

IV. EQUIPMENT

I. Optics Safety Report

Prepared by

F. R. Huson

TABLE OF CONTENTS

LIST OF FIGURES

TABLE OF CONTENTS (Cont'd)

LIST OF TABLES

IV. I. OPTICS SAFETY REPORT

(1) GENERAL DESCRIPTION

The reason for the optics system in a bubble chamber is to record as simply and as accurately as possible any bubble in the chamber. This must be done immediately after the bubble is formed to avoid error due to the bubble moving. The criteria for the optics system are:

1.0 General system; wide angle optics at top with Scotchlite illumination.

2.0 Appropriate positions for the cameras such that the system is simple, minimizes error, and maximizes fiducial volume, and can photograph plates and TST's (Track Sensitive Target).

3.0 Good resolution so as to resolve small bubbles.

4.0 Distorting lens vs. non-distorting.

1.0 General System.

The advantages of a chamber with the piston at the bottom and fisheye optics at the top have been discussed in many BNL reports (e.g., BNL 8266(R) proposal for a 14-foot chamber). The use of Scotchlite for bright field illumination in large bubble chambers is simple and works. Dark field illumination (coat-hangers, mirrors, straight through illumination, etc.) for hydrogen bubble chambers is difficult because of the small angle of the scattered light from bubbles (due to the small index of refraction ~1.1). It does not seem feasible at this time to use Scotchlite as a dark field system. Fisheyes minimize the size of the window needed for the optics and illumination systems. Spherical fisheyes are larger than some other possible shapes but are simpler and have less critical tolerance concentricity. The major goal for NAL concerning a large bubble chamber is to have a working chamber as soon as possible, constructed with a minimum of money and personnel.

These criteria necessitate using already proven designs. There are 3 designs with similar criteria to the NAL chamber; i.e., the ANL 12-foot optics, the BNL 7-foot optics and the CERN 3.7 meter optics. The ANL 12-foot optics have a 140° field angle and 50% distortion at 70° to the optic axis. These optics are suitable for a chamber that is longer along the beam than it is high. The BNL 7-foot optics have a 90° field angle and no distortion. These optics are suitable for a chamber that is higher than it is long. The CERN 3.7 meter optics have a 108° field angle and 22% distortion at 54° to the optic axis. These optics are suitable for a chamber of about equal length and height. Thus, we have selected the CERN 3.7 meter fisheye and mounts (see Figure 1) since they best satisfy our criteria.

The film to be used is Kodak 2482 pan 70mm, perforated on both sides with standard perforations. The properties of this film are given in an enclosure. Standard 70mm film was selected so that existing scanning and measuring equipment could be used to analyze the film. If the film were narrower, bubbles on the film would be smaller than 10μ; larger film would be more expensive.

The fisheyes are hemispherical. The smallest fisheye is made as small as possible; it is just large enough to contain the lens and flash. It serves as a vacuum window such that the lens and flash are in a room temperature atmosphere and can be removed with little difficulty. If there were one less window, then either the flash would be in vacuum next to a cold window making it difficult to change, or if that window were warm there would be a heat leak ($H = e\sigma T^4 A$ = tens of watts) into the chamber and no safety against breakage of the chamber window. That is, if the chamber window broke and let cold liquid hit a warm window there would be some small probability the window or seal would break; thus, the middle window is called both a heat shield window and safety window. The radii of the windows in the CERN design

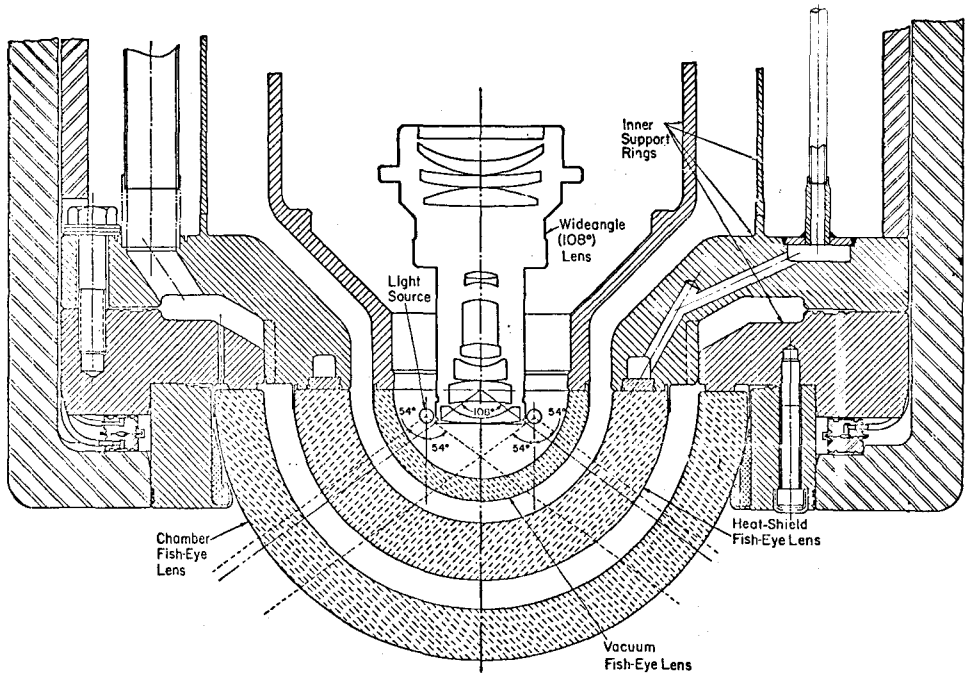

Fig. 1. Detail of a Camera Port of the 15-Foot Bubble Chamber, Showing the Fisheye Lenses

could have been smaller and would have saved some money; however, there was not time for NAL to redesign the optics because of the long delivery time for fisheyes. There is an engineering advantage in having more space to perform the necessary tasks to obtain a photograph.

2.0 Camera Positions.

The design criteria for the number of cameras and their positions are:

a. Be able to use the minimum number of cameras: three for normal experiments.

b. Have a sufficient number of cameras to be able to de experiments that require plates, track-sensitive targets, etc. Some solutions, particularly for plates, require five cameras.

c. Have two down-stream cameras that can photograph tracks in the nose of the chamber. The nose on the chamber is a very cheap way of adding 2.5 feet to the chamber for hadron physics.

d. The three cameras used for hadron physics should have their optic axis approximately perpendicular to the beam so that narrow depth of field lenses are not excluded.

e. Optimize the stereo angle such that the azimuthal and dip angle errors are minimum; also, keep in mind ease of scanning.

The first conclusion reached was to put six cameras in the chamber This satisfied a. and b. above plus giving the advantage that two experiments (e.g., one neutrino and one hadron) could be performed simultaneously without putting them on the same film strip.

The second conclusion was to add a "beanie" to the chamber for the optic ports. By adding $3m^3$ (10%) to the volume of the chamber, we could add $7m^3$ (33%) to the volume visible to three cameras. Also, the visible volume matched much better the shape of the chamber. This solution also suggests strongly a depth of field of 750-4200mm for the optics.

There are many possible orientations for the cameras. The one we concluded was best is shown in Figure 2. Some of the properties are given in the following table:

TABLE I.

CAMERA POSITION

		(1)	(2)	(3)	(4)	(5)	(6)
			ν Cameras			Hadron Cameras	
Nodal point in inches	x	-28.5	9.0	9.0	- 4.0	37.9	37.9
	y	0	-35.0	35.0	0	-28.3	28.3
	z	-78.5	-83.625	-83.625	-89.0	-73.0	-73.0
Optic axis	φ	0	90	270	0	120	240
	θ	-20.0	-22.0	-22.0	0	-23.25	-23.25
Possible Vol visible to (3) cameras			28			26	

Ch - $33.3m^3$

Chamber Center x = 0 y = 0 z = 0

3.0 Resolution.

The large depth of field required for the 15-foot chamber gives the limit on the resolution. The phase difference (Δ) over the depth of field is given by:

$$\Delta = \frac{d^2}{8\lambda}\left(\frac{1}{\ell} - \frac{1}{\ell^1}\right)$$

where d is the diameter of the entrance pupil, ℓ is the distance from the lens to a point in the chamber, ℓ^1 is the distance from the lens to where Δ = 0. For the 15-foot chamber 750mm $<\ell<$4200mm and ℓ^1 = 2000mm. The wave length of the light used is fixed by the following limitations:

a. Kodak 2482 pan film is not sensitive to $\lambda>625m\mu$

b. Scotchlite is good for $500<\lambda<700m\mu$ and best at $550m\mu$

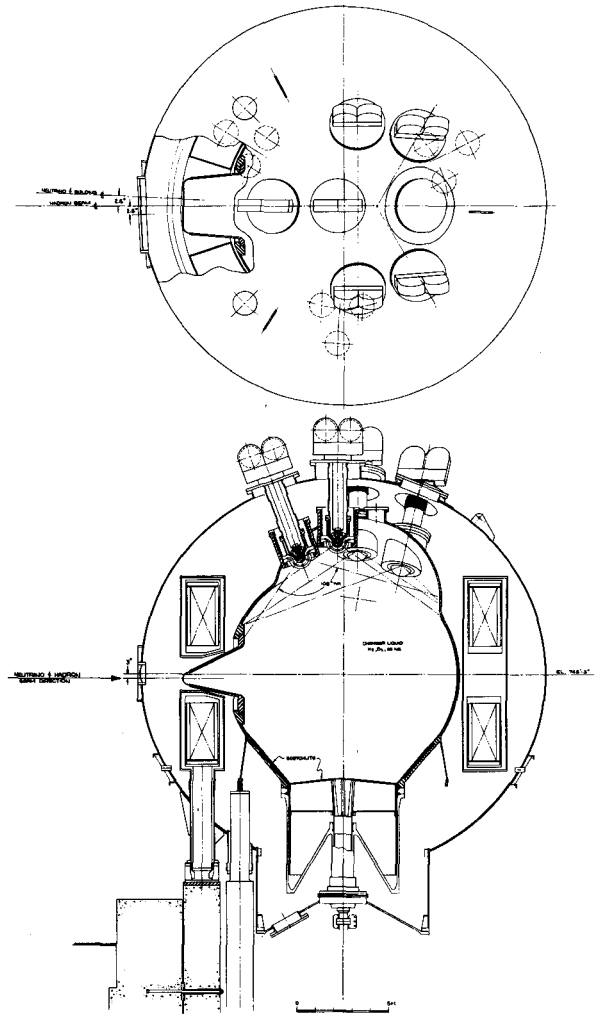

Fig. 2 Chamber Assembly

Thus, we have chosen λ = 540mμ, for example a Wratten #58 filter. Figures 3 and 4 taken from the BNL 14-foot proposal (BNL 7266(R)) shows the effect of Δ on resolution. Normally Δ is kept to less than a quarter wave length (Rayleigh criterion), however, we would like to make d as large as possible and thus Δ since d determines the limit on the resolution

$$D \text{ (diameter of Airy disk)} = \frac{\lambda f}{d}$$

The compromise is to let Δ go to $\lambda/2$ at 750mm (see Figure 5), this gives d = 2.0mm the largest possible entrance pupil to give the necessary depth of field.

An interesting quantity is the ratio of bubble image diameter without diffraction to the diameter of the Airy disk.

$$X = \frac{Bf}{\ell} \Big/ \frac{\lambda f}{d} = \frac{Bd}{\lambda \ell}$$

where B is the diameter of a bubble in space. This quantity is a function of only bubble diameter, entrance pupil diameter, wave length and object distance. As long as we require the large depth of field and thus fixing the entrance pupil we have no way of varying X. When X is less than one, the contrast of the image starts to degenerate and finally disappears. The γ of the film will change this effect somewhat.

Table II lists six possible lenses. Number (1) is the lens in the specification we have sent out for bid. Numbers (2), (3) and (6) are non-distorting lenses with full depth of field. Number (4) is a narrow depth of field lens and Number (5) is the CERN 3.7 meter lens.

All aberrations for these lenses should be small compared to the diffraction limit, that is less than 5μ on the film. The only exception to this is radial distortion. If there is radial distortion it should have a very simple form, for example:

$$\frac{\Delta r}{r} = a\theta + b\theta^2$$

where r is the radial distance on the film from the optic axis and θ is

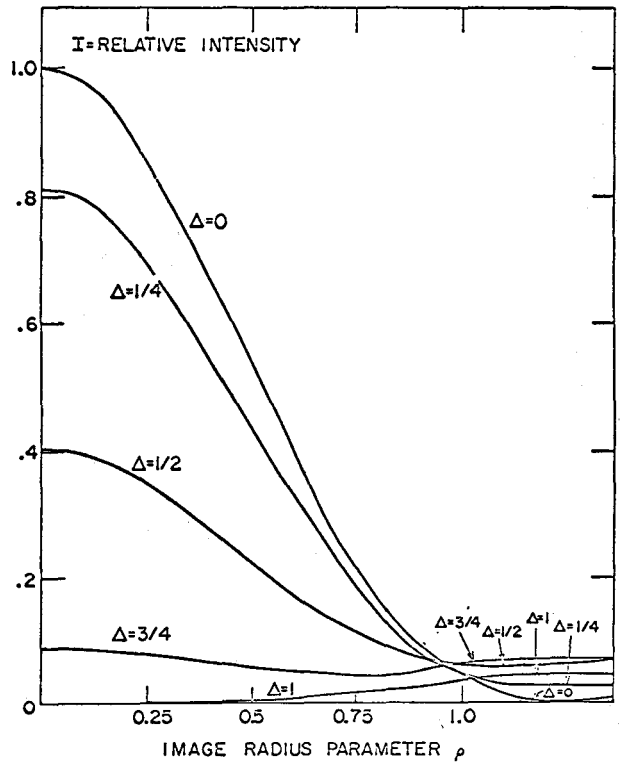

Fig. 3. Change of Image Shape With Distance From Focal Point

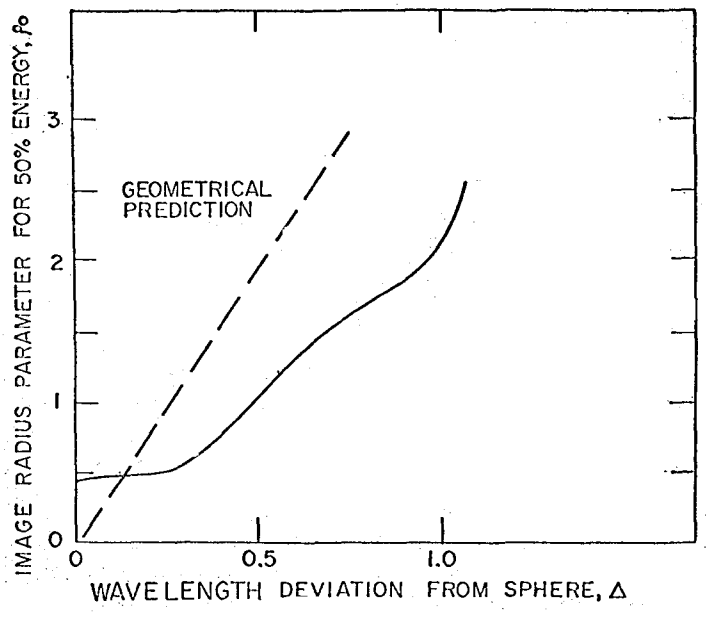

Fig. 4. Variation of Radius for 50% Energy With Wave-Front Deviation Δ

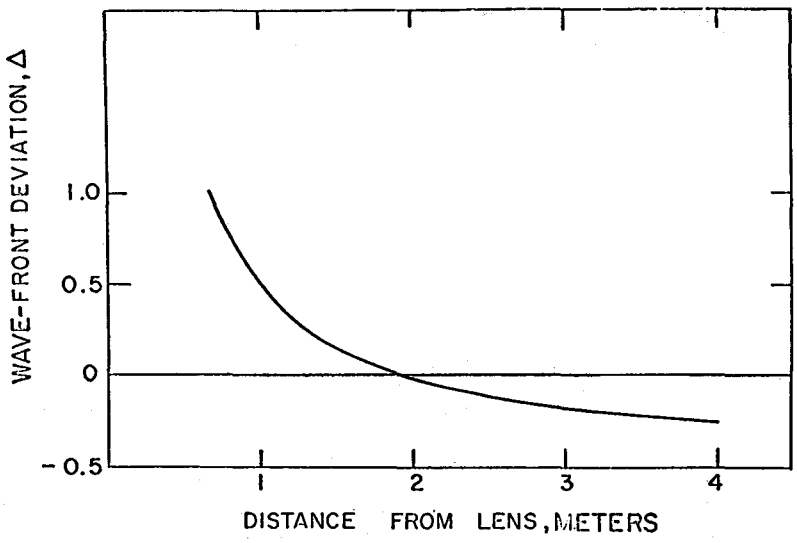

Fig. 5. Wave-Front Deviation in Wavelength

TABLE II

POSSIBLE LENSES

	(1)	(2)	(3)	(4)	(5) CERN 3.7m	(6)
Image. Min. (usually diff. limit)	10μ	7.5μ	10μ	10μ	11μ	10μ
Field Angle	108°	108°	90°	108°	108°	108°
Image Diameter	75mm	75mm	75mm	150mm	88mm	94mm
Depth of Field	750-4200mm	750-4200mm	750-4200mm	1250-2750mm	750-4200mm	750-4200mm
Focal Length	37mm	27.4mm	37mm	55mm	41mm	37mm
Distortion	28%	0	0	0	22%	0
Demagnification	20-114	28-153	20-114	23-50	18-102	20-114
X for .5mm Bubble	.44-2.5	.44-2.5	.44-2.5	1.12-2.15	.44-2.5	.44-2.5
Vol. visible to (3) cameras	26-28m^3	26-28m^3	20-22m^3	~8m^3	25-27m^3	23-25m^3

the angle to the optic axis. The lens should also be corrected for chromatic aberration.

4.0 Distorting Lens v. Non-Distorting Lens.

The advantages of a distorting lens are the following:

a. The lens can easily be made telecentric and thus the tolerance on film flatness is not critical.

b. The light intensity over the whole image is more uniform for a distorting lens.

c. The demagnification is less.

d. There is a better match of volume in the chamber mapped to equal area on the film.

e. It is easier to design a distorting lens.

The one disadvantage is that the image is distorted. Figure 6 is a map of the barrel distortion for 25% distortion at 54° (Lens (1)) and a map for no distortion (Lens (2)).

The information that we have obtained from optics manufacturers about a non-distorting lens is that it may be necessary to either make a symmetric lens, which is very difficult since the space for the objective is not large, or to use an aspheric lens. The difficulty with an aspheric is that it may have small distortions that would take many parameters to correct.

We worry very much about having an image on film smaller than 10μ. This begins to approach the limit of the film (2-5μ) and may well be too small for CRT measuring devices. The only other recourse to use a non-distorting lens is either use a larger film or cut more of the edges off the image. To use a larger film would mean a change in analysis equipment for all users and more expense for film. Figure 7 shows the volume of the chamber cutoff using Lens (6) in Table II.

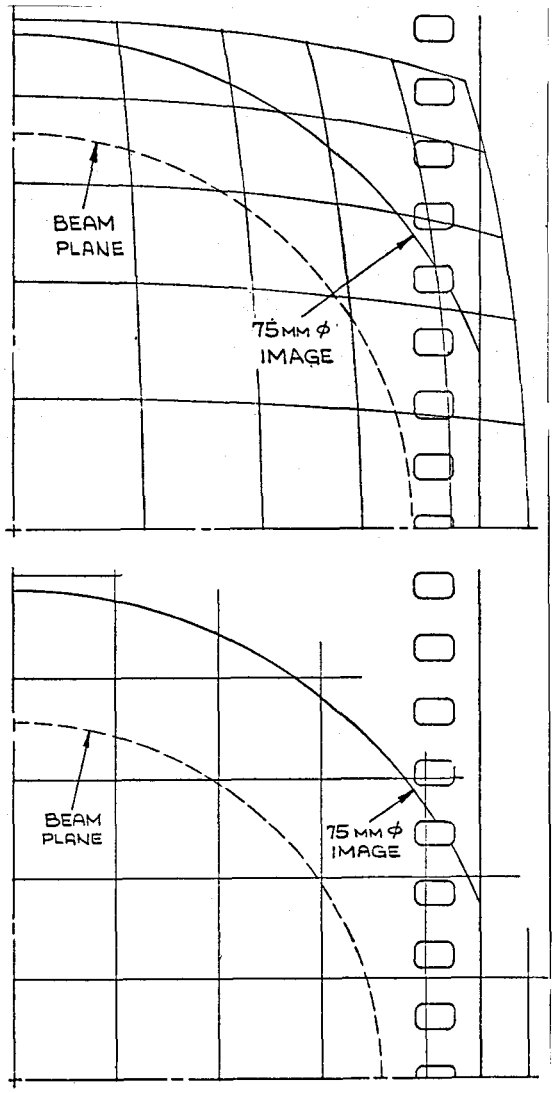

Fig. 6. One Quarter Image for Lens (1) and (2) of Table II

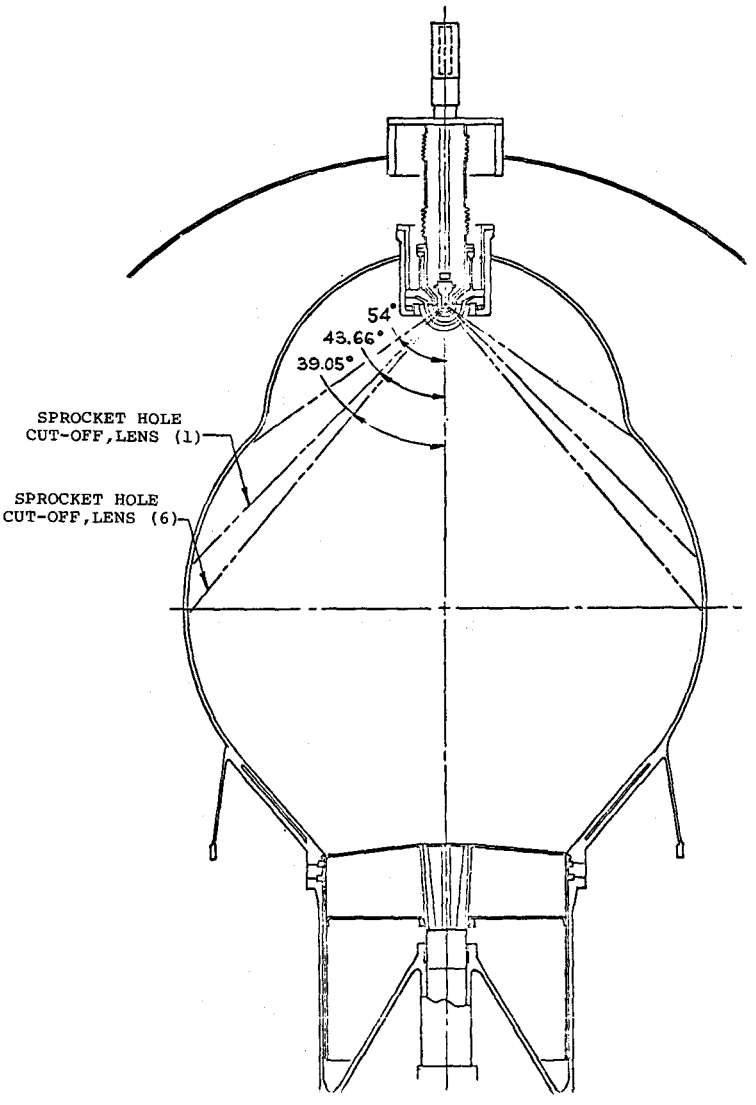

Fig. 7. Volume of Chamber Cut-Off Using Lens (6) in Table II

Conclusion

We conclude that the image on the film should not be smaller than 10μ. We want to keep the demagnification to not much larger than 100. We want to use standard 70mm film since it is sufficient. Our conclusion is that we should obtain six lenses of the type (1). To buy two different sets of three lenses is very expensive. The CERN 3.7 meter lenses cost more than the development of new lenses; thus, we cannot buy three CERN lenses and three other lenses as cheaply as we can buy six lenses of type (1). This does not exclude buying other type lenses in the future.

(2) STRESS ANALYSIS

In this section we will look at the stresses of each of the parts of an optic port. NAL Drawing No. 2623.ME-25250 has a complete parts list which serves as a guide for this report. We will first list the properties of the various materials used (Table III) and then go through each of the parts as listed on the drawing.

The pressures used will be noted as each item is treated. Normal operation conditions and maximum stress conditions will be given.

1.0 Allowable Stresses.

The stresses quoted in this report were calculated by F. R. Huson. The calculations are kept in the bubble chamber files. These calculations are based on simple geometric shapes and approximations.

2.0 Individual Pieces.

2.1 Chamber Window - Item 1.

The main chamber window (BSC-7 glass from O'Hara) is mounted onto 42.5Ni-Fe so that the thermal contractions are matched (see Figure 8). Thus, the only thermal stresses are produced by temperature differences. Normal conditions for this window will be considered to be 150 psi outside, and vacuum inside. This gives a maximum compressive stress in the glass of 725 psi (see Figure 9) and no tensile stresses. The shear in the epoxy is

TABLE III

PROPERTIES OF MATERIALS

Material	Yield (psi) 300°K	Yield (psi) 77°K	Maximum Stress	$\frac{L_{293}-L_{25}}{L_{293}} \times 10^{-5}$	d (10^{-6}/°K) 300°K	d (10^{-6}/°K) 77°K	c(joules/cm°K) 300°K	c(joules/cm°K) 77°K	K (mW/cm°K) 300°K	K (mW/cm°K) 77°K	E)10^6 psi) 300°K	E)10^6 psi) 77°K	ν
316L	25,000	~50,000	15,000	297	1.6	.8	3.7		120	70	28		.3
36Ni-Fe	40,000		15,000	41*	1.5*		4.2		104	~70	20.5	19.5	.3
42.5Ni-Fe	40,000		15,000	136*	5.3*		4.0		108	~70	21		.3
Fused Silica	~6,000		1,000	~0	.6	-.6	1.66	.4	13.4	6	10.5	9.8	.16
O'Hara BSC-7	~6,000	~8,000	1,000	135**	7.5*	2.9**	1.8	.45	10.2	4.2	9.1	8.6	.2
Indium	500 - 4,000			700	32	22							
Teflon	~1,500			2,100					2.6	2.3	.058+		
Scotch-weld 2216 B/A	Shear Modulus* 260 psi at 300°K 2,650 psi at 77°K Maximum shear stress*** 2,300 psi at 300°K (higher at colder temperature)												

* Measured by Hans Kautzky

** See Figure 8

\+ Mark's 6-193

*** Spec. Sheet from 3M Company

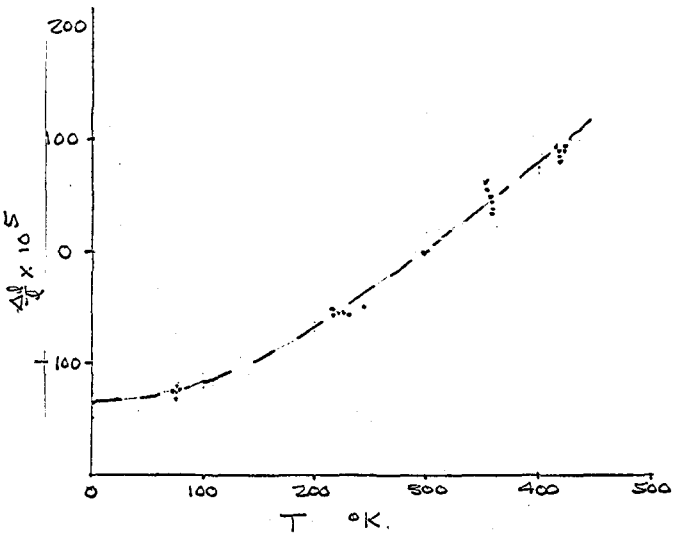

Curve is following fit.

$$\left(\frac{\Delta\ell}{\ell}\times 10^5 + 380\right)^2 = .95T^2 + 59600$$

$$\alpha = \frac{d\frac{\Delta\ell}{\ell}}{dT} = \frac{.95\times 10^{-5}\,T}{\sqrt{.95T^2+59600}}$$

T	α
77°	2.9×10^{-6}
298°	7.5×10^{-6}

Fig. 8. ANL Data for $\frac{\Delta\ell}{\ell}$ of BSC-7 from O'Hara

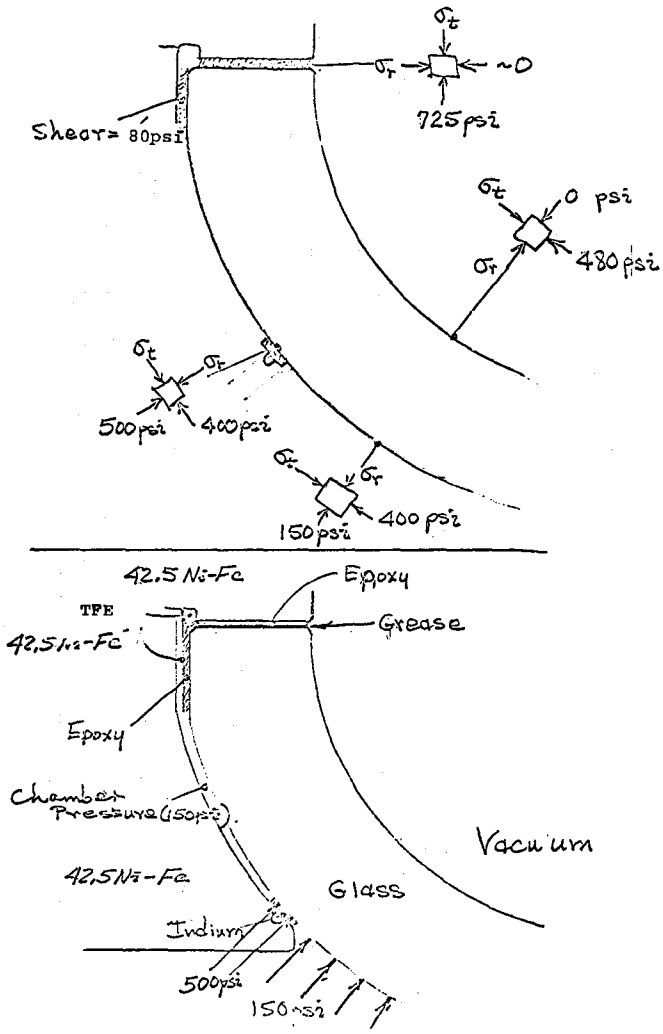

Fig. 9. Stresses for Chamber Window

approximately 80 psi. This assumes a good mating between the edge of the glass and the cement. The cement is not allowed to adhere to the glass on the flat surface by putting grease on the glass. This is done so that temperature gradients between the 42.5Ni-Fe and glass can occur since the cement will slip on the grease. The cylindrical 42.5Ni-Fe where the cement-glass bond is made will be at a temperature between the temperature of the glass and the main 42.5Ni-Fe piece. Care will be taken to not have a build-up of cement near the outer edge of the glass (see Figure 9) by filling the space there with a soft material. Such a build-up could cause chipping on the corner edge of the glass.

We assume that the maximum internal pressure would occur for 15 psi inside and vacuum outside (i.e., vacuum in the chamber). This gives a maximum tensile stress in the glass of 32.5 psi, and shear in the epoxy of 80 psi.

The maximum stress in the glass can occur from temperature differences. Thus, we take a maximum stress of 1000 psi and calculate the maximum ΔT. This is the worst gradient possible; e.g., all the glass at one temperature except for a thin film.

$$E = \frac{\sigma(1-\nu)}{\Delta\ell/\ell} = \frac{\sigma(1-\nu)}{\alpha\Delta T}$$

$$\Delta T = \frac{\sigma(1-\nu)}{\alpha E} = \begin{matrix} 11.7°K \text{ at } 300°K \\ 32°K \text{ at } 25°K \end{matrix}$$

This also holds for a glass-metal or epoxy surface if one assumes the metal or epoxy is rigid. Therefore, we should not have a local temperature difference greater than 11.5°K for the chamber window. If we let "local" be the thickness of the window then

$$\frac{\Delta T}{\Delta X} = \frac{11.7}{1.37} = 8.5°K/\text{in.}$$

We note that for any gradient other than a step function the stresses will be less.

We can now estimate a cooldown rate for the chamber window. During cooldown both sides of the window will be in contact with cooler gas, since helium gas will be put in vacuum Space #1 during cooldown. However, the worst situation would be for all of the heat to be removed at the edge of the glass. The amount of heat per °K is:

$$Q = VC = 11{,}000 \text{ joules/°K}$$

The rate of transfer for a given dT/dx is:

$$H = AK \frac{dT}{dx} = 31 \text{ watts}$$

Therefore, the cooldown rate is:

$$R = \frac{H}{Q} = \frac{AK}{VC} \frac{dT}{dx} = 10°K/hr \text{ at } 300°K$$

Taking into account the variation of R as a function of T gives the rate shown in Figure 10. For this rate it would take at least 18 hours to cool down.

It must be pointed out that the above calculations for cooldown rate are rough estimates and that the actual cooldown rate will be determined by tests in the optics test pot. The criteria that must be adhered to is the 11.7°K temperature difference (see Figure 10) across the window thickness or between the 42.5Ni-Fe and the glass. Experience with the 7-foot bubble chamber optics has shown that the actual cooldown rate is larger than the calculated by approximately a factor 2.

2.2 Heat Shield Window - Item 2.

The fused silica heat shield window is mounted to Invar. Under normal operating conditions, this window has vacuum on both sides. The temperature of the Invar-fisheye interface is 25°K; the temperature of the center of the fisheye is approximately 125°K. The only stresses are due to the difference in thermal contraction between Invar and fused silica. This puts a maximum shear in the Scotchweld of 70 psi and a compressive stress in the fused silica

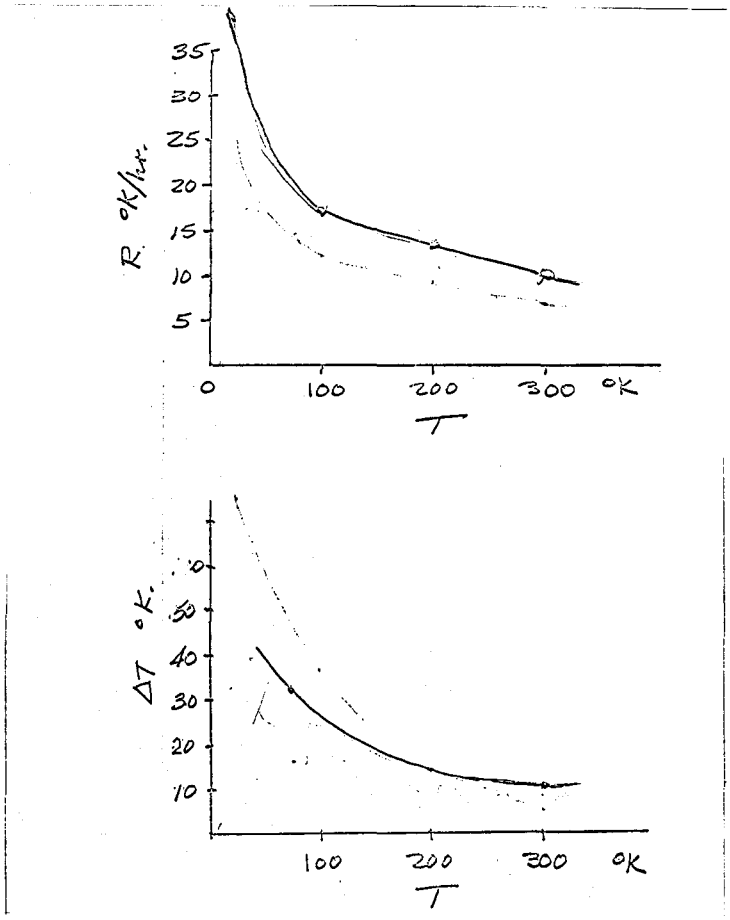

Fig. 10. Cooldown Rate S and Local Temperature Difference Allowable vs. T

of less than 53 psi. The compressive stress is due to the Invar .030 inch cylinder shrinking around the fisheye.

In this particular case it is important that the edge of the quartz slips on the greased Scotchweld (similar to Figure 9) since if it does not, the fused silica will have a stress of 4000 psi.

In the event vacuum Space #1 goes to 150 psi the maximum stress in the quartz is 315 psi. The shear in the Scotchweld is approximately 80 psi.

If vacuum Space #2 goes to 15 psi, the shear in the Scotchweld is 75 psi.

2.3 Vacuum Chamber Window - Item 3.

The fused silica vacuum chamber window is mounted to Invar. The operating temperature for both pieces is room temperature. The stresses for normal operation are 33.5 psi tensile membrane stress at the Invar surface and less than 55 psi shear stress in the Scotchweld bond. The fused silica-Invar mount is not greased in this case since this bond helps insure a good seal between atmosphere and vacuum Space #2. The probability that this fisheye gets cold is very small.

If there were a pressure of 150 psi in Space #2, the maximum membrane stress would be 452 psi at the inner surface and 420 psi compressive stress on the edge.

2.4 Chamber Window Retaining Flange - Item 4.

This ring has two functions: First, to hold the chamber window in the event the epoxy joint fails and, second, to center the optics with respect to the nozzle. The stresses in this ring are all very small.

The important characteristics of this piece are its tolerances. There are three regions of concern:

a. At the upper outside edge this ring must be centered relative to the chamber window. To obtain this centering to within 2 mils, we maintain a radial gap of 5 $\pm$ 2 mils during bolting.

b. During cooldown the nozzle contracts 14 mils on the radius more than the ring. Therefore, we leave a radial gap of 20 $\pm$ 2 mils. The Teflon ring (Item 36) will serve to center the ring in the nozzle.

c. There is a radial gap of 15 $\pm$ 2 mils between the chamber window and the retainer ring. We note that if the ring is 20°K colder than the chamber window this gap decreases by only .73 mils.

2.5 Diaphram Seal Ring - Item 5.

This inflatable ring has two functions: First, to make a seal between the main vacuum and chamber pressure and, second, to give the necessary force to hold the optics in place. In normal operation the pressure of the chamber will hold the optics in place; however, if the chamber has vacuum and the vacuum tank has 15 psi and the magnet is on, the ring must at least hold:

Pressure	= 5,000 lb
Invar x 7 (Mag.)	4,700 lb
Other Mass	~300 lb
	10,000 lb

which gives a pressure of 320 psi on the two indium seals. This means that the minimum pressure inside the ring must be 140 psi. In fact, the pressure in the seal should be such that it produces 500 psi in the indium for a .250 inch flash of indium or 220 psi.

The tolerances and thermal contractions on the metal parts are such that the seal will have to move between .963 and .988 (Seal thickness = .963). Also the 42.5Ni-Fe will contract 15 mils

radially more than the 316L stainless steel ring. This means the radial displacement will be between 15 and 30 mils.

Both of these criteria; i.e., inflation between .000 and .025 mils and slippage between the two pieces of 15 to 30 mils, has been tested in a similar test apparatus and neither the material nor the vacuum seal failed.

2.6 Chamber Window Mounting Flange - Item 6.

The normal situation is to have a force up on the inner edge due to chamber pressure on the chamber window. This gives a stress of 1750 psi in the flange and a deflection upward of less than 0.2 mils.

During cooldown this flange contracts radially 7 mils more than the Invar heat shield window flange. Therefore, we leave a radial gap of 13 $\pm$ 2 mils between them. The Teflon ring (Item 37) acts as a centering device.

If the space between the chamber window and its retaining ring has 150 psi pressure, the .030 inch cylinder will have a stress of 8000 psi. If Space #1 has 15 psi and the chamber is under vacuum this cylinder will have a stress of less than 1800 psi.

We note that the chamber window surface must be 2.5 mils lower than the heat shield window surface at room temperature to have them equal at 25°K.

2.7 Heat Shield Window Flange - Item 7.

The thermal stress in the .030 inch cylinder holding the fused silica is calculated under Item 2.

Under normal operation there is a thermal gradient (300°K to 25°K) in the 0.1 inch cylinder. The maximum thermal stress possible is:

$$\sigma = \frac{E}{1-\nu} \frac{\Delta \ell}{\ell} = 8700 \text{ psi}$$

If the chamber window leaked and there was a pressure of

150 psi on the outside of the heat shield window and flange there would be a stress of 1750 psi in the flange. It would deflect upwards at its inner diameter 0.002 inches.

If the vacuum tank has a pressure of 150 psi there would be a compressive hoop stress of 11,200 psi in the cylinder. The collapse pressure for the cylinder is 500 psi. A 10g vertical pulse on the optics will produce less than 0.00008 inch deflection of the lenses perpendicular to the optic axis.

2.8 Vacuum Chamber Window Flange - Item 8.

Under normal operation conditions there are 15 psi inside this cylindrical element and vacuum on the outside. This gives a hoop stress of 220 psi in thelarge cylinder and 750 psi in the .030 inch cylinder that holds the vacuum window.

Should this flange be cold shocked (immersed in liquid hydrogen) the minimum stress is:

$$\sigma = \frac{\Delta \ell}{\ell} \frac{E}{1-\nu} = 8700 \text{ psi}$$

Should this flange have an external pressure of 150 psi, the stress in the cylinder is 2240 psi.

2.9 Window Ring Spacer - Item 9.

The maximum stress in this piece is 1070 psi.

The joint on each end of this ring must be greased with vacuum grease to make a good thermal contact.

2.10 Fisheye Thrust Ring - Item 10.

The maximum stress due to chamber pressure of 150 psi plus inflatable seal force is 3100 psi. The axial deflection is 1.33 mils.

2.11 Plug-eye Bolt - Item 11.

Eliminated

2.12 Plug-bolt - Item 12.

These plugs are made of Invar. They have an interference fit of .0002 to .0008 inches and will be press fit warm.

In addition the 42.5Ni-Fe contracts 1 mil more than the Invar.

2.13 Special Cap Screw - Item 13 (See Table IV).

There are eight of these 5/8 inch - 42.5Ni-Fe bolts. The torque on the bolts should be 40 ft. lb. This will give a load of 2250 to 8500 lb per bolt.

2.14 Diaphram Lifting Lug (6) - Item 14.

These lugs carry the weight of the inflatable seal during assembly.

2.15 Invar Stud (6) - Item 15 (See Table IV).

There are 3-5/16 inch studs in each half cylinder. The load is just weight (~1000 lb) or 160 lb per bolt. A torque of 5 ft lb will give 800 lb/bolt.

2.16 Standard Stud (6) - Item 16 (See Table IV).

Again just weight (~1200 lb) or 200 lb per bolt.

2.17 Indium Seals - Item 17.

2.18 Indium Seals - Item 18.

2.19 Indium Seals - Item 19.

2.20 Indium Seals - Item 20.

2.21 Indium Seals - Item 21.

2.22 Indium Seals - Item 22.

2.23 Indium Seals - Item 23.

2.24 Warm Buna-N O-Ring Seal - Item 24.

2.25 Belleville Nozzle Washer - Item 25.

The load on these bolts is:

a.	Chamber Pressure (150 psi)	42,500 lb
b.	Inflatable Seal	15,700
c.	Minus Atmosphere	-1,700
		56,500 lb

or 2350 lb per bolt. If we put 200 ft lb of torque on the bolts, we will obtain 10,000 lb per bolt or more than a factor 4 in

TABLE IV

BOLTS

Number	Item	Size	Material	Maximum Load	Torque	Load	Stress
8	13	5/8"-18	42.5Ni-Fe	2400	100 ft lb	10,500 lb	37,000 psi
6	15	5/16"-	Invar	160	$\leq$5	$\leq$800	$\leq$15,000
6	16	5/16"-		200	$\leq$5	$\leq$800	$\leq$15,000
8	31	1/4"-20	St. Stl.	small	--	--	--
12	32	3/4"-16	St. Stl.	2500	100	12,000	20,000
8	33	1/2"-20	St. Stl.	2360	30	3,600	22,000
24	34	1-1/8"-7	St. Stl.	2350	200	10,000	14,000
16	35	1/2"-20	St. Stl.	1180	30	3,600	22,000

safety. In addition the Belleville Washer can unspring $1 - \frac{2350}{3290} \times .059 = .017$ inches before the 56,500 lb load would move the flange.

2.26 Warm Belleville (48) (16 Bolts) - Item 26.

The necessary load to make up the indium and O-ring seals is 1180 lb per bolt. Under normal conditions there is no other load. If the vacuum tank has pressure, the seal is made better. If vacuum Space #2 has 150 psi pressure then the bolts would see a 1000 lb load or less than the 1180 lb above. The bolts will have 20 ft lb torque which gives 2400 lb tension. The Belleville washers take 515 lb to flatten them, thus we need three washers to give sufficient load even if the bolt loosens slightly. We note that there is not a strong argument for or against using these washers

2.27 Belleville at Invar Joint (36) (12 Bolts) - Item 27.

In this situation the stainless steel bolts contract 5.6 mils more than the Invar, plus the 42.5Ni-Fe contracts radially 15 mils more than the Invar. The bolts need at least 2500 lb per bolt to make the indium seal. The three washers take 5160 lb to flatten them and have a total deflection of 3x37-111 mils, or 46.5 lb per mil. Thus to allow for the 5.6 mils above, the load must be less than 4900 lb per bolt. Thus the bolt torque will be 30 ft lb to give a tension of 3600 lb per bolt warm and 3860 lb per bolt cold.

2.28 Nut for Cylinder Stud (6) Stainless Steel - Item 28.

A torque of 5 ft lb gives 800 lb per bolt.

2.29 Dowel Pin (6) Stainless Steel - Item 29.

2.30 Washer (6) Stainless Steel - Item 30.

2.31 Cap Screw for Item 14 (6) Stainless Steel - Item 31.

(See Table IV)

2.32 Bolts for Heat Shield-Chamber Window Flange (12)
Stainless Steel - Item 32. (See Table IV)
See Item 27. - 30. ft lb will give 3600 lb/bolt.

2.33 Socket Head Cap Screw (8) Stainless Steel - Item 33.
(See Table IV)
We need 2360 lb per bolt to make the indium seal, thus a torque of 20 ft lb.

2.34 Nozzle Bolts (24) Stainless Steel - Item 34. (See Table IV)
See Item 25. - 200 ft lb torque gives 10,000 lb per bolt.

2.35 Bolts (16) Stainless Steel - Item 35. (See Table IV)
See Item 26. - 20 ft lb torque gives 2400 lb per bolt.

2.36 Teflon Centering Rings - Item 36.

2.37 Teflon Centering Rings - Item 37.

2.38 Teflon Centering Rings - Item 38.

2.39 Bellows Assembly Between Optics and Vacuum Tank (See Drawing No. 2623.ME-25432)
The two bellows are designed for 150 psi external pressure, have a time constant of $\leq$.010 seconds and have been mass spectrometer checked for leaks. One of the bellows was tested for 10^6 cycles.
The maximum stress in the cylinder for 150 psi in the vacuum tank would be 4800 psi.
The top flange (32 inch diameter) would have a stress of 14,000 psi if the vacuum tank has 150 psi inside.

2.40 Optics Port Plug (See Drawing No. 2623.ME-25421)
For 150 psi in the chamber and vacuum in the vacuum tank the membrane stress in the spherical section is 3600 psi and the maximum stress in the cylinder is 1350 psi.

(3) OPERATION

1.0 Refrigeration System.
The design of the optics cooling loop is discussed in the Cooling

Loop Section. The six optics ports are cooled in the parallel using a counterflow heat exchanger that limits the ΔT in to out to less than 30°K. This keeps cold refrigerant from shocking the optics.

The normal heat load is about 2000 watts for cooldown in 48 hours and 500 watts for normal operation divided as follows:

Conduction Warm to Cold	35 watts
Radiation	35
Miscellaneous	15
	85 watts per port
	x 6 = 510 watts

There can be an error the order of 100 watts due to the emissivity of the Invar. This load could be cut to approximately 300 watts by using superinsulation in vacuum Space #2.

2.0 Optics Window Vacuum System.

The Optics Window Vacuum System serves to insulate the camera assembly from the chamber liquid and to protect the three windows in each of six ports from condensable vapors which could fog these windows The system basically consists of three manifolds, two 300 ℓ/s ion pumps, two 260 ℓ/s turbo-molecular pumps and the required valves for cross connections and isolation (See Drawing No. 2627.MD-25798). The system serves one optics vacuum Space #1 (between the large and medium windows) and one optics vacuum Space #2 (between the medium and small windows) in each of six ports. The system will operate satisfactorily with only one ion and one turbo-molecular pump, but two of each have been included for back-up in case of pump failure, for increased flexibility, and to permit isolation of Spaces #1 from Spaces #2 under normal operating conditions.

Normally the six #1 Spaces are connected to Manifold A and pumped by Ion Pump A; the six Spaces #2 are connected to Manifold B and pumped by Ion Pump B. Should any of the twelve spaces develop a small leak it

is removed from Manifold A (or B) and valved into Manifold C, where it is pumped by Turbo Pump C or D. Should either (or both) of Manifolds A or B require a turbo pump, they can be pumped by Turbo D while Turbo C continues to pump on Manifold C. Finally, both Manifolds A and B can be pumped by either Ion Pump A or B when the cross connect valve between Manifolds A and B is open.

In case of a pressure rise above 5×10^{-5} torr (as measured by cold cathode gauges), in any of the three manifolds, all valves connecting that manifold to the optics vacuum spaces will automatically close in less than one second. If the pressure in any manifold continues to rise to 0.5 torr (as measured by thermocouple gauges) all valves in the system will automatically close. Additional protection is provided by 130 psig relief valves in each of the three manifolds and 15 psig repture disks in the two Ion Pumps.

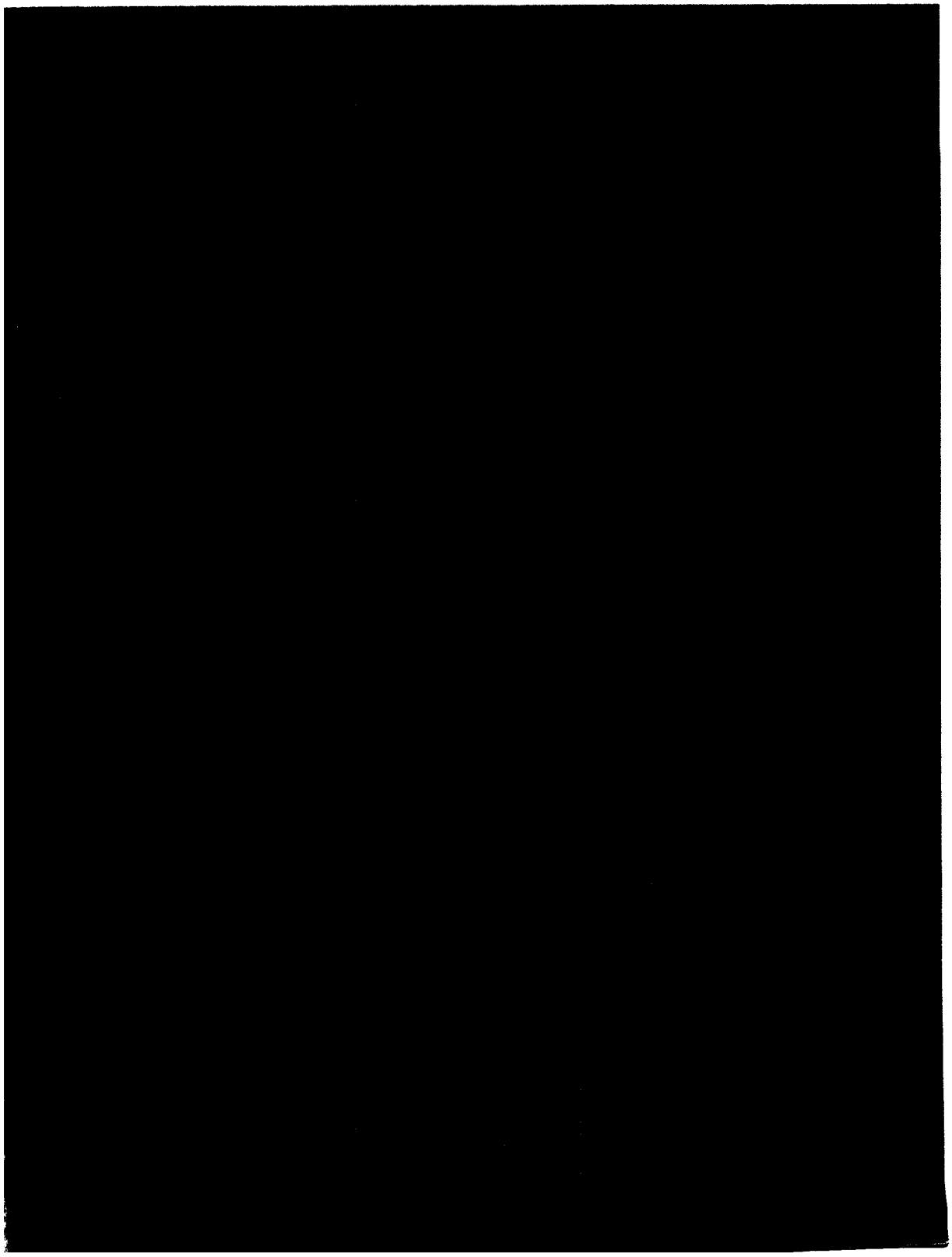

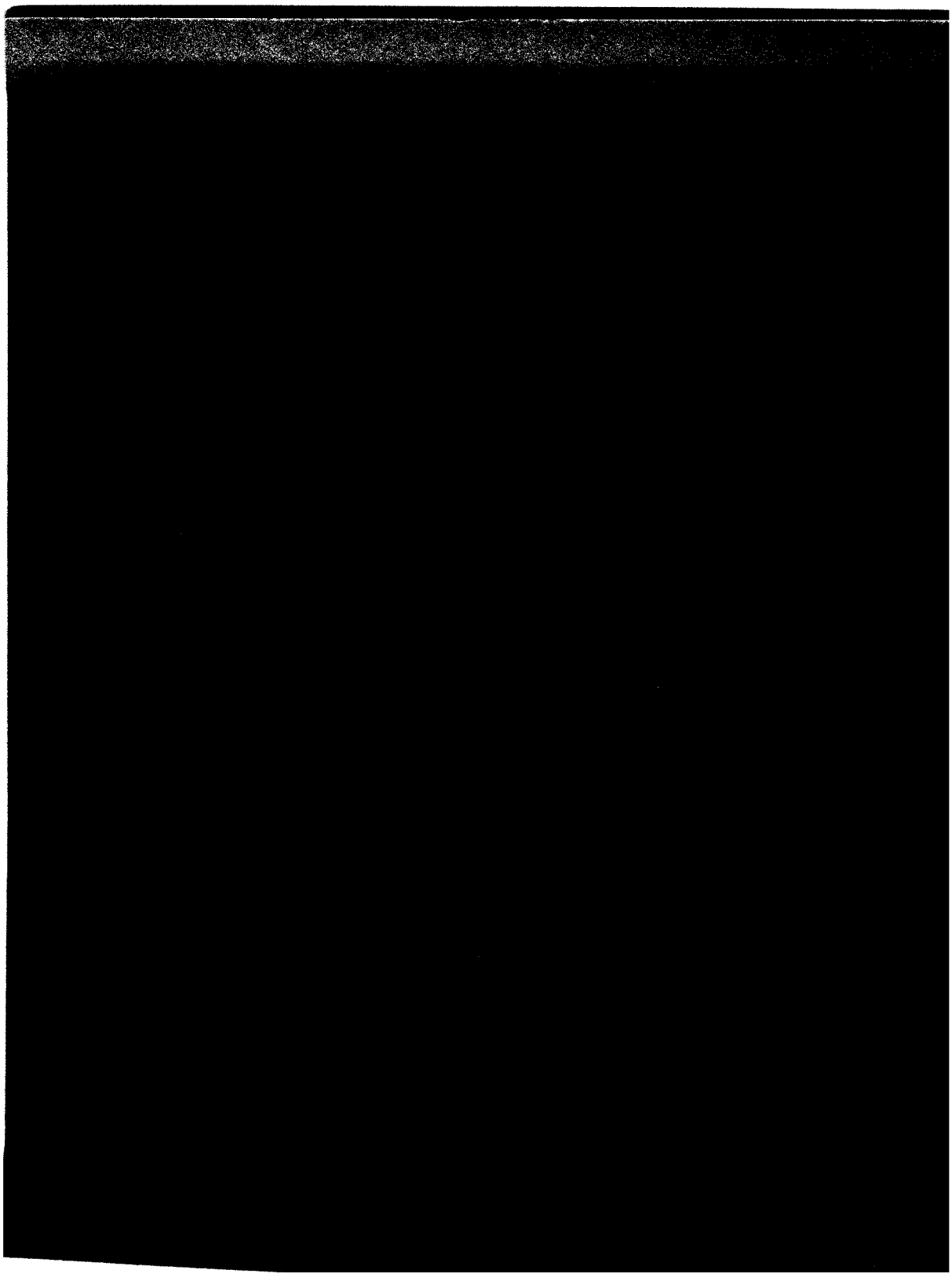

IV. EQUIPMENT

J. Failure Mode Analysis: OPTICS

Prepared by

F.R.Huson

IV. J. Failure Mode Analysis: OPTICS

The Optics has 3 fisheyes (see drawing No. 2623.ME-25250). The 2 smaller are quartz and can withstand thermal shock between 25°K and 300°K without breaking. This is also true of the Invar mounts holding these windows.

Loss of Vacuum Between Small and Medium Fisheyes

The loss of vacuum in this vacuum space will not cause loss of main vacuum or the optics vacuum between the large and medium fisheyes. The heat leak to the chamber will be the order of kilowatts. The liquid in the chamber will be dumped back to the dewar and the vacuum will be fixed.

Loss of Vacuum Between Large and Medium Fisheyes

Since the medium fisheye is nearly 25°K everywhere except the center where it is ~125°K, nothing fails. The liquid in the chamber will be dumped back to the dewar and the vacuum fixed.

Large Fisheye Broken

As soon as the pressure rises above 5×10^{-5} torr the 1 1/2 inch valves to the vacuum space between the large and medium fisheye close (in about one second). From this point on this case is equivalent to "Loss of Vacuum Between Large and Medium Fisheyes".

Small Fisheye Broken

As soon as the pressure rises above 5×10^{-5} torr the 1 1/2 inch valves to the vacuum space between the small and medium fisheye close (in about one second). From this point on this case is equivalent to "Loss of Vacuum Between Small and Medium Fisheyes".

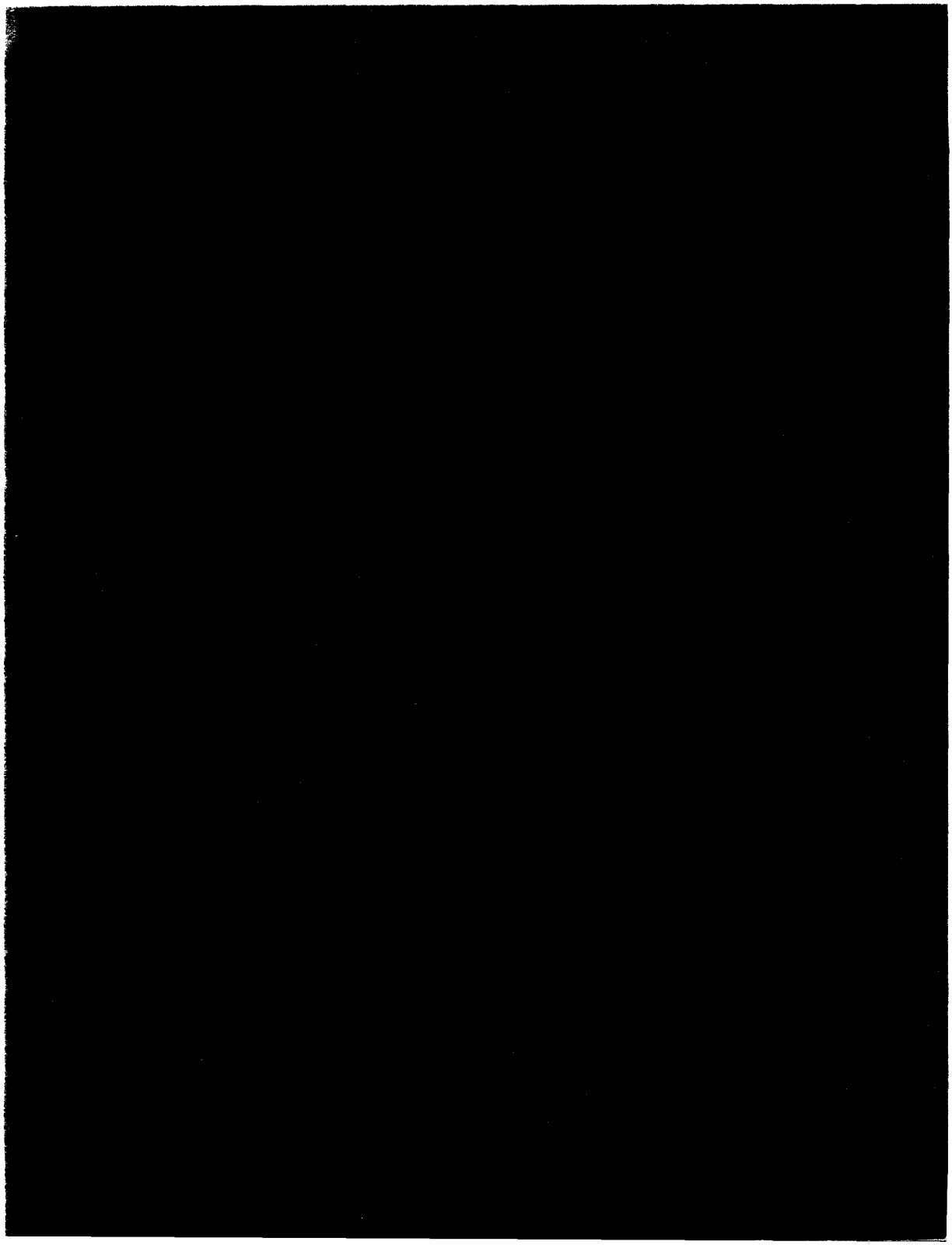

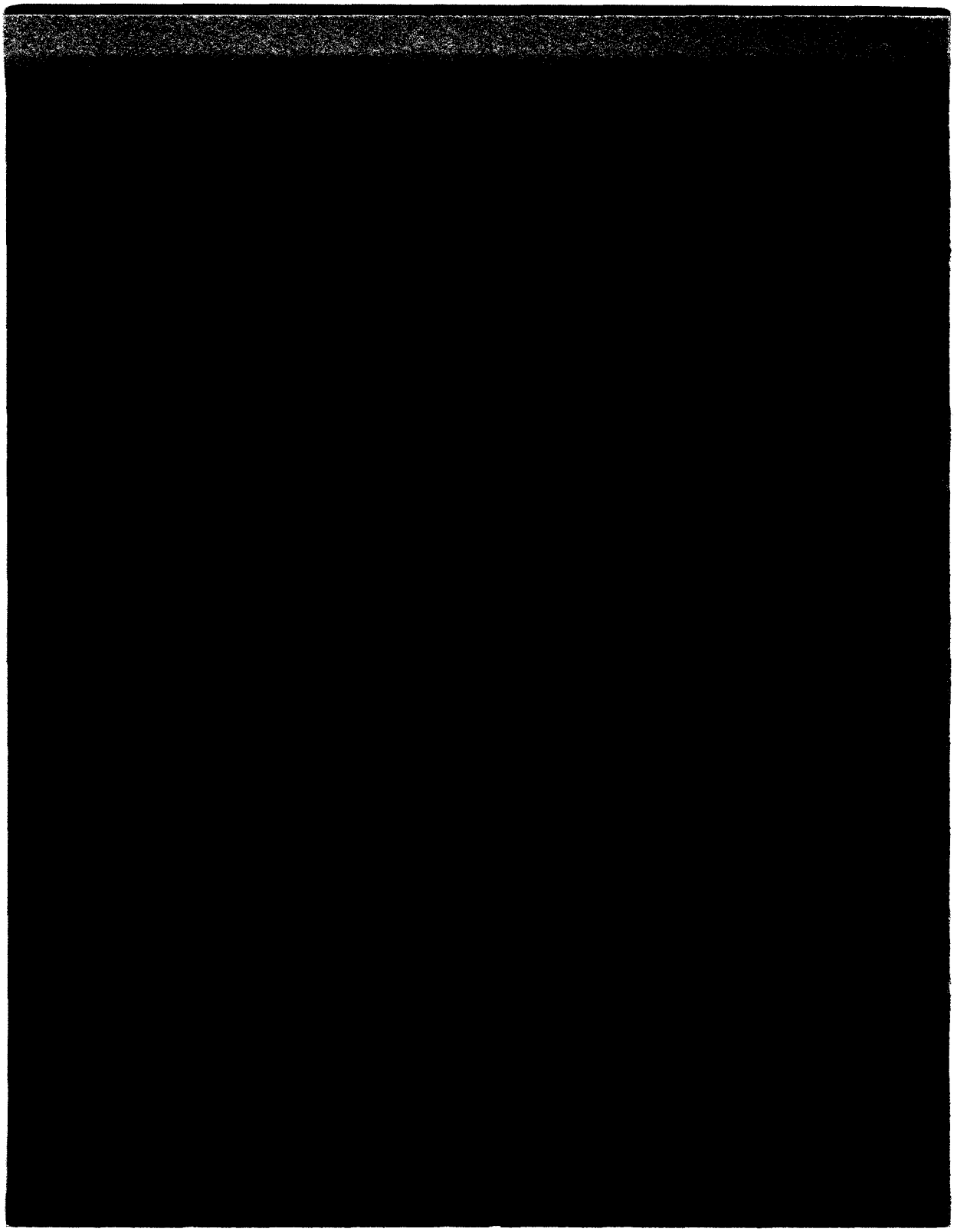

IV. EQUIPMENT

K. Magnet

1. Superconducting Magnet for the 15-foot NAL Bubble Chamber - Design Report

Prepared by

John Purcell

TABLE OF CONTENTS

LIST OF FIGURES

LIST OF FIGURES (Cont'd)

LIST OF TABLES

IV. K. 1. SUPERCONDUCTING MAGNET FOR THE 15-FOOT NAL BUBBLE CHAMBER - DESIGN REPORT

(1) BASIC PARAMETERS

Following the agreement between NAL and ANL on the design, fabrication, and delivery by ANL of the Superconducting Magnet for the 30,000 Liter Bubble Chamber, and after subsequent discussion between NAL and ANL, the main features of the magnet were decided upon as follows:

- The magnet clear bore, including cryostat, is 13 feet.

- The clear opening for chamber snout and beam entry is 22 inches vertically and 48 inches horizontally. The opening is unobstructed by the magnet system. The downstream beam opening presents a 90° horizontal aperture, but is obstructed by two vertical struts.

- The magnet is equipped with a separate vacuum jacket, which is adequate for independent testing of the magnet out of the chamber and for operation inside the vacuum vessel of the chamber.

- The overall size of the magnet, including its cryostat and vacuum tank, is designed to fit inside the 22 foot sperical vacuum jacket of the chamber.

- The magnet and its cryostat will be supported on three legs at the bottom. The transfer lines and power leads will be fed from the top.

- The central field is aimed at 30 kgauss, in accordance with budget possibilities.

- No iron return path or shield will be provided.

- The total cost, including complete tests at Argonne and Helium Refrigerator is to be $2,000,000.

- The delivery of the magnet to NAL, after complete tests at Argonne, is to be June, 1972.

(2) BASIC TECHNICAL CHOICES

From the previous specifications and after a preliminary investiga-

tion of the whole system, the following parameters were fixed; inner diameter of the winding 14 feet, separation between coil halves 39 inches, amount of superconducting material for 30 kgauss 660,000 kA feet. The final cost is mainly affected by the cost of the conductor and of the cryostat. The design should devote the greatest care to minimizing fabrication cost of these two components.

Prior to the more detailed design of the magnet, a certain number of technical decisions were made. These were based on the experience gained from the ANL 12-Foot Bubble Chamber and on the more recent developments in superconducting magnet technology, and are believed to ensure the most economical design and construction together with complete reliability in performance and safety of the magnet.

- The winding will be made of single pancakes, each pancake being independent of the others and mechanically self-supported against radial and hoop stresses. This favors a greater simplicity in the construction, handling, and assembly of the winding. It also simplifies the design of the spacers between pancakes and eliminates the need for radial clamps and for clamped crossovers between pancakes.

- An average current density of 2000 A/cm^2 has been found as a good compromise between the available space and magnet efficiency on one hand and the stability performances on the other, together with the need for limited peak field and stresses inside the winding.

- A cooling strip between turns is not necessary, as the cooling capacity for stabilization can be provided both by edge cooling and by partial face cooling through narrow transverse grooves built in the conductor itself. Apart from the obvious economical gain in eliminating the cooling strip and the simplification in winding operations, the main advantage of this solution is to allow the maximum cross section area for the conductor itself, at a given average current density, thus reducing the power dissipation in the conductor in the normal state and the necessary cooling capacity for stabilization. It also minimizes the

total resistance of the magnet in the extreme case of a complete transition to normal state and favors the removal of the stored energy through external resistors at a minimum discharge voltage.

- The conductor has to be made of twisted fine superconducting filaments, in order to reduce to a negligible level the eddy current time constants in the conductor and to improve the intrinsic stability.

- Splicings of the superconducting material should be avoided inside the pancakes, in view of the high current density and of the limited cooling capacity available.

(3) CONDUCTOR CHARACTERISTICS

A current of 5000 A has been adopted. This current is high enough to keep the number of turns and the self inductance reasonably small and is low enough to favor a low heat loss from the power leads, and a reasonably economical power supply and bus bar distribution. The resulting length per pancake also represents a practical limit for the production of a continuous length of material for each pancake.

Taking into account the space necessary for stainless steel reinforcing strips, turn-to-turn insulation and inter-pancake spacers, the current density in the conductor itself must be about 3500 A/cm^2, which gives a cross section area of 1.45 cm^2.

An aspect ratio of 10:1 has been chosen for the conductor dimensions after estimating the available cooling capacity. A higher ratio would reduce both the fraction of edge cooling and the face cooling grooves in the conductor. A smaller ratio would increase the number of pancakes and spacers, thus affecting the efficiency and cost.

The conductor dimensions were taken as 1.5 in. x 0.15 in., with an approximate length of 3100 ft. in each pancake.

The structure of the conductor was determined after a technical and economical optimization based on present technology and industrial capabilities. One of the major requirements was the need for twisted

superconducting filaments. Twisting of filaments uniformly distributed through the whole area of the conductor was found impractical and very expensive, due to the large size and the high aspect ratio. Furthermore, such a conductor would be highly anisotropic because of filament flattening. It was then decided to split the conductor into components: a copper backing strip, two side strips with cooling grooves, and a smaller strip containing the superconducting filaments. This composite conductor is then soldered together with 50-50 lead-tin solder.

The superconducting inner strip is 0.5 in. x 0.1 in.; an aspect ratio of 5:1. Preliminary tests on samples of the same outer dimensions but with a different superconductor content showed an anisotropic effect of about 15%. This is quite acceptable, and smaller than the difference between the maximum radial and axial fields which will be observed in the magnet.

The number of filaments is 60, and the copper to superconductor ratio in the inner strip is 4:1. This last ratio corresponds to a current density in the superconductor filaments of 70,000 A/cm^2; a common value at 60 kgauss. The size of the filaments is about 15 mils, which ensures adequate current sharing properties together with reliable manufacturing processings. The filaments are twisted at the rate of one twist per foot. This twist pitch rate must be kept as large as practical to enable easy and reliable manufacturing. The preceding parameters will be discussed in a later section with regard to stabilization.

The stabilizing copper strip was initially devised in a single component of over all cross section 1.5 in. x 0.15 in. with a longitudinal groove 0.504 in. x 0.107 in. on one side and edge cooling. Bids from the copper manufacturers showed that such a strip would be too expensive. Most of the manufacturers declined to quote. The reasons may be found in the unusual strip profile compared to standard fabrication, the high tolerances requested for the strip and groove dimensions and the limitation of unitary lengths in current production.

It was then decided to split the copper strip into three components, which could be welded or soldered together in order to achieve the required profile. For the assembly of the whole composite, soft soldering was found to be the most practical. It is reliable and economical. Another advantage is that the soldering of the superconducting strip together with the three copper strips is done in one operation. The subdivision of the copper strip is shown in Figure 1. The backing strip sets the overall width of the conductor at 1.48 in. The smaller copper strips are 0.48 in. wide, allowing a small recess from the backing strip at the edge after assembly. They have transverse grooves 0.020 in. deep and 0.125 in. wide at the back giving a 50% surface for cooling. The superconducting inner strip, being only 0.1 in. thick, is laid well below the copper surface level, so that no force can be directly transmitted to this strip from turn-to-turn pressure.

The final soldering process of the conductor is subjected to a development contract presently underway. The main specifications are the following:

- The bond thickness must be kept below 0.002 in.
- The flatness tolerance of the assembled conductor is 0.005 in.
- TIR and the parallelism 0.002 in. maximum.
- The solder should be a 50-50 lead-tin content or a higher lead content material, but the tin content should not exceed 50% due to the detrimental effect of tin at low temperature.
- Special care has to be taken with regard to flux corrosion and flux trapping and the bond quality and homogeneity must be checked, voids greater than 1.0 in. are not permissible. A continuous ultrasonic testing technique, checked by X-ray inspection, has to be developed as part of the contract.

The mechanical problems raised by the use of soft solder concern the shear stresses due to hoop stress or to differential thermal contraction, for which the chosen solder exhibits adequate properties,

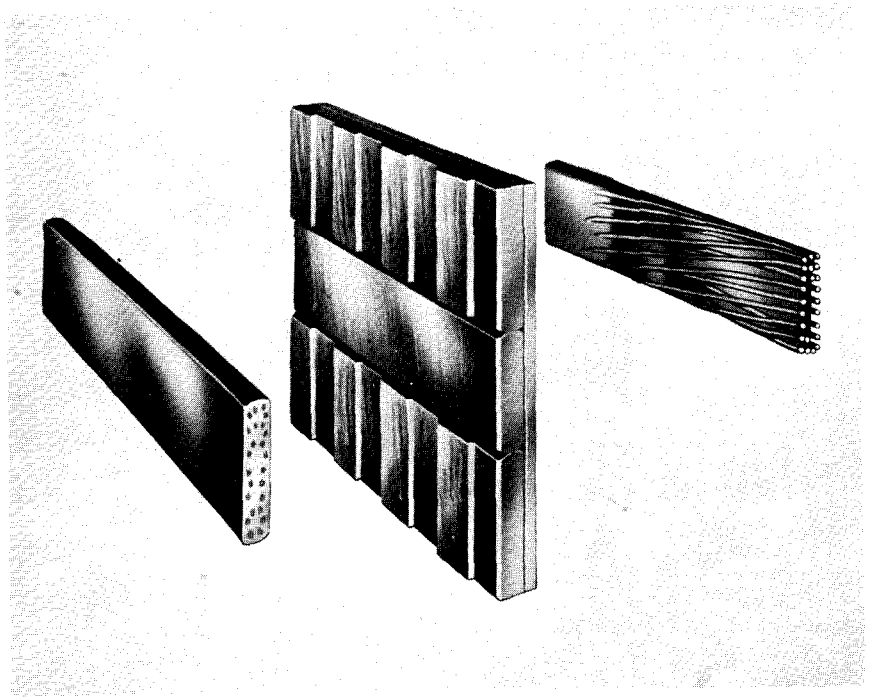

Fig. 1. Photo of magnet conductor. The various components are soft soldered together.

and the transmission of the radial forces applied to the conductor. For 70% of the turns, these forces result in a compressive stress on the solder, whilst for the outer turns, where the field is reversed, the conductor tends to be pulled out from the copper strip. But in this case, the maximum stress is only 120 psi, which is negligible.

(4) COIL CHARACTERISTICS

From the preceding sections, most of the coil parameters are already determined and the remaining factors for optimization are the number of pancakes and the number of turns per pancake. In fact, the choice of these parameters was mainly dependent on the maximum length which could be manufactured for the conductor and which is about 3100 ft. giving about 65 turns per pancake. For 30 kgauss central field we need about 22 pancakes per coil. Variations of these parameters does not significantly affect the performance of the magnet, as can be seen in Table I.

In practice the length of conductor and the number of turns may vary from one pancake to another. The pancakes will be stacked with the shorter lengths at the extremities. The number of turns will be between 63 and 66 with an average of 65.

The complete characteristics of the coils are given in Table II. The field distribution is shown in Figures 2, 3a, 3b and 4, which correspond respectively to the bubble chamber volume, the winding cross section, and the volume outside the magnet. A flux line plot is given in Figure 5.

As already indicated, the magnet will be made of 43 identical single pancakes. The conductor will be wound with a stainless strip 0.075 in. thick in parallel, in order to provide mechanical support for hoop stresses. Mylar insulation 10 mils thick will be placed on each face of the conductor. This double insulation will allow a continuous short-circuit testing during winding. The last turn of the stainless

TABLE I

VARIATION OF MAGNET PARAMETERS WITH NUMBER OF PANCAKES
FOR 30 KGAUSS CENTRAL FIELD

Total Number of Pancakes		40	42	44
Turns per Pancake		70.2	67.4	64.9
Length of Conductor (ft.)		3,390	3,240	3,110
Total Length of Conductor (ft.)		135,600	136,080	136,840
Stored Energy (Mjoules)		395.81	394.85	394.35
Max. Field on Conductor (kgauss)		52.7	52.04	51.35
Max. Radial Field (kgauss)		40.9	40.5	40.1
Field Uniformity in Chamber $\Delta B/B_o$ (%)				
R_{cm}	Z_{cm}			
100	0	+3.1	+2.8	+2.4
150	0	+2.1	+1.3	+0.4
0	100	-9.3	-8.9	-8.4
0	150	-21.9	-21.1	-20.3
100	100	-2.	-1.5	-1.

TABLE II

MAGNET CHARACTERISTICS

Winding inside diameter	14 ft.
Winding outside diameter	16 ft. 8 in.
Spacing between coils	39 in.
Length of bottom coil	38.25 in.
Length of top coil	36.75 in.
Number of pancakes bottom coil	22
Number of pancakes top coil	21
Number of turns per pancake (average)	65
Total number of turns	2860
Length of conductor per pancake (average)	3100 ft.
Total length of conductor	134,000 ft.
Weight of conductor	55 tons
Weight of stainless steel strip	26 tons
Operating current	5000 A
Ampere-turns	14.3×10^6
Current density in conductor	3700 A/cm^2
Average current density	1885 A/cm^2
Central field	30.06 kgauss
Maximum axial field	51.4 kgauss
Maximum radial field	40.1 kgauss
Maximum field on end pancake at R = 220 cm	45.3 kgauss total
	26.6 kgauss axial
	37.3 kgauss radial
Self-inductance	31.7 Henrys
Stored energy	396 Mjoules
Compressive force between coils at bridge	5920 tons
Maximum compressive force between coils	11,250 tons
Liquid helium consumption	50 liters/hr.
Shield heat load	300 watts
Shield cooling method	He gas cooled by LN_2
Helium vessel pressure rating	45 psia (external and internal)
Cryostat weight	45 tons

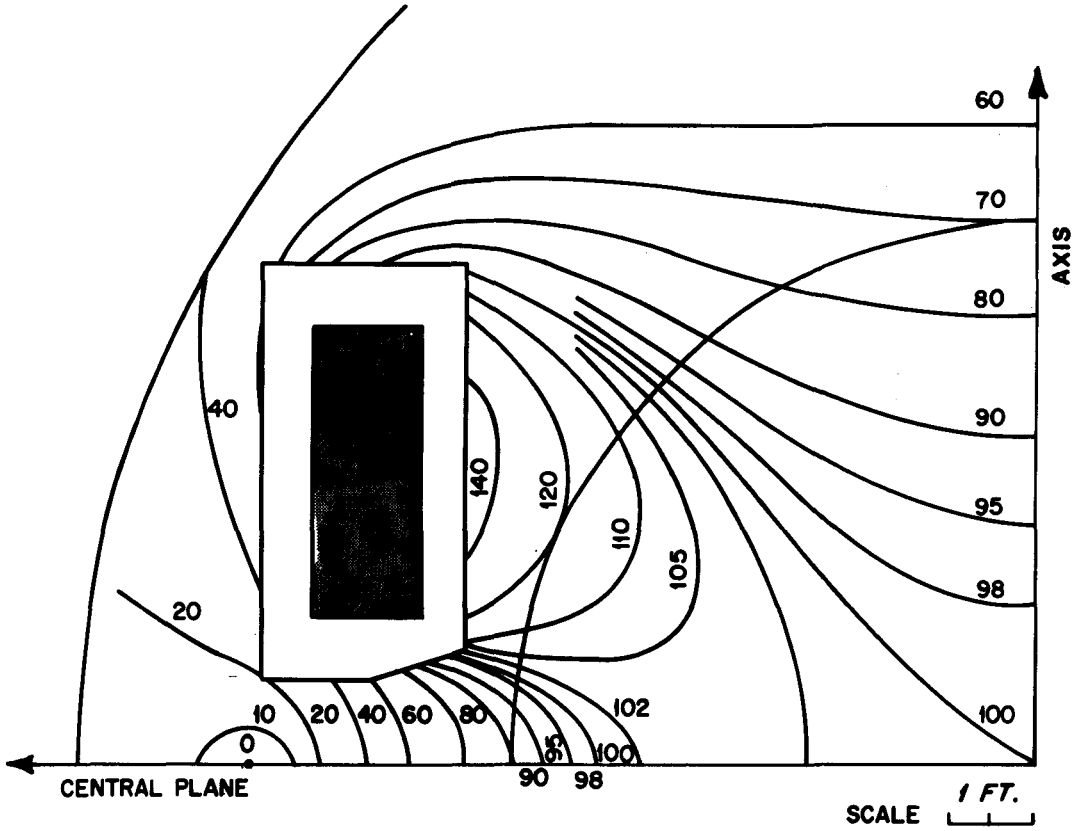

FIG. 2 – CONSTANT – FIELD LINES IN CHAMBER TOTAL FIELD IN % OF CENTRAL FIELD

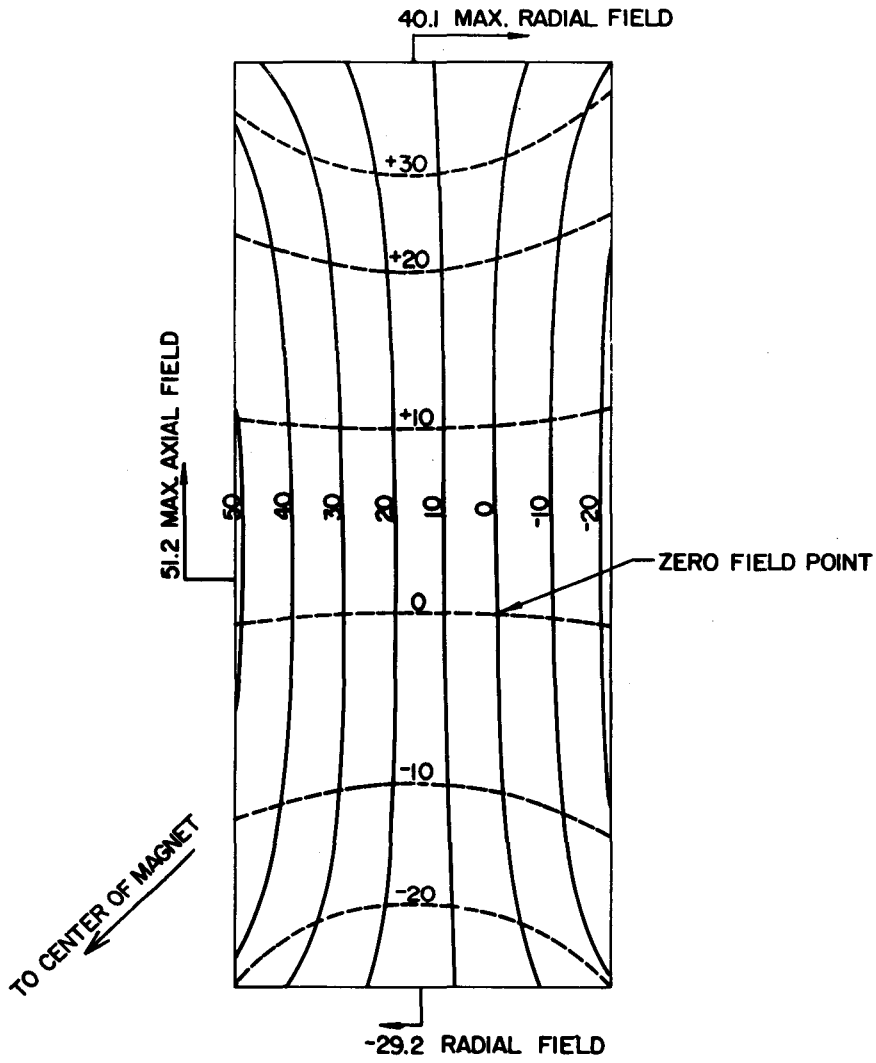

FIG. 3a

CONSTANT-FIELD LINES (k GAUSS) (V) COIL
SOLID LINES: VERTICAL FIELD
DOTTED LINES: HORIZONTAL FIELD

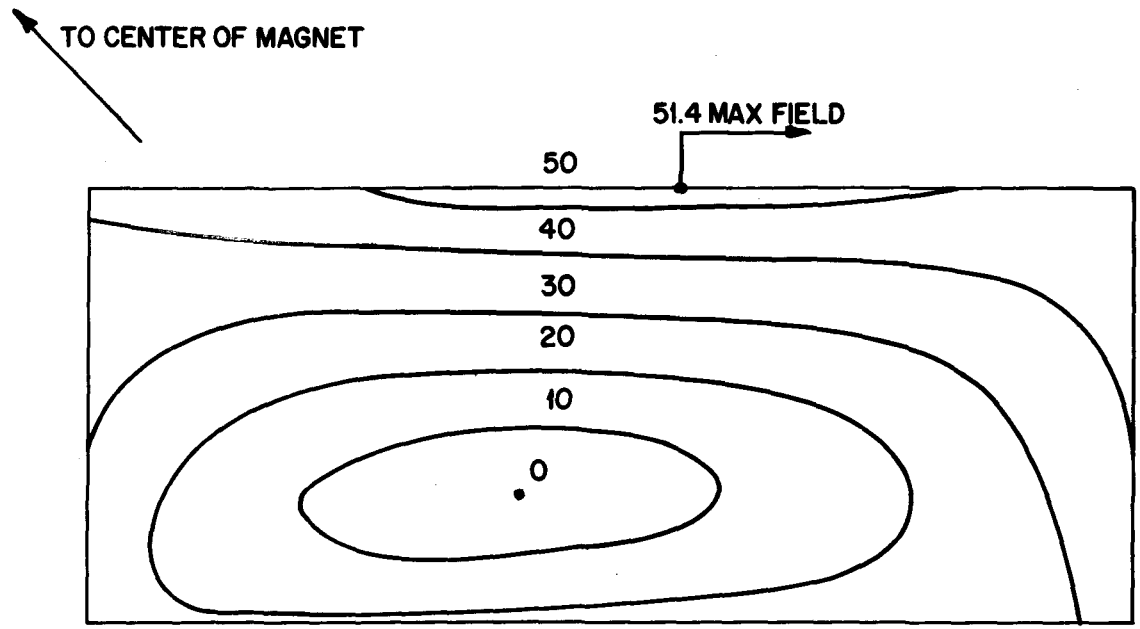

FIG. 3b – CONSTANT-FIELD LINE IN COIL TOTAL FIELD (k GAUSS)

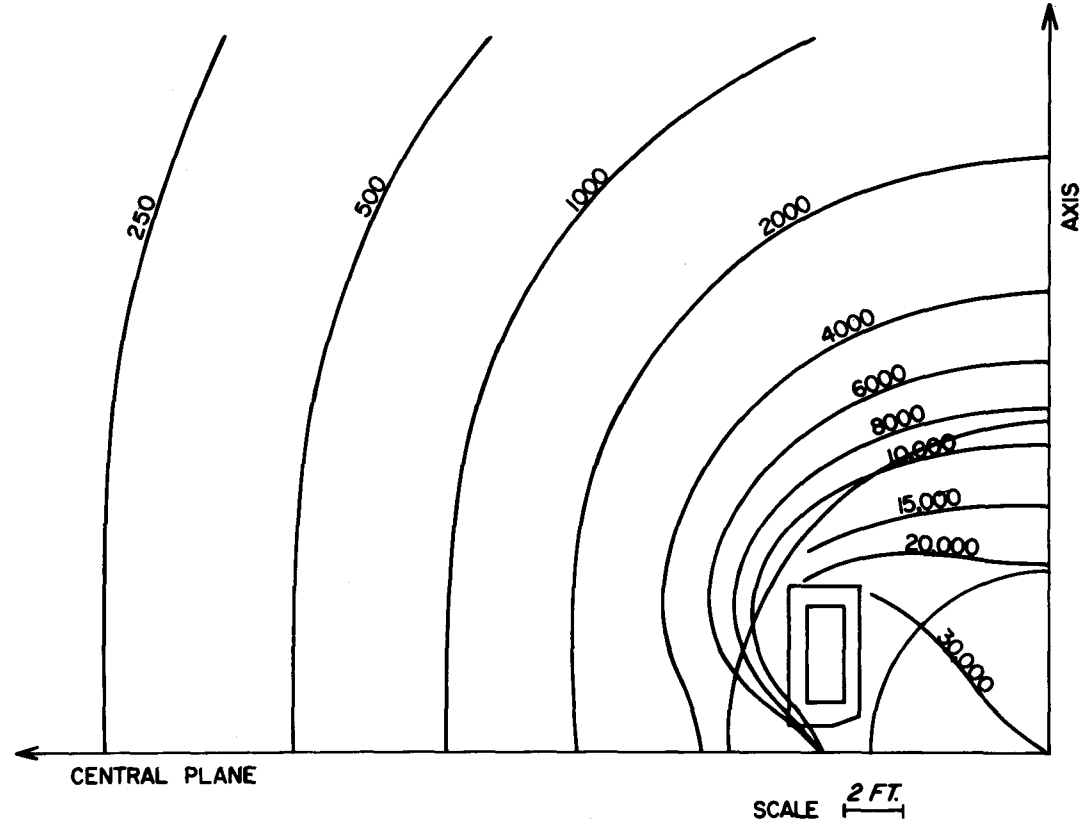

FIG. 4 STRAY FIELD PLOT (TOTAL FIELD IN GAUSS)

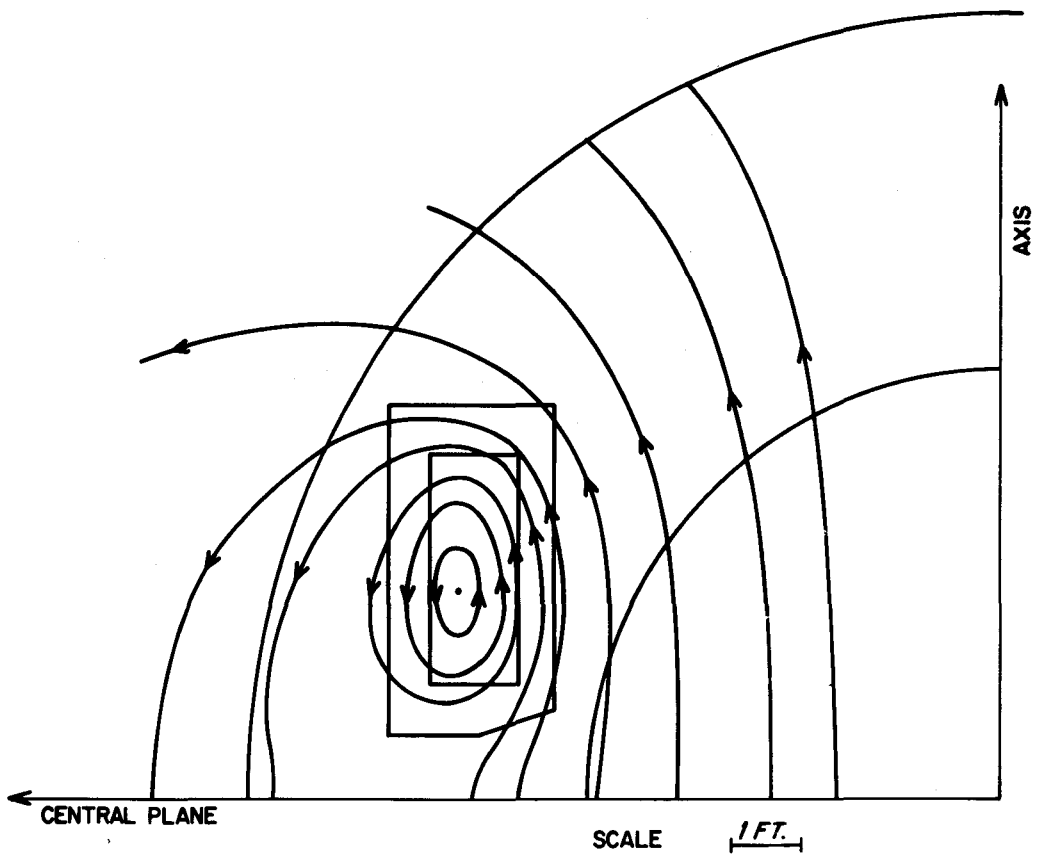

FIG.5 MAGNETIC FLUX LINES

steel strip will be edge-welded to the preceding turn to make each pancake self-supporting for the hoop load and to eliminate the need for radial clamps. The stainless steel strip is 1.5 in. wide, exceeding the conductor width by 20 mils. The compressive force between pancakes will be supported only by the stainless steel. This has the advantage of releasing some of the tolerances on the width of the conductor and of eliminating any possible compressive load concentration on the edge of the conductor with the risk of buckling of the wide copper strip in case of local bond deficiency of the solder.

The coils will be wound at ANL using existing winding line components from the 12 ft. magnet. One winding table only will be needed, as no epoxy will be used in the present magnet. New tension devices have been constructed for the conductor and the stainless steel strips.

Spacers between pancakes will be .25 in. thick Micarta (linen reinforced phenolic). These are 1 in. wide and will give 50% coverage of the surface of the coil. Each coil stack will be clamped directly to the bottom plate of the cryostat as described in a following section.

Figure 6 shows assembly of the coils at NAL. Figure 7 shows the electrical connection between pancakes.

(5) STRESS ANALYSIS

The distribution of compressive or axial pressures across the whole section of the winding is shown in Figure 8. The maximum average pressure, which occurs on the eigth pancake starting from the gap and on the middle turns of this pancake, is 2690 psi. Assuming a 50% coverage of the spacers, the stainless steel strip will be submitted to a maximum axial pressure of 17,200 psi.

The hoop stresses in the pancakes have been determined by using the simplified assumption of a homogeneous solid disc under the actual field distribution, then by redistributing these stresses in the materials according to their respective cross sections and moduli of elasticity.

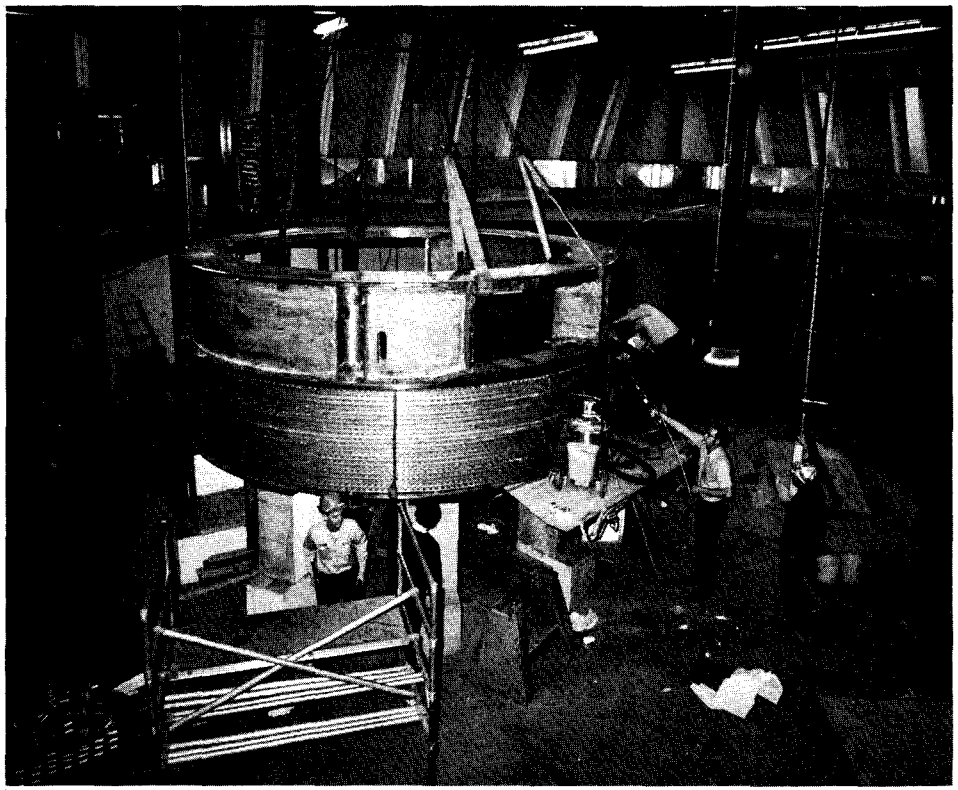

Fig. 6. NAL Bubble Chamber Magnet Assembly.

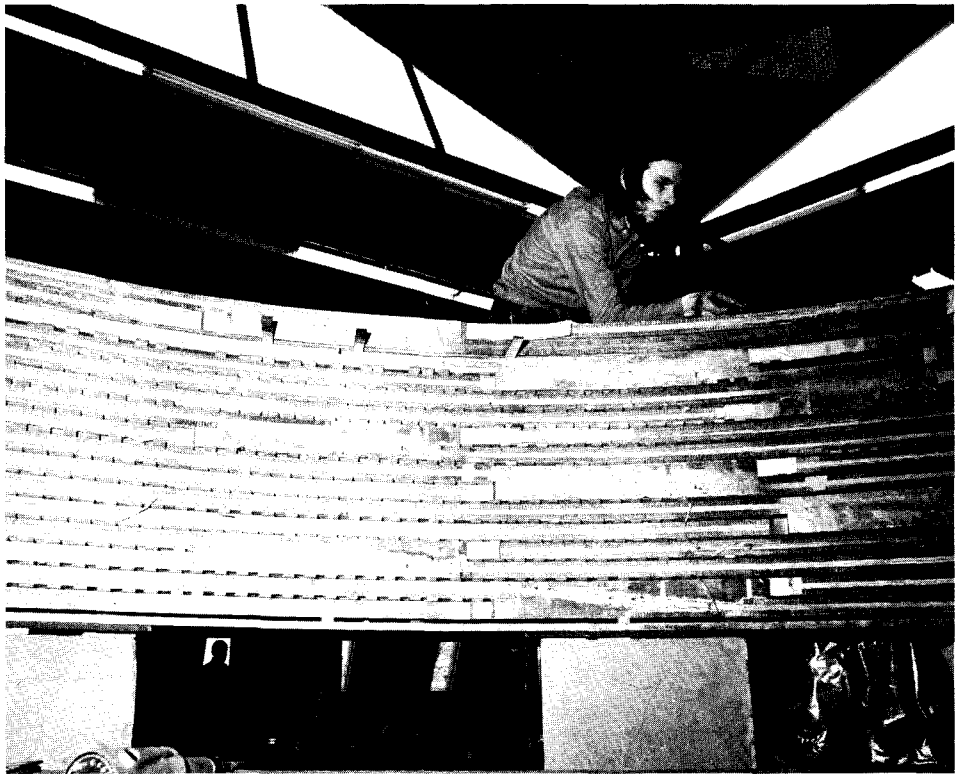

Fig. 7. Interior View Showing Electrical Connections.

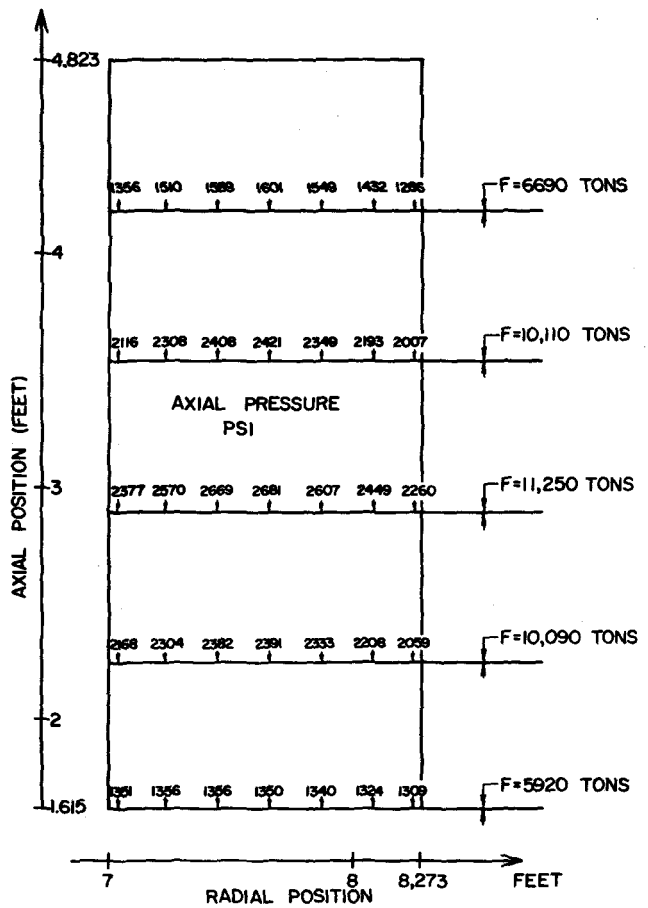

Fig. 8. Distribution of Vertical Forces in the Winding.

The maximum hoop stress occurs on the inner diameter of the pancake with a maximum hoop load of 4080 lbs. per turn. Using moduli of elasticity of 30×10^6 psi for stainless steel and 17×10^6 psi for copper (average modulus up to 10,000 psi hoop stress) the maximum hoop stresses are then 10,300 psi for the copper and 17,000 psi for the stainless steel. These hoop stresses decrease nearly linearly with the radius and on the outside diameter the stresses are 8200 psi for the copper and 13,500 psi for the stainless steel.

Actually, the hoop stress distribution must differ slightly from that indicated above due to the non-homogeneous structure of the winding and to the presence of Mylar between turns. However, the difference was found very small when using a more elaborate program[1)], provided that no gap be allowed between turns during windings. In fact much greater discrepancies can arise from the choice of the moduli of elasticity for the materials involved. In any case, the integration of the hoop stresses along the radial thickness of the coil must result in the total hoop load, which can be directly obtained from the average axial field in the pancake. In the present case, the field varies nearly linearly from the inside to the outside radius from 51 kgauss to -22 kgauss, giving an average field of 14.5 kgauss. With a total of 325,000 amp x turns in the pancake, the total hoop load in the latter is then 247,000 lbs. or an average of 3820 lbs. per turn, which corresponds to what was found in the above analysis.

Another change in the hoop stress distribution arises from the fact that, in the present magnet, it is planned not to clamp the extremity of the inside turn in order to avoid any stress concentration on this portion of the conductor and on the electrical inner joint which could result from the clamping method. Consequently, the coil will have a tendency to unwind itself, starting from the inner turn. This tendency is overcome by the friction between turns due to radial forces. The radial pressure on the first turn is 97 psi, which gives a total radial force

of 76,500 lbs. on this turn. In order to balance the hoop load of 4080 lbs. found before, a friction coefficient of 0.053 would be sufficient, which is very low even between copper or stainless steel to Mylar interface. Supposing that the friction coefficient was smaller, the preceding radial force acting for friction would become about two times higher, reducing the necessary friction coefficient to 0.027. It can be concluded that only a small length of the conductor will tend to slip outwards. The amplitude of the displacement of the inner end of the conductor can be found from the expansion of the coil itself under the magnetic hoop load. This expansion is of the order of 0.054% on the inside diameter. If one turn is effectively allowed to slip, the end will move only 0.28 in. A last remark can be added to the present discussion. As shown above, if we follow the conductor starting from the inner end, we must reach one point where the accumulated friction force is sufficient to balance the hoop force. From this point the tendency of slipping between turns disappears completely as the hoop stress itself is balanced at each point of the conductor in the two opposite directions.

The stress analysis described above only applies to the electromagnetic forces. The stresses given here should be combined with the thermal stresses due to differential contraction between copper and stainless steel during cooldown and with the pre-stresses induced by tension during winding. The first stresses have been estimated as 2830 psi in the copper and -3770 psi in the stainless steel strip, using a differential contraction of 30×10^{-5}. On the other hand, the winding tensions are planned to be 4500 psi for the copper and 9000 psi for the stainless.

(6) COIL STABILITY

We first examine the "external" stability of the conductor based on the classical "full stabilization" criterion, which is independent of the nature of internal instabilities.

As previously indicated, two modes of cooling are provided for the

conductor, edge cooling and face cooling. The power dissipated in the conductor when 100% normal is per cm of length:

$$W = \frac{3 \times 10^{-8}}{1.28} (5000)^2 = 0.585 \text{ watt/cm}$$

This is the power at the highest field point where the resistivity of the copper is 3×10^{-8} Ω - cm.

For edge cooling 75% of the surface is exposed to liquid helium (only one edge of the conductor can contact the spacers); i.e., 0.572 cm^2 per cm of length and the heat exchange coefficient can be safely taken as 0.4 watt/cm^2, which enables the removal of 0.288 watt/cm. For face cooling the exposed surface is 2.5 cm^2/cm. From Wilson's data[2] the heat transfer coefficient for the channels in the conductor should be higher than 0.15 watt/cm^2, which gives a heat exchange of 0.375 watt/cm. Then the total heat exchange capacity for the conductor is 0.66 watt/cm and the stability factor is 0.97, which indicates that full stabilization is achieved with the provided cooling.

"Internal" stability refers to the behavior of the superconducting filaments inside the copper matrix. Two effects are responsible for internal instabilities: magnetization of the superconducting material with associate "flux jumps" and eddy currents due to flux variations during charging or discharging of the magnet.

With regard to the first effect, no attempt has been made to achieve complete intrinsic stability for the present magnet, as the size of the filaments would have been too small and their number too large for a practical, reliable, and economical conductor fabrication. Furthermore, such a requirement is not necessary in view of the external stabilization indicated above. The characteristic which in this case is considered important for internal stability is the current-sharing characteristic of the superconducting filaments. This can be explained in a simple way: when a filament is heated, its current capacity is reduced

accordingly and can become smaller than the transported current, in which case part of this current is transferred to the copper, with resistive heat dissipation taking place both in the copper and in the superconductor. The current-sharing transition must be smooth and reversible in order to avoid large jumps, but most important the heat transfer capacity from superconductor to copper must be sufficient to allow the filaments to return to their initial temperature and full current capacity after the occurrence of the perturbation. This condition will be analyzed for the present magnet in the most critical case of maximum current and maximum field.

The current-sharing characteristic of the conductor is shown in Figure 9 where the current and the dissipated power are plotted both for the copper and the superconductor as a function of the voltage along the conductor. The copper resistance is 2.35×10^{-8} Ω/cm. The maximum voltage with all the current in copper is then 117 μ V/cm and the maximum power dissipated in the superconductor occurs when the current is equally shared between copper and superconductor and is equal to 147 mW/cm.

On the other hand, the heat transfer characteristic between superconductor and copper can be expressed by the following relation, first derived by Fairbanks[3)]

$$W = 8 \pi k (\overline{T} - T_o)$$

Where k is the thermal conductivity of the superconductor, T_o the copper temperature assumed uniform, T the average temperature in the superconductor and W the heat flux per cm of length for one filament. If N is the number of filaments, $W_{max} = 147 \times 10^{-3}/N$. Maximum $\overline{T}$ also represents the critical temperature at the current of 2500 A and field of 60 kgauss and is found equal to 5.7°K[4)]. Supposing the copper temperature to be 4.7°K and taking a very conservative value of K = 0.5 mW/cm for Nb-Ti, the above formula gives N = 12.

The number of 60 filaments adopted for the conductor then ensures

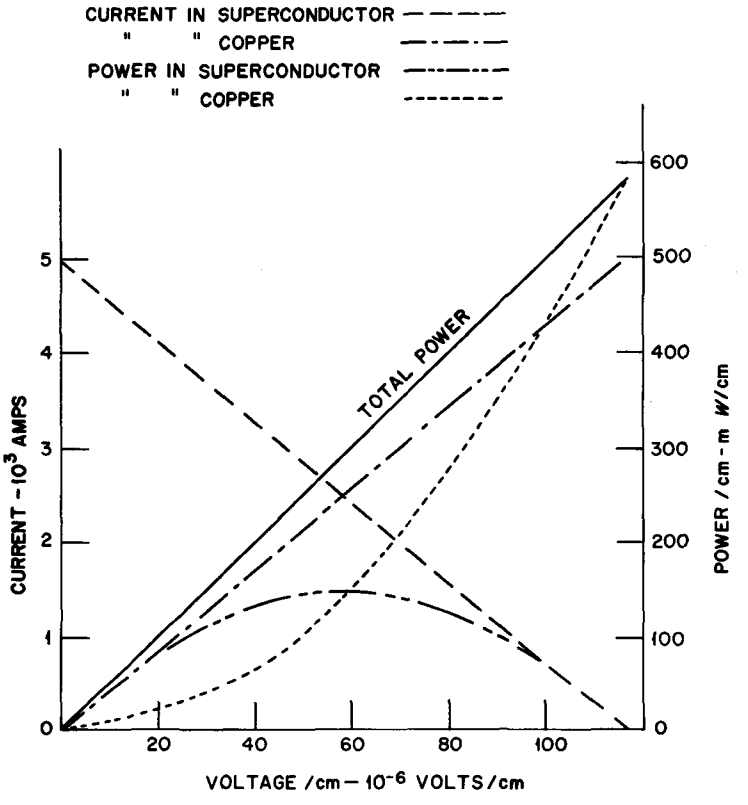

Fig. 9. Current-Sharing Characteristic of the Conductor.

a very safe current-sharing characteristic for this conductor.

In the preceding analysis, the thermal resistance of the bond between superconductor and copper has been neglected, as it is expected to be very small with the method of fabrication anticipated for the conductor. The bond quality has been defined in the specifications by its transfer length which must be smaller than one inch.

The second effect mentioned before concerns the eddy currents in the conductor. By twisting the filaments, the amplitude of these currents can be reduced to a level well below the critical current. A characteristic length is universally used for determining the useful twist rate:

$$\ell_c^2 = J_c \rho / \frac{dB}{dt} \times 10^8$$

In the present case J_c = 70,000 A/cm^2, $\rho = 3 \times 10^{-8}$ Ω-cm, d = 0.038 cm, and dB/dt = 2 Gauss/sec. with a charge voltage of 10 volts. This gives ℓ_c = 63 cm which indicates that the pitch of the twist should be well below 126 cm. This has been specified as 14 in. maximum, or 35 cm.

In fact, the main reason for twisting the filaments is to reduce the time constant of the eddy currents in order to eliminate any perturbation of the field shape in the useful volume. An expression for the time constant has been given by Morgan[5], which applied to the pitch of 14 in. gives T = 54 sec. Though this value may be far from exact, as it does not take into account the actual number and configuration of filaments, it indicates well enough that long time-constant field perturbation will not occur in the present magnet.

(7) CRYOSTAT

The cryostat is designed to operate with a source of liquid helium and to utilize the sensible heat of the boil-off gas to intercept incoming heat. The expected boil-off rate is 50 liters per hour. This mode of operation as compared to a refrigerator has the advantage of reduced boil-off in the event the magnet has to be run from a liquid source for

a short period of time. By keeping a reserve of 3000 to 4000 liters of liquid in the storage dewar, the magnet can be operated for 60 to 80 hours without requiring the operation of the liquefier. This allows shutdown for maintenance without interrupting the magnet operation.

Pressure ratings of the cryostat were chosen to minimize the cost and weight without impairing the operation. The vacuum vessel is rated for normal operating conditions and is vented to the chamber vacuum for large internal or external pressures. This approach still has the advantage of separate vacuums for the chamber and magnet; i.e., the cold surface is not exposed to possible hydrogen leakage and the magnet will not be affected by poor chamber vacuum. Venting the magnet vacuum to the chamber vacuum increases the maximum allowable pressure in the chamber vacuum to the buckling strength of the helium vessel rather than that of the light weight magnet vacuum vessel. Pressure rating of the helium vessel is based on possible pressure rise during emergency conditions. The rating of 45 psi results in a 3/4 in. wall thickness which stiffens the bridge support structure.

The magnet cryostat (Figures 10 and 11) is a vessel 128 in. high x 213.5 in. O.D. x 156 in. I.D. (stiffeners on the outer vessel increase the O.D. to 222 in.). The components which make up the cryostat are a stainless steel vacuum vessel, two stainless steel helium vessels separated by a stainless steel bridge assembly and an aluminum radiation shield covered with several layers of aluminized Mylar.

The helium vessel and vacuum vessel are designed to meet the following conditions:

1. To withstand 45 psia pressure both internal and external on the helium vessel.
2. To establish a design that would minimize the weight and cost of the cryostat fabrication and assembly.
3. To use 16,000 psi for a safe stress level for the vessels at at room temperature conditions.

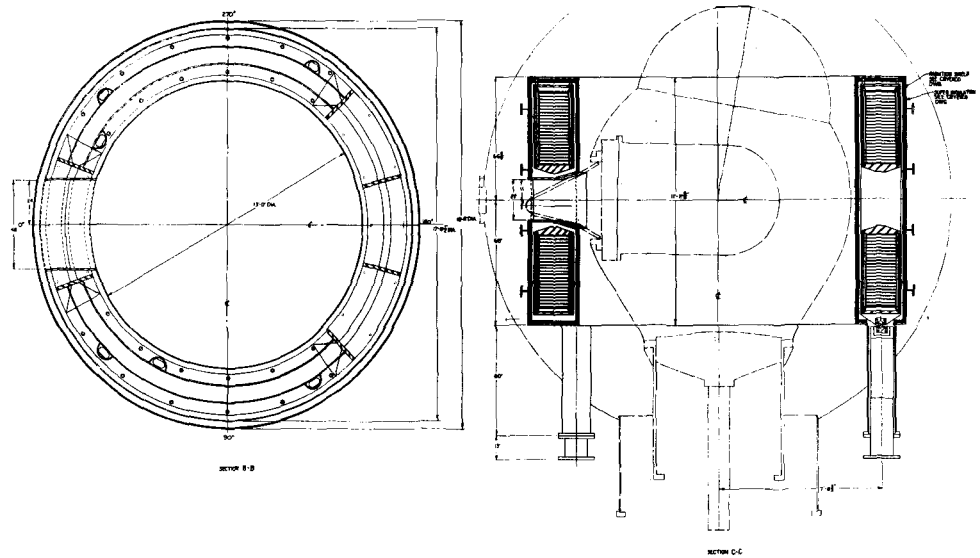

Fig. 10. Overall cross section of bubble chamber and magnet.

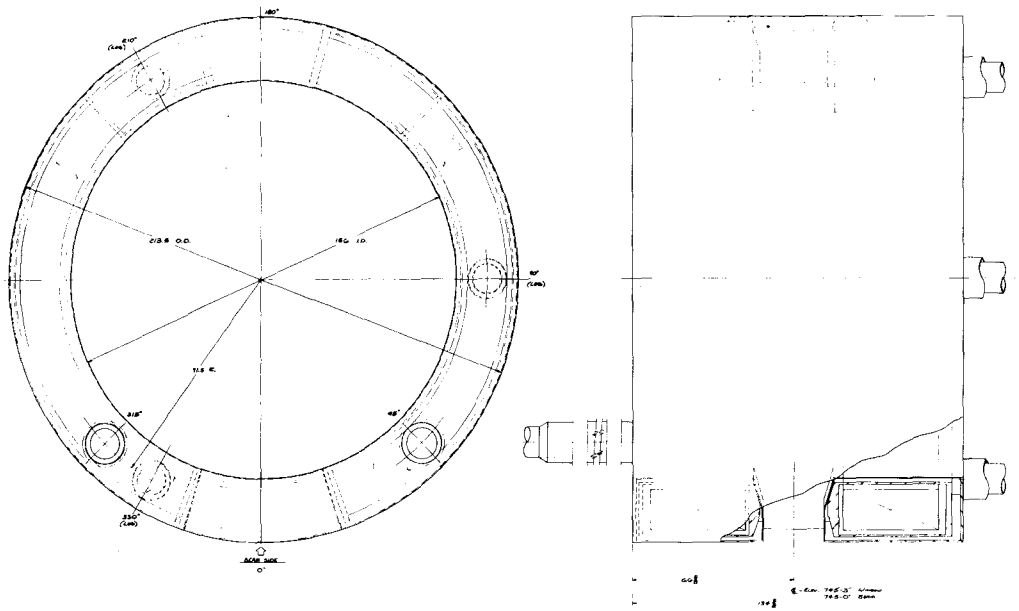

Fig. 11. Top view and cross section of magnet.

4. To use a 30,000 psi stress level for the design of the helium vessel bridge structure in tension and bending. This stress level was established because:
   a. The bridge will be at 4.2°K when the magnetic forces are applied.
   b. The forces are applied slowly due to the slow charging rate of the magnet.
   c. The magnetic forces cannot accidently exceed those calculated for a central field of 30 kgauss.
5. The vacuum vessel is designed for 5 psia internal pressure and 20 psia external pressure. Rupture discs are provided to protect the vessel under emergency conditions.
6. To support 500,000 lbs. vertical external load and 50,000 lbs. horizontal load.

The helium vessel modules are stainless steel cylindrical shells with cover plates. These assemblies envelope the coils and are welded to the bridge structure to form a unitized vessel rated at 45 psi internal and external pressure.

Two 12 in. pipes are located in the top plate of the helium vessel. These pipes provide access openings for the power leads, instrumentation, cryogenic piping and the emergency dump system.

The helium vessel is supported from the bottom by three equally spaced legs fabricated from 12 in. pipes with cooling passages attached for intercepting heat. Between the three support legs and the helium vessels are pivot-type bearing boxes. These boxes are designed to move 0.3 in. horizontally during cooldown of the cryostat and to support a vertical load of 3 g's and a horizontal load of .2 g's.

The aluminum radiation shield with cooling coils, completely envelopes the helium vessel. Suitable openings are provided in the shield to prevent collapse of the shield during vacuum pumpdown or an overpressure due to a broken rupture disc in the vacuum jacket.

The bridge assembly is the support base for the coils in each module. The coils are clamped to the bridge structure by means of 1 in. aluminum tie rods and a clamping ring. The tie rods are spaced in pairs on 18° centers. The tie rods are screwed into the bridge structure and extend through a 5/8 in. stainless steel clamp ring. The spacers between the clamp ring and the coil vary in thickness. Radially positioned midway between the tie rods are spacers 0.500 in. thick. When the nuts on the tie rods are tightened they deflect the clamp ring approximately 0.070 in. This spring effect loads the coils midway between the tie rods to approximately 6500 lbs. each or a total force of 130,000 lbs. The tie rods are then tightened to a stress of 15,000 psi which produces a force applied to the coils of 480,000 lbs. When the tie rods are tightened they will elongate about 0.060 in. The spring action produced by the deflected clamp ring and the elongated tie rods will maintain a clamping force on the coils during cooldown and also as the coils tend to "bed down" under the compressive load caused by the magnetic field.

The bridge assembly also provides beam windows at 0° and at 180°. The beam entry window located at 0° is a clear opening 22 in. high x 48 in. wide. The beam exit window located at 180° is also a clear opening of 90° included angle with two vertical support struts 5 in. thick located radially 15° each side of the 180° centerline.

The bridge structure has six, 6 in. vertical pipes spaced in suitable locations to provide communication between the upper and lower coil modules. They will be used for passage of helium (gas and liquid), for intercoil connections, instrumentation wires and cooldown piping.

(8) VACUUM VESSEL

The vacuum vessel is fabricated out of stainless steel and is designed for an internal pressure of 5 psi and an external pressure of 20 psi. Rupture discs with the above ratings will be installed in the vacuum vessel to protect the system in the event of either a bubble chamber

or helium vessel failure. The vacuum pump for the cryostat is attached to a pumpout port located in one of the vessel support legs. The cooling tubes for the radiation shield enter the system through a bayonet fitted flange connected to a fitting in the vacuum pumpout line.

(9) RADIATION SHIELD

The cryostat contains a thermal radiation shield in the vacuum space between the helium vessel and outer vessel. The radiation shield is constructed of aluminum and is cooled by circulating cold helium gas through piping on the shield. The gas is circulated by a small compressor and is cooled with liquid N_2. Average temperature of the shield will be about 90°K, and the heat load about 300 watts. It will be insulated from the warm wall with aluminized Mylar. Aluminized Mylar will also be used between the shield and the vessel. Due to space limitations, a radiation shield will not be used in the region of the inlet beam window. Here only aluminized Mylar insulation will be used. The shield is slotted at various places to reduce the forces due to eddy currents when the magnet is discharged.

(10) LEADS

The magnet current leads will be brought out of the top of the cryostat as shown in Figure 12. The leads will introduce about 12 watts in to the helium bath. They will have a loss almost this great at zero current. This is because the leads are designed to operate with zero gas flow for 10 min. without burning out. A flow alarm will be installed in the lead gas exhausts. If flow is interrupted for any reason the magnet energy can be dumped without burning out the leads.

(11) LIQUEFIER (See also Section V)

Liquid helium will be supplied to the magnet system by a 100 liter per hour liquefier. The machine will be furnished as a packaged system by a commercial firm. Liquid is stored in a gas shielded, 10,000 liter

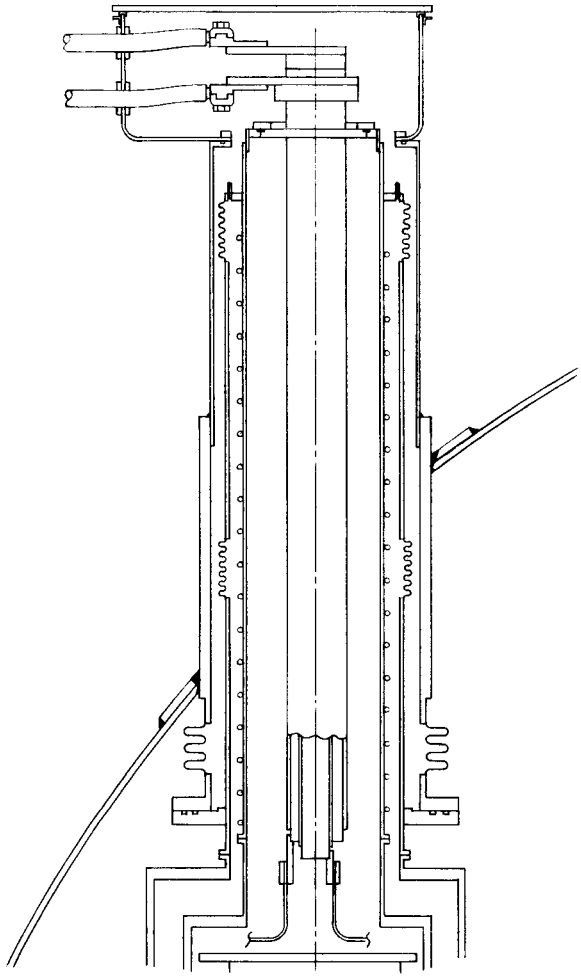

Fig. 12. Vertical penetration used for leads.

dewar. Pressure in the dewar will be maintained at 4 psig and liquid will be transferred to the magnet as needed to maintain the liquid level. Dual purifiers will be utilized in the system so reactivation of one can take place while the other one is operating. The purifier system is designed for 500 ppm impurity level. The machine can operate as a refrigerator, for cooldown of the magnet, and can produce 2000 watts of refrigeration at 50°K, dropping to 1000 watts at 20°K. A complete flow sheet is shown in Figure 13.

(12) COOLDOWN (See also Section V)

The magnet will be cooled to operating conditions in four stages. It is estimated that thermal stresses will limit the maximum cooldown rate to 20 kW. In the first stage helium gas will be circulated through a "cooldown heat exchanger" by the liquefier compressor. Liquid nitrogen will be used to cool the heat exchanger which is located near the magnet. After about 120 hours of cooling the magnet will be at 115°K.

About 29,000 liters of liquid nitrogen will be required. At this point the liquid nitrogen is replaced by liquid hydrogen for the second stage cooling.

Fifty hours later the magnet will have been cooled to 40°K, consuming 11,000 liters of liquid hydrogen. At this point the liquefier is connected as a refrigerator for third stage cooling down to 20°K. The fourth stage is to transfer liquid helium from the storage dewar to the magnet to cool down to 4°K and fill with liquid. About 500 liters of liquid helium will be evaporated in cooling the magnet from 20°K to 4°K and another 5150 liters required to fill it. The expected cooldown rate is shown in Figure 14 and the magnet heat capacity in Figure 15.

(13) INSTRUMENTATION (See also Section VI)

Each pancake will have a potential tap so the joint resistance can be checked. A thermocouple will be placed on each pancake to monitor temperature and temperature gradients during cooldown. Continuous liquid

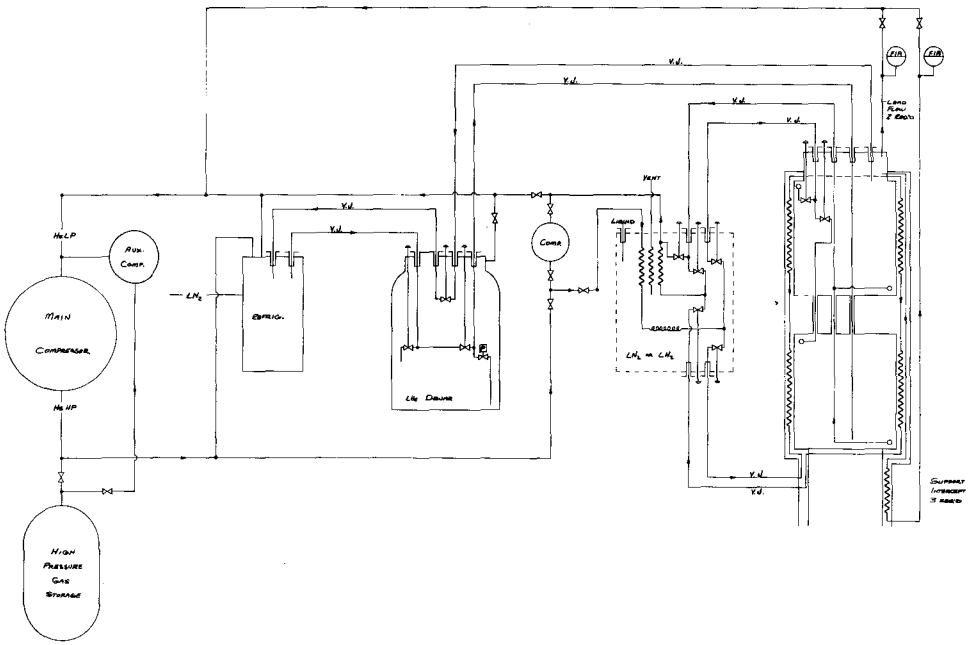

Fig. 13. Magnet system flow sheet.

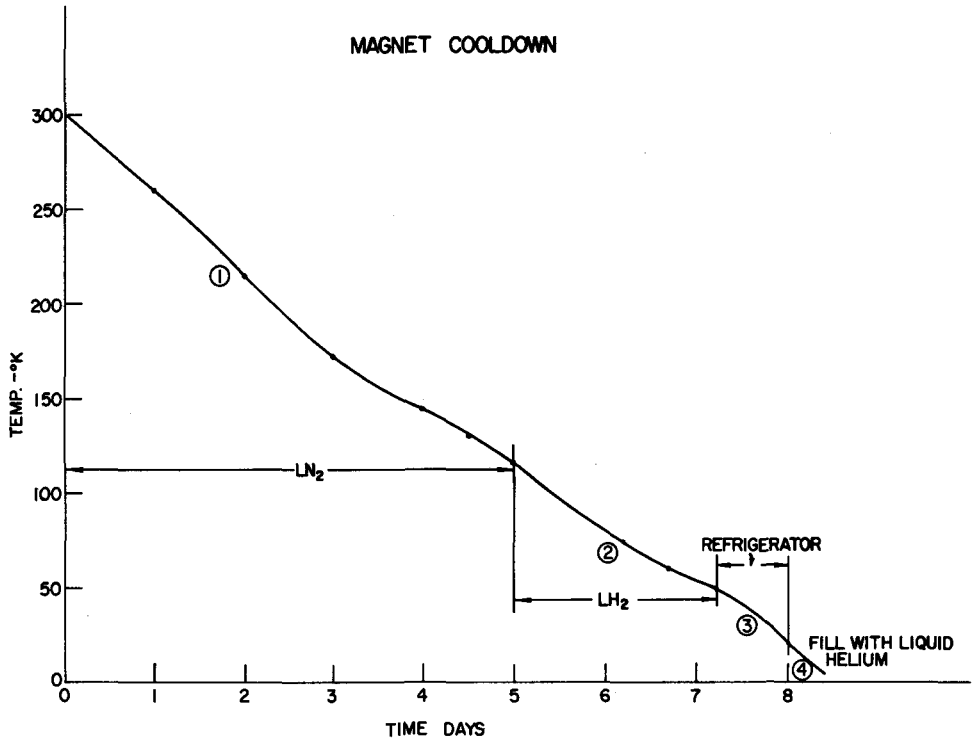

Fig. 14. Magnet Cooldown

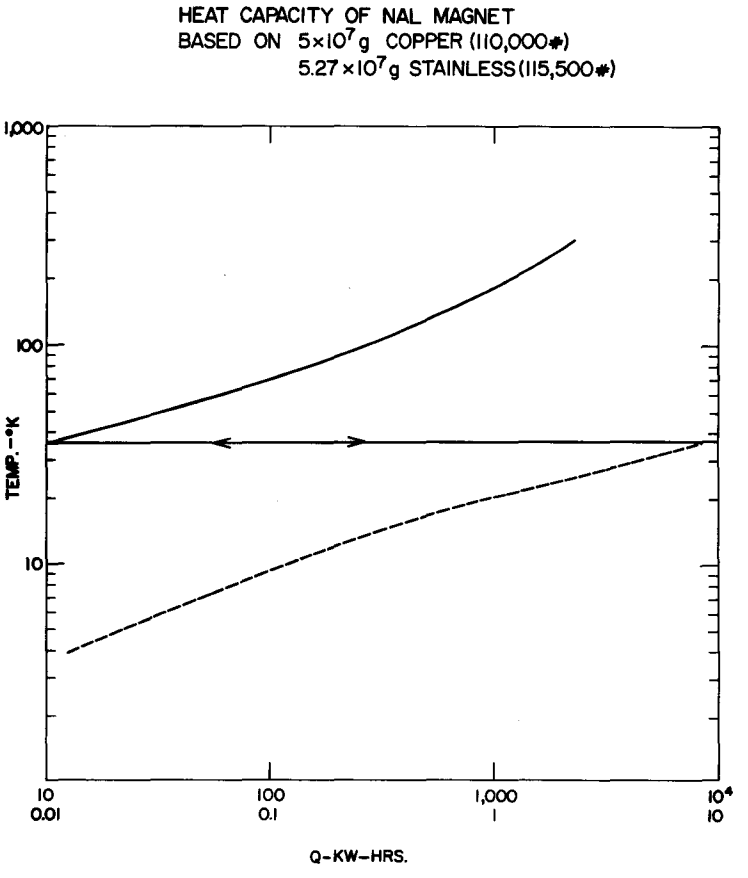

Fig. 15. Heat Capacity of NAL Magnet

level indication will be provided by several superconducting indicators in series along the height of the coil. A continuous level indicator will be placed in the top pipe that contains the leads and the level will be controlled in the top pipe that contains the fill line. Strain gauges will be bonded to the stainless steel clamp rings to indicate any changes in the amount of bending to determine if the coils are loosening up.

(14) POWER SUPPLY

The power supply will furnish 10 volts at 5000 amps which will charge the magnet at a maximum rate of 0.33 amp/sec. Current sensing will be accomplished by an electronic transducer with a basic stability of 10^{-4}, this will be the limiting factor in the power supply stability.

Control of the power supply will be similar to that of the 12-foot HBC magnet; i.e., on-off. For more information on this type of power supply the reader is referred to ANL/HEP 6813, "The Superconducting Magnet System for the 12-Foot Bubble Chamber".

(15) DUMP RESISTOR

To decrease the field rapidly a 0.036 ohm dump resistor is provided. The resistor will be constructed of stainless steel and immersed in a water bath. Enough water will be used to absorb the 400 Mjoules by the heat capacity of the water. Upon dumping at full field the magnet terminal voltage will go to 180 volts. The design is intended for 1000 volts to give adequate safety factor. The time constant of the magnet and dump resistor is about 14 min.

(16) MAGNET VACUUM SYSTEM

The basis for the design of the magnet vacuum system assumed two conditions: 1) that rapid pumpdown of the vacuum system was not necessary or desirable due to the danger of damaging the superinsulation and 2) once the magnet is cold no further pumping will be necessary.

Using these basis assumptions the vacuum system design proceeded. A 6 inch 1500 liter/sec. diffusion pump was chosen as the main pumping unit, to be close mounted to the magnet leg. The forepump and line were chosen several sizes larger than necessary to provide a sufficiently low foreline pressure for the diffusion pump when the diffusion pump is passing its maximum throughput. This turned out to be a 40 CFM Stokes Vacuum Pump with a 4 inch IPS foreline.

Following is a schematic of the vacuum system. Tabulated below is the interlock and startup procedure.

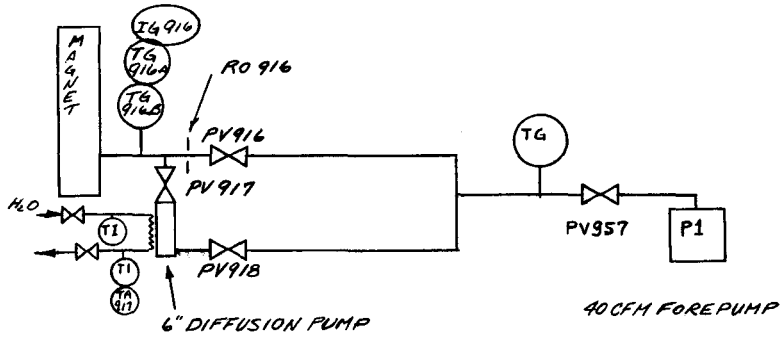

1. Start P1 -- if TG reads less than 1 ATM P1 will not start until line is vented.
2. Start P1 -- PV957, PV916, PV919 open automatically to prevent superinsulation damage. Manual override for PV916 on rear of panel allows PV916 to remain closed if desired. This requires operator decision. To further prevent superinsulation damage RO917 (a one inch diameter orifice) is placed downstream of valve PV917.
3. All valves have manual override to close only on rear of panel.
4. When TG916B reads 100μ or less diffusion pump is opened to system and turned on. PV916 is closed.

5. Should power loss occur PV957, PV916, PV917 will close automatically.
6. To restart operator supervisor decision is required. Four inch line must be vented and pump restarted after closing PV916 and PV918. When TG and TG916B are shown to be micron range or less PV917 may be reopened.
7. The diffusion pump is protected with a water temperature switch TA917 which actuates an alarm and cuts off the diffusion pump heater. Operator decision is required to restart the diffusion pump heater.

The entire system is capable of withstanding 150 psig internal pressure, but safety devices located on other parts of the system prevent pressure from rising above 45 psig.

Pumpdown time is unknown due to the superinsulation in the system and the water it tends to hold. Once dry, pumpdown to 10^{-6} should take roughly 4 to 5 hours.

(17) DETAILED STUDIES

The following is a list of additional calculations and reports on the magnet:

1. Magnetic Engineering Associates

   Report, J.J.Nolan, 1/26/71: Forces on the Heat Shield of the 15-Foot NAL Bubble Chamber Magnet

   Report, L.M.Lontai, 3/10/71: Magnetic and Thermal Stresses in the Windings; Prestressing With Winding Tension

2. Argonne National Laboratory

   J.Purcell Memo, 2/23/71: NAL Superconducting Magnet Design Review Meeting

3. Cryogenic Engineering Co.

   J.Dehaan, 5/5/71: Calculations Relating to Design & Analysis of Helium Cryostat for 30 Kilogauss Magnet for NAL

4. Magnetic Corp. of America

   Report, 6/9/71: Investigation of the Stability and Quench Characteristics of the Conductor for the NAL Bubble Chamber Magnet

5. R.B.Jacobs Associates, Inc.

   Letter, 7/8/71: Adequacy of Leg Heat-Intercept Exchangers on NAL Magnet Cryostat

   Letter, 6/16/71: Emergency Venting of NAL Magnet Cryostat

   All calculations for above.

6. Cryogenic Consultants, Inc.

   P.C.VanderArend, 8/20/71: Summary Description of Cooling System for Magnet Pancakes

   P.C.VanderArend, 8/19/71: Review of Stearns-Roger Drawings

7. Battelle Memorial Institute

   Letter, 11/11/71: Review of Stearns-Roger Design Calculations for the Magnet Cryostat

8. Stearns-Roger Corp.

   Kass Taylor: All stress calculations on magnet cryostat.

REFERENCES

1) Herve, Program SPRMFI, Internal Report, February 20, 1969

2) M.N.Wilson, Pure and Applied Cryogenics, Vol. 6, p. 109 (1966)

3) D.F.Fairbanks, The Transition to Current-Sharing in Composite Conductors, Norton Internal Report, 1967

4) R.Hampshire, J.Sutton, and M.T.Taylor, Effect of Temperature on the Critical Current Density of Nb-44% Ti Alloy, Conference on Low Temperatures and Electric Power, London, March 24, 1969

5) G.H.Morgan, Theory of the Twisted Multicore Superconducting Wire in a Uniform Magnetic Field, BNL 13792

Appendix I

THE NAL 2-FOOT MAGNET TEST

During the first test of the NAL 2-foot magnet a normal region developed at 6,000 amps. At the time this was thought to be due to the leads but could not be verified. The leads were rebuilt to carry higher currents, and the magnet was retested November 19, 1971.

During the test one power lead became plugged so no intercept flow could be taken, and a bad leak developed in the top of the cryostat. This leak prevented the cryostat pressure from building to a level sufficient to give proper heat intercept flows, resulting in a high heat leak.

The magnet was charged several times and each time the power supply primary circuit breaker tripped between 5,000 and 6,000 amps. This circuit breaker was rewired and the magnet was charged to 7,110 amps before the circuit breaker tripped. During all of these charges, the magnet was carefully monitored for normal regions and none were observed. The magnet was also allowed to stay at different current levels for several minutes to see if any normal region would develop. The 7,100 amps developed about 40 kgauss peak transverse field and about 25 kgauss peak radial field.

The magnet was then charged to 5,900 amps and held while the lead intercept flow was completely valved off, and the liquid level allowed to drop. After 15 to 20 minutes, the liquid level dropped about one inch below the bottom of the top pancake, and the magnet slowly began to quench. During the quench, the top pancake appeared to go partially normal with the remaining pancakes remaining superconducting.

The 2-foot magnet was disassembled and the conductor inspected with the same ultrasonic equipment that is being used for the final conductor.

Inspection of the 2-foot magnet conductor indicated about ten voids, 3 to 4 inches long. One area about 4 inches long was completely unsoldered. The normal criteria for conductor to be used in the large magnet is: voids shall be no longer than one inch. The performance of the conductor in the 2-foot, with its larger voids, leaves little doubt as to the electrical stability of the conductor in the large magnet, operating at 5,000 amps.

IV. EQUIPMENT

K. Magnet

2. INVESTIGATION OF THE STABILITY AND QUENCH CHARACTERISTICS OF THE CONDUCTOR FOR THE NAL BUBBLE CHAMBER MAGNET: SUMMARY OF CALCULATIONS

Prepared by

Z. J. J. Stekly

IV. K. 2. INVESTIGATION OF THE STABILITY AND QUENCH CHARACTERISTICS OF THE CONDUCTOR FOR THE NAL BUBBLE CHAMBER MAGNET: SUMMARY OF CALCULATIONS

This report is a summary of the work carried out under Contract No. 31-109-38-2511 from the Argonne National Laboratory. The purpose of the effort was to examine the conductor stability, the effect of motion and the propagation of the normal region in the coil being built by Argonne National Laboratory for the National Accelerator Laboratory bubble chamber.

Calculations were made of the following:

1. Transient characteristics of the conductor.
2. Temperature rise due to motion.
3. Terminal characteristics and velocity of propagation of the normal region along the conductor.
4. Calculation of the quench transient.

The main results are presented in tabular or graphical form in the main body of the report. Detailed descriptions or analyses are presented in the detailed calculations.

Conductor Description

The basic conductor configuration is shown in Figure 1. The conductor consists of a central section (labeled superconductor in Figure 1) which has 60 strands of Nb-Ti imbedded in copper. This central section is then soldered to three copper pieces to form the composite conductor. The two side pieces are grooved to allow helium flow.

The conductor is wound into place with a strip of steel for structural purposes. The steel is .020" larger than the copper so that under the worst conditions the conductor could slide a length of .020".

The central section of the conductor has a copper to superconductor ratio of 3.5 to 1. It has a design current of 5000 A and a critical current of 6000 A at 50 kilogauss. The twist rate is one per foot of length.

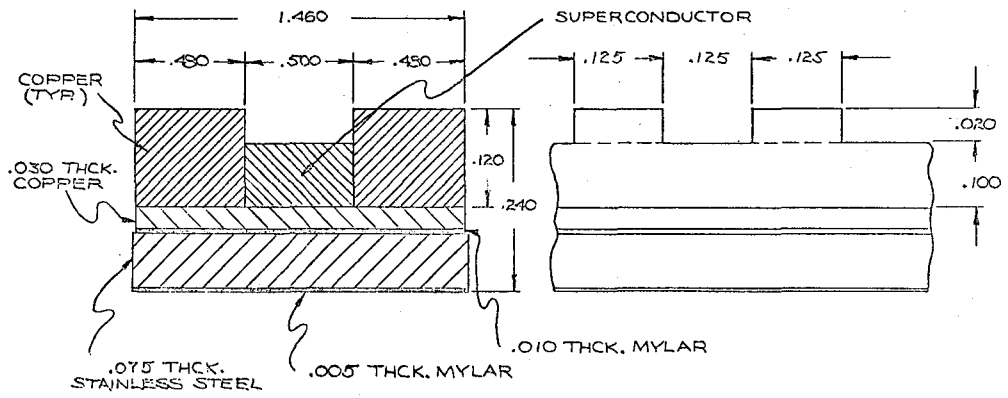

FIGURE 1. CROSS-SECTION OF CONDUCTOR

Transient Characteristics

The question of stability of the current flow in the central section of conductor is of primary importance. Since this section has a lower copper to superconductor ratio the time constants for several phenomena were computed and are tabulated below (unless shown otherwise all calculations are at 50 kilogauss):

Characteristic Times

		msec.
Growth of Instability	(no thermal cond.)	.058
	(with thermal cond.)	146
Decay of heating		77
Redistribution of current		154
Cooling of conductor	(nucleate boiling)	0.655
	(film boiling)	23
Relaxation of magnetization currents	B=5T	19200
	B=0	67200

Two growth rates were computed for instabilities. The .058 msec growth rate results if thermal conduction is neglected. This instability is completely damped out by the fact that it takes 154 msec for the current to redistribute throughout the conductor (assuming all the superconductor disappeared). If thermal conductivity is taken into account (but no heat transfer to liquid helium) the estimated growth time of the instability is 146 msec. The decay of heating due to currents in the copper occurs in 77 msec. so that this instability will also have its growth limited. Further, the cooling time for the conductor (by heat transfer to liquid helium occurs in 0.655 msec. in nucleate boiling and 23 msec. in film boiling. Both of these cooling rates are faster than the growth rate of the instability.

Based on the above it can be concluded that the conductor is stable provided helium is present.

Effect of Motion

The stainless steel being wider than the composite by 0.020 inch creates the possibility of relative movement by this amount. This slid-

ing generates heat which can drive a portion of the conductor normal. An approximate analysis of this situation is presented in the detailed calculations. Using average values for the properties, the following estimates result:

Time for slip to take place	333μsec
Estimated temperature at sliding surface	14.2°K
Average energy per unit mass (copper only)	4.66×10^{-3} j/g
Average temperature after slide (copper only)	12.2°K

The above calculations assume that the ratio of static to dynamic coefficient of friction is 0.5 and that the slip occurs at the maximum radial field (4T). If the slip occurs at lower fields then the energy release is less.

In the above calculations no account was taken of the heat transferred to the liquid helium. This is indeed a good model since the thermal time constant for film boiling is 23 msec.

While the above computation represents a worse case because of the use of maximum radial field and maximum sliding distance the temperature. rise in any slide is probably enough to drive the current out of the superconductor. However, based on estimates of the transient behavior, the conductor should recover to a fully superconducting state.

Terminal Characteristics of the Conductor and Propagation Velocity Along the Conductor

The characteristics of the conductor were computed for two cases: (1) For the current uniformly distributed throughout the copper substrate, and (2) for the current restricted to the central portion of the conductor.

The results are summarized for the terminal characteristics and for the velocity of propagation in the detailed calculations.

If one assumes that the superconductor suddenly disappears then, locally, while 5000 A is passing through the conductor the propagation of the normal region along the conductor occurs at approximately 1700 cm/sec. x .077 sec = 131 cm. One would expect that the normal region would subse-

quently recede-- provided helium was still present.

Quench Transient

The propagation of the normal region in a single pancake is shown in Figure 2. This transient was computed neglecting any heat transfer to liquid helium between pancakes, but taking into account the specific heats of helium, insulation and stainless steel.

Details of the computation are presented in the detailed calculations.

Conclusions

Except for the fact that conductor motion will drive regions of the windings into the normal state all calculations done so far show that the conductor should be stable under transient conditions. The stability of operation depends on having helium present at the heat transfer surfaces. Disturbances large enough to vapor bind the small passages could lead to a quench.

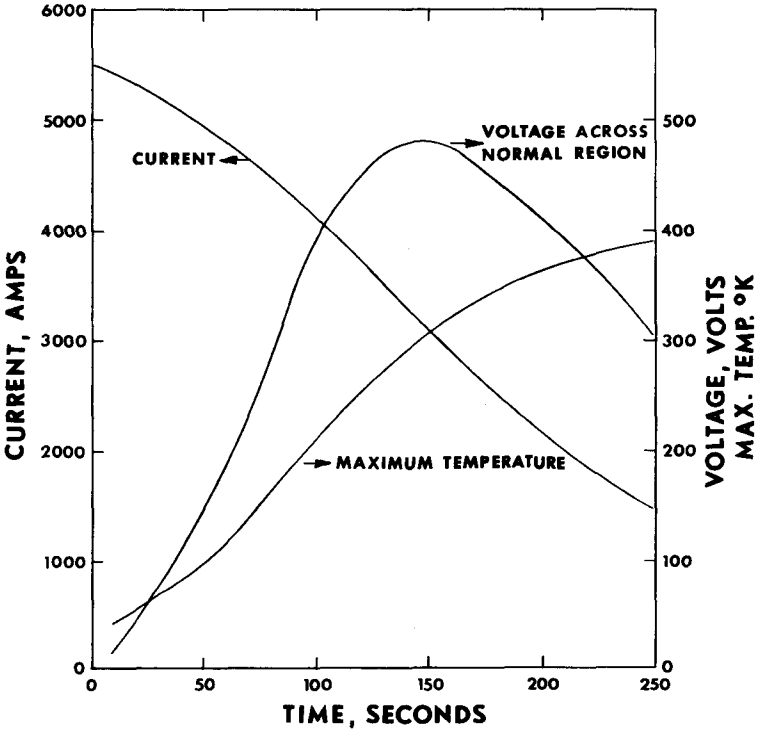

FIGURE 2. QUENCH TRANSIENT FOR 30,000 LITER BUBBLE CHAMBER MAGNET

IV. EQUIPMENT

K. Magnet

Prepared by

J. Purcell and Z. J. J. Stekly

IV. K. 3. VOIDS IN SOLDER BOND

VOIDS IN SOLDER FOR NAL BC CONDUCTOR

J. PURCELL

In the design report we used α as the ratio of power dissipated in the conductor when it is 100% normal to the power the helium bath can take away and remain in nucleate boiling. The calculated value of the α is 0.97 and experimental results from the 2' magnet indicate it is much less than this. Consideration of this α is valid in that it predicts recovery of the coil if a large region were to go completely normal. Recovery of a normal region does not require a bond between the superconductor and the copper strips because the current divides and flows in each strip as long as some contact is made along the length of the conductor. Figure 1 shows how the power will vary in the superconducting strip as it goes from normal to superconducting. The curve was calculated using the actual amount of copper in the superconducting strip and the following values:

$\rho_{cu} = 3 \times 10^{-8}$

Cu to superconductor in strip = 4:1

R inner strip = 11.6×10^{-8} Ω/cm

R_{cu} strips = 3×10^{-8} Ω/cm

I = 5,000 Amps

Note that this recovery power does not depend on bonding between the superconductor and the copper.

Stekly originally introduced α as a stability factor which is given by $\alpha = \frac{I^2 \rho}{APH\ (T_c - T_b)}$

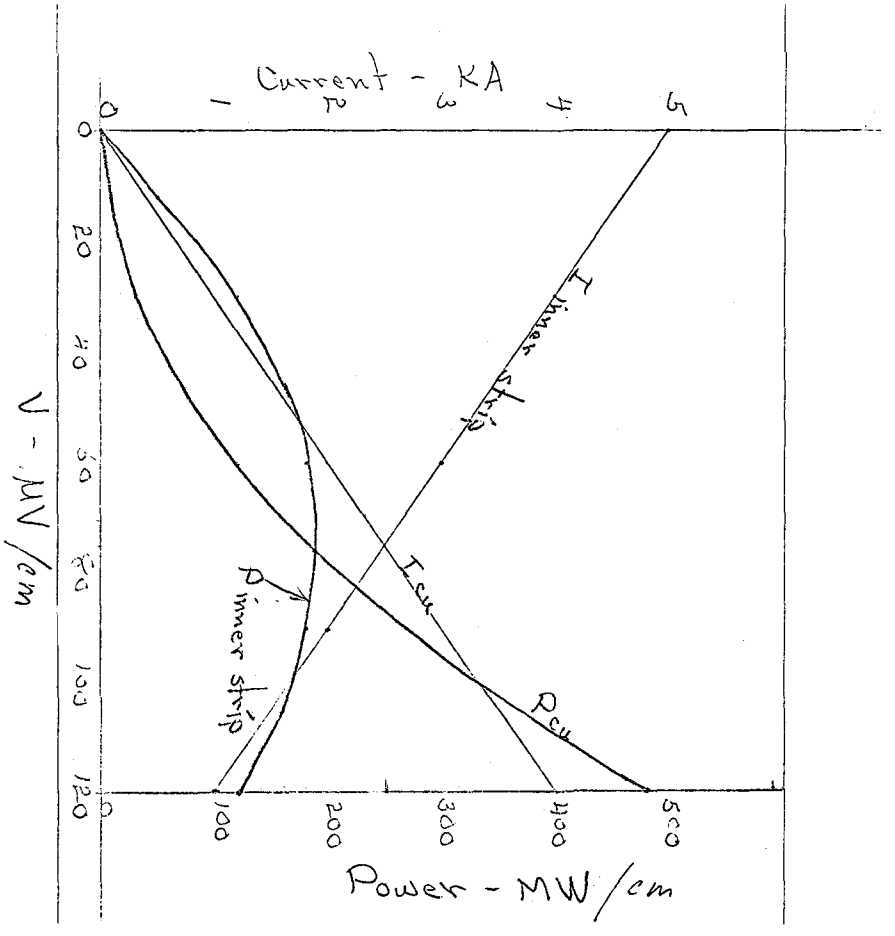

FIGURE 1. V-I CURVE

where P = cooled perimeter

A = cross sectional area of conductor

H = film coefficient to LHe, $\approx$ 1 ω/cm^2 °K

T_c = critical temperature of the superconductor, 6-8 °K for N_b Ti

T_b = temperature of bath $\approx$ 4 °K

This α deals with the slope of the V-I curve as it starts into current sharing. If α is less than 1 the conductor will go smoothly into current sharing. Applying this criteria to just the inner conductor, we obtain an α of 0.38 which indicates the inner conductor willgo into current sharing on its own without the benefit of the additional copper. This is all that is necessary for stability since the fully normal stability is taken care of by the additional copper in parallel.

Voids in the solder bond do not detract from the stability of the conductor but a long unbonded length will increase the charging loss of the magnet. If a short length, ($\approx$ 1 cm) wants to go normal during charging, the normal region will spread until it reaches a region bonded well enough for current transfer to take place. For example a 1 foot length of unbonded conductor will dissipate 18 watts at 5,000 amperes during the time it is normal. Recovery time of such a normal region will be a few seconds. At the charge and discharge rates expected for the NAL magnet, the charging losses will be small and the increase due to poor bonding is negligible.

The importance of voids is determined by the effect on the mechanical properties of the coil. In the end pancakes the conductor is subjected to a vertical force due to the radial field component. This force represents a shear load on the solder bond. To calculate this shear load:

$B_{max.}$ radial = 40 kG = 4 tesla

I = 5,000 Amps.

F = BI = (4) 5,000 = 20,000 Newtons/meter

$$F = \frac{20,000\ (2.2)}{9.8} = 4,500 \text{ lbs/meter}$$

$$F = \frac{4,500}{39.4} = 114 \text{ lbs/in.-length}$$

The conductor is 0.5 inch wide

$A = 0.5\ in^2/in.-\ length$

$$S_{shear} = \frac{F}{A} = \frac{114}{0.5} = 228 \text{ psi.}$$

This shear stress will appear on the solder bond with no solder in the crack between the conductor and the edge strip. The strength of a soldered joint is around 6,000 psi although this decreases with time, at room temperature, to about 4,800 psi. The sustained load carrying capacity of solder joints decreases to 300 or 400 psi over a period of years at room temperature. The particular load on the magnet solder can only occur at low temperatures so it is doubtful that the aging will be as severe.

Near the outside of the coil, the magnetic forces are in a direction to pull the conductor away from the backing strip. This force results in a tensile stress of about 50 psi.

If a small amount of mechanical failure occurs in the solder bond it will be harmless. It seems prudent, however, to prevent failures that will result in a turn or two unbonded.

Any unbonded region more than two inches in length will be repaired. This will prevent large stresses from accumulating and causing large scale failure.

Our present experience has been that any voids that appear are small (pin holes) and that only a major malfunction of the soldering line will produce voids of any size. In the event of malfunction probably several feet of conductor will be unbonded.

MAGNETIC CORPORATION OF AMERICA
67 Rogers Street
Cambridge, Massachusetts 02142
617/868-3300

October 1, 1971

Mr. George T. Mulholland
Bubble Chamber
National Accelerator Lqboratory
P.O. Box 500
Batavia, Illinois

Dear George,

After discussing the effect of delaminating the "train tracks" with you over the phone, we set about calculating the allowable delaminated lengths along the following model which is essentially what you suggested:

Starting from a conductor that has been driven into the normal region, we examine the recovery process. Recovery occurs as usual in the non-delaminated lengths of the conductor. Upon reaching the end of the delaminated length, recovery will continue taking place if the current in the section containing the superconductor is below the minimum propagating current as determined by the total cross-sectional area and cooling perimeter of the section containing the conductor. As recovery proceeds, the section containing the superconductor will increase in current and will continue to recede until either the current in that section increases to the minimum propagating value or the normal region shrinks to a critical size, at which point complete recovery occurs.

I am sending you a table containing the maximum allowable delaminated lengths for no effect on the VI curve, as well as the allowable length for complete recovery at 5,000 amps in the conductor. The three graphs are plots of the current at which full recovery is expected to occur as a function of the delaminated length.

I want to point out that the computations assumed no thermal contact between the delaminated sections, and as such, the actual performance of the conductors should be somewhat better than the calculations show.

If you have any questions, don't hesitate to give me a buzz.

Sincerely yours,

John

Z. J. J. Stekly
Technical Director

Enclosures
wm

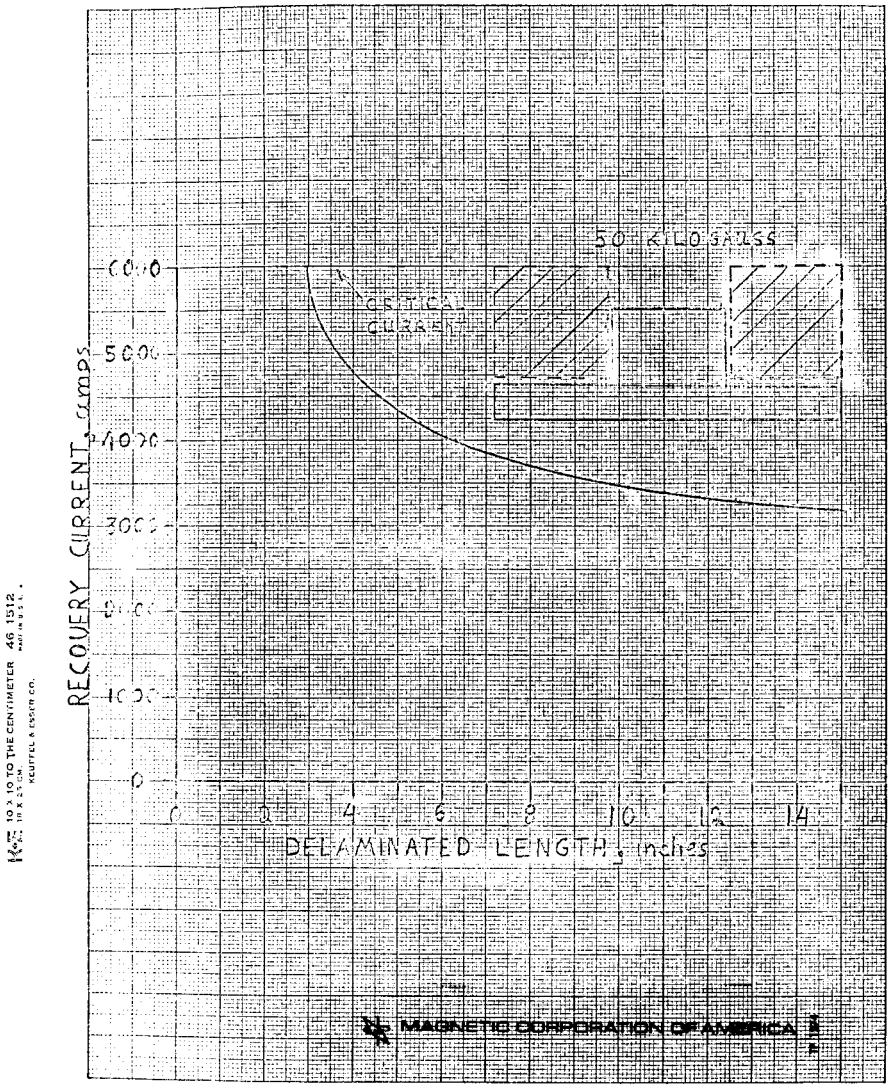
50 KILOGAUSS
CRITICAL CURRENT
RECOVERY CURRENT, amps
6000
5000
4000
3000
2000
1000
0
0
2
4
6
8
10
12
14
DELAMINATED LENGTH, inches
MAGNETIC CORPORATION OF AMERICA

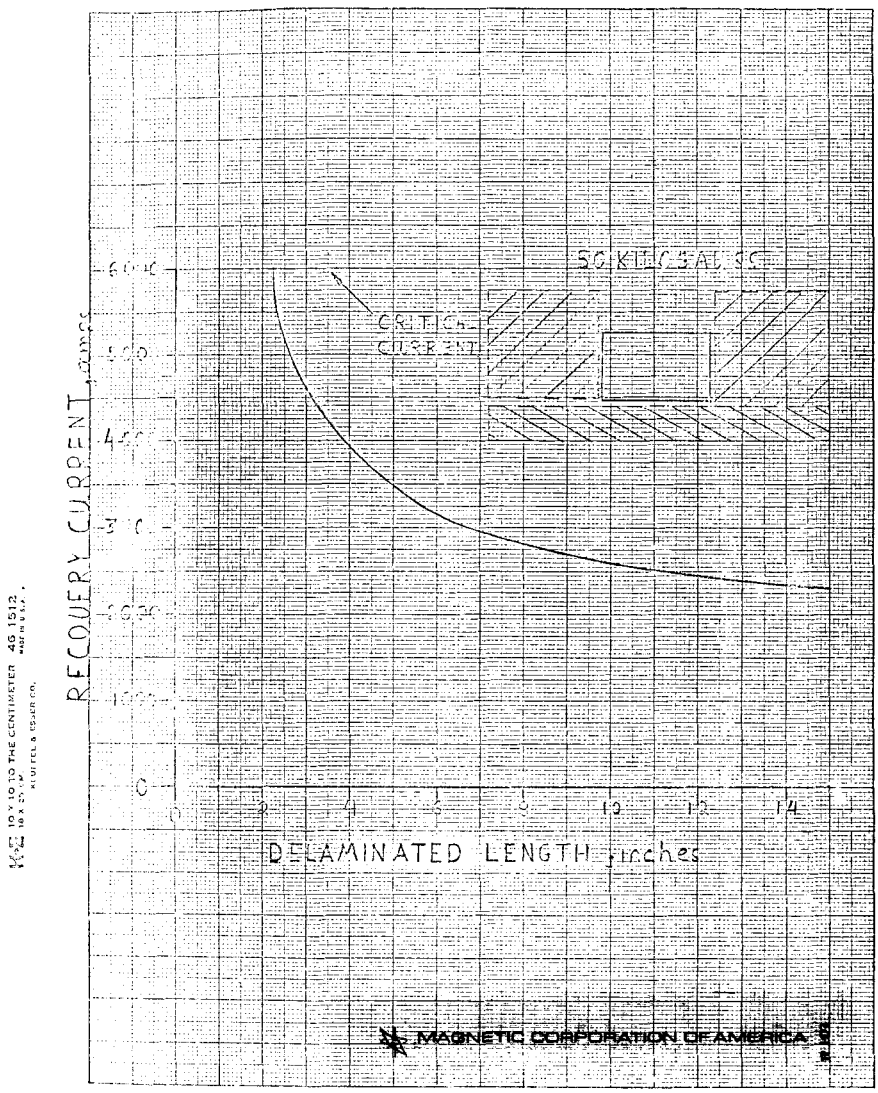
RECOVERY CURRENT, amps
CRITICAL CURRENT
SOLID SEAL
DELAMINATED LENGTH, inches
MAGNETIC CORPORATION OF AMERICA

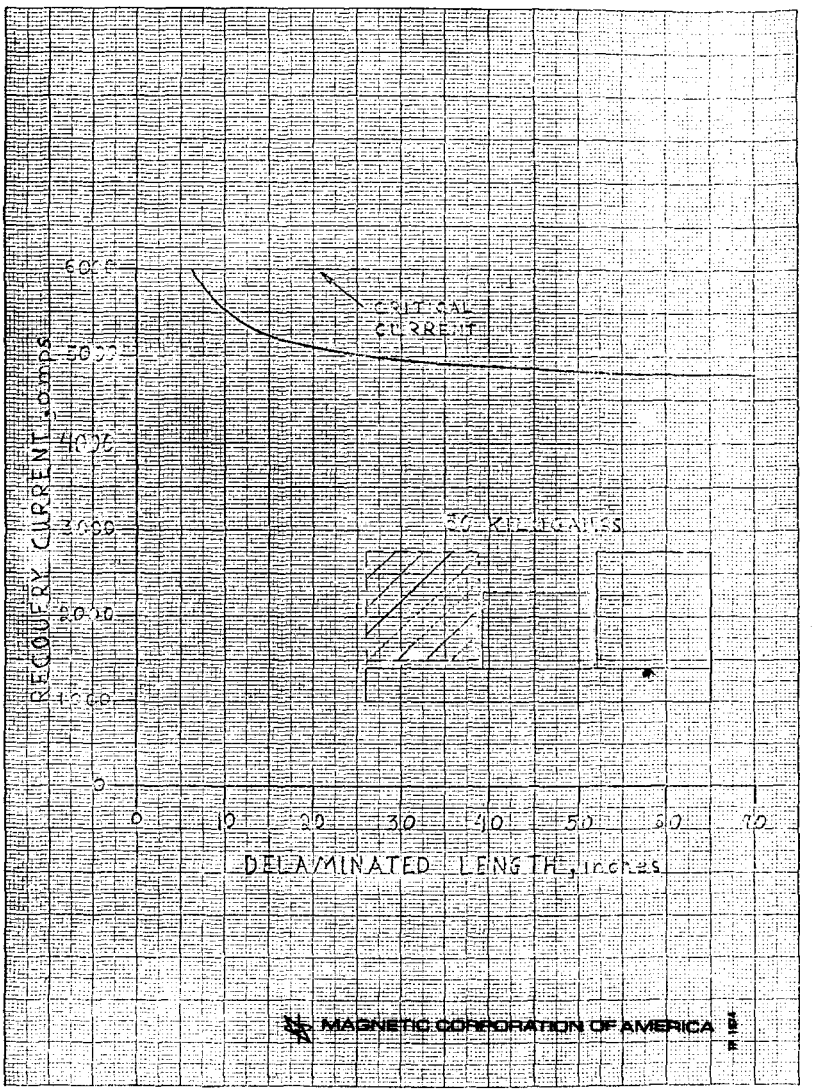

TOTAL DELAMINATED LENGTHS

	No Effect on V-I Curve	No Recovery at 5000A
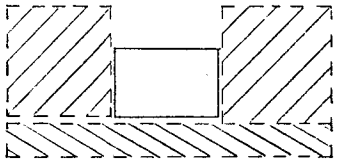	1.24 in.	2.68 in.
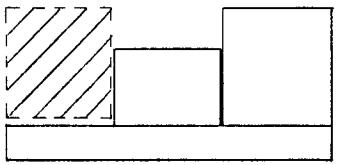	6.58 in.	26.1 in.
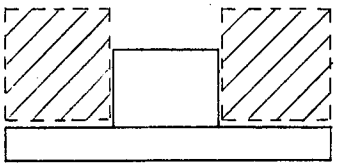	2.76 in.	3.7 in.

MAGNETIC CORPORATION OF AMERICA

IV. EQUIPMENT

K. Magnet

4. MAGNETIC AND THERMAL STRESSES IN THE WINDINGS: SUMMARY OF CALCULATIONS

Prepared by

L. M. Lontai

IV. K. 4. MAGNETIC AND THERMAL STRESSES IN THE WINDINGS: SUMMARY OF CALCULATIONS

Prestressing with Winding Tension

The analysis of the magnetic and thermal stresses is based on the anisotropic winding analysis derived for the 12' HBC. The results are plotted on Figure 1.

The peak magnetic hoop stresses are at the ID:

$\sigma_{\theta}|^{cu}$ ~ 9600 psi
$\sigma_{\theta}|^{ss}$ ~16640 psi } tensile
$\sigma_{\theta}|^{Mylar}$ ~ 1020 psi

The peak radial stress is σ_r ~-1080 psi (comp.) at r ~92 inches.

The thermal hoop stresses developed at the ID due to differential contraction are:

$\sigma_{\theta}|^{cu}$ ~ 3980 psi tensile
$\sigma_{\theta}|^{ss}$ ~-8420 psi compressive
$\sigma_{\theta}|^{Mylar}$ ~13610 psi tensile

The radial stress is small but tensile, indicating that the windings tend to loosen up unless they are radially clamped. Considering the differential contraction between the Micarta spacers and the coil build indicates that this will induce a radial compressive (clamping) stress in the windings of σ_r ~-640 psi, thus allowing the above thermal hoop stresses to develop!

Therefore, the peak operating hoop stresses at the ID are:

$\sigma_{\theta}|^{cu}$ ~13580 psi
$\sigma_{\theta}|^{ss}$ ~ 8820 psi } tensile
$\sigma_{\theta}|^{Mylar}$ ~14630 psi

The analysis of prestressing by winding tension indicates that for a winding stress of 4500 psi in the conductor, the stainless steel should

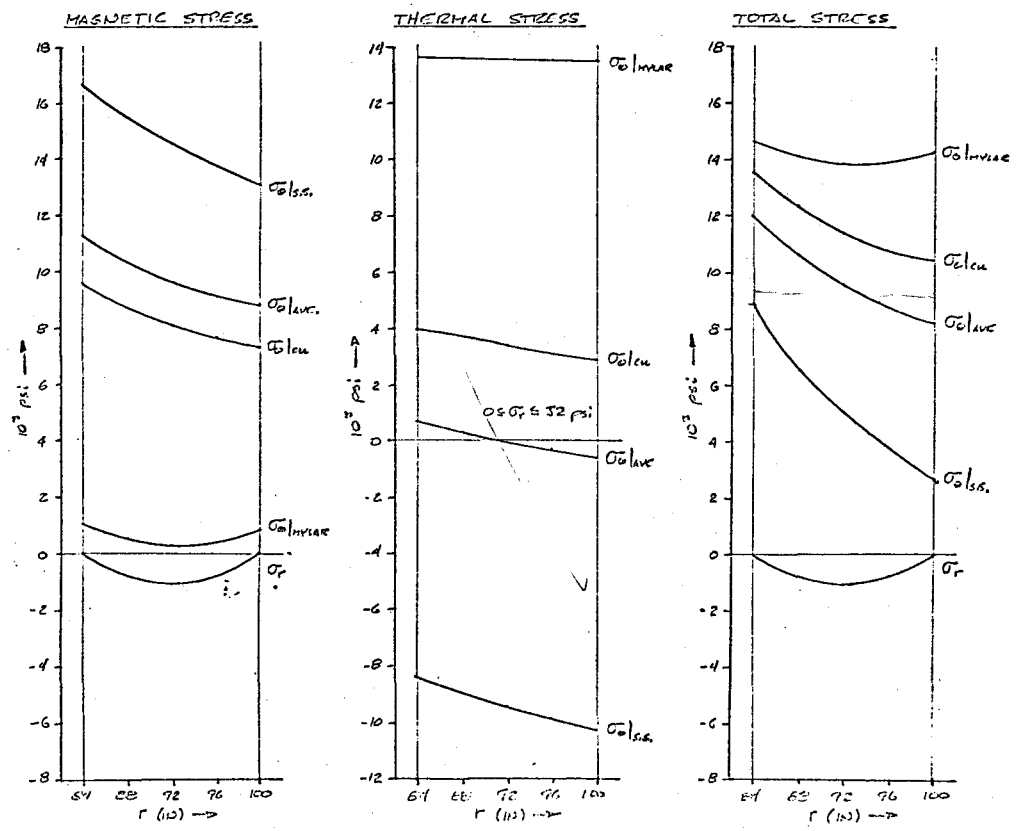

FIGURE 1. MAGNETIC AND THERMAL STRESSES

be wound under more than 20,000 psi tension in order to achieve a significant compensation for the cooldown thermal stresses.

Unwinding of Conductor ID

The end of the ID turn unwinds about .04 inches due to the differential thermal contraction between the whole ID conductor turn and the rest of the windings.

The unwinding resulting from the magnetic loading is about .145 inches with a coefficient of friction of $\eta \sim .028$ which allows the whole ID turn to move. (The unwinding $\Delta\ell$ is tabulated in the calculations.)

Therefore, the maximum unwinding of the end of the ID turn is about .185 inches resulting in a maximum relative motion between the ID ends of two adjacent oppositely wound pancakes of about .37 inches.

Axial Buckling of Pancakes

No real problem.

IV. EQUIPMENT

K. Magnet

5. Status Reports

Prepared by

John Purcell

TABLE OF CONTENTS

IV. K. 5. STATUS REPORT

JANUARY 31, 1971

Superconductor

Supercon managed to get short samples from the first two billets they ran and these have been tested at ANL. Both samples had very good current carrying capacity with the field parallel to the face of the conductor. The currents were of 7,050 and 6,800 amperes in a field of 52 kG, which is the peak axial field in the magnet. Current in a radial field of 40 kG was only 5,750 and 4,920 amperes. This is the same radial field that the conductor will experience in the magnet. If the radial field current carrying capacity is the limiting factor in the final conductor, it will be easy to grade the material to get the highest current capacity in the regions of high radial field. Only two pancakes will be exposed to the radial field of 40 kG, whereas almost all of the pancakes see the 52 kG axial field.

Supercon now hopes to get about 1,000 ft of conductor from one of the first two billets. If they manage this, we will wind it into the 2-ft bore test magnet and proceed with testing. Supercon's schedule appears to be consistent with their earlier predictions of about one month delay from the original schedule.

Cryostat

The cryostat procurement is proceeding on schedule. The clamp rings are almost ready to ship to ANL and the fabrication portion of the contract is in progress. Some minor design changes have occurred as a result of the design review meeting, but these will not cause delay.

Stainless Steel Strip

This material is still scheduled for delivery by February 15. The Mylar is at ANL.

Current Leads

Only one bid was received on the leads; however, it is acceptable and the price is less than the budget amount.

Refrigerator

An order has been placed with Cryogenic Technology Inc. for the refrigerator. The price is within the budget and delivery is December 31, 1971.

Cooldown Heat Exchanger

Bids due February 8, 1971.

Other Comments

We have occupied Building 12 and the crane is installed. Work is progressing in setting up the winding line. The dummy copper has been received at ANL so the dummy coil might be wound this month.

The dipole for short sample testing is behaving better. Two of its coils performed satisfactorily in a recent test. One more coil must be made operational.

At the design review meeting, several problems were discussed. Some of these conversations produced data that has been included in the cryostat design. Other questions require more calculations and steps are being taken to have consultants perform some of these tasks.

SCHEDULE OF PROJECT EVENTS

AS OF JANUARY 31, 1971

Event	Original Schedule Date as of 7/28/70	New Date	Actual Date
Order superconductor	1 Sept 70		11 Sept 70
Cryostat Contract signed	1 Nov 70		22 Dec 70
Model Magnet completed	1 Dec 70	19 Mar 71	
Refrigerator order placed	1 Jan 71	15 Feb 71	13 Jan 71
Winding line installation complete	1 Feb 71	15 Mar 71	
First pancake wound	7 Feb 71	1 April 71	
All coils wound for first module	1 May 71	1 June 71	
First cryostat components arrive ANL	1 Mar 71		
Start assembly, first module	15 Mar 71	1 Apr 71	
Start assembly, second module	15 Aug 71		
First module finished	1 Oct 71		
Second module finished	1 Dec 71		
Refrigerator received ANL	1 Mar 72		
Complete cryostat	1 May 72		
Finish test of magnet	1 June 72		

STATUS REPORT

MARCH 31, 1971

Superconductor

The superconductor procurement is progressing very nicely now and we expect delivery of the first four lengths about the middle of April. (See Appendix A for more on this subject.)

Cryostat

The 5-in. thick material for the bridge was ultrasonically tested for flaws or laminations and none were found. The material has now been cut to size and is being welded into the large rings.

Current Leads

The design of the current leads has now been approved and Magnetic Corp. of America will submit a revised proposal at a somewhat different price.

Refrigerator

A meeting was held with the C.T.I. Corporation to verify all the refrigerator details. The flow sheet has been approved and certified drawings will be available in about one month.

Cooldown Heat Exchanger

A meeting was held with C.C.I. The technical details of the heat exchanger were agreed upon and certified drawings will be available in about one month.

Winding Line

The winding line is in operation and a dummy coil has been wound. We used about 1,000 ft of ordinary ETP copper which allows a winding of 25 turns. The finished coil was very flat and the winding went smoothly. We had some problems with the brakes on the tensioning device in that they tended to gall the conductor material as it passed through the tensioner. Minor modifications are presently being made to solve this

problem. In general, the winding line appears to work very well and it looks like a rate of one coil per day is feasible once we obtain conductor.

APPENDIX A

One billet of superconductor will produce a length of about 3,100 ft, enough for one pancake winding. We need 44 lengths for the magnet and 1 length to wind a test magnet, a total of 45 lengths.

Supercon planned to initially run 2 billets through the fabrication process to make sure their production procedures were all right. Both of these billets had problems and the conductor was badly damaged. We had hoped to get some good conductor from these billets, but the damage prohibited usage.

Supercon felt the problem was in the die angle used in the drawing bench. They felt it worthwhile to verify this by running 4 more billets through the complete process. This has been done and the 4 billets turned out good. These will be delivered to ANL as finished conductor about the middle of April. When these 4 lengths of conductor are received, we will wind the test magnet from one length and wind 3 pancakes with the remaining 3 lengths.

Cleaning and assembly of the remaining billets are in process now and extrusion is scheduled for April 5 and 6. The finished 41 billets should start arriving at Argonne by June 15.

SCHEDULE OF PROJECT EVENTS

AS OF MARCH 31, 1971

Event	Original Schedule Date as of 7/28/70	New Date	Actual Date
Order superconductor	1 Sept 70		11 Sept 70
Cryostat contract signed	1 Nov 70		22 Dec 70
Model magnet completed	1 Dec 70	25 Apr 71	
Refrigerator order placed	1 Jan 71	15 Feb 71	13 Jan 71
Winding line installation complete	1 Feb 71	15 Mar 71	19 Mar 71
First pancake wound	7 Feb 71	30 Apr 71	
All coils wound for first module	1 May 71	20 July 71	
First cryostat components arrive ANL	1 Mar 71		8 Feb 71
Start assembly, first module	15 Mar 71	15 June 71	
Start assembly, second module	15 Aug 71		
First module finished	1 Oct 71	1 Aug 71	
Second module finished	1 Dec 71	1 Sept 71	
Refrigerator received ANL	1 Mar 72	30 Dec 71	
Complete cryostat	1 May 72	1 Feb 72	
Finish test of magnet	1 June 72		

STATUS REPORT

APRIL 30, 1971

Superconductor

The first four billets of superconductor have been taken completely through the extrusion and drawing process and are now ready for soldering. One of the lengths had to be cut during drawing so it is short and provided only three usable pieces. Soldering these strips is planned to begin during the week of May 17, with delivery expected shortly thereafter.

Supercon has decided to process the 45 remaining billets. These were extruded April 20 and are now in Toronto going through the drawing process.

Delivery of the superconductor remains our biggest problem although this issue is slowly evolving into a believable schedule. We are presently expecting the first delivery in early June. This shipment will be relatively small; the bulk of the material is presently scheduled for shipment beginning July 1971. (See the attachment for a complete current schedule of this activity.)

The copper backing strip is all in hand now and looks very good. The side strip material is almost down to size and final sizing should proceed beginning May 3. Some difficulty was encountered in notching the side strips to hold proper dimensions. A sample was made with 1/8-in. notches, rather than 1/4-in., and this looks satisfactory. Notching of the side strips is scheduled to start May 10.

The soldering equipment is essentially complete and some successful test runs have been made.

Cryostat

Work is continuing on the bridge and it is presently on schedule.

Current Leads

A purchase order for the leads has been issued to Magnetic Corp.

of America.

Cooldown Heat Exchanger

We now have all the drawings on this exchanger and fabrication is in process.

Winding Line

The winding line is complete but idle until conductor arrives.

SCHEDULE OF PROJECT EVENTS

AS OF APRIL 30, 1971

Event	Original Schedule Date as of 7/28/70	New Date	Actual Date
Order superconductor	1 Sept 70		11 Sept 70
Cryostat contract signed	1 Nov 70		22 Dec 70
Model magnet completed	1 Dec 70	1 June 71	
Refrigerator order placed	1 Jan 71	15 Feb 71	13 Jan 71
Winding line installation complete	1 Feb 71	15 Mar 71	19 Mar 71
First pancake wound	7 Feb 71	7 June 71	
All coils wound for first module	1 May 71	1 Sept 71	
First cryostat components arrive ANL	1 Mar 71		8 Feb 71
Start assembly, first module	15 Mar 71	1 Aug 71	
Start assembly, second module	15 Aug 71	1 Sept 71	
First module finished	1 Oct 71	1 Sept 71	
Second module finished	1 Dec 71	1 Oct 71	
Refrigerator received NAL	1 Mar 72	30 Dec 71	
Complete cryostat	1 May 72	15 Mar 72	

STATUS REPORT

MAY 31, 1971

Superconductor

As can be seen from the attached schedule, the superconductor is now progressing nicely. Part of the coils for the 2-ft test magnet have been wound, and we expect to test the magnet shortly.

Short-sample testing of the conductor proved to be quite difficult due to the high currents and fields involved. A system has been developed to induce high currents in a sample with a 100-amp power supply. With this system we can get 10,000 amps of test current with high sensitivity to resistance changes. Resistance changes of 10^{-9} ohm are easily detectable. The new system will simplify future short-sample testing.

Cryostat

See the enclosed monthly report from Stearns-Roger Inc.

Cooldown Heat Exchanger

See enclosed monthly report from Cryogenic Consultants, Inc.

SCHEDULE OF PROJECT EVENTS

AS OF MAY 31, 1971

Event	Original Schedule Date as of 7/28/70	New Date	Actual Date
Order superconductor	1 Sept 70		11 Sept 70
Cryostat contract signed	1 Nov 70		22 Dec 70
Model magnet completed	1 Dec 70	25 June 71	
Refrigerator order placed	1 Jan 71	15 Feb 71	13 Jan 71
Winding line installation complete	1 Feb 71	15 Mar 71	19 Mar 71
First pancake wound	7 Feb 71	5 Jul 71	
All coils wound for first module	1 May 71	1 Sept 71	
First cryostat components arrive ANL	1 Mar 71		8 Feb 71
Start assembly, first module	15 Mar 71	1 Aug 71	
Start assembly, second module	15 Aug 71	1 Sept 71	
First module finished	1 Oct 71	1 Sept 71	
Second module finished	1 Dec 71	1 Oct 71	
Refrigerator received NAL	1 Mar 72	30 Dec 71	
Complete cryostat	1 May 72	15 Mar 72	

STATUS REPORT

JUNE 30, 1971

Superconductor

The windings were finished for the 2-ft magnet and it has been tested. The magnet was designed to test the stability of the conductor rather than the short sample characteristics. This results in a high current but a lower field than will exist in the large magnet.

Cooldown of the magnet went very well requiring only 300 liters of liquid helium to cool the 2,000-lb magnet to 4°K. Charging began when the magnet was covered with liquid helium. The magnet was noisy in that the loose turns could be plainly heard as they slid into place as the magnet was energized. It is difficult to model the mechanical motion that will occur in the large magnet, however, the 2-ft model demonstrated that large mechanical movements did not disturb the stability.

Electrical stability of the magnet was determined with a heater wound along a 3-ft length of conductor in the winding. The magnet was charged to some current level and then the heater power was increased until the 3-ft section of conductor was driven normal. Heater power was then increased to its maximum of 300 watts in an attempt to force the magnet to quench. This was done for magnet currents of 4,000, 4,500, 5,000, and 5,500 amperes. In every case, the length of conductor went normal with 100 watts of heater power (33 watts per ft) and the normal region would not propagate with a maximum heater power of 300 watts (100 watts per ft).

At 6,000 amperes a thermal instability occurred in the power leads which led to a slow quench of the magnet. Several minutes are required for the normal region to propagate and this agrees with the calculations that have been made.

During the quench, a sharp rise in current was recorded. This could not be explained until the magnet was removed from the cryostat

and the connection to the bottom pancake was found to be broken. Apparently when the lead broke, it was shorted to the third coil from the bottom and continued to carry the main magnet current. The two bottom coils were disconnected and discharged between themselves with a small amount of arcing between pancakes.

The model demonstrated that the conductor stability is adequate for the large magnet. Since power dissipation in a normal region varies as the current squared, 6,000 amperes is 36/25 or 144% of rated power at 5,000 amperes.

We plan to install heavier current leads, repair the broken connection, and run the model again in the next few weeks. This run will not be to demonstrate adequate stability, but to see how high the model will go. It might be a useful magnet for future use.

Two full-length pieces of conductor have been completed and these will be wound in final coils.

As can be seen from the attached conductor schedule, it has slipped about two weeks.

Cryostat

See enclosed monthly report.

Cooldown Heat Exchanger

See enclosed monthly report.

SCHEDULE OF PROJECT EVENTS

AS OF JULY 16, 1971

Event	Original Schedule Date as of 7/28/70	New Date	Actual Date
Order superconductor	1 Sept 70		11 Sept 70
Cryostat contract signed	1 Nov 70		22 Dec 70
Model magnet completed	1 Dec 70	25 June 71	29 June 71
Refrigerator order placed	1 Jan 71	15 Feb 71	13 Jan 71
Winding line installation complete	1 Feb 71	15 Mar 71	19 Mar 71
First pancake wound	7 Feb 71	20 July 71	
All coils wound for first module	1 May 71	1 Sept 71	
First cryostat components arrive ANL	1 Mar 71		8 Feb 71
Start assembly, first module	15 Mar 71	1 Aug 71	
Start assembly, second module	15 Aug 71	1 Sept 71	
First module finished	1 Oct 71	1 Sept 71	
Second module finished	1 Dec 71	1 Oct 71	
Refrigerator received NAL	1 Mar 72	30 Dec 71	
Complete cryostat	1 May 72	15 Mar 72	

STATUS REPORT

JULY 31, 1971

Superconductor

Conductor for two pancakes has been received and wound into coils. Two more lengths have been soldered and are now at Supercon awaiting shipment. Problems were encountered during the soldering of the third length resulting in about 100 ft of poorly soldered conductor starting from 2,700 ft from the lead end. We plan to repair the bad soldering upon arrival at Argonne.

To prevent further slipping in the superconductor schedule, we are working closer with Supercon, primarily in scheduling. Present delivery schedule calls for the final shipment to be made the week of October 11.

Cryostat

The cryostat is proceeding on schedule. The bridge and upper helium vessel have arrived on site.

Coil Winding

The coil winding line worked very well in winding the first two coils. A photograph of the first coil is attached. The coils are very true and no problems are expected in the stacking.

SCHEDULE OF PROJECT EVENTS

AS OF AUGUST 20, 1971

Event	Original Schedule Date as of 7/28/70	Date	Actual Date
Order superconductor	1 Sept 70		11 Sept 70
Cryostat contract signed	1 Nov 70		22 Dec 70
Model magnet completed	1 Dec 70	25 June 71	29 June 71
Refrigerator order placed	1 Jan 71	15 Feb 71	13 Jan 71
Winding line installation complete	1 Feb 71	15 Mar 71	19 Mar 71
First pancake wound	7 Feb 71	20 July 71	20 July 71
All coils wound for first module	1 May 71	15 Sept 71	
First cryostat components arrive ANL	1 Mar 71		8 Feb 71
Start assembly, first module	15 Mar 71	24 Sept 71	
Start assembly, second module	15 Aug 71	15 Oct 71	
First module finished	1 Oct 71	15 Oct 71	
Second module finished	1 Dec 71	27 Oct 71	
Refrigerator received NAL	1 Mar 72	30 Dec 71	
Complete cryostat	1 May 72	15 Mar 72	

STATUS REPORT

SEPTEMBER 30, 1971

In order to assemble the superconductor, two side strips and one bottom strip into a composite strip ready for winding into final superconducting coils, it was decided to enter into a contract for this development work with Supercon, subsidiary of Norton Company. During the development phase of this contract it was necessary to try many unique ideas in designing fixtures and process control for the work. This work involved fabrication of a composite soldered unit meeting the specifications required for the completed product. The development work was considered completed and the production phase for the 44 required coils was started. During the production runs involving long lengths of material, approximately 3,300 lineal feet, a number of additional problems arose. These problems were primarily in the soldering of the 4 pieces required for the composite into a completed unit meeting the specification requirements. A number of coils were made with continuing development of fixtures and process controls that finally produced the required results.

Six of the early production runs received at ANL have a number of unbonded areas that will require rework. Argonne will rework 2 of these 6 units. The remaining 4 will be shipped back to Supercon for a rerun through their furnace using the improved assembly clamping system. In addition to these 6 units, one of the later production runs will be rerun at Supercon for a simple repair. There are also 2 additional units that will require extensive repair primarily the composite backing strip. ANL is working out a repair procedure for these 2 units and expects that this repair will be done at Supercon upon completion of the remaining production run of the total 44 units. Of the remaining units that have been fabricated by Supercon, 14 additional units were shipped to Argonne with 3 remaining at Supercon. This group was

fabricated with improved fixtures and process controls and appears to be quite good. These units will be inspected at Argonne but no major repairs are expected to be necessary.

The present schedule is for Supercon to complete the production fabrication by November 10, 1971, and to complete all necessary repairs by November 19, 1971. Coil winding at ANL will continue simultaneously with the estimated completion of all coils at ANL by the end of November.

Cryostat

The contract with Stearns-Roger Corporation is progressing quite satisfactorily. The major cryostat parts have been shipped to Argonne and the vacuum vessel is due to be shipped about the middle of October. The assembly contract with Stearns-Roger has been approved. Stearns-Roger has sent their Construction Superintendent, Mr. Joseph Santerno, to Argonne to prepare for the required assembly work. He will make arrangements with the local construction unions for scheduling the necessary labor mix needed to complete the work.

Liquefier

A contract was made with C.T.I. for the production of a liquefier. This work has been progressing quite well and the contract required that it be delivered to NAL upon completion by the vendor. NAL has considered the possibility of some slight modifications in this work. Since the delivery is to be made to NAL it was decided that the contract would be changed from an Argonne responsibility to an NAL primary responsibility.

Miscellaneous

ANL is experiencing some overrun on the original estimated costs for this work; therefore, in order to minimize any overrun, a review of the remaining work, searching for possible reduction in cost, is being made in cooperation with NAL. A tentative plan is to finish the coil winding at Argonne and do the final assembly and testing at NAL. This

plan will result in reducing the projected costs of the job since the assembly and test will be completed at NAL, thereby reducing the costs of initial assembly and disassembly at ANL and the difficult job of moving the completed unit from Argonne to NAL as was originally planned.

SCHEDULE OF PROJECT EVENTS

AS OF SEPTEMBER 30, 1971

Event	Original Schedule Date as of 7/28/70	Date	Actual Date
Order superconductor	1 Sept 70		11 Sept 70
Cryostat contract signed	1 Nov 70		22 Dec 70
Model magnet completed	1 Dec 70	25 June 71	29 June 71
Refrigerator order placed	1 Jan 71	15 Feb 71	13 Jan 71
Winding line installation complete	1 Feb 71	15 Mar 71	19 Mar 71
First pancake wound	7 Feb 71	20 July 71	20 July 71
All coils wound for first module	1 May 71	20 Nov 71	
First cryostat components arrive ANL	1 Mar 71		8 Feb 71
Start assembly, first module	15 Mar 71	30 Nov 71	
Start assembly, second module	15 Aug 71	17 Dec 71	
Sirst module finished	1 Oct 71	17 Dec 71	
Second module finished	1 Dec 71	29 Dec 71	
Refrigerator received NAL	1 Mar 72	30 Dec 71	
Complete cryostat	1 May 72	15 May 72	

STATUS REPORT

OCTOBER 31, 1971

Superconductor

The assembly of the composite conductor is complete with the exception of one length, Supercon No. 42. After final inspection, it was found that 13 lengths of conductor have questionable solder bonds. Supercon is rearranging the soldering line and expects to start the rework November 15. It will be finished near December 8.

Superconductor No. 42 has not been soldered yet because the short sample tests are inconclusive. Tests performed at ANL show a low current capacity while tests performed at Supercon on individual filaments give a normal current capacity. Some sort of instability that has not been explained seems to be the problem. Further heat treating and testing will be done on No. 42 to verify its acceptance during the rework period.

Coil Winding

Coil winding has begun on a two-shift basis and should soon be at a rate of eight to ten per week. Building "A" at NAL will not be ready for use until December 1, so the first shipment of finished coils to NAL is scheduled for November 30. Coil stacking will then commence at NAL on a two-shift basis to recover the time lost in waiting for building "A".

Cryostat

The contract with Stearns-Roger Corporation is progressing satisfactorily. The vacuum vessel has arrived at ANL. All the cryostat parts will be shipped by truck to NAL sometime after December 1.

SCHEDULE OF PROJECT EVENTS

AS OF OCTOBER 31, 1971

Event	Original Schedule Date as of 7/28/70	Date	Actual Date
Order superconductor	1 Sept 70		11 Sept 70
Cryostat contract signed	1 Nov 70		22 Dec 70
Model magnet completed	1 Dec 70	25 June 71	29 June 71
Refrigerator order placed	1 Jan 71	15 Feb 71	13 Jan 71
Winding line installation complete	1 Feb 71	15 Mar 71	19 Mar 71
First pancake wound	7 Feb 71	20 July 71	20 July 71
All coils wound for first module	1 May 71	20 Nov 71	
First cryostat components arrive ANL	1 Mar 71		8 Feb 71
Start assembly, first module	15 Mar 71	30 Nov 71	
Start assembly, second module	15 Aug 71	17 Dec 71	
First module finished	1 Oct 71	17 Dec 71	
Second module finished	1 Dec 71	29 Dec 71	
Refrigerator received NAL	1 Mar 72	30 Dec 71	
Complete cryostat	1 May 72	15 May 72	

STATUS REPORT

NOVEMBER 30, 1971

Superconductor

Superconductor No. 42 has not yet passed the ANL tests for stability. The present plan is to try more heat treatment on No. 42 and if this does not improve the conductor to an acceptable level, then three shorter lengths of good conductor will be substituted for No. 42. Using three short lengths will necessitate two splices within the pancake. A method for making splices has been worked out, and some strength tests have been made in the laboratory at liquid helium temperature to verify the mechanical integrity of the splices.

A second test was run on the 2-ft magnet and the current was taken to 7,100 amperes. A description of this test is attached to this report.

The superconductor repair at Supercon has been slow to get started because it took more time than expected to get the soldering line rearranged. Repair of one length has now been completed and the quality appears to be as good as the regular production runs. It is expected that the repairs will be completed by the end of December.

Coil Winding

Twenty coils have been wound and the winding is now almost routine. The second shift has been dropped because we will soon be finished with the thirty lengths that are on hand and will be waiting for delivery from Supercon.

Coil Assembly

The first load of seven coils was shipped to NAL December 7 without incident. Actual coil assembly will commence in Building "A" during the week of December 13.

Cryostat

Stearns-Roger Corporation have completed a new schedule, cost, and assembly procedure for completing the cryostat at NAL.

SCHEDULE OF PROJECT EVENTS

AS OF NOVEMBER 30, 1971

Event	Original Schedule Date as of 7/28/70	Date	Actual Date
Order superconductor	1 Sept 70		11 Sept 70
Cryostat contract signed	1 Nov 70		22 Dec 70
Model magnet completed	1 Dec 70	25 June 71	29 June 71
Refrigerator order placed	1 Jan 71	15 Feb 71	13 June 71
Winding line installation complete	1 Feb 71	15 Mar 71	19 Mar 71
First pancake wound	7 Feb 71	20 July 71	20 July 71
All coils wound for first module	1 May 71	15 Dec 71	
First cryostat components arrive ANL	1 Mar 71		8 Feb 71
Start assembly, first module	15 Mar 71	13 Dec 71	
Start assembly, second module	15 Aug 71	17 Jan 72	
First module finished	1 Oct 71	17 Jan 72	
Second module finished	1 Dec 71	29 Jan 72	
Refrigerator received NAL	1 Mar 72	30 Dec 71	
Complete cryostat	1 May 72	15 June 72	

STATUS REPORT

DECEMBER 31, 1971

Superconductor

Continued testing of various heat treated samples of superconductor No. 42 have not shown it to be acceptable. It appears this length of conductor will have to be rejected. We have investigated splicing together short lengths of material to replace No. 42 but the short lengths that are available have some broken filaments and are not usable.

With one pancake missing, the number of pancakes in the magnet will be 43 instead of 44. One of these pancakes is wound from a shorter length and is only 52 turns. This results in a total decrease in the number of turns of about 3%. At an operating current of 5,000 amperes, this would give a central field of 29.1 kG instead of 30 kG as originally planned. A 3% increase in operating current to 5,150 amperes would bring the field back to 30 kG. This should be possible since the 2-ft tests showed the conductor had good electrical stability and the increased current with fewer turns would produce approximately the same mechanical forces as the original design.

Conductor repair has been progressing and should be completed during the week of January 24. Some of the repaired conductor has been inspected at ANL and wound into coils. The material is high quality and no problems have been encountered.

Coil Winding

Thirty-three coils have been wound and 27 have been shipped to NAL.

Coil Assembly

The bottom coil assembly of 22 pancakes will be completed during the week of January 24. After the instrumentation and bridge are installed, coil stacking will commence on the top coil assembly.

Concurrently with the stacking, welding will start on the lower helium vessel.

Cryostat

All the cryostat parts have been moved to NAL and are ready for assembly.

SCHEDULE OF PROJECT EVENTS

AS OF DECEMBER 31, 1971

Event	Original Schedule Date as of 7/28/70	Date	Actual Date
Order superconductor	1 Sept 70		11 Sept 70
Cryostat contract signed	1 Nov 70		22 Dec 70
Model magnet completed	1 Dec 70	25 June 71	29 June 71
Refrigerator order placed	1 Jan 71	15 Feb 71	13 June 71
Winding line installation complete	1 Feb 71	15 Mar 71	19 Mar 71
First pancake wound	7 Feb 71	20 July 71	20 July 71
All coils wound for first module	1 May 71	15 Dec 71	
First cryostat components arrive ANL	1 Mar 71		8 Feb 71
Start assembly, first module	15 Mar 71	13 Dec 71	13 Dec 71
Start assembly, second module	15 Aug 71	4 Feb 72	
First module finished	1 Oct 71	4 Feb 72	
Second module finished	1 Dec 71	25 Feb 72	
Refrigerator received NAL	1 Mar 72	30 Dec 71	
Complete cryostat	1 May 72	15 June 72	

IV. EQUIPMENT

L. Failure Mode Analysis: MAGNET

Prepared by

John Purcell

STATUS REPORT

MARCH 31, 1972

Coil Assembly

All the coils have been wound and the coil assembly at NAL has been completed. After discussing the possibilities with NAL bubble chamber personnel, it was decided to use only 43 pancakes, giving 2,782 turns compared to the original design of 2,860 turns.

The winding equipment in building 12 is completely dismantled.

Cryostat

Welding has been completed on both the upper and lower helium vessels. The vessels have been successfully tested to 60 psig, or 125% of working pressure. ASME code requires 115% test pressure.

In leak checking the vessels some difficulty arose in obtaining a suitable vacuum (less than 10^{-3} torr). After pumping for several days it was found that the poor vacuum was due to moisture coming from the Micarta. Rather than attempting to pump the Micarta dry, a cold trap was used to freeze out the water vapor in the pumpout line. This worked well and a leak check was performed with good sensitivity. No leaks were found.

SCHEDULE OF PROJECTS EVENTS

AS OF FEBRUARY 29, 1972

Event	Original Schedule Date as of 7/28/70	Date	Actual Date
Order superconductor	1 Sept 70		11 Sept 70
Cryostat contract signed	1 Nov 70		22 Dec 70
Model magnet completed	1 Dec 70	25 June 71	29 June 71
Refrigerator order placed	1 Jan 71	15 Feb 71	13 June 71
Winding line installation complete	1 Feb 71	15 Mar 71	19 Mar 71
First pancake wound	7 Feb 71	20 July 71	20 July 71
All coils wound for first module	1 May 71	15 Dec 71	
First cryostat components arrive ANL	1 Mar 71		8 Feb 71
Start assembly, first module	15 Mar 71	13 Dec 71	13 Dec 71
Start assembly, second module	15 Aug 71	4 Feb 72	4 Feb 72
First module finished	1 Oct 71	4 Feb 72	4 Feb 72
Second module finished	1 Dec 71	25 Feb 72	21 Feb 72
Refrigerator received NAL	1 Mar 72	30 Dec 71	
Complete cryostat	1 May 72	15 June 72	

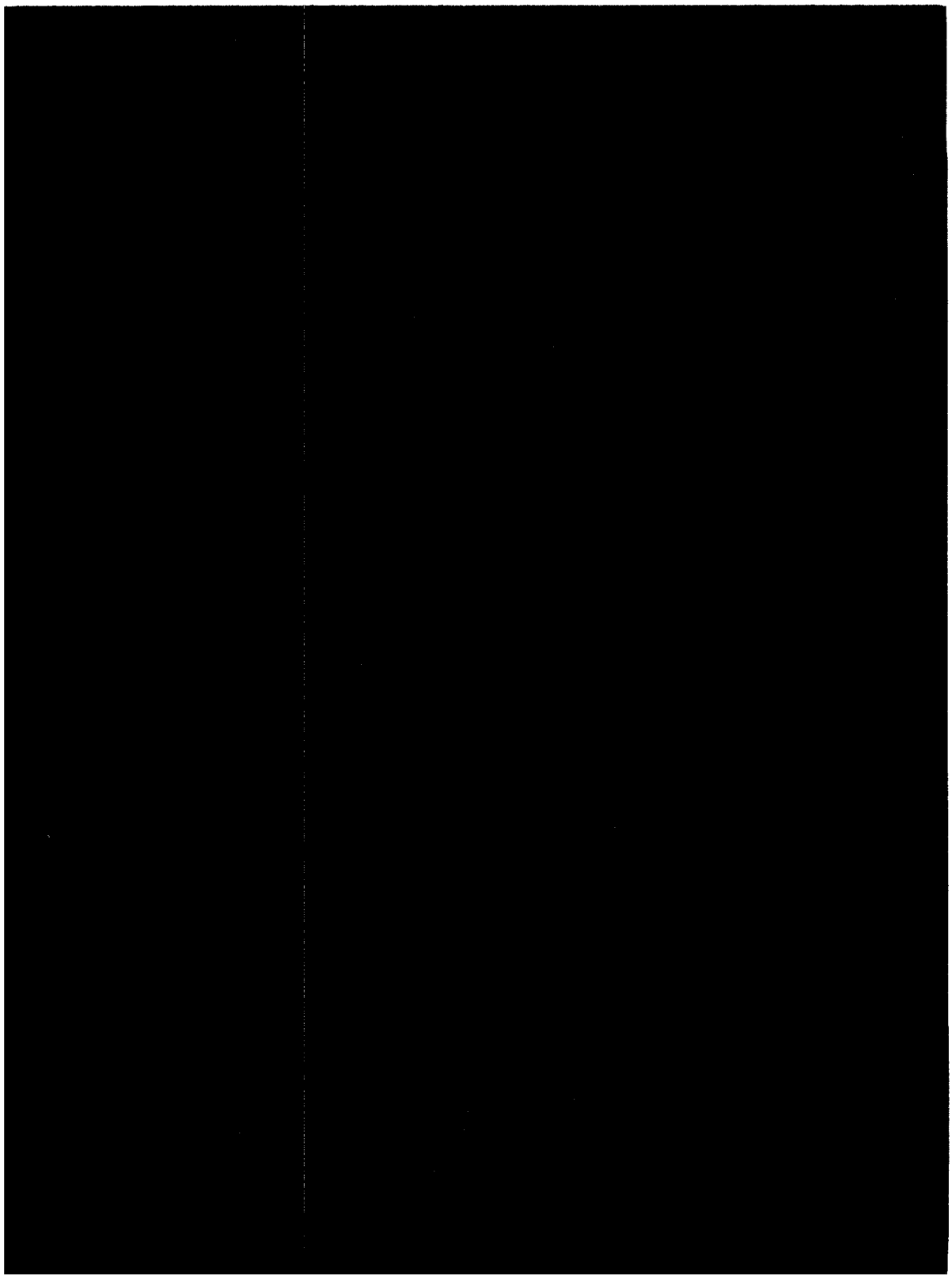

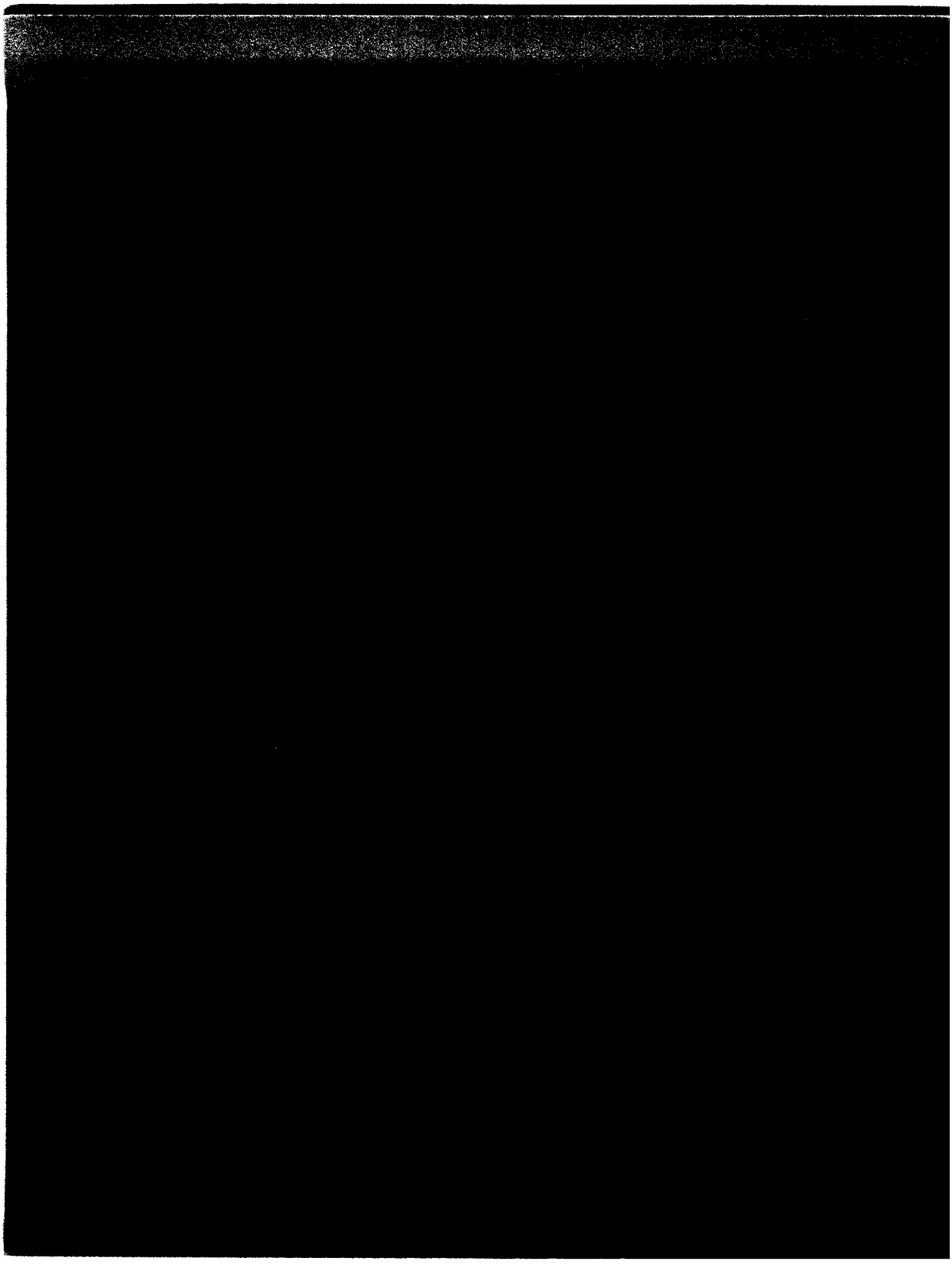

IV. L. Failure Mode Analysis: MAGNET

Cryostat

Normal operating pressure of the cryostat is 16.7 psia and it's design pressure is 45 psia. The cryostat is protected from overpressure by a 30 psi rupture disk connected to a 12 inch vent line. Pressure drop calculations have been made by R.B.Jacobs for the system and the following table applies. This table gives time to empty the cryostat as a function of average vented fluid temperature, assuming the cryostat is held at a pressure of 30 psig.

Temperature (°K)	Time to Empty (sec.)
4.2	3.04
10	8.7
20	18.7
30	22.8
40	26.1
50	29.8
100	42.2

Stekly and co-workers have calculated the propagation time for a normal region in a single uncooled pancake. Some values of peak temperature and voltage as a function of time are given in the following table.

Time (sec.)	Voltage Across Normal Region	Max. Temperature (°K)
10	20	40
20	43	55
30	78	67
40	110	80
50	150	100

The conclusion from these calculations is that if a coil starts going

normal in an uncontrolled manner, local heating will result in a pressure rise to blow the rupture disk and the coil will continue to go normal surrounded by helium gas. In no case can the coil go completely normal while immersed in helium liquid. The 1.5 megawatts that would occur with a completely normal coil cannot happen under liquid and the vent is not sized to handle the resulting flow.

Loss of Vacuum

If the main vacuum of the chamber goes to atmosphere nothing happens to the magnet. If the pressure in the chamber vacuum sphere exceeds 20 psia, hydrogen will fill the magnet vacuum vessel. The condensing hydrogen will produce less than 50 kw of heating in the magnet cryostat. Once the cryostat rupture disk is blown the 50 kw cause a pressure buildup of less than 1 psi. The coil would probably begin to quench, but so slowly that pressure rise is no problem.

Dump Resistor and Power Leads

Energy stored in the magnet will normally be discharged into the dump resistor, a set of stainless steel plates immersed in a water bath. The resistor has been tested to 140% power, one section at a time. Normal dump peak voltage will be 180 volts with a time constant of about 14 minutes. The power leads between the magnet, power supply and dump resistor consist of 6 -900 mcm cables each. Care has been taken in the layout to minimize the number of current carrying joints. Purged housings will enclose the magnet leads and buss to a point beyond the vacuum sphere. Thermostats connected to the alarm panel will be placed on the connections between the buss and the magnet power leads.

Low Liquid Level

During normal operation 3,000 to 4,000 liters of liquid helium will be kept in reserve in the 10,000 liter liquid storage dewar. The liquefier can be shut down for many hours, either due to malfunction or rou-

tine maintenance, without affecting the operation of the magnet.

A low liquid level could occur with a plugged liquid transfer line. If the liquid drops below it's normal operating point, an alarm will be activated. The magnet energy will be discharged into the dump resistor and the transfer line will be cleared to resume service. If for some reason the energy is not dumped, the top pancake will eventually begin to go normal. This will result in a pressure rise, blowing the rupture disk and the remainder of the coils will go normal in a gas atmosphere.

Cooldown Heat Exchanger

Liquid hydrogen is used during a portion of the magnet cooldown cycle. A small volume of liquid hydrogen will be contained in the cooldown heat exchanger and vented to a normal hydrogen vent. The hydrogen is used to cool helium gas that is then passed through the magnet. Hydrogen will be used when the magnet is about 115°K down to 40°K.

Plugged Heat Intercepts

The major heat intercept flows are the power leads and the support legs. Each of these flows is alarmed. The power leads are designed to operate with full current and half flow indefinitely and at no flow for 10 minutes without overheating. This gives adequate time to dump the magnet energy with a low flow alarm. If all the intercepts were to plug the cryostat pressure would rise giving an alarm in addition to the low flow alarms. One intercept plugging completely will result in a heat leak too high to continue magnet operation. The magnet must be drained and the plug removed to continue operation.

Conductor Breakage

Great care has been taken in the magnet design to minimize the possibility of conductor breakage; however, the forces are large and conductor breakage must be considered a credible accident. If a conductor breaks, a large amount of damage will have already occurred in the magnet

so the safety concern is for the chamber assembly.

When a conductor breaks, the 5,000 ampere magnet current will continue to flow through the resulting arc. The arc voltage will be 20 to 40 volts. A power dissipation of 100 to 200 kw will raise the cryostat pressure very quickly to the relief point of 30 psig. The cryostat fluid contents will be vented and the arc will continue eroding the copper conductor. As the arc gap, and thus the arc voltage, increases, further voltage breakdown will occur in the spaces between the pancakes. The arc voltage will always be rather low and will not erode the cryostat wall.

Although considerable damage will be done to the magnet windings in the event of conductor breakage, no overpressure of the magnet cryostat will occur; the cryostat will completely contain the arc; and the field decay rate is only slightly greater than normal. The chamber will not be affected by conductor breakage.

Severed Buss

If the power leads from the magnet to the power supply or dump resistor are broken when the magnet is not energized nothing happens.

Severing the leads to the dump resistor with the magnet energized will not cause harm unless the magnet energy is dumped. If a dump is attempted in this state a large arc will be drawn at the contacts of the dump switch and the terminal voltage of the magnet will rise until a breakdown occurs within the magnet.

A break in the leads between the power supply and dump resistor will cause the magnet energy to be dumped as if the dump switch were opened.

Severing the power leads between the magnet and dump resistor when the magnet is energized will result in an arc between the severed ends. If the severed ends are pushed apart a few inches the arc voltage will go up, resulting in a voltage breakdown in the magnet.

Failure of the dump resistor, by open circuit will result in high magnet voltage and internal breakdown. The dump resistor is protected

from this sort of failure by parallel paths. Failure of the dump resistor by shorting is harmless in that it only slows dowm the magnet dump and reduces the power dissipation in the dump resistor.

Extreme care must be taken to prevent open circuits either in the d-c power buss or the dump resistor.

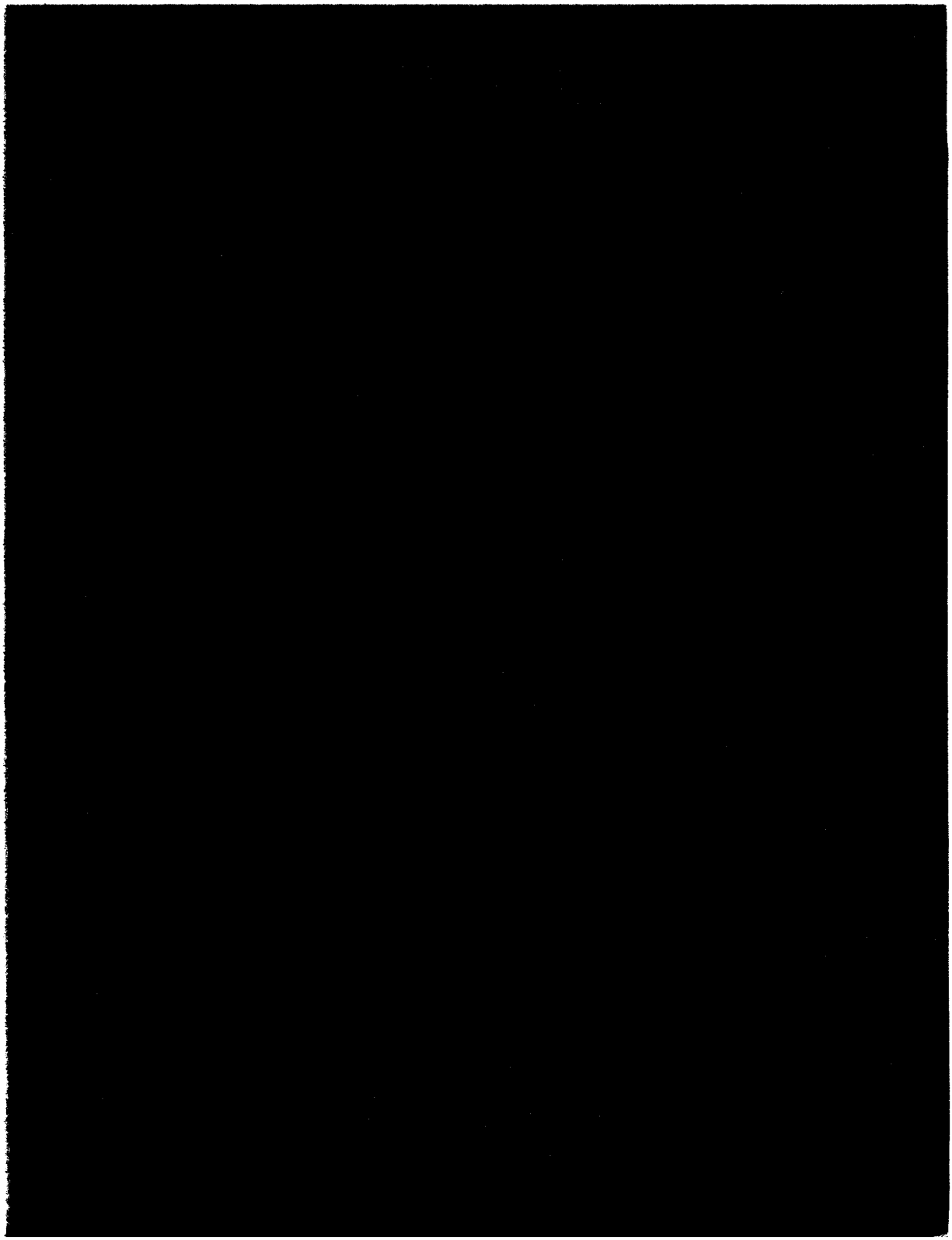

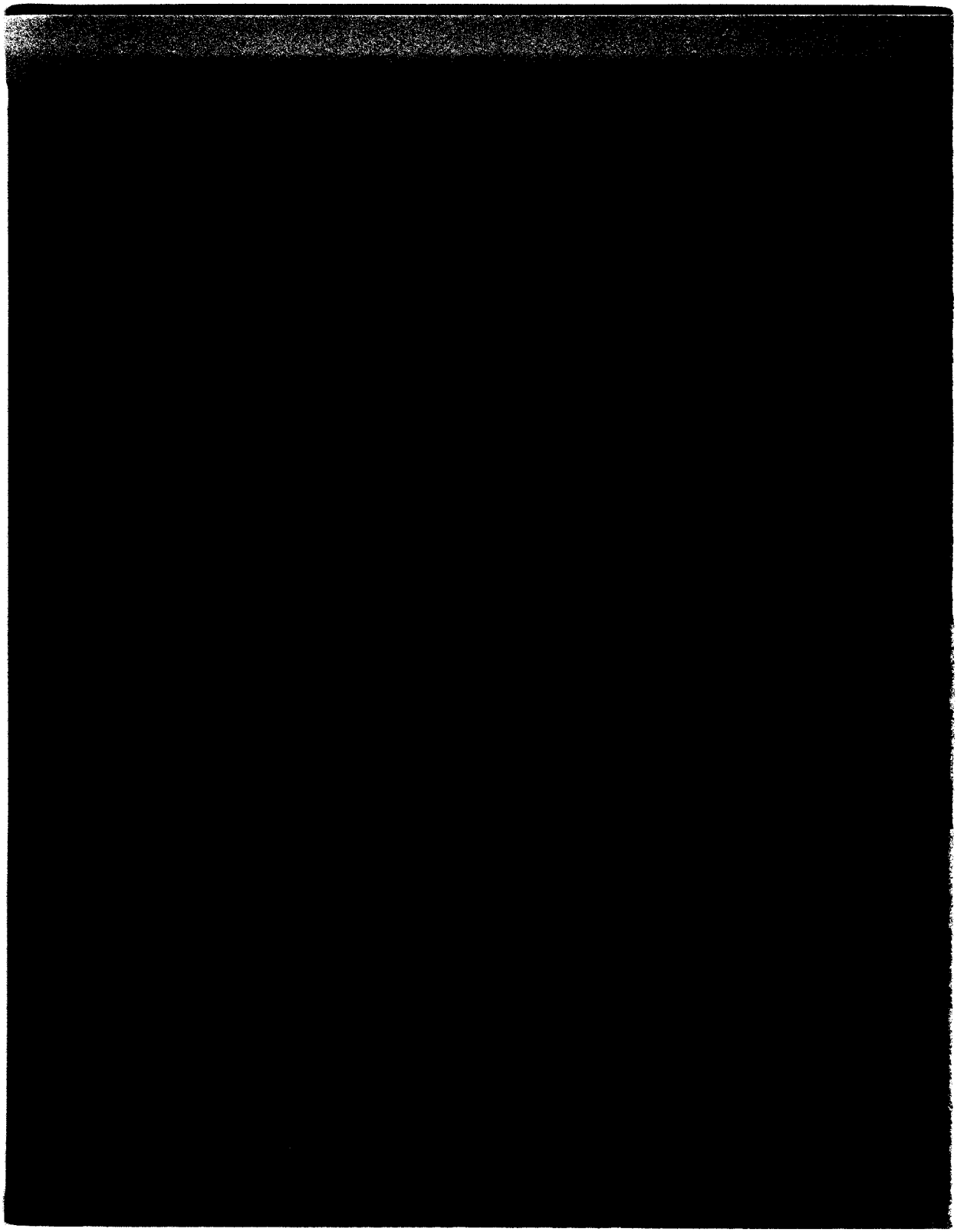

IV. EQUIPMENT

M. Main Vacuum

Prepared by

C. B. Pallaver

IV. M. MAIN VACUUM

(1) DESIGN PHILOSOPHY

The function of the main tank vacuum system is to provide an insulating vacuum such that:

a. The heat leak into the chamber is less than 0.2 W/ft^2.

b. The piping system will withstand 150 psig and -425°F in an emergency condition without permanent damage.

c. The system will dynamically maintain insulating vacuum conditions* if exposed to a small leak of chamber media.

d. All vacuum gauges, valves, and miscellaneous hardware shall be capable of withstanding 150 psig.

e. The vacuum tank also serves as secondary protection in case of failure of the inner vessel.

f. Foresystem. The effective pumping speed of the foresystem has a capacity of 1200 cfm at 10^{-1}mm. The ultimate pressure of the foresystem is 3×10^{-3} torr.

g. High Vacuum System. The system effective pumping speed is 1000 cfm below 10^{-3} torr.

---

* A vacuum of 10^{-4} torr with a background gas of hydrogen will allow a heat leak of 0.2 W/ft^2 to the super insulated chamber.

(2) COMPONENTS

The various components which comprise the main vacuum tank are:

PV901 - Right Angle Valve	- Size 20 inch Conductance 15,000 liters/second Pneumatically operated (Mfg.: Torr Vacuum)
PV902 - 10-Inch Butterfly Valve	- Pneumatically operated (Mfg.: Jamesbury)
Cold Trap	- Size 20 inch Chilled water or liquid N_2 Conductance 9800 liters/second (Mfg.: Torr Vacuum)
PV903 - 6-Inch Butterfly Valve	- Pneumatically operated (Mfg.: Jamesbury)
Diffusion Pump	- Size 20 inch Design speed 17,500 liters/second Operating range $1x10^{-3}$ to $1x10^{-9}$ torr Heaters 12 kW, 480v (Mfg.: Norton Equipment)
PV904 - 8-Inch Butterfly Valve	- Pneumatically operated (Mfg.: Jamesbury)
PV905 - 6-Inch Butterfly Valve	- Pneumatically operated (Mfg.: Jamesbury)
Blower	- Effective pumping speed 1200 cfm Ultimate $3x15^{-3}$ torr Maximum continuous operation 15 torr Normal starting 50 torr Motor 15 hp, 460v (Mfg.: Leybold Heraeus)
Forepump	- Effective pumping speed 150 cfm Ultimate $2x10^{-2}$ torr Motor 20 hp, 460v (Mfg.: Leybold Heraeus) Note: Bypass line provided between blower and forepump.

(3) INSTRUMENTS, ASSORTED

Capable of reading main vacuum pressure from $5x10^{-6}$ mm vacuum to 20 psig with interlocking capabilities at all levels of pressure.

(4) PIPES

All pipe from booster and forepump isolation valves to main vacuum tank are 304 stainless steel capable of withstanding pressure up to 150 psig.

(4) SYSTEM START UP

a. Close PV901 and PV902. These valves isolate main tank from vacuum piping system.
b. Open all other valves in vacuum system; PV903, PV904, and PV905.
c. Make sure cooling water is flowing to blower, forepump and diffusion pump.
d. Start forepump, when vacuum on PG904 reads less than 100 microns, open PV902; close PV904. The main vacuum tank is now being evacuated.
e. When TG902B reads 12 mm start booster pump, close PV905. Open PV904.
f. Check purge gas system is flowing to diffusion pump heaters.
g. When TG902A reads less than 100 microns, turn on diffusion pump and make sure liquid N_2 is in cold trap.
h. After diffusion pump is at proper temperature, close PV902.
i. Open PV901 and PV905. Close PV904.

(6) MONITOR AND CONTROL SYSTEM

Pressures in the main vacuum tank can be monitored in the following ranges:

10^{-2} torr to $5x10^{-6}$ torr

0 - to 1,000 milli torr

0 - 20 torr

0 - 20 psia

All of these instruments have full scale double limit controllers capable of opening or closing any valve in the vacuum or flow systems or triggering any alarm circuit.

(7) NORMAL OPERATION

Pressure in the main tank when stabilized and chamber full of liquid hydrogen should read no worse than $5x10^{-5}$ torr and not much better than $5x10^{-7}$ torr. The only maintenance required is checking pump oil level and reading pressures at regular intervals.

(8) POSSIBLE PROBLEMS AND SYSTEM REACTION

a. Overheating of Diffusion Pump. Temperature sensor on diffusion pump will give alarm at predetermined setting, then at a higher level, automatically shut off power to diffusion pump.

b. Loss of Purge Gas at Diffusion Pump. Pressure sensor will give alarm at predetermined setting, then at a lower level, automatically shut off power to diffusion pump.

c. Power Failure. Entire vacuum system is connected to the emergency power bus (15 second delay). If emergency power fails, valves at the booster and forepump will be automatically closed.

d. Vacuum Failure.

1) Main tank vacuum pressure rises above $5x10^{-5}$ torr but below $5x10^{-4}$.

Indication:

1. Medium level alarm on control room alarm panel.
2. Pressure can be read on IG902 which tripped alarm.

Action:

1. Record IG902 pressure until vacuum improves.

2) Main tank vacuum pressure rises above $5x10^{-4}$ but below 500 mi-

crons.

Indication:

1. High level alarm on control room alarm panel.
2. Pressure can be read on IG902 and TG902A.
3. Chamber cooling loops demanding high consumption of liquid hydrogen.
4. Chamber pressure rising.

Action:

1. Lower chamber pressure.
2. Shut off power to diffusion pump.
3. Open PV902.
4. Close PV901.
5. Determine cause of leak.

3) Main tank vacuum pressure rises above 500 microns but below 20 mm.

Indication:

1. High level alarm on control room panel.
2. Pressure can be read on TG902A and TG903.
3. Chamber cooling loops unable to reduce chamber pressure.

Action:

1. PV902,PV903 automatically closed.
2. Dump chamber to dewar.

4) Main tank vacuum pressure rises above 20 mm.

Indication:

1. High alarm in control room alarm panel.
2. Pressure can be read on TG903 and PS902.

Action:

1. PV904 closes automatically.
2. Chamber is without insulation, open chamber vents to keep pressure down.
3. If chamber pressure rises to 150 psia it automatically

vents up the stack.

Note: See NAL Drawing 2627.MC-25971 included.

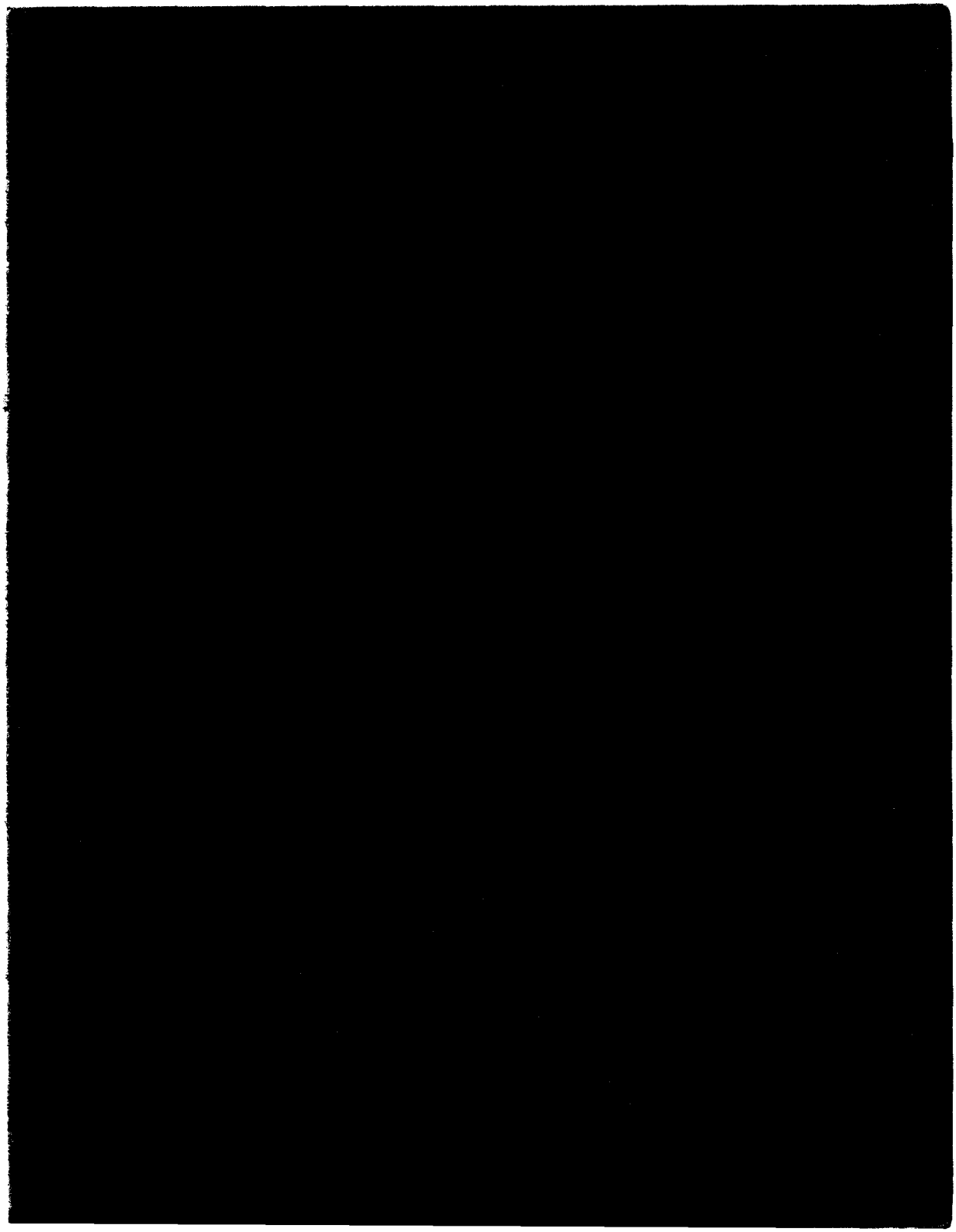

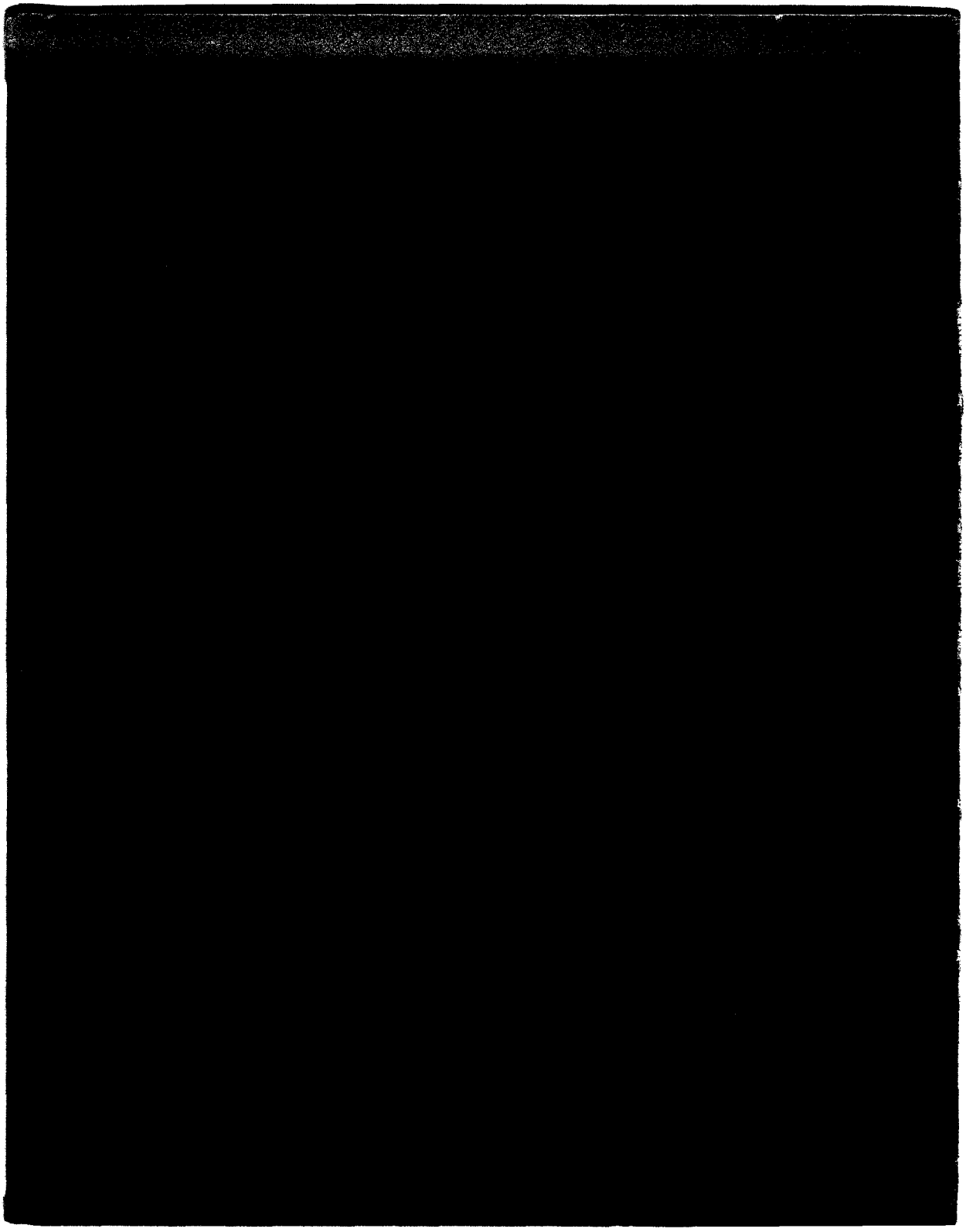

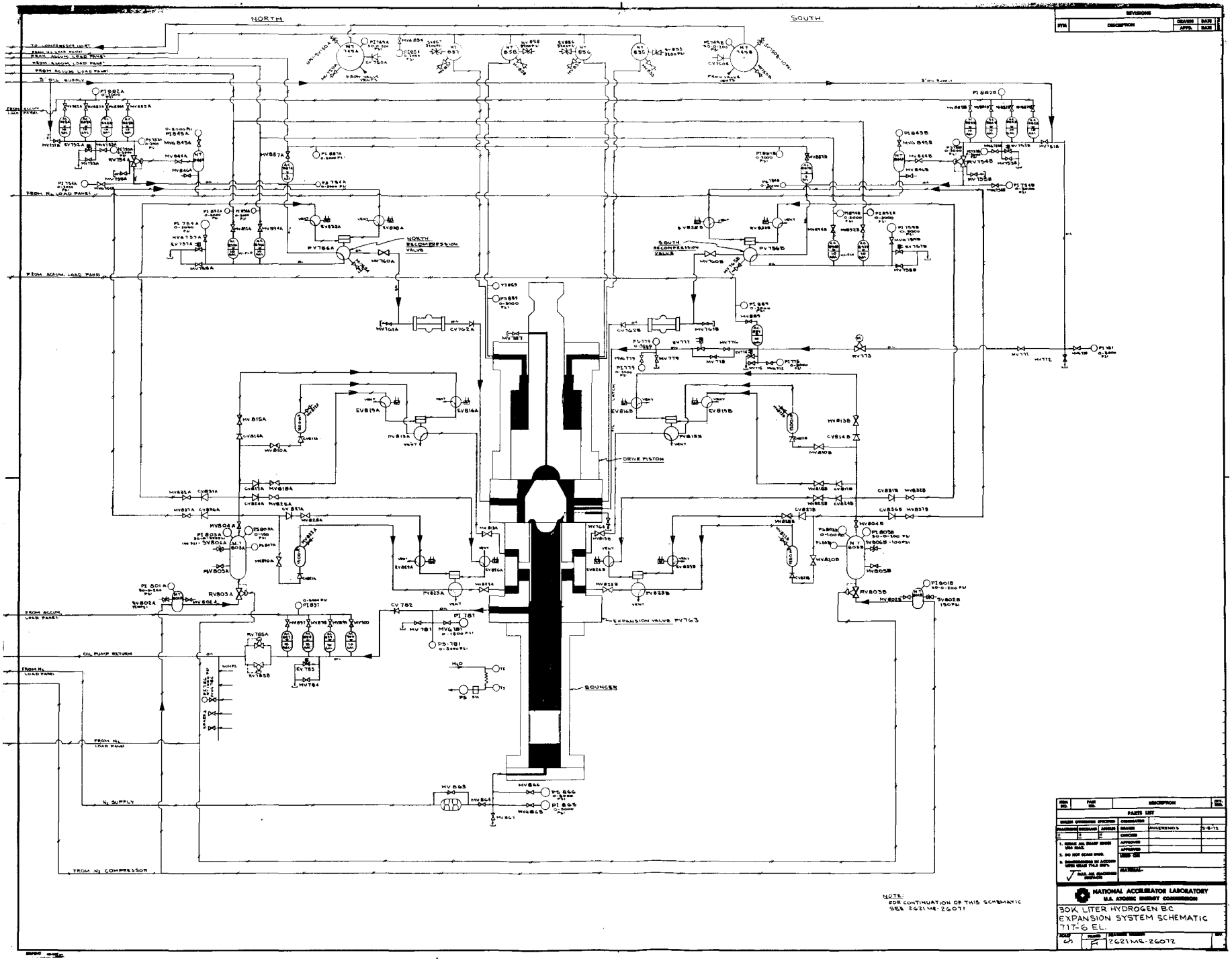
NORTH
SOUTH
FROM ACCUM. LOAD PANEL
FROM N2 LOAD PANEL
OIL PUMP RETURN
FROM N2 COMPRESSOR
NORTH RECOMPRESSION VALVE
SOUTH RECOMPRESSION VALVE
DRIVE PISTON
EXPANSION VALVE PV763
BOUNCER
NOTE:
FOR CONTINUATION OF THIS SCHEMATIC
SEE 2621ME-26077
NATIONAL ACCELERATOR LABORATORY
U.S. ATOMIC ENERGY COMMISSION
30K LITER HYDROGEN BC
EXPANSION SYSTEM SCHEMATIC
717'-6 EL.
2621ME-26072

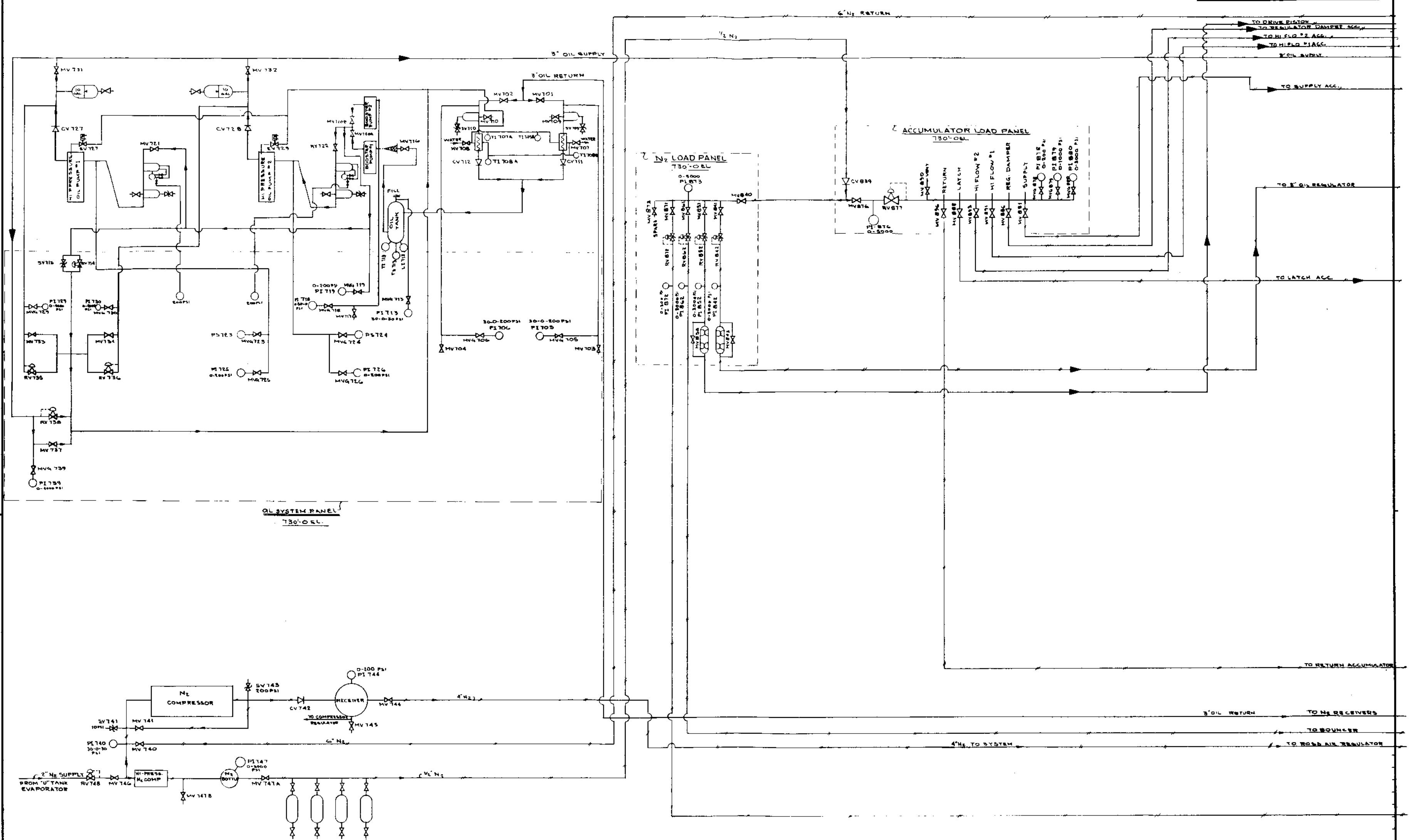

NOTE:
FOR CONTINUATION OF THIS SCHEMATIC
SEE 2621ME-26072

DRAWN	AVGERINOS 5-8-72

NATIONAL ACCELERATOR LABORATORY
U.S. ATOMIC ENERGY COMMISSION

30K LITER HYDROGEN B.C
EXPANSION SYSTEM SCHEMATIC
730'-0 EL

SIZE F — 2621ME-26071

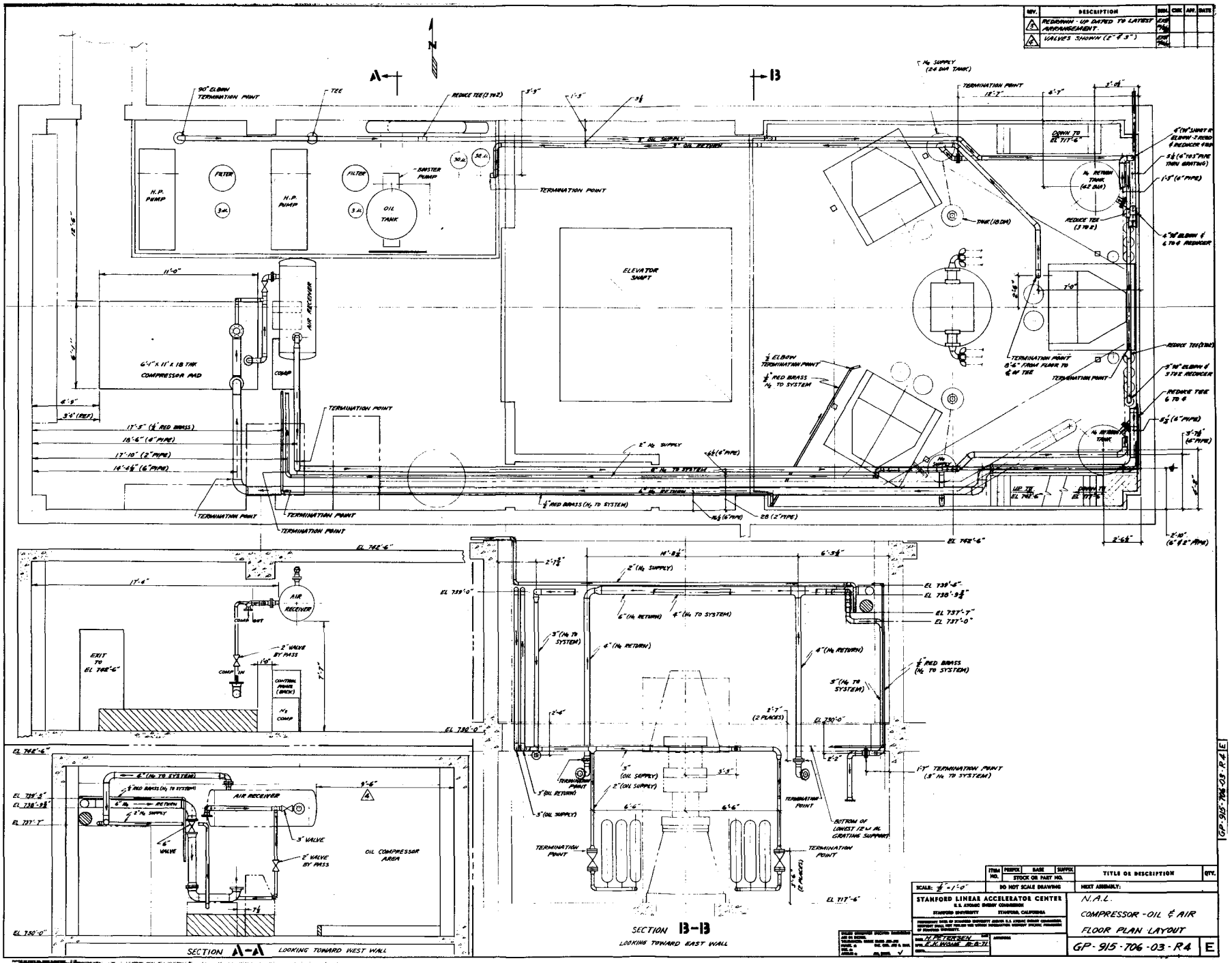

ITEM NO.	PREFIX	BASE	SUFFIX	TITLE OR DESCRIPTION	QTY.
		STOCK OR PART NO.			

SCALE: 3/4" = 1'-0" DO NOT SCALE DRAWING

NEXT ASSEMBLY:

STANFORD LINEAR ACCELERATOR CENTER
U.S. ATOMIC ENERGY COMMISSION
STANFORD UNIVERSITY STANFORD, CALIFORNIA

N.A.L.
COMPRESSOR - OIL & AIR
FLOOR PLAN LAYOUT

DRN. N. PETERSEN DATE
SPR. E.K. ROWE 12-8-71

GP-915-706-03-R4 E

GP-915-706-03-R4 E

NATIONAL ACCELERATOR LABORATORY
U.S. ATOMIC ENERGY COMMISSION

2621.ME-33202

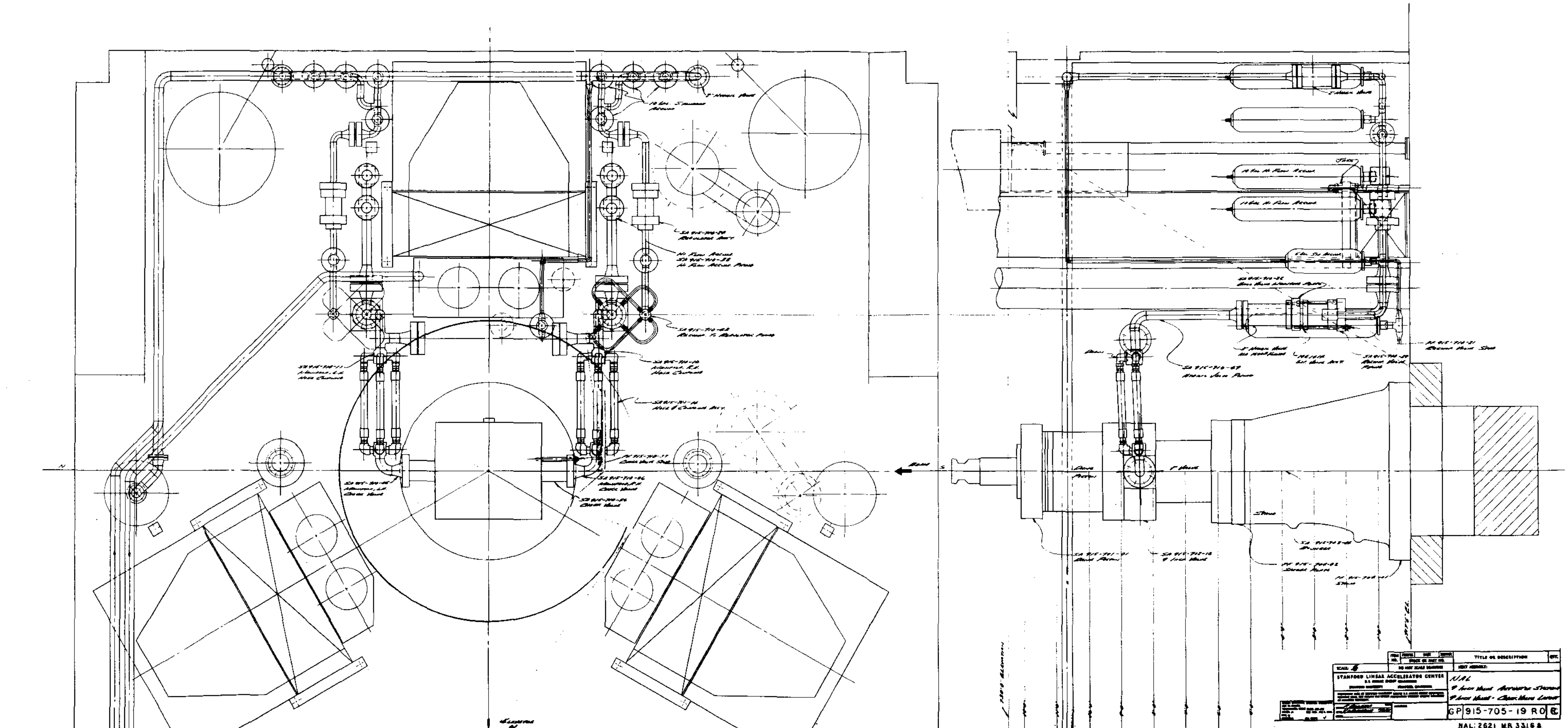

NATIONAL ACCELERATOR LABORATORY
U.S. ATOMIC ENERGY COMMISSION

2621.MR-33168

SCALE	FILMED	DRAWING NUMBER	REV.

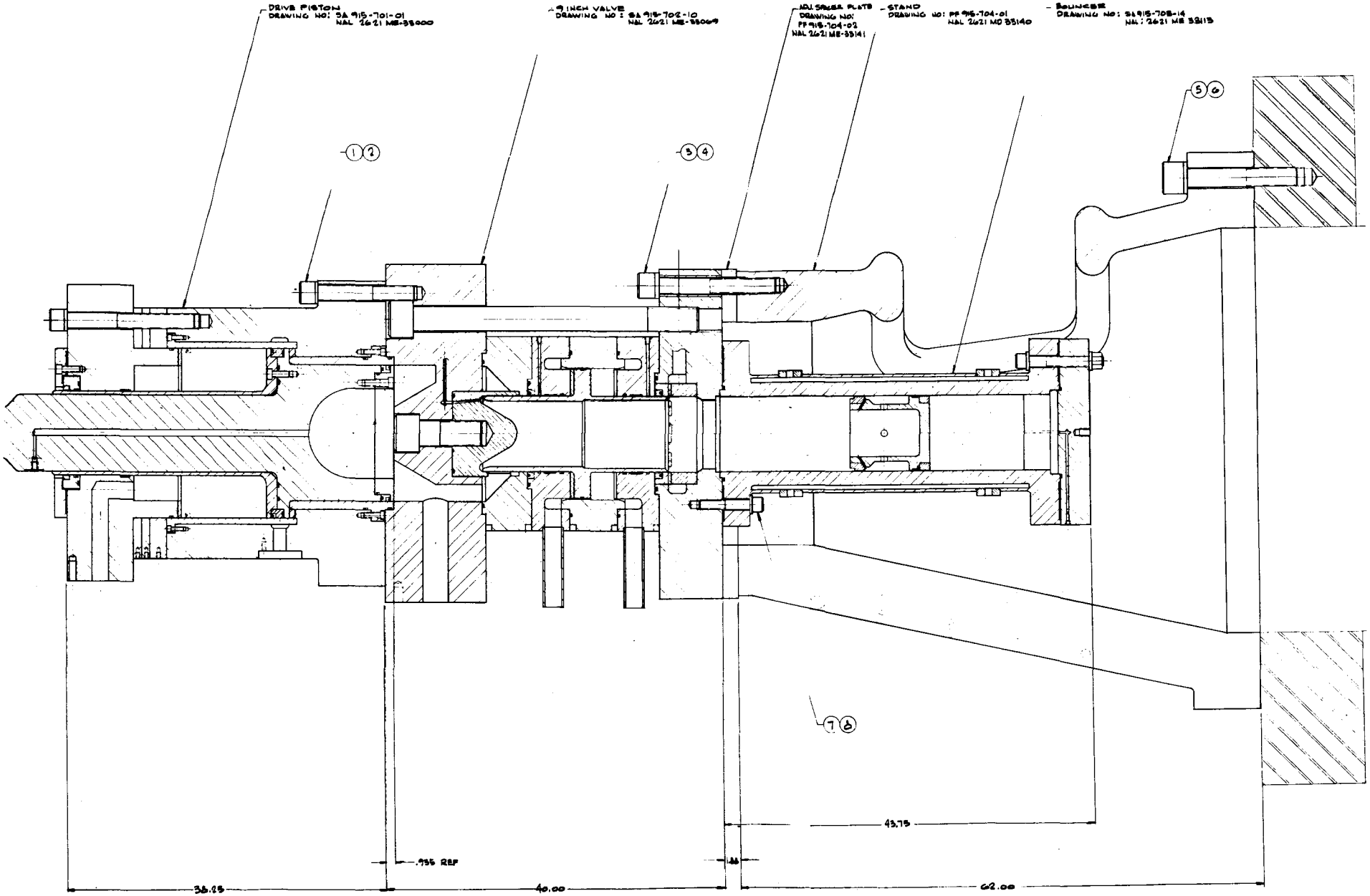

NATIONAL ACCELERATOR LABORATORY U.S. ATOMIC ENERGY COMMISSION			
2621.MR-33280			
SCALE	FILMED	DRAWING NUMBER	REV.

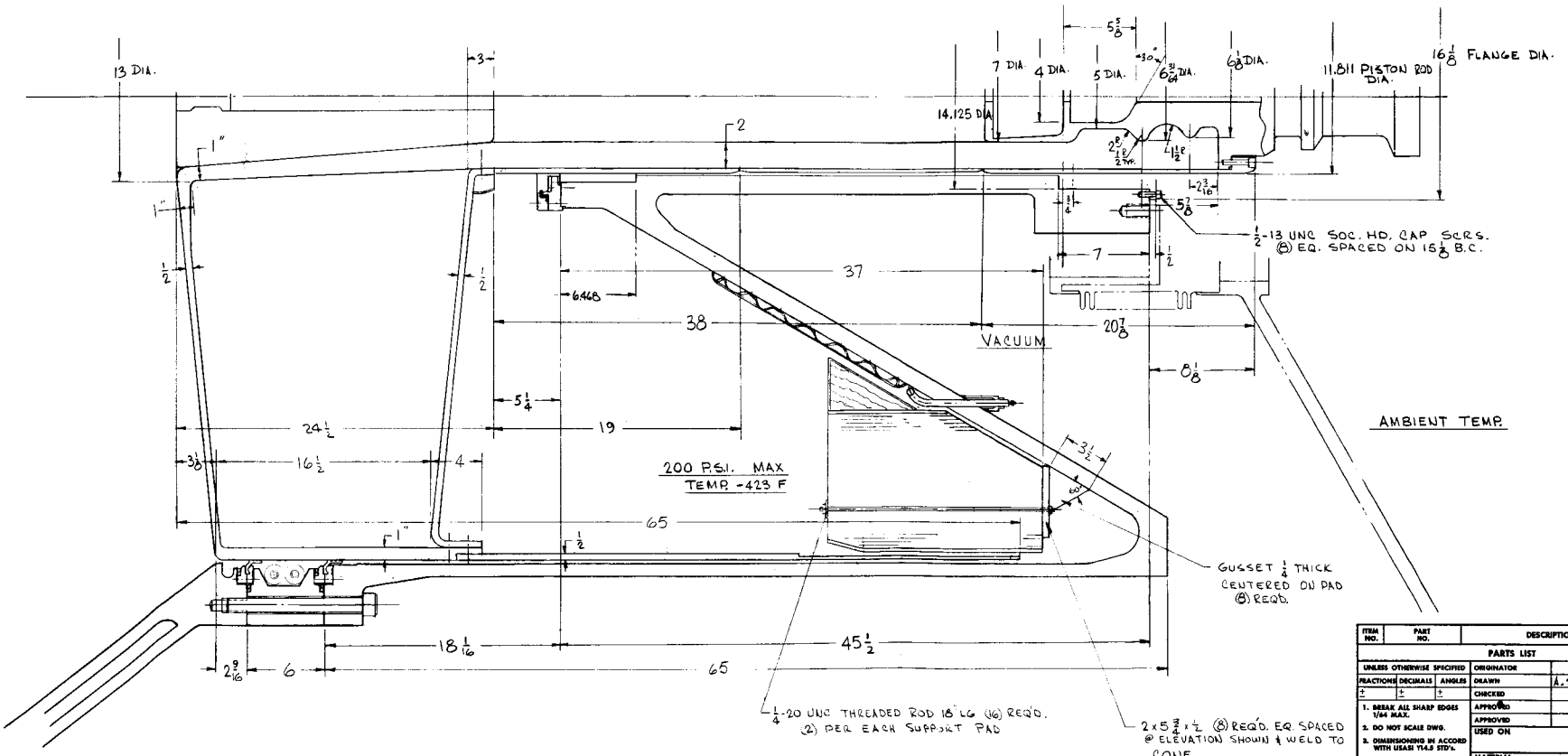

REVISIONS				
SYM	DESCRIPTION	DRAWN / APPD.	DATE	DATE

ITEM NO.	PART NO.	DESCRIPTION	QTY. REQ.

PARTS LIST

UNLESS OTHERWISE SPECIFIED			ORIGINATOR		
FRACTIONS	DECIMALS	ANGLES	DRAWN	A. SKRABOLY	5/18/71
±	±	±	CHECKED		
1. BREAK ALL SHARP EDGES 1/64 MAX.			APPROVED		
2. DO NOT SCALE DWG.			APPROVED		
3. DIMENSIONING IN ACCORD WITH USASI Y14.5 STD'L.			USED ON		
√ MAX. ALL MACHINED SURFACES			MATERIAL -		

NATIONAL ACCELERATOR LABORATORY
U.S. ATOMIC ENERGY COMMISSION

PISTON & ROD GUIDE ASSY.

SCALE	FILMED	DRAWING NUMBER	REV.
1/4=1"	FA	2621.MD-25378	A

BRUNING 40-107 —

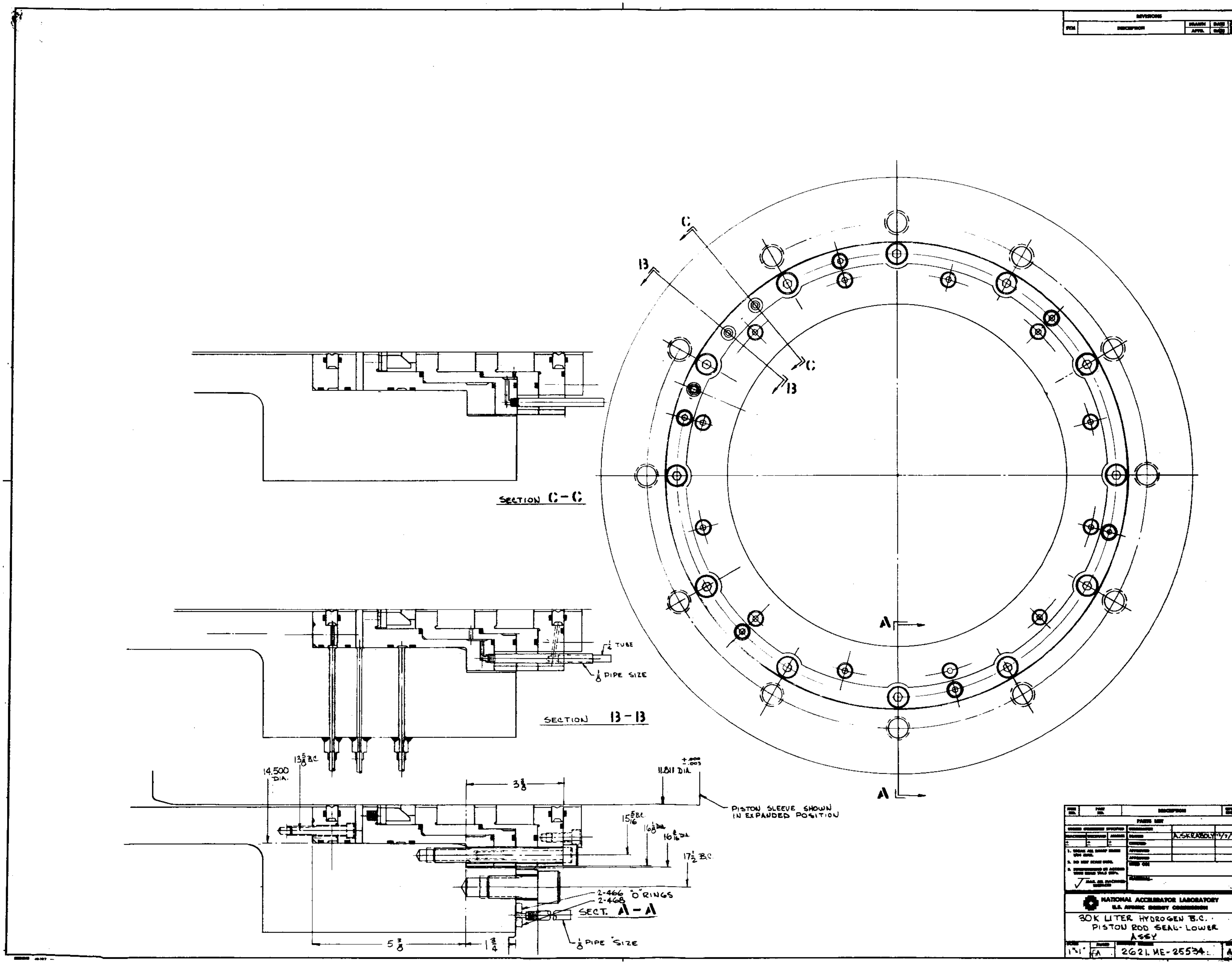
SECTION C-C
1/4 TUBE
1/8 PIPE SIZE
SECTION B-B
14.500 DIA.
13 5/8 B.C.
3 3/8
11.811 DIA. +.000 -.003
PISTON SLEEVE SHOWN IN EXPANDED POSITION
15 5/16 B.C.
16 3/8 DIA.
16 5/8 DIA.
17 1/2 B.C.
2-466 "O" RINGS
2-468
SECT. A-A
5 3/8
1 3/4
1/8 PIPE SIZE
A
B
C
A.SKRABOLY
NATIONAL ACCELERATOR LABORATORY
U.S. ATOMIC ENERGY COMMISSION
30K LITER HYDROGEN B.C.
PISTON ROD SEAL-LOWER ASSY
1"=1"
FA
2621.ME-25534

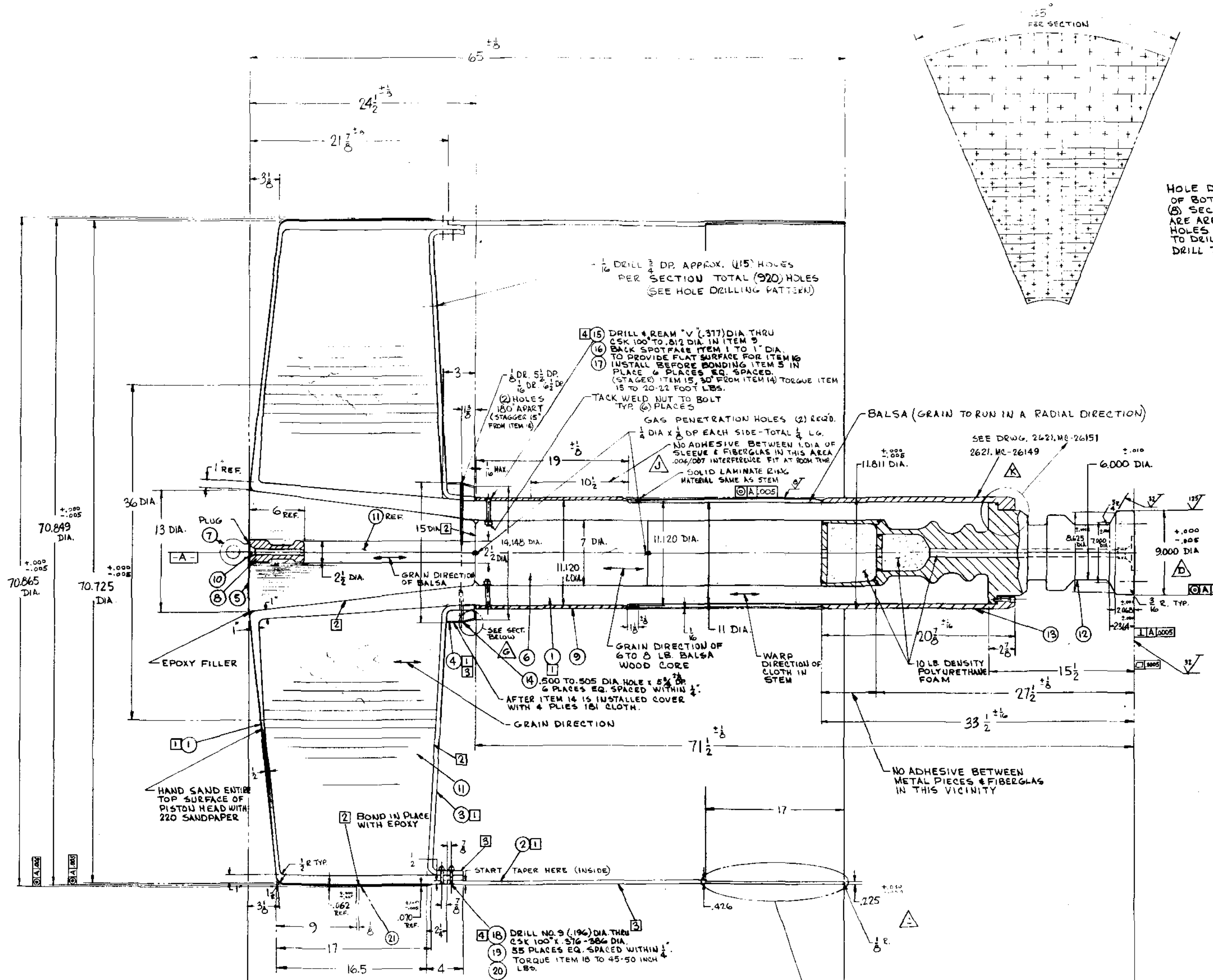

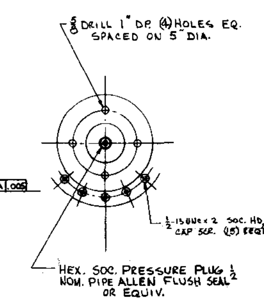

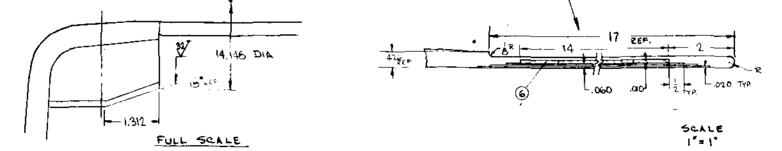

REVISIONS			
SYM	DESCRIPTION	DRAWN / APPD.	DATE
A	REVISED & REDRAWN	A.S.	11/4/70
B	REVISED PER BRUNS. PRINT	A.S.	12/11/70
C	TAPER ADDED	A.S.	12/22/70
D	WAS 8" DIA.	A.S.	12/30/70
E	REVISED PER BRUNS. PRINT	A.S.	8/3/71
F	REVISED	A.S.	10/5/71
G	TAPPER ADDED	A.S.	2/15/72
H	FINALIZED	A.S.	3/14/72
J	NOTE ADDED	A.S.	4
K	REVISED LOWER SLEEVE	A.S.	6/29/72

ITEM NO.	PART NO.	DESCRIPTION	QTY. REQ.
21		TEFLON (25% GLASS FILLED)	
20		NUT	110
19		WASHER	110
18		SCREW	110
17		NUT	6
16		WASHER	6
15		SCREW	6
14		ROLLPIN	6
13	2621.ME-25837	PISTON ROD SLEEVE	1
12	2621.MC-25569	PISTON ROD FITTING ASSY.	1
11	2621.MD-25464	WOOD CORE	8
10	2621.MB-25462	PLUG BOLT	1
9	2621.MC-25464	BEARING	1
8	2621.MC-25436	PISTON PLUG	1
7	2621.MC-25463	EYE BOLT ASSY.	1
6		BALSA WOOD 6-8 LB. DENSITY	A.R.
5		PLUG ASSY.	1
4		SUPPORT RING	1
3		BAFFLE	1
2		SKIRT	1
1		PISTON HD & STEM	1

PARTS LIST

UNLESS OTHERWISE SPECIFIED			ORIGINATOR		
FRACTIONS ± 1/64	DECIMALS ± —	ANGLES ± ¼	DRAWN	A. SKRABOLY	11/4/70
1. BREAK ALL SHARP EDGES 1/64 MAX.			CHECKED		
2. DO NOT SCALE DWG.			APPROVED		
3. DIMENSIONING IN ACCORD WITH USAS Y14.5 1966.			APPROVED		
125 MAX. ALL MACHINED SURFACES			USED ON		
			MATERIAL: NOTED ABOVE		

NATIONAL ACCELERATOR LABORATORY
U.S. ATOMIC ENERGY COMMISSION

30K LITER HYDROGEN B.C.
EXPANSION PISTON

SCALE	FRAMED	DRAWING NUMBER	REV.
¼:1"	FK	2621.ME-25129	K

NOTES:

1. MATERIALS
   ITEM 1 PISTON HD. TO BE 181 & STEM TO BE 143 (OR 341) FIBERGLAS CLOTH IMPREGNATED WITH RESIN EPON 826 & CL (BRUNS CORP. RESIN FORMULA 199.) PLIES OF 181 FROM PISTON HD. & 143 OR 341 FROM STEM TO BE STEP OVERLAPPED & INTEGRALLY JOINED TOGETHER OVER THE 24.5 TAPERED TRANSITION AREA.
   ITEMS 2, 3, & 4 TO BE 181 FIBERGLAS CLOTH IMPREGNATED WITH RESIN EPON 828 & CL (BRUNS. RESIN FORMULA 199).
2. ADHESIVE TO BE ARALDITE 106 OR EQUIV. AT ALL BONDED JOINTS EXCEPT AS NOTED.
3. SEAL ALL TRIMMED & MACHINED SURFACES WITH BRUNS. RESIN FORMULA 188.
4. DIP IN BRUNS. RESIN FORMULA 199 BEFORE INSTALLATION.
5. -A- IS DEFINED AS THE ℄ FORMED BY ROTATING ABOUT THE TWO 60° CENTERS AT EACH END.

REVISIONS				
SYM	DESCRIPTION	DRAWN / APPD.	DATE / DATE	FILMED

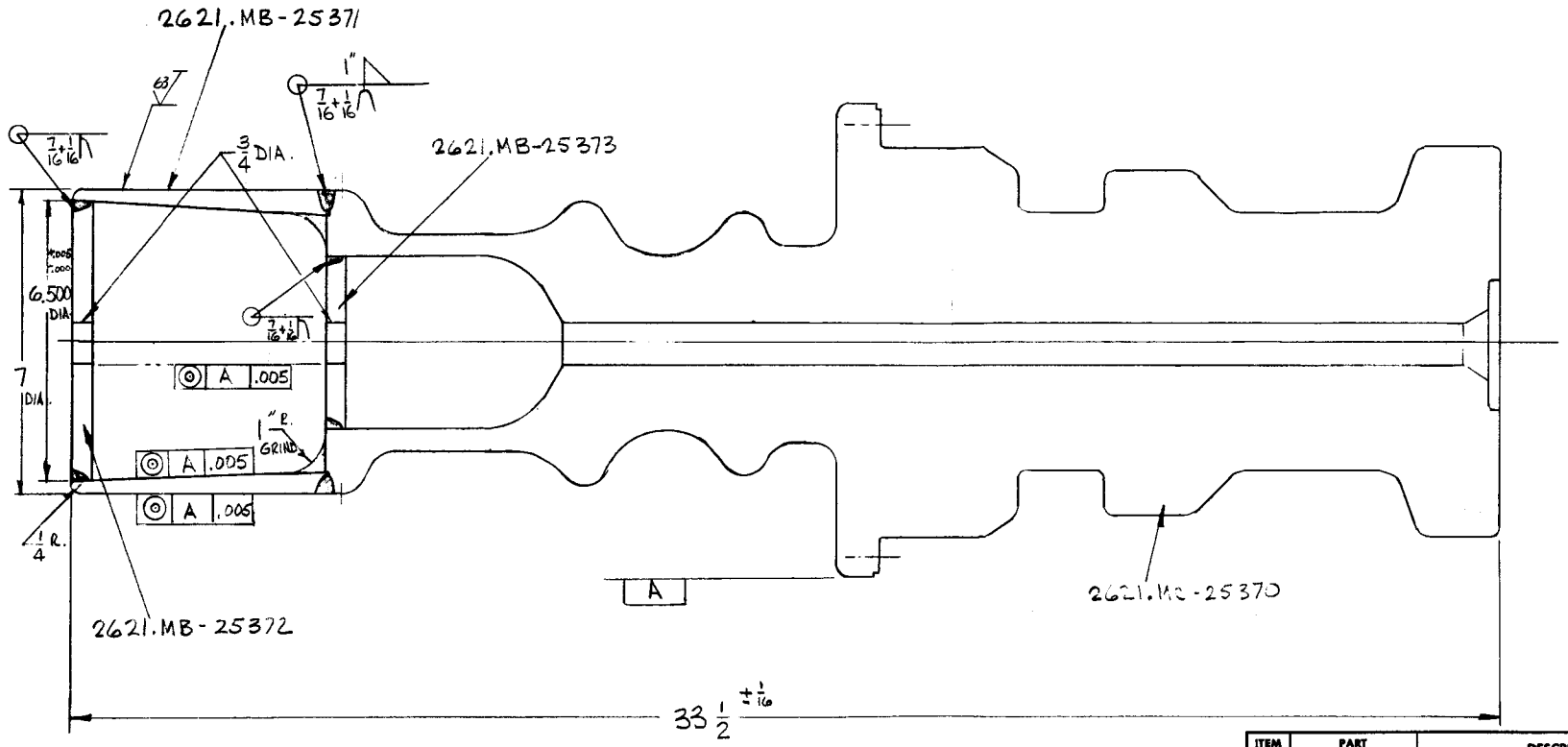

ITEM NO.	PART NO.	DESCRIPTION	QTY. REQ.

PARTS LIST

UNLESS OTHERWISE SPECIFIED	ORIGINATOR		
FRACTIONS / DECIMALS / ANGLES	DRAWN		
± 1/32 / ± .2 / ± 2°	CHECKED	A. SKRABOLY	5/13/71
1. BREAK ALL SHARP EDGES 1/64 MAX.	APPROVED		
2. DO NOT SCALE DWG.	APPROVED		
3. DIMENSIONING IN ACCORD WITH USASI Y14.5 STD's.	USED ON	2621.ME-25129	
125/250 MAX. ALL MACHINED SURFACES	MATERIAL-		

NATIONAL ACCELERATOR LABORATORY
U.S. ATOMIC ENERGY COMMISSION

PISTON ROD FITTING ASSY.

SCALE	FILMED	DRAWING NUMBER	REV.
1/2=1"	FM	2621.MC-25369	A

BRUNING 40-107

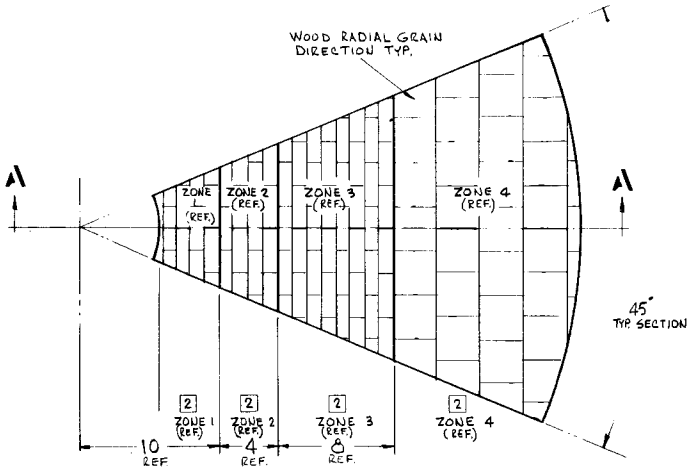

ZONE	TYPE OF WOOD	DENSITY LB/FT³
1	DOUGLAS FIR	34.0
2	BALSA WOOD	15.5
3	BASA WOOD	11.0
4	BALSA WOOD	6.0

TABLE I

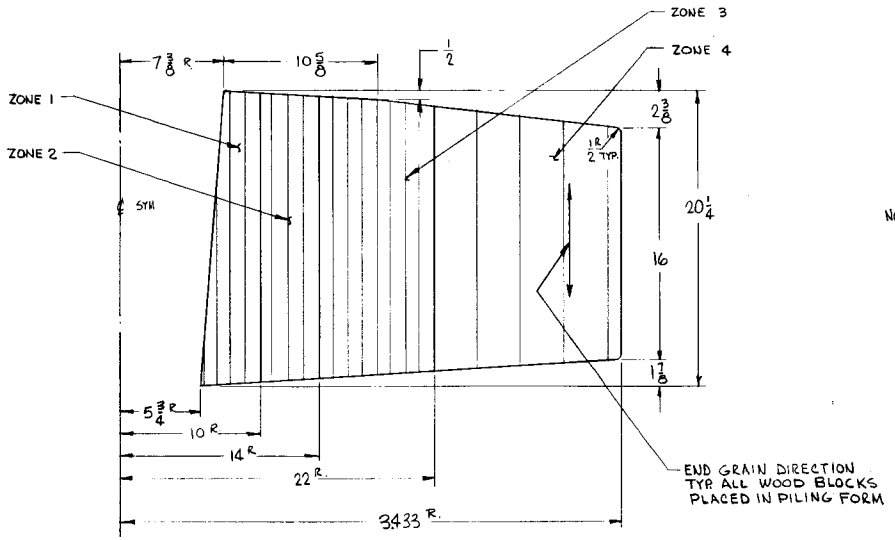

SECTION A – A

NOTES:

1. FOR TYPE OF WOOD & DENSITY REQUIRED IN EACH ZONE SEE TABLE I
2. [2] JOINTS FROM ONE ZONE TO ANOTHER TO BE BONDED, OVERLAP, BLOCK TILED, CONFIGERATION AS SHOWN TO DEVELOPE A JOINT WITH A SHEAR STRENGTH EQUAL TO OR BETTER THAN THAT OF THE ADJOINING ZONE.
3. ADHESIVE TO BE CASCOPHEN RS-240M WITH CATALYST FM-124 (THE BORDEN CHEMICAL COMPANY 350 MADISON AVE., NEW YORK, N.Y.

REVISIONS				
SYM	DESCRIPTION	DRAWN / APPD.	DATE	PLANNER
A	REVISED	A.S.	10/5/71	

ITEM NO.	PART NO.	DESCRIPTION	QTY. REQ.
PARTS LIST			

UNLESS OTHERWISE SPECIFIED			ORIGINATOR		
FRACTIONS	DECIMALS	ANGLES	DRAWN	A.SKRABOLY	8/11/71
± 1/32	± .010	± 1/2°	CHECKED		
1. BREAK ALL SHARP EDGES 1/64 MAX.			APPROVED		
2. DO NOT SCALE DWG.			APPROVED		
3. DIMENSIONING IN ACCORD WITH USASI Y14.5 STD'L.			USED ON		
√ MAX ALL MACHINED SURFACES			MATERIAL SEE TABLE		

NATIONAL ACCELERATOR LABORATORY
U.S. ATOMIC ENERGY COMMISSION

30K LITER HYDROGEN B.C.
WOOD CORE

SCALE	FILMED	DRAWING NUMBER	REV.
1"=1"		2621.MD-25461	A

BRUNING 40-107

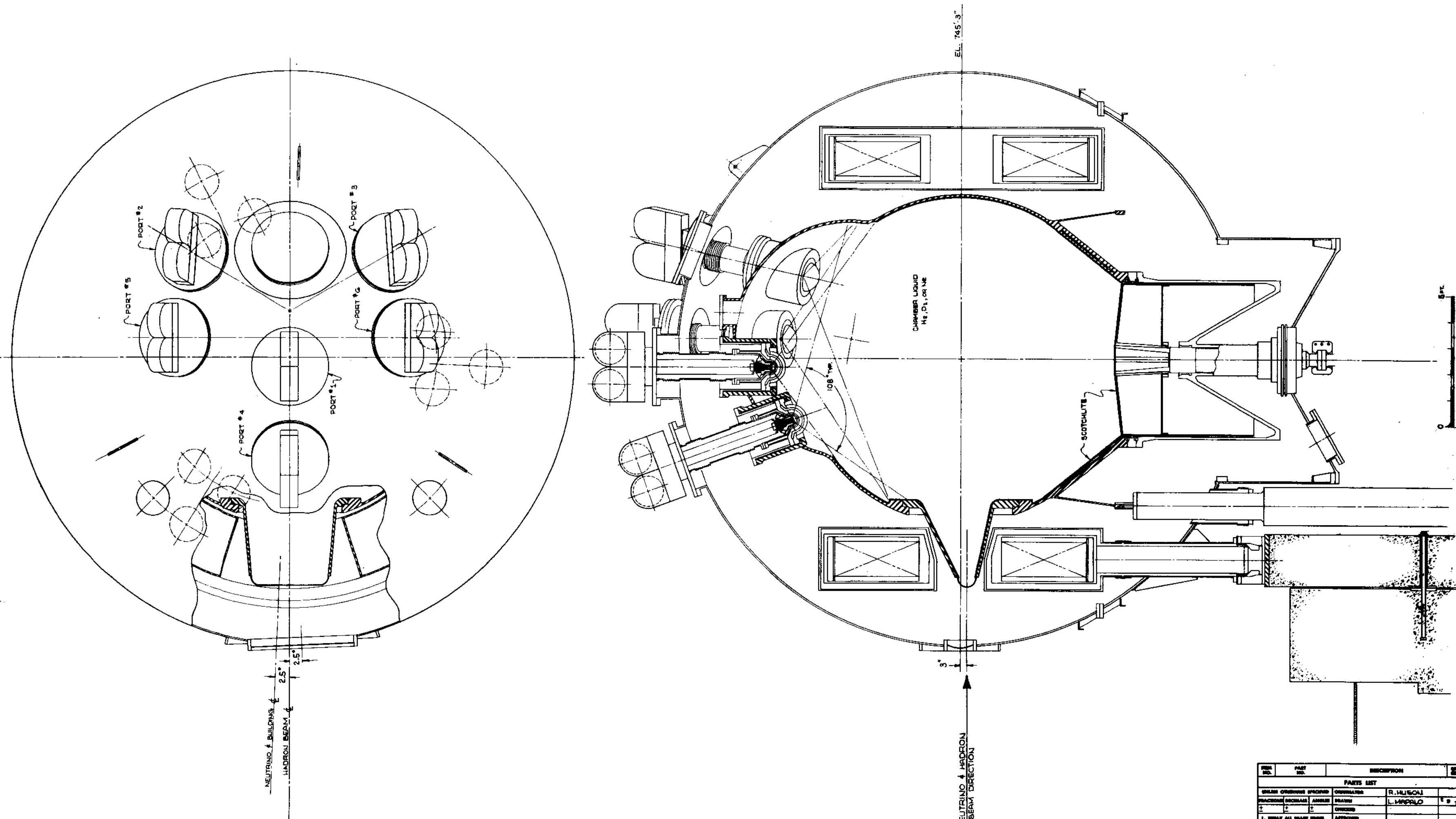

REVISIONS			
SYM.	DESCRIPTION	DRAWN / APPD.	DATE / DATE

ITEM NO.	PART NO.	DESCRIPTION	QTY. REQ.
PARTS LIST			

UNLESS OTHERWISE SPECIFIED			ORIGINATOR	R. HUSON	
FRACTIONS	DECIMALS	ANGLES	DRAWN	L. MAPALO	
±	±	±	CHECKED		
1. BREAK ALL SHARP EDGES 1/64 MAX.			APPROVED		
2. DO NOT SCALE DWG.			APPROVED		
3. DIMENSIONING IN ACCORD WITH USAS Y14.5 STD'S.			USED ON		
MAX. ALL MACHINED SURFACES			MATERIAL		

NATIONAL ACCELERATOR LABORATORY
U.S. ATOMIC ENERGY COMMISSION

30 K LITER HYDROGEN BUBBLE CHAMBER
GENERAL ASSEMBLY
ILLUSTRATION

SCALE 1/40" = 1"

DRAWING NUMBER 2629-ME-25308

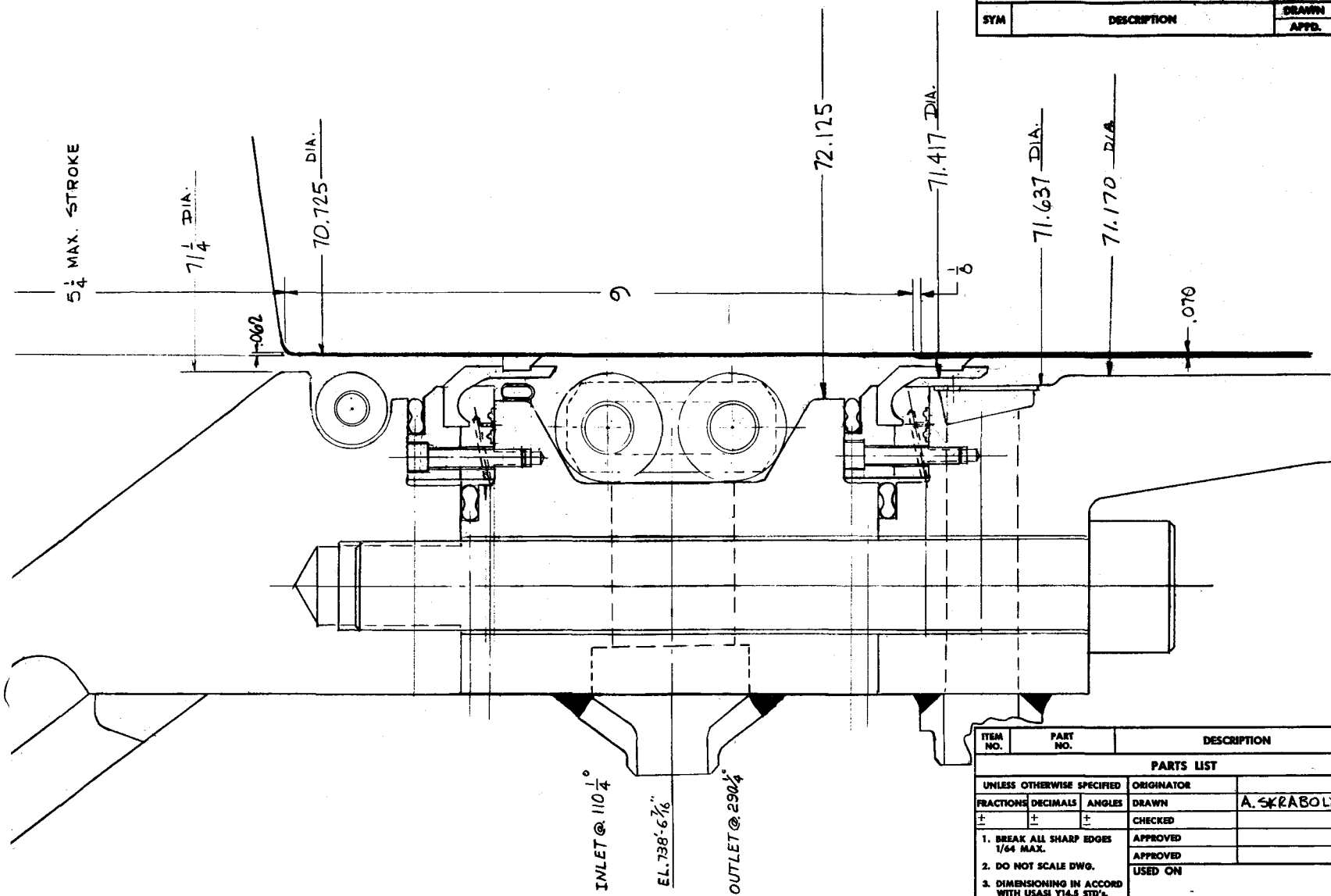

REVISIONS			
SYM	DESCRIPTION	DRAWN APPD.	DATE

ITEM NO.	PART NO.	DESCRIPTION	QTY. REQ.

PARTS LIST

UNLESS OTHERWISE SPECIFIED			ORIGINATOR		
FRACTIONS	DECIMALS	ANGLES	DRAWN	A. SKRABOLY	3/15/71
±	±	±	CHECKED		
1. BREAK ALL SHARP EDGES 1/64 MAX.			APPROVED		
2. DO NOT SCALE DWG.			APPROVED		
3. DIMENSIONING IN ACCORD WITH USASI Y14.5 STD's.			USED ON		
√ MAX. ALL MACHINED SURFACES			MATERIAL-		

NATIONAL ACCELERATOR LABORATORY
U.S. ATOMIC ENERGY COMMISSION

30K LITER HYDROGEN B.C. LIP SEAL SECTION

SCALE	FILMED	DRAWING NUMBER	REV.
1"=1"	f	2621.MC-25336	

40-107 —

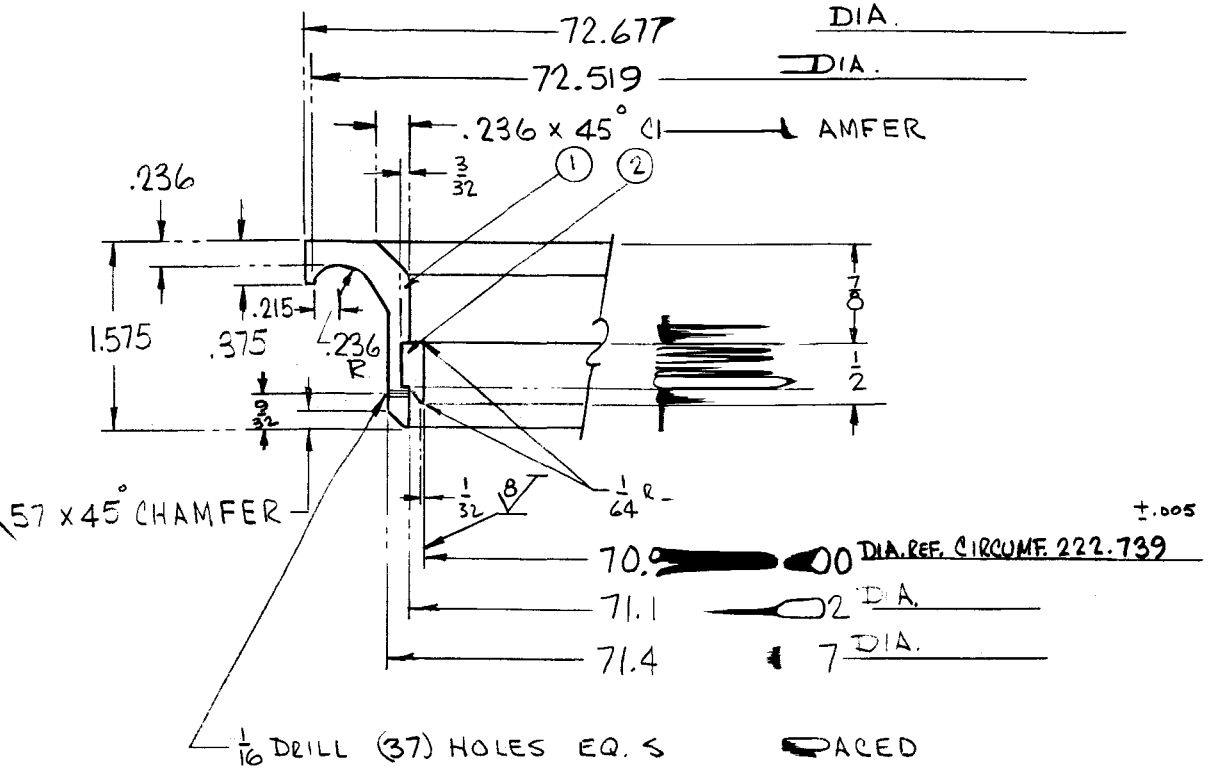

REVISIONS				
SYM	DESCRIPTION	DRAWN / APPD.	DATE / DATE	FILMED
A	WAS 70.940 DIA. CIR. 222.865	A.S.	4/4/72	

ITEM NO.	PART NO.	DESCRIPTION	QTY. REQ.

PARTS LIST

UNLESS OTHERWISE SPECIFIED			ORIGINATOR		
FRACTIONS	DECIMALS	ANGLES	DRAWN	A. SKRABOLY	3/20/72
± 1/2	± .005	± 1/4°	CHECKED		
1. BREAK ALL SHARP EDGES 1/64 MAX.			APPROVED		
2. DO NOT SCALE DWG.			APPROVED		
3. DIMENSIONING IN ACCORD WITH USASI Y14.5 STD's.			USED ON		
125 √ MAX. ALL MACHINED SURFACES			MATERIAL- ① FIBERGLAS EPOXY ② BERYLLIUM COPPER		

NATIONAL ACCELERATOR LABORATORY
U.S. ATOMIC ENERGY COMMISSION

30K LITER HYDROGEN B.C. LOWER-PISTON LIP SEAL

SCALE	FILMED	DRAWING NUMBER	REV.
1=1"	FA	2621. MB-25973	A

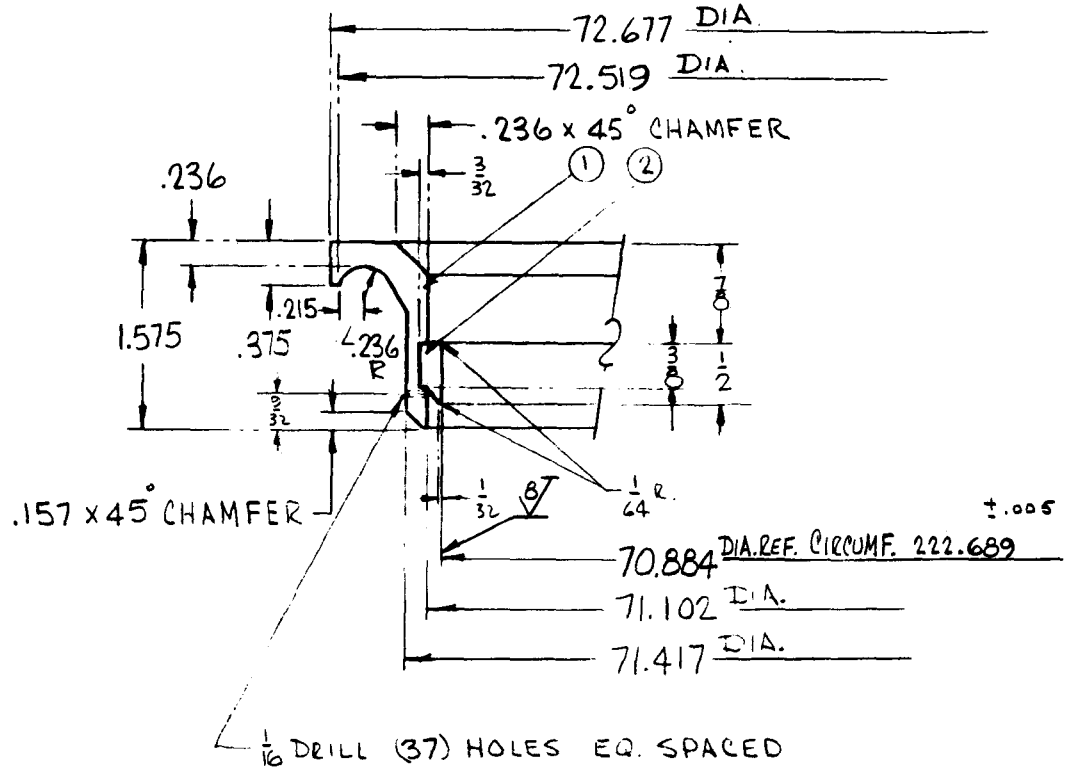

REVISIONS			
SYM	DESCRIPTION	DRAWN / APPD.	DATE
A	WAS 70.924 DIA. CIR. 222.815	A.S.	4/4/72

ITEM NO.	PART NO.	DESCRIPTION	QTY. REQ.

PARTS LIST

UNLESS OTHERWISE SPECIFIED			ORIGINATOR		
FRACTIONS	DECIMALS	ANGLES	DRAWN	A. SKRABOLY	3/20/72
± ~	± .005	± 1/4°	CHECKED		
			APPROVED		
			APPROVED		

1. BREAK ALL SHARP EDGES 1/64 MAX.
2. DO NOT SCALE DWG.
3. DIMENSIONING IN ACCORD WITH USAS Y14.5 STD's.

125 MAX. ALL MACHINED SURFACES

USED ON

MATERIAL- ① FIBERGLAS EPOXY
② BERYLLIUM COPPER

NATIONAL ACCELERATOR LABORATORY
U.S. ATOMIC ENERGY COMMISSION

30K LITER HYDROGEN B.C.
UPPER - PISTON LIP SEAL

SCALE	FILMED	DRAWING NUMBER	REV.
1=1"	FA	2621.MB-25974	A

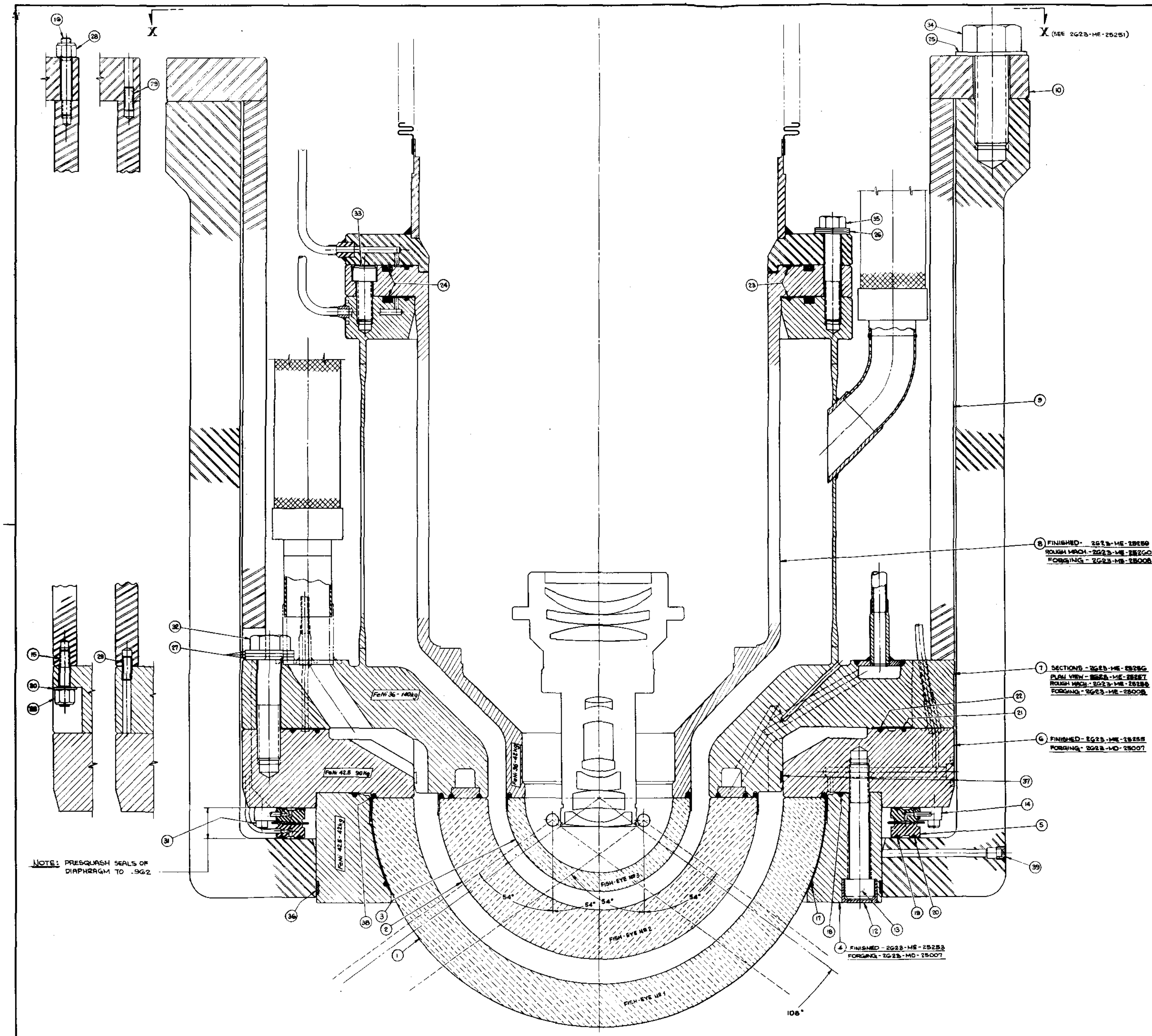

REVISIONS

SYM	DESCRIPTION	DRAWN / APPR.	DATE
A	ITEM #11 NOW DELETED	L.M.	9-29-7[illegible]
B	ADDED ITEM # 39	L.M.	4-11-7[illegible]

ITEM NO.	PART NO.	DESCRIPTION	QTY. REQ.
39	2623-MB-26018	TEFLON SEAL ORIFICE	1
38		1/8 SQ. TEFLON FILLER	3
37		TEFLON CENTERING SPACER	[illegible]
36	2623-MC-25262	TEFLON JETTING SEAL	1
35		1/2-20UNF-2A x 3" LG. HEX. HD. MACH. SCR./SAFETY WIRE HOLES - STN. STL.	[illegible]
34		1 1/2-7 UNC-2A x 5" LG. [illegible] SCR./SAFETY WIRE HOLES - STN. STL.	[illegible]
33		1/2-20UNF-2A x 1 1/4 LG. SOC. HD. CAP SCREW - STN. STL.	[illegible]
32		[illegible]	12
31		[illegible] SOC. HD. CAP SCREW/SAFETY WIRE HOLES - [illegible]	12
30		5/16 STD. PLAIN WASHER, STN. STL. [illegible]	6
29		5/16 DIA. x [illegible] LG. STD. DOWEL, STN. STL.	[illegible]
28		"HI-KEY" NUT [illegible] HI-SHEAR CORP. [illegible]	12
27	PHOSPHORUS BRONZE	"SCHNORR" DISC SPRING [illegible] 40mm O.D. x [illegible]	[illegible]
26	PHOSPHORUS BRONZE	"SCHNORR" DISC SPRING [illegible]	[illegible]
25	PHOSPHORUS BRONZE	"SCHNORR" DISC SPRING [illegible] 60mm O.D. x 30.5mm I.D. x [illegible]	[illegible]
24		"O" RING - 1/4 WIDE x [illegible] I.D. AN-6227-[illegible]	2
23		INDIUM SEAL (2% SILVER), [illegible] x 12.[illegible] MEAN DIA. ([illegible])	[illegible]
22		INDIUM SEAL (2% SILVER), [illegible] x 16.030 MEAN DIA. ([illegible])	1
21		INDIUM SEAL (2% SILVER), [illegible] x [illegible] MEAN DIA. ([illegible])	1
20		INDIUM SEAL (2% SILVER), [illegible] x [illegible] MEAN DIA. ([illegible])	[illegible]
19		INDIUM SEAL (2% SILVER), [illegible] x 19.[illegible] MEAN DIA. (60 [illegible])	[illegible]
18		INDIUM SEAL (2% SILVER), [illegible] x 15.[illegible] MEAN DIA. (48 [illegible])	1
17		INDIUM SEAL (2% SILVER), [illegible] x 13.625 MEAN DIA. (42 [illegible])	[illegible]
16	2623-MB-[illegible]	STD. STUD - REWORK	[illegible]
15	2623-MB-[illegible]	INVAR STUD	6
14	2623-MB-[illegible]	DIAPHRAGM LIFTING LUG	6
13	2623-MB-25265	SPECIAL CAP SCREW	8
12	2623-MB-25264	PLUG, BOLT	8
~~11~~	~~2623-MB-[illegible]~~	~~PLUG, EYE BOLT~~ △	~~4~~
10	2623-ME-25262	FISH-EYE THRUST RING	1
9	2623-ME-[illegible]	WINDOW RING SPACER	1
8	2623-ME-2625[illegible]	#3 WINDOW FLANGE	1
7	2623-ME-25256 2623-ME-25257	#2 WINDOW FLANGE - SECTIONS - PLAN VIEW	1
6	2623-ME-25255	#1 WINDOW FLANGE	1
5	2623-ME-25254	DIAPHRAGM SEAL FLANGE	1
4	2623-ME-25253	RETAINING FLANGE, WINDOW #1	1
3	2623-MB-25004	FISH-EYE WINDOW #3	1
2	2623-MC-25008	FISH-EYE WINDOW #2	1
1	2623-MC-25002	FISH-EYE WINDOW #1	1

PARTS LIST

UNLESS OTHERWISE SPECIFIED			ORIGINATOR	CERN	
FRACTIONS	DECIMALS	ANGLES	DRAWN	L. MAPALO	1-18-71
±	±	±	CHECKED		
1. BREAK ALL SHARP EDGES 1/64 MAX.			APPROVED		
2. DO NOT SCALE DWG.			APPROVED		
3. DIMENSIONING IN ACCORD WITH USASI Y14.5 STD.			USED ON		
√ MAX. ALL MACHINED SURFACES			MATERIAL-		

NATIONAL ACCELERATOR LABORATORY
U.S. ATOMIC ENERGY COMMISSION

30k LITER HYDROGEN BUBBLE CHAMBER
OPTICS SYSTEM
OPTICAL FISH-EYE ASS'Y. (SECTION)

SCALE	FILMED	DRAWING NUMBER	REV.
1"=1"	FA	2623-ME-25250	A

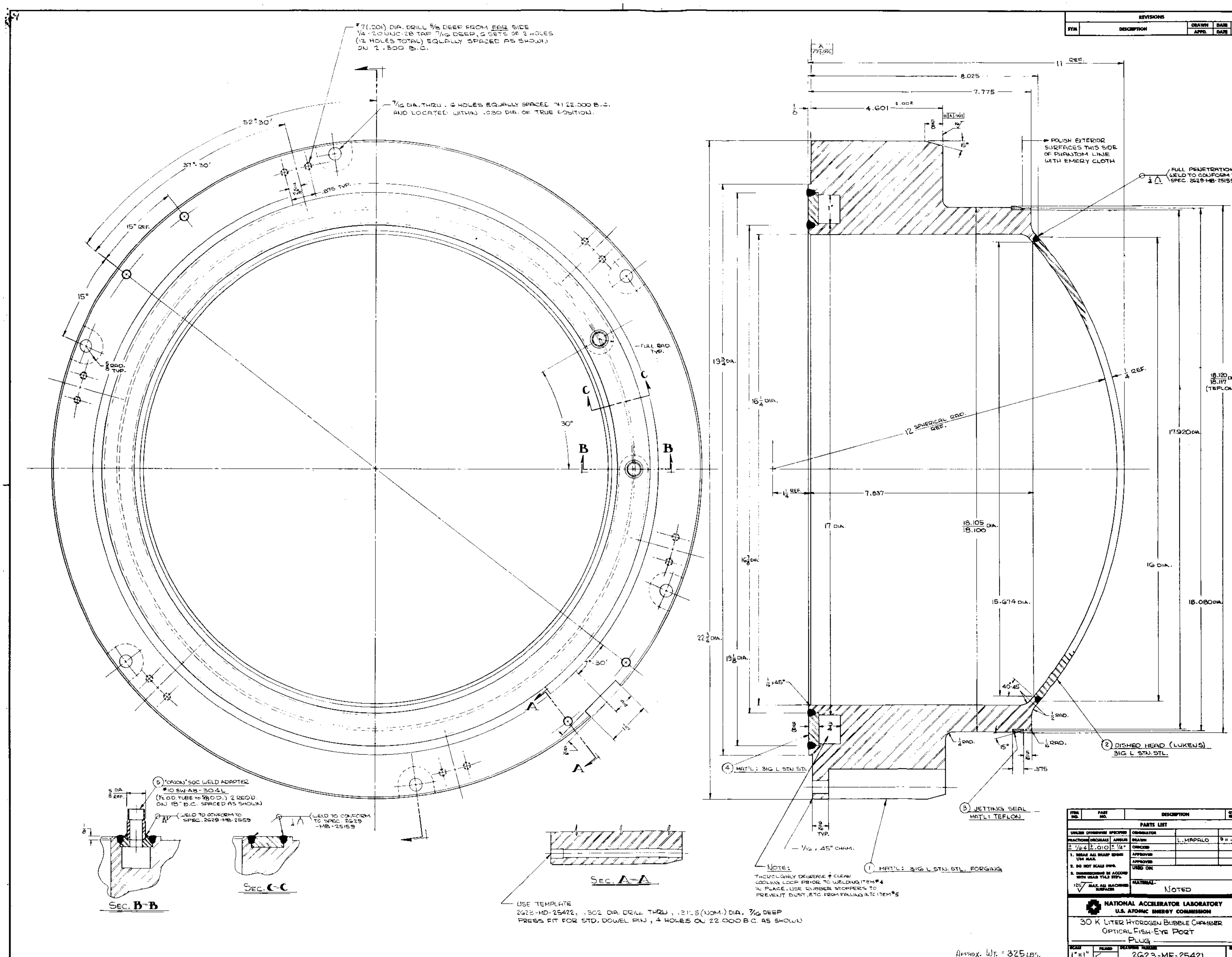
#7(.201) DIA. DRILL 5/8 DEEP FROM FAR SIDE
1/4-20 UNC-2B TAP 7/16 DEEP, 6 SETS OF 2 HOLES
(12 HOLES TOTAL) EQUALLY SPACED AS SHOWN
ON 2.300 B.C.
7/16 DIA. THRU. 6 HOLES EQUALLY SPACED ON 22.000 B.C.
AND LOCATED WITHIN .030 DIA. OF TRUE POSITION.
52°-30′
37°-30′
15° REF.
15°
5/8 RAD. TYP.
.875 TYP.
7/16 TYP.
FULL RAD. TYP.
30°
7°-30′
C
B
A
3/4
1 1/2
5/16
5 DIA. 8 REF.
5 "CAJON" SOC WELD ADAPTER
#10 SW-AB-304L
(1/2 O.D. TUBE TO 5/8 O.D.) 2 REQ'D.
ON 18" B.C. SPACED AS SHOWN
WELD TO CONFORM TO SPEC. 2629-MB-25159
WELD TO CONFORM TO SPEC. 2629 -MB-25159
SEC. B-B
SEC. C-C
SEC. A-A
USE TEMPLATE
2623-MD-25422, .302 DIA. DRILL THRU, .3125 (NOM.) DIA. 7/16 DEEP
PRESS FIT FOR STD. DOWEL PIN, 4 HOLES ON 22.000 B.C. AS SHOWN
11 REF.
8.025
7.775
4.601 ±.002
5/8
15°
POLISH EXTERIOR SURFACES THIS SIDE OF PHANTOM LINE WITH EMERY CLOTH
FULL PENETRATION WELD TO CONFORM TO SPEC. 2629-MB-25159
1"
19 3/4 DIA.
16 1/4 DIA.
1/4 REF.
12 SPHERICAL RAD. REF.
18.120 / 18.117 DIA. (TEFLON)
17.920 DIA.
1 1/4 REF.
7.837
17 DIA.
18.105 / 18.100 DIA.
16 7/8 DIA.
16 DIA.
15.674 DIA.
18.080 DIA.
22 3/4 DIA.
19 1/8 DIA.
1/16 x 45°
40°-45′
1/2 RAD.
3/8
3/4
1/4 RAD.
15°
1/16 RAD.
5/16
.375
4 MAT'L: 316 L STN. STL.
2 DISHED HEAD (LUKENS) 316 L STN. STL.
3 JETTING SEAL MAT'L: TEFLON
9/16 TYP.
1/16 x 45° CHAM.
NOTE:
THOROUGHLY DEGREASE & CLEAN COOLING LOOP PRIOR TO WELDING ITEM #4 IN PLACE. USE RUBBER STOPPERS TO PREVENT DUST, ETC. FROM FALLING INTO ITEM #5
1 MAT'L: 316 L STN. STL. FORGING
APPROX. WT. = 325 LBS.
REVISIONS
SYM
DESCRIPTION
DRAWN
APPD.
DATE
ITEM NO.
PART NO.
DESCRIPTION
QTY. REQ.
PARTS LIST
UNLESS OTHERWISE SPECIFIED
FRACTIONS ± 1/64
DECIMALS ±.010
ANGLES ± 1/4°
1. BREAK ALL SHARP EDGES 1/64 MAX.
2. DO NOT SCALE DWG.
3. DIMENSIONING IN ACCORD WITH USASI Y14.5 STD's.
125 MAX. ALL MACHINED SURFACES
ORIGINATOR
DRAWN L. MAPALO 9-11-71
CHECKED
APPROVED
APPROVED
USED ON
MATERIAL NOTED
NATIONAL ACCELERATOR LABORATORY
U.S. ATOMIC ENERGY COMMISSION
30 K LITER HYDROGEN BUBBLE CHAMBER
OPTICAL FISH-EYE PORT
PLUG
SCALE 1"=1"
FILMED
DRAWING NUMBER 2623-ME-25421
REV.

REVISIONS			
SYM	DESCRIPTION	DRAWN / APPD.	DATE
A	REDRAWN	AVGERINOS	6-24-72
B	REVISED	AVGERINOS	6-17-11

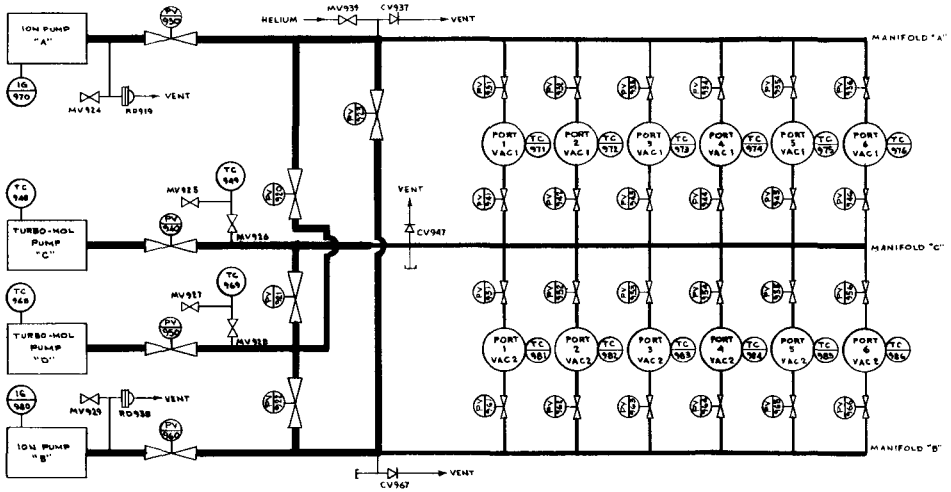

ITEM NO.	PART NO.	DESCRIPTION	QTY. REQ.

PARTS LIST

UNLESS OTHERWISE SPECIFIED			ORIGINATOR		
FRACTIONS	DECIMALS	ANGLES	DRAWN	AVGERINOS	6-24-72
±	±	±	CHECKED		
1. BREAK ALL SHARP EDGES 1/64 MAX.			APPROVED		
2. DO NOT SCALE DWG.			APPROVED		
3. DIMENSIONING IN ACCORD WITH USAS Y14.5 STD's.			USED ON		
√ MAX ALL MACHINED SURFACES			MATERIAL -		

NATIONAL ACCELERATOR LABORATORY
U.S. ATOMIC ENERGY COMMISSION

30K LITER HYDROGEN B.C.
OPTICS VACUUM SYSTEM
SCHEMATIC

SCALE	FILMED	DRAWING NUMBER	REV.
NONE	FB	2627MD-25798	B

SYM.	DESCRIPTION	DRAWN / APPD.	DATE / DATE
A	ADDED ITEM # 9	LM	1-24-72
B	ADDED ITEMS 10 THRU 24 INCL.	LM	4-14-72

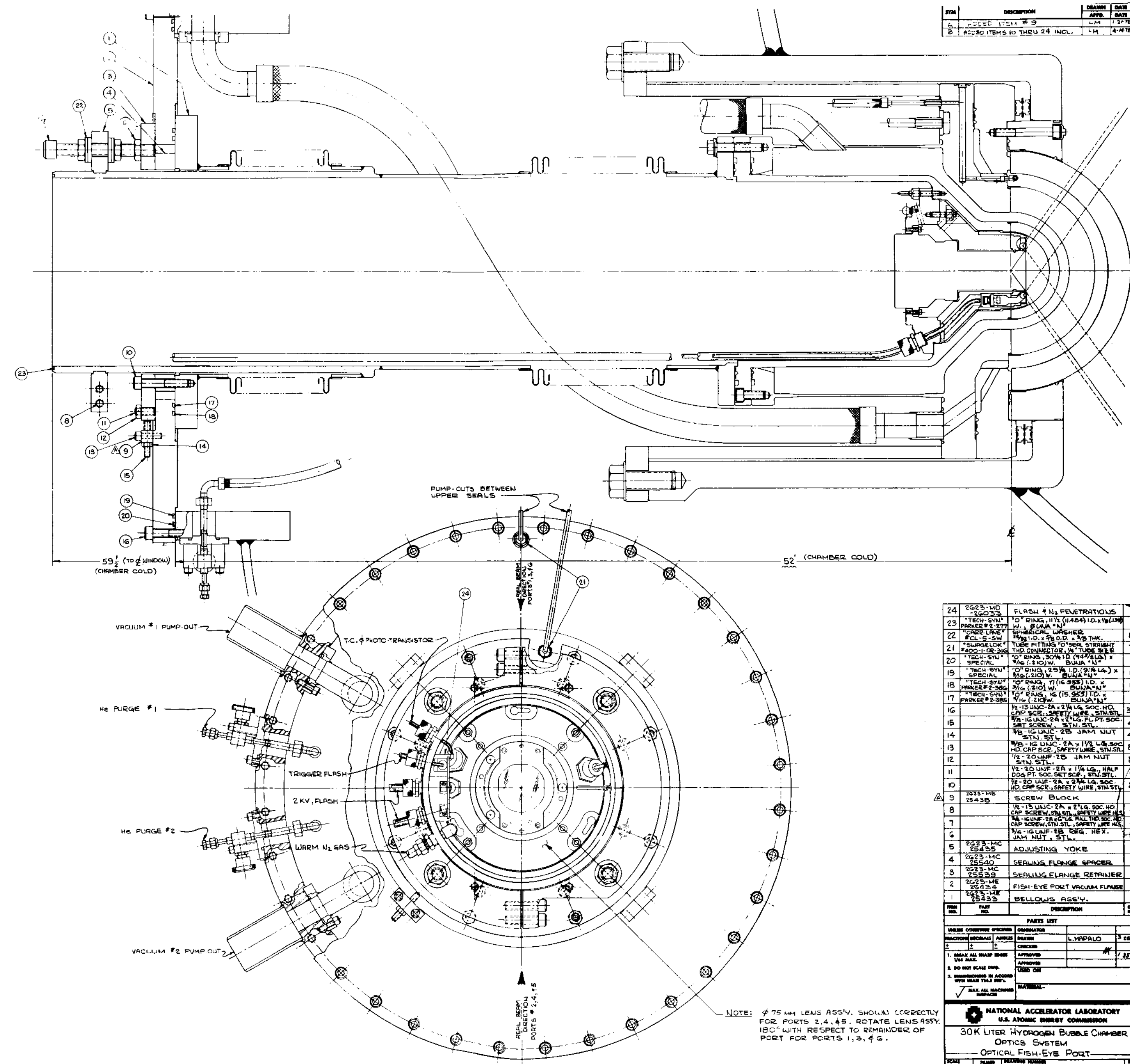

NOTE: ⌀ 75 mm LENS ASS'Y. SHOWN CORRECTLY FOR PORTS 2,4,&5. ROTATE LENS ASSY. 180° WITH RESPECT TO REMAINDER OF PORT FOR PORTS 1,3,&6.

ITEM NO.	PART NO.	DESCRIPTION	QTY. REQ.
24	2623-MD-26033	FLASH & N_2 PENETRATIONS	1
23	"TECH-SYN" PARKER #2-277	"O" RING, 11½ (11.484) I.D. x ⅛ (.139) W., BUNA "N"	1
22	"CARR-LANE" #CL-5-SW	SPHERICAL WASHER 17/32 I.D. x ⅝ O.D. x 3/8 THK.	8
21	"SWAGELOK" #400-1-OR-316	TUBE FITTING "O" SEAL STRAIGHT THD. CONNECTOR, ¼" TUBE SIZE	2
20	"TECH-SYN" SPECIAL	"O" RING, 30¼ I.D. (94 7/8 LG.) x 3/16 (.210) W. BUNA "N"	1
19	"TECH-SYN" SPECIAL	"O" RING, 29¼ I.D. (91¾ LG.) x 3/16 (.210) W. BUNA "N"	1
18	"TECH-SYN" PARKER #2-386	"O" RING, 17 (16.955) I.D. x 3/16 (.210) W. BUNA "N"	1
17	"TECH-SYN" PARKER #2-385	"O" RING, 16 (15.955) I.D. x 3/16 (.210) W. BUNA "N"	1
16		½-13 UNC-2A x 2¼ LG. SOC. HD. CAP SCR., SAFETY WIRE, STN. STL.	36
15		⅜-16 UNC-2A x 2" LG. FL. PT. SOC. SET SCREW, STN. STL.	4
14		⅜-16 UNC-2B JAM NUT STN. STL.	4
13		⅜-16 UNC-2A x 1½ LG. SOC. HD. CAP SCR., SAFETY WIRE, STN. STL.	8
12		½-20 UNF-2B JAM NUT STN. STL.	8
11		½-20 UNF-2A x 1¼ LG., HALF DOG PT. SOC. SET SCR., STN. STL.	8
10		½-20 UNF-2A x 2¾ LG. SOC. HD. CAP SCR., SAFETY WIRE, STN. STL.	8
9 (A)	2623-MB 25438	SCREW BLOCK	4
8		½-13 UNC-2A x 2" LG. SOC. HD. CAP SCREW, STN. STL., SAFETY WIRE HLS.	4
7		¾-16 UNF-2A x 6" LG. FULL THD. SOC. HD. CAP SCREW, STN. STL., SAFETY WIRE HLS.	4
6		¾-16 UNF-2B REG. HEX. JAM NUT, STL.	12
5	2623-MC 25435	ADJUSTING YOKE	1
4	2623-MC 25540	SEALING FLANGE SPACER	1
3	2623-MC 25539	SEALING FLANGE RETAINER	1
2	2623-ME 25434	FISH-EYE PORT VACUUM FLANGE	1
1	2623-ME 25433	BELLOWS ASS'Y.	1

PARTS LIST

UNLESS OTHERWISE SPECIFIED					
FRACTIONS ±	DECIMALS ±	ANGLES ±	ORIGINATOR		
			DRAWN	L. MAPALO	3-26-71
			CHECKED		
			APPROVED	MK	1-25-72
			APPROVED		

1. BREAK ALL SHARP EDGES 1/64 MAX.
2. DO NOT SCALE DWG.
3. DIMENSIONING IN ACCORD WITH USAS Y14.5 STD'S.

√ MAX. ALL MACHINED SURFACES

USED ON

MATERIAL-

NATIONAL ACCELERATOR LABORATORY
U.S. ATOMIC ENERGY COMMISSION

30K LITER HYDROGEN BUBBLE CHAMBER
OPTICS SYSTEM
— OPTICAL FISH-EYE PORT —

SCALE	PLANO	DRAWING NUMBER	REV.
½"=1"		2623-ME-25432	B

REVISIONS				
SYM	DESCRIPTION	DRAWN / APPD.	DATE / DATE	FILMED

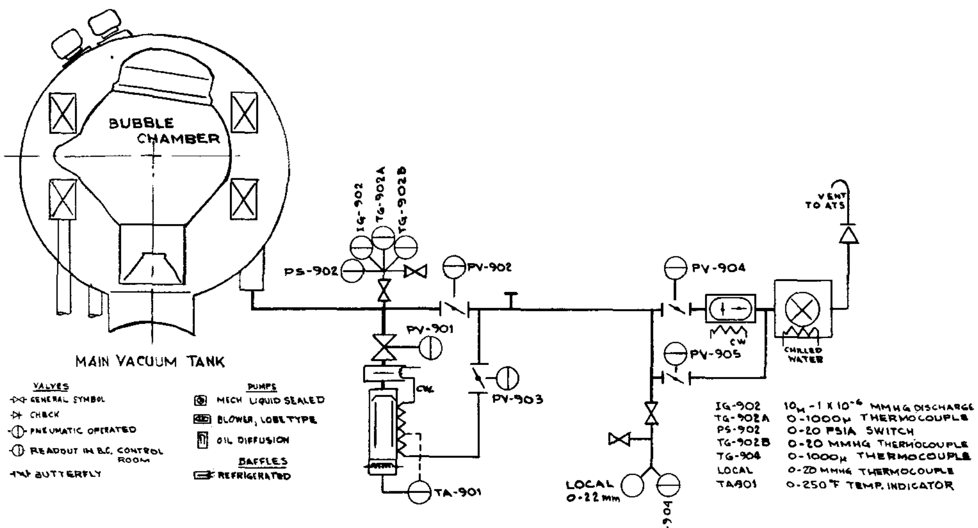

MAIN VACUUM TANK SYSTEM

ITEM NO.	PART NO.	DESCRIPTION	QTY. REQ.

PARTS LIST

UNLESS OTHERWISE SPECIFIED					
FRACTIONS ±	DECIMALS ±	ANGLES ±	ORIGINATOR		
			DRAWN	AVGERENOS	3-20-72
			CHECKED		
			APPROVED		
			APPROVED		

1. BREAK ALL SHARP EDGES 1/64 MAX.
2. DO NOT SCALE DWG.
3. DIMENSIONING IN ACCORD WITH USASI Y14.5 STD's.

√ MAX. ALL MACHINED SURFACES

USED ON

MATERIAL-

NATIONAL ACCELERATOR LABORATORY
U.S. ATOMIC ENERGY COMMISSION

30K LITER HYDROGEN B.C.
MAIN VACUUM SYSTEM
SCHEMATIC

SCALE	FILMED	DRAWING NUMBER	REV.
∽	F	2627MC-25971	

BRUNING 40-107 —